DOCTORAL THESIS

Siting Strategies for Variable Renewable Generation Assets in Capacity Expansion Planning Frameworks

Author:
David-Constantin RADU

Supervisor:
Prof. Damien ERNST

President of the jury:
Prof. Louis WEHENKEL, *University of Liège*

Examination committee:
Raphaël FONTENEAU, PhD, *University of Liège*
Edwin HAESEN, PhD, *ENTSO-E*
Asst. Prof. Jakub JURASZ, *Wrocław Univ. of Science and Technology*
Prof. Hrvoje PANDŽIĆ, *University of Zagreb*
Asst. Prof. Sylvain QUOILIN, *University of Liège*

A thesis submitted in fulfilment of the requirements for the degree of Doctor of Philosophy

at

LIÈGE université
Sciences Appliquées

December 2, 2021

Acknowledgements

In arguably the most exciting of times for energy research, I would like to express my gratitude to Prof. Damien Ernst for providing me the opportunity to embark on this journey, as well as to Prof. Louis Wehenkel, Assoc. Prof. Hrvoje Pandžić, Asst. Prof. Jakub Jurasz, Asst. Prof. Sylvain Quoilin, Raphaël Fonteneau and Edwin Haesen for offering me the chance to successfully conclude it. I would also like to thank all my collaborators for their valuable input on my work along these years. In particular, my deepest gratitude goes to my colleague Mathias Berger, whose stamina, work ethics and technical depth have left an undeniable mark on my research output and who is also the main reason why these years were not a solitary professional journey.

I wish to thank Catherine, Samia and Daniela for their efforts towards improving my everyday life in a foreign country. For the same reason, I would like to acknowledge the crucial role of beautiful people like Daniele, Ioannis, Mathias, Miguel, Queralt or Raphaël, whose friendship was a much needed distraction along these years.

I thank Raul for being a live example of hard work and successful goal achievement and for very skillfully knowing when to abuse his elder brother duties. His role in my becoming a doctoral candidate in a technical field can only be matched by the contribution of my parents, Maria and Remos, whose decades-long efforts on all possible levels led me to where I am today. Finding proper means of acknowledging them would be futile but what is clear to me is that this success is as much theirs as it is mine. Last but not least, I cannot be thankful enough for having Cristina by my side in all the ups and downs along these years. Her unconditional support and patience for work hours extending deep into overtime were instrumental to the successful completion of this journey.

To everyone out there fighting the good fight.

Abstract

Siting Strategies for Variable Renewable Generation Assets in Capacity Expansion Planning Frameworks

by David-Constantin RADU

In the eve of a climate crisis generated by the sustained combustion of fossil fuels across various economic sectors, decarbonising worldwide power systems has been a cornerstone in reaching net-zero targets in the upcoming decades. To this end, widely-available renewable energy sources (RES) such as solar irradiance or wind have been recently harnessed at scale in order to replace fossil-based generators in the electricity mix of power systems around the world. However, such resources are inherently variable on time scales ranging from minutes to years and integrating them in power systems typically complicates planning and operational procedures. Several solutions have been advocated to alleviate these issues, including the large-scale deployment of electricity storage systems or the implementation of demand response programs. Alternatively, since RES are heterogeneously-distributed in space and time, it has been suggested that siting RES electricity production assets so as to exploit this diversity may reduce the aggregate output variability of power plants as well as the residual electricity load (i.e., total load minus renewable production). The concept of renewable sources spatiotemporal complementarity formalises this idea and makes for the chief concept investigated in this thesis.

The manuscript starts by revealing how connecting remote RES sites could lead to reduced probabilities of low-generation events. Then, a framework explicitly designed to assess the spatiotemporal complementarity between geographically dispersed RES assets is introduced and leveraged to devise optimisation models seeking to identify deployment patters with maximum complementarity among sites. Once an optimisation problem for siting RES assets based on complementarity criteria is made available, the value of spatiotemporal complementarity for power systems is assessed. Essentially, this is made possible via a multi-stage approach that works as follows. In the first stage, a highly-granular siting problem identifies a suitable set of sites where RES assets could be deployed according to a pre-specified criterion (e.g., spatiotemporal complementarity, output maximisation). In the second stage, the subset of previously identified sites is passed to a capacity expansion planning framework that sizes the power generation, transmission and storage assets that should be deployed and operated in order to satisfy pre-specified electricity demand levels at minimum cost. Furthermore, a third stage may also be leveraged should a more accurate estimation of the impact of different siting criteria on the operation of power systems is sought. This stage is formulated as a classical unit commitment and economic dispatch problem and, given the capacities of power generation, transmission and storage assets resulted from the second stage, provides a more detailed view on the daily operation of the power system assets. Finally, inspired by the workings of the aforementioned routine, a method to reduce the spatial dimension and decrease the computational burden of capacity expansion planning problems while preserving a detailed representation of RES assets is proposed.

Contents

List of Figures

List of Tables

List of Abbreviations

AR6	Sixth Assessment Report of the IPCC
CAPEX	Capital expenditure
CCGT	Combined-cycle gas turbine
CEP	Capacity expansion planning (framework)
CH_4	Methane
CO_2	Carbon dioxide
COP	Conference of Parties
DC-OPF	Linearized (DC equations) optimal power flow
EC	European Commission
EEZ	Exclusive Economic Zone
ENTSOE	European Network of Transmission System Operators (for Electricity)
EU	European Union
FLP	Full LP
FOM	Fixed operation and maintenance cost
GHG	Greenhouse gases
GIS	Geographic information system
IEA	International Energy Agency
IEC	International Electrotechnical Commission
IP	Integer program
IPCC	The Intergovernmental Panel on Climate Change
IRENA	International Renewable Energy Agency
(HV)AC	(High voltage) Alternate current
(HV)DC	(High voltage) Direct current
k€/M€/b€	Thousand/million/billion €
(k)m	(kilo)metre
kt/Mt	kilo-/megaton
km^2	kilometre-square
Li-Ion	Lithium-ion electrochemical storage
LP	Linear program
MENA	Middle East & North Africa

MILP	Mixed-integer linear program
MIR	Mixed-integer relaxation
MW/GW/TW	Mega-/Giga-/Terawatt
MWh/GWh/TWh	Mega-/Giga-/Terawatt-hour
N/A	Not applicable
N_2O	Nitrous oxide
nm	Nautical miles
O&M	Operation and maintenance (expenditures)
OCGT	Open-cycle gas turbine
OPEX	Operational expenditure
OPSD	Open Power System Data
ppm	Parts-per-million
PCA	Principal component analysis
PHS	Pumped-hydro storage unit
PMR	Peak memory requirement
PV	Photovoltaics
PV_d	Distributed PV
PV_u	Utility-scale PV
QP	Quadratic program
RES	Renewable energy sources
RLP	Reduced LP
ROR	Run-of-river hydro power plant
SITE	Siting stage of the SM
SA	Simulated annealing
SM	Solution method
SRT	Solver runtime
STO	Reservoir-based hydro power plant
TSCE	Total system cost error
TSO	Transmission system operator
TYNDP	Ten-Year Network Development Plan
UCED	Unit Commitment and Economic Dispatch
UK	United Kingdom
UNFCCC	United Nations Framework Convention on Climate Change
USA	United States of America
VOM	Variable operation and maintenance cost
W_{off}/W_{on}	Offshore/Onshore wind

List of Symbols

Indices

g	dispatchable generation technology index
l	location, site
i	transmission corridors index
n	bus, node
r	RES generation technology index
s	storage technology index
t	time index
w	time window
τ	time slice index

Sets

$\mathcal{C}$	set of network cycles
$\mathcal{D}$	set of technologies providing firm (i.e., non-variable) capacity
$\mathcal{G}$	set of dispatchable generation technologies
$\mathcal{I}$	set of transmission corridors, $\mathcal{C} \subset \mathcal{N}_B \times \mathcal{N}_B$
$\mathcal{I}_n^+, \mathcal{I}_n^-$	set of inbound and outbound links into node n, respectively
$\mathcal{I}^{ac}$	set of non-controllable (i.e., AC) transmission assets, with $\mathcal{I}^{ac} \subseteq \mathcal{I}$
$\mathcal{J}_{\mathrm{w}}^L$	subset of critical locations within L during time window w, with $\lvert\mathcal{J}_{\mathrm{w}}^L\rvert = N_{\mathrm{w}}^L$
l^*	set of candidate sites whose removal from $\mathcal{L}$ minimises the difference in criticality indicators
$\mathcal{L}$	set of candidate sites
$\mathcal{L}_0$	set of RES sites with legacy capacity
$\mathcal{L}_n$	set of candidate sites in subregion n, with $\cup_{n \in \mathcal{N}_B} = \mathcal{L}$
L	subset of locations, with $L \subseteq \mathcal{L}$
L_n	set of (candidate) RES sites at partition $n \in \mathcal{N}_B$
$L_n^{\mathtt{SITE}}$	set of RES sites selected at partition $n \in \mathcal{N}_B$ by the siting algorithm
L_n^r	subset of RES sites using technology $r \in \mathcal{R}$ at partition $n \in \mathcal{N}_B$
$L_r^{\mathtt{SITE}}$	subset of RES sites using technology $r \in \mathcal{R}$ and selected by the siting algorithm

L_r^{FLP}	subset of RES sites using technology $r \in \mathcal{R}$ and selected by the full LP
$\mathcal{N}_B$	subregions considered for deployment, with $\lvert\mathcal{N}_B\rvert = B$
$\mathcal{R}$	set of RES technologies not properly sited
$\mathcal{S}$	set of storage technologies
$\mathcal{T}$	set of time indices, with $\lvert\mathcal{T}\rvert = T$
$\mathcal{T}_{\mathrm{w}}$	set of time indices comprising time window w, with $\lvert\mathcal{T}_{\mathrm{w}}\rvert = \delta$
$\mathcal{T}_\tau$	time slice
$\mathcal{W}$	set of time windows, with $\lvert\mathcal{W}\rvert = W$
$\mathcal{W}_C^L$	set of critical time windows
$\mathcal{Z}$	set of integers denoting wind speed regimes

Time Series

$\mathbf{s}_l$	renewable resource at location l, with element s_{lt} at time step t
$\boldsymbol{\pi}_l$	capacity factor at location l, with element π_{lt} at time step t

Functions

$\mathfrak{c}^L$, $\mathfrak{f}_C(L)$	criticality indicator associated with locations set L
$\mathfrak{g}_{ij}$	function mapping pairs of wind regime labels to binary digits
$\mathfrak{h}_l$	transfer function returning per-unit capacity factors from resource time series $\mathbf{s}_l$
$\mathfrak{q}_l$	mapping evaluating resource quality at location l
$\mathfrak{z}$	function mapping wind signals to wind regimes $\in \mathcal{Z}$
$\tilde{\boldsymbol{\pi}}_l$	average capacity factor at site l

Parameters

c	global criticality threshold [$\in \mathbb{N}$]
k_n	number of sites to be selected in region $n \in \mathcal{N}_B$, with $\sum_n k_n = k$ [$\in \mathbb{N}$]
lat, lon	latitude and longitude, respectively [deg]
r	neighbourhood radius in the SA algorithm [$\in \mathbb{N}$]
v_{min}^{α}, v_{max}^{α}	wind speed thresholds [m/s]
v_{cut}^{out}	cut-out wind speed [m/s]
$v_t^{j(i)}$, $v_t^{k(i)}$	voltage angle at source and sink bus of line $i \in \mathcal{I}^{ac}$, respectively [p.u.]
v_t^{ref}	reference voltage angle [p.u.]
A_{nl}	matrix entry indicating whether location l belongs to subregion $\mathcal{L}_n$ [$\in 0, 1$]

C_{ic}	matrix entry indicating whether line i is element of cycle c [$\in \{-1, 0, 1\}$]
D_{lw}	matrix entry indicating whether location l is critical during window w [$\in 0, 1$]
I	number of iterations performed by the SA algorithm [$\in \mathbb{N}$]
N	number of neighbouring solutions drawn by the SA algorithm at each iteration [$\in \mathbb{N}$]
$M_{ij}^{(l_1,l_2)}$	matrix of complementarity factors between pair of sites (l_1, l_2), with entries m_{ij}
$T(i)$	temperature schedule for the SA algorithm
x_i	series reactance of line $i \in \mathcal{I}^{ac}$ [Ω]
$\alpha_{l\mathrm{w}}$	local criticality threshold at location l and time step t [$\in \mathbb{R}_+$]
β	accuracy score of the siting algorithm [%]
δ	time window length [$\in \mathbb{N}$]
$\delta\tau$	time slice length [$\in \mathbb{N}$]
δ_g^{mdt}	minimum down time of generator $g \in \mathcal{G}$ [$\in \mathbb{N}$]
δ_g^{mut}	minimum up time of generator $g \in \mathcal{G}$ [$\in \mathbb{N}$]
$\tilde{\Delta}$	objective difference between solutions in the SA algorithm
Δ_g^+	upward ramp-rate of dispatchable generation technology $g \in \mathcal{G}$ [MW/h]
Δ_g^-	downward ramp-rate of dispatchable generation technology $g \in \mathcal{G}$ [MW/h]
ϵ_{site}	reference site surface utilization factor [%]
η_g	thermal efficiency of generation technology $g \in \mathcal{G}$ [%]
η_s^C	charging efficiency of storage technology $s \in \mathcal{S}$ [%]
η_s^D	discharging efficiency of storage technology $s \in \mathcal{S}$ [%]
η_s^{SD}	self-discharging efficiency of storage technology $s \in \mathcal{S}$ [%]
γ_r	reduction factor for RES technology $r \in \mathcal{R}$ [%]
$\bar{\kappa}_l$	technical potential of a given RES technology at location l [$\in \mathbb{R}_+$]
$\bar{\kappa}_i$	maximum allowable installed capacity of line $c \in \mathcal{C}$ [$\in \mathbb{R}_+$]
$\bar{\kappa}_{nx}$	maximum allowable installed capacity of technology $x \in \{\mathcal{G}, \mathcal{R}, \mathcal{S}\}$ at node $n \in \mathcal{N}_B$ [$\in \mathbb{R}_+$]
κ_n	target installed capacity in region $n \in \mathcal{N}_B$ [GW]
$\underline{\kappa}_l$	legacy capacity of a given RES technology at location l [$\in \mathbb{R}_+$]
$\underline{\kappa}_i$	legacy capacity for transmission line $i \in \mathcal{I}$ [$\in \mathbb{R}_+$]
$\underline{\kappa}_{nx}$	legacy capacity for technology $x \in \{\mathcal{G}, \mathcal{R}, \mathcal{S}\}$ at node $n \in \mathcal{N}_B$ [$\in \mathbb{R}_+$]
λ_{nt}	electricity demand at node n and time t [MW]
$\bar{\lambda}_w$	system-wide electricity demand during time window w [MW]
$\hat{\lambda}_n$	peak electricity demand at node n [MW]
μ_j	minimum required operational level of technology $j \in \{\mathcal{G}, \mathcal{S}\}$ [MW]
$\nu_g^{CO_2}$	specific CO_2 emissions associated with generation technology $g \in \mathcal{G}$ [kt_{CO_2}/MWh]
Π_l	equivalent capacity credit of RES site $l \in \mathcal{L}$ [-]
Π_{nr}	equivalent capacity credit of RES technology $r \in \mathcal{R}$ at node $n \in \mathcal{N}_B$ [-]

ρ_r power density of RES technology $r \in \mathcal{R}$ [MW/km^2]
ϕ_s charge-to-discharge ratio of storage technology $s \in \mathcal{S}$ [-]
ϕ_s^{EP} energy-to-power ratio of storage technology $s \in \mathcal{S}$ [-]
Φ_n planning reserve margin at node $n \in \mathcal{N}_B$ [%]
θ^{ens} economic penalty for demand curtailment [€/MWh]
θ_f^l FOM cost of RES site $l \in \{\mathcal{L}\}$ [€/MW $\times$ year]
θ_v^l VOM cost of RES site $l \in \{\mathcal{L}\}$ [€/MWh]
θ_f^j FOM cost of technology $j \in \{\mathcal{G}, \mathcal{R}, \mathcal{S}, \mathcal{I}\}$ [€/MW $\times$ year]
θ_v^j VOM cost of technology $j \in \{\mathcal{G}, \mathcal{R}, \mathcal{S}, \mathcal{I}\}$ [€/MWh]
θ_f^l FOM cost of RES site $l \in \{\mathcal{L}\}$ [€/MW $\times$ year]
θ_v^l VOM cost of RES site $l \in \{\mathcal{L}\}$ [€/MWh]
θ_{SU}^g start-up cost of generator $g \in \{\mathcal{G}\}$ [€/start-up]
θ_{SD}^g shut-down cost of generator $g \in \{\mathcal{G}\}$ [€/start-up]
θ_{ramp}^g ramping cost of generator $g \in \{\mathcal{G}\}$ [€/MWh]
Ψ^{CO_2} system-wide CO_2 budget [Mt]
σ_{site} reference site surface area [km^2]
ς scalar representing the share of yearly demand covered by the sited RES technologies [-]
ω_t weight of each operating condition $t \in \mathcal{T}$ in the objective function and CO_2 emissions [h]
ω_s weight of each operating condition $t \in \mathcal{T}$ in the operation of storage units [h]
ξ_τ^n RES feed-in target in region n during time slice τ [$\in \mathbb{R}_+$]
ζ^l annualized investment cost at RES site $l \in \{\mathcal{L}\}$ [€/MW]
ζ^j annualized investment cost of technology $j \in \{\mathcal{G}, \mathcal{R}, \mathcal{S}, \mathcal{I}\}$ [€/MW]
ζ_S^s annualized investment cost of the energy component of storage tech. $s \in \{\mathcal{S}\}$ [€/MW]

Optimisation Variables

e_{nst} state of charge of storage technology $s \in \mathcal{S}$, at node $n \in \mathcal{N}_B$ and time $t \in \mathcal{T}$ [$\in \mathbb{R}_+$]
K_l installed capacity of RES site $l \in \mathcal{L}$ [$\in \mathbb{R}_+$]
K_i installed capacity of transmission line $i \in \mathcal{I}$ [$\in \mathbb{R}_+$]
K_{nj} installed capacity of of generation technology $j \in \{\mathcal{G}, \mathcal{R}\}$ at node $n \in \mathcal{N}_B$ [$\in \mathbb{R}_+$]
K_{ns} power component capacity of storage technology $s \in \mathcal{S}$ [$\in \mathbb{R}_+$]
p_{nst}^C charging flow of storage technology $s \in \mathcal{S}$, at node $n \in \mathcal{N}_B$ and time $t \in \mathcal{T}$ [$\in \mathbb{R}_+$]
p_{nst}^D discharging flow of storage technology $s \in \mathcal{S}$, at node $n \in \mathcal{N}_B$ and time $t \in \mathcal{T}$ [$\in \mathbb{R}_+$]
p_{it} power flow over line $i \in \mathcal{I}$ at time $t \in \mathcal{T}$ [$\in \mathbb{R}$]
p_{nt}^{ens} unserved demand at node $n \in \mathcal{N}_B$ and time $t \in \mathcal{T}$ [$\in \mathbb{R}_+$]
p_{njt} feed-in of generation technology $j \in \{\mathcal{G}, \mathcal{R}\}$, at node $n \in \mathcal{N}_B$ and time $t \in \mathcal{T}$ [$\in \mathbb{R}_+$]

p^{ramp}_{ngt}	first difference of feed-in of generator $g \in \mathcal{G}$, at bus $n \in \mathcal{N}_B$ and time $t \in \mathcal{T}$ $[\in \mathbb{R}]$
p_{lt}	feed-in of RES site $l \in L_n$ at time $t \in \mathcal{T}$ $[\in \mathbb{R}_+]$
$q^{CO_2}_{ngt}$	CO_2 emissions of generation tech. $g \in \mathcal{G}$ at node $n \in \mathcal{N}_B$ and time $t \in \mathcal{T}$ [kt]
S_{ns}	energy component capacity of storage technology $s \in \mathcal{S}$ $[\in \mathbb{R}_+]$
u_{ngt}	commitment variable for dispatchable generator $g \in \mathcal{G}$, at bus $n \in \mathcal{N}_B$ and time $t \in \mathcal{T}$ $[\in 0, 1]$
u^{SD}_{ngt}	shut-down decision variable for generator $g \in \mathcal{G}$, at bus $n \in \mathcal{N}_B$ and time $t \in \mathcal{T}$ $[\in 0, 1]$
u^{SU}_{ngt}	start-up decision variable for generator $g \in \mathcal{G}$, at bus $n \in \mathcal{N}_B$ and time $t \in \mathcal{T}$ $[\in 0, 1]$
x_l	variable used to indicate whether location l is selected for deployment $[\in 0, 1]$
y_w	variable used to indicate whether window w is critical $[\in 0, 1]$

Chapter 1

Introduction

First, this chapter frames the research questions pursued in the thesis in the context of the ongoing climate crisis. It starts by discussing the role of power systems in the decarbonisation efforts of societies before addressing the need for planning tools required to understand this process in its full complexity. The concept of spatiotemporal renewable resource complementarity is then introduced in the context of renewable generation asset siting decisions. Then, the contributions of the thesis are briefly stated and a detailed description of the structure of the manuscript follows. Finally, the list of peer-reviewed publications forming the core of the current manuscript is provided.

1.1 Context and Motivation

In times characterized by the socio-economic effects of a coronavirus pandemic, the world appears to be on the brink of another crisis that affects the climate system as a whole (e.g., the atmosphere, the oceans, the land masses or the biosphere, as well as the interaction between them) and has long been the subject of a fierce debate on whether it has anthropogenic roots or not. In this regard, the Sixth Assessment Report (AR6) of the Intergovernmental Panel on Climate Change (IPCC) recently concluded that "it is unequivocal that human influence has warmed the atmosphere, ocean and land" [1].

The warming of these climate elements is a direct consequence of the fact that the natural carbon sinks (e.g., oceans, forestry) could not keep up with the emissions associated with the ever-increasing use of fossil fuels since the start of the industrial revolution in the 1850s. This imbalance has steadily led to an accumulation of greenhouse gases (GHG, i.e., mainly CO_2, CH_4 and N_2O) in the atmosphere which, in turn, started the process of climate system warming. In the same report [1], the IPCC quantified some of the effects of this compounded stock of GHG. On average, the global surface temperature in the first two decades of this century has been 1 °C higher than at the end of the 1800s. In addition, more frequent and extreme heat waves, heavy precipitation events, as well as agricultural and ecological droughts are all side-effects (with high confidence in the anthropogenic factor) of climate system warming. All these effects are expected to persist over the current century, given the inertia of the climate system. Nonetheless, in order to mitigate the damage inflicted upon it, corrective measures (i.e., limiting GHG emissions) are necessary across all economic sectors and with a global reach.

The multi-lateral agreement at the 21st Conference of Parties (COP21) of the UNFCCC marked an unprecedented milestone in the fight against climate change [2]. This agreement came as a hybrid of legally binding and non-binding provisions for tackling the climate crisis and was adopted by 196 countries with the chief goal of limiting the warming of the global climate system by 2100 to "well below 2 °C" compared to pre-industrial levels. Out of the five scenarios proposed in the AR6 in order to assess the climate response to corrective measures throughout the rest of the century, two of these were found to limit the increase of the global surface temperature in line with the COP21 targets. In both these scenarios, yearly GHG emission rates are curbed after 2025, net-zero CO_2 emissions are reached around or shortly after 2050 and negative CO_2 emissions are required for the remainder of the century.

Reaching net-zero energy systems in a matter of decades is going to be a daunting task. The International Energy Agency (IEA) recently commented on the implications of such an endeavour in their "Net-Zero by 2050" report [3]. This study clearly states that "the path to net-zero emissions is narrow" and that it requires

swift action on multiple levels, from the deployment of renewable energy technologies (e.g., wind, solar photovoltaics), to the electrification of energy-intensive and currently fossil-based sectors (e.g., transportation), the development of cost-efficient storage technologies or the advent of carbon-free fuels (e.g., hydrogen) and the transition towards more efficient energy utilization in the residential and commercial sectors. The "World Energy Transitions Outlook" study of the International Renewable Energy Agency (IRENA) doubles down on this idea and emphasizes the fact that current national and regional climate pledges "do no more than stabilise global emissions" [4]. It also draws attention to the critical importance of limiting investments in the oil and gas industries, phasing out fossil fuel subsidies across sectors (from coal-based power generation to aviation fuels) and being pragmatic with respect to the role of carbon capture technologies in the decarbonisation of energy systems. Similar pathways are envisioned by stakeholders even at regional levels. The "Net-Zero America" study of the Andlinger Center for Energy and the Environment at Princeton University concludes that curbing GHG emissions in the USA requires "large-scale mobilization of capital, policy and societal commitment" [5]. The authors suggest that the transition towards a net-zero economy relies on extensive efforts in six directions, namely, electrification and end-use energy efficiency, investment in power generation and transmission capacity, adoption of zero-carbon fuels and feedstocks, CO_2 capture and utilization, reduced emissions of GHGs other than CO_2 and enhancing the natural carbon sinks. Similarly, the "14^{th} Domestic Five-Year-Plan" report of the fastest growing and second largest economy in the world (China) envisions a series of measures to achieve carbon neutrality in its economy by 2060 [6]. Among others, halting any new coal-based power plant project, accelerating the development of wind-, solar- or hydro-based projects, as well as incorporating a carbon pricing system by 2030 when domestic CO_2 would have peaked are considered [7]. At European level, the 2019 "Clean Energy for all Europeans" [8] and the 2021 "European Green Deal" [9] packages gather a set of policy initiatives paving the way towards the implementation of a long-term climate strategy of the European Union (EU) aiming at carbon-neutrality by 2050. The actions suggested in these packages span across multiple economic sectors, from energy transformation to industry, transport or agriculture and are the cornerstone of a recently drafted European Climate Law supposed to safeguard their implementation towards 2050 and beyond.

1.1.1 The Role of Power Systems in the Decarbonisation of Economies

One of the common denominators across all these studies [3]–[5], [7], [9] is the fact that power and heat generation have to be at the forefront of decarbonisation efforts. According to the 15^{th} Special Report of the IPCC [10], electricity and heat production was the economic sector with the highest contribution to the global GHG emissions in 2010, with a share of 25%. This is not particularly surprising considering that coal and natural gas were, the same year, ranked as the first and third

sources of electricity production worldwide, with 40.3% and 22.5% shares, respectively [11]. However, over the following ten years alone, electricity generation from renewable sources (RES) has gained substantial ground. While RES were covering a share of 20% of total electricity generation in 2010, ten years later they were supplying 29% (in addition to the 10% covered by other low-carbon generation, such as nuclear power plants) [3]. This was made possible mainly via a swift adoption of wind and solar photovoltaics (PV). More specifically, the capacity of the former technology went from 180 GW to 690 GW between 2010 and 2020, while an astounding 17-fold uptake in solar PV capacity (40 GW to 710 GW) happened between the same two years [12]. Nonetheless, according to the "Net-Zero 2050" report of the IEA, such deployment rates should be consistently maintained over the next three decades to stand a chance of meeting the climate neutrality targets in due time [3]. That is, while global wind and solar PV additions in 2020 represented 114 GW and 134 GW, respectively, they should reach 350 GW and 630 GW, respectively, by mid-century. Such deployment efforts would enable 88% of the electricity generation to be supplied by RES by 2050, in addition to 43% of residential heating needs, 35% of industrial heat requirements and 8% of road transport energy needs. Practically, power systems would transition from the economic sector with the biggest share of GHG emissions to one that relies entirely on low-carbon generation technologies.

A key aspect to consider when designing such systems is that, as stated in [13], the power sector "not only contributes to climate change but is also vulnerable to climate change". This vulnerability of power systems against the various effects of the climate crisis has recently been showcased in Africa (when Cyclone Idai forced the South-African Transmission System Operator (TSO) to begin shedding load) [14], Texas (where a recent cold spell caused over 30 GW of dispatchable capacity to go offline, which resulted in massive load shedding across the state) [15] or, more recently, Northwestern Europe (where floods caused several substations to trip, thus leaving thousands without electricity for sustained periods of time) [16]. Thus, with the inevitable advent of weather-driven generation technologies (e.g., wind or solar PV, among others), the vulnerability of power systems to climate change and its effects becomes a relevant issue to consider when planning the future energy systems [17].

1.1.2 Centralised versus Distributed Power System Development

The development of power systems has historically happened in a centralised fashion, yet more recently the distributed generation paradigm has started to gain ground and play a crucial role in the context of their decarbonisation. On the one hand, the *centralised* development paradigm refers to the production of electricity through large-scale generation facilities connected to high-voltage transmission lines and usually located far from end-consumers. This paradigm has mainly been driven

by i) the economies of scale and the potential for efficiency gains in thermal generation units (e.g., coal, nuclear or gas-fired power plants which could be scaled up while decreasing the cost of producing electricity), ii) the low operational costs of transmission technologies and iii) the necessity of locating polluting (e.g., coal-based) facilities far away from populated areas. It is worth noting that, even though this paradigm relied extensively on the development of large-scale thermal or hydro generation facilities, more recent offshore wind farms or gigawatt-scale solar PV or onshore wind parks still constitute centralised generation facilities.

On the other hand, the *distributed* development paradigm refers to the generation of electricity via a series of technologies located in the vicinity of the place where it is consumed. These technologies include, e.g., solar PV panels, combined heat and power units, fuel cells or Diesel-fuelled back-up generators, and can serve anything from a single home to large industrial or residential facilities. In the latter case, distributed generation units are usually part of a microgrid (operating in island mode or connected to the distribution system), as well. The drivers behind the distributed development paradigm include, among others, i) the possibility of energy access in areas where the establishment of centralised facilities and transmission infrastructure is not practical, ii) the potential of a more reliable energy supply, as it enables consumers to hedge against network outages or iii) the provision of an alternative to distribution network expansion and the sense of energy independence and economic hedging it provides to end-customers.

1.1.3 The Relevance of Planning Tools in Decarbonisation Efforts

Regardless of whether the development of the power system occurs in a centralised or distributed fashion, the process of power (or, more generally, energy) systems planning involves a complex blend of technical, economic and policy considerations and often times drives the development course of the underlying system for several decades. As such, mathematical models have been developed in order to assist stakeholders in the process and inform them with respect to the benefits and risks of certain planning decisions or development pathways [18]. In time, these models have evolved into powerful tools for the design, analysis and implementation of energy system decarbonisation policies. Such models are typically referred to as *expansion planning models* and usually focus on a specific subset of power system assets, e.g., generation technologies (via *generation expansion planning* [19]) or transmission infrastructure (via *transmission expansion planning* [20]). Another approach (and the approach followed in this thesis) tackles the planning of power systems by simultaneously accounting for multiple classes of power system assets, e.g., generation, transmission or storage technologies [21], in a distinct class of problems that will be referred to as *capacity expansion planning* problems (or frameworks), or CEPs. It should be noted that the *planning* in CEP refers to investment decisions in the

long term and not to the scheduling of units on shorter time frames, e.g., day- or week-ahead.

In broad terms, the capacity expansion planning (CEP) problem provides information about which technologies (and in which quantities) are necessary to supply a given demand under certain technical, economic or policy constraints. This problem is formulated as an optimization problem that can have a monetary objective (e.g., cost minimization or profit maximization) or can seek to optimize some non-monetary indicator (e.g., minimizing CO_2 emissions or the installed capacity of a given technology). Its constraints model i) the physical processes governing the operation of the system (e.g., power flows in transmission lines), ii) the technical limits of certain technologies (e.g., ramp rates of dispatchable generation units), as well as iii) potential economic or policy considerations (e.g., monetary or emissions budgets). Depending on how accurate the representation of these modelling aspects is, the CEP problem can be expressed through a wide range of formulations, e.g., from simplified continuous linear formulations preserving the basic features of the system (and often times the most relevant features in a planning context) to non-convex non-linear formulations emulating as accurately as possible the components of the system, as well as their dynamics and interaction [19], [20]. With respect to the objective of the underlying investment decisions, the CEP problems are usually classified in two categories. On the one hand, the *central planner* approach seeks to maximize social welfare resulting from a given (set of) investment decision(s). In this class of problems, the central planner is an entity assumed to control the planning and operation of all power system assets (e.g., transmission, generation, storage, etc.). On the other hand, the *decentralised* approach seeks to maximize profits of market agents (i.e., producers, consumers) in a competitive environment overseen by an entity in charge of controlling the market, i.e., the market operator [22]. The CEP problems proposed and leveraged in this thesis are cast as continuous linear programs and follow the central planner approach.

Throughout the literature, there exists plenty of tools implementing CEP problems and whose implementations are at different stages of development. A brief summary of such tools is provided in the following. A familiar name in the industry is The Integrated MARKAL EFOM Model (TIMES) developed by the IEA [23], which is implemented in GAMS and comes with a GNU v3 license and applications covering a wide range (from global to local) of spatial scales [24]. In addition, the Balmorel framework (also implemented in GAMS and) published under an ISC license [25] has long been used for planning of energy systems over long temporal horizons. The tool has been used for assessments in Central America [26] or Europe [27], [28], among others. Similarly, the OSeMOSYS framework [29], implemented in GNU Mathprog and released under a Apache 2.0 license, has been used for over a decade for long-term planning studies at European [30] and even global scales [31].

More recently, the Python-based PyPSA framework was released as a toolbox focusing on long-term CEP problems with high spatial and temporal resolutions [32]. It comes with an MIT license and was leveraged in multiple large-scale applications in Europe [33], [34], China [35], Africa [36] or India [37]. PyPSA is also the modelling framework on top of which the contributions of this thesis are built. Then, Calliope also comes as a Python-based open-source framework for planning energy systems with high spatial and temporal resolutions [38]. It is released under an Apache 2.0 license and has been used for large-scale studies in Europe [39], Africa [40] or even at district level [41]. Furthermore, GenX is a Julia-based CEP framework recently made available under a GNU v2 license [42], with case studies in the US [5] and Europe [43]. More recently, the REISE framework, implemented in Julia and released under a MIT license [44] has also received a great deal of attention with a US-focused case study [45]. The proposed list of selected tools is by no means exhaustive, yet it contains frameworks that meet the following criteria: i) they are provided with open-source licenses, ii) they are relatively mature in their development timeline (i.e., peer-reviewed studies using them are available) and iii) they are developed mainly for planning purposes (as opposed to frameworks that are mainly used for operational studies, e.g., Dispa-SET [46] or PowerModels.jl [47]). For a more comprehensive list of such frameworks, the reader is directed to the work of Ringkjøb et al [48].

1.1.4 Siting of Renewable Generation Assets in Planning Studies

The relatively recent uptake of RES in power systems across the world [12] has rendered their planning an increasingly complex task. The chief reason behind this issue is the variability of the underlying resources (e.g., wind speed or direction, solar irradiance) over both short (i.e., minutes to hours) [49] and long (years to decades) [50] time frames. This inherent variability has costly consequences on the design and operation of the system (e.g., the activation of fast-responding dispatchable generation in times of renewable resource scarcity in order to match the electricity demand) and has prompted researchers to acknowledge the critical importance of spatially- and temporally-resolved models in long-term planning studies. In one of the first article on this topic, Pfenninger et al. conclude that "resolving time and space becomes important to accurately answer questions about the energy system" [51]. In addition, Wohland et al. state that "improved spatial planning [...] offers multiple options to mitigate [...] renewable generation variability" [50]. However, the obvious issue arising with spatially- and temporally-resolved models is the resulting problem size which, when it doesn't translate into instances that are intractable altogether, leads to impractical solving times [52].

In consequence, modellers have resorted to various techniques that enabled them to reduce the size of resulting problems. From a temporal standpoint, plenty of research has been conducted to develop time series reduction techniques able to

identify subsets of data containing the most relevant features from a power system planning standpoint [53]. Less work has been conducted on spatial dimension reduction, though, even though the authors of [51] suggest that the "spatial detail may be critically important for renewables: their economic potential and generation costs depend greatly on their location". Nevertheless, expansion planning studies for systems with high shares of RES have been usually tackled by spatially aggregating renewable resources at rather coarse resolutions, e.g., at country-level (that is, the wind or solar resource is represented via one single time series for an entire country). Examples of such studies abound in the literature and they all suffer from the same drawback, as renewable resources cannot be accurately modelled in countries or regions with otherwise diverse RES regimes across their territory, such as Germany or France in [54], [55] or Europe or any other region in [56]. The impact of this drawback on the design of power systems and the incurred costs has been assessed in recent years in a series of publications.

For instance, Krishnan et al. [57] revealed that representing RES via one time series per US state (i.e., 48 profiles per RES technology, as the study focuses on the contiguous territory) leads to sub-optimal results, with overall less renewable generation capacity and more conventional generation capacity compared to the set-up where RES are modelled via the native spatial resolution of the underlying model (i.e., 356 profiles for onshore wind and 134 profiles for solar PV, respectively). Another work [58] investigated the same issue, this time at a spatial scope covering the state of California. They conclude that using highly-granular RES data (in this case, the locations of individual sites were determined based on a previous screening step) leads to 10% cost savings and 20% curtailment mitigation in systems with increased RES penetration levels compared to set-ups where RES assets are modelled at a county level. Then, a similar study performed by Hörsch and Brown also reveals up to 10% cost differences and interesting wind-solar trade-offs between model instances based on the European power system where RES are modelled via 37 (i.e., one profile per country) or 362 profiles [59]. More recently, a study by Frysztacki et al. [60] further supports these findings with a study focusing on the European power system. They confirm the findings of [57], [59] and point out that modelling RES via 1024 different profiles leads to 10.5% lower system costs and significant installed capacity differences compared to more simplified set-ups using only 37 distinct profiles per renewable resource. Thus, all these studies point out the value of spatially-resolved RES modelling as a key feature in achieving proper siting of such assets in expansion planning frameworks.

1.1.5 On the Spatiotemporal Complementarity of Renewable Resources

A conventional method for siting RES assets considers resource quality (i.e., the average capacity factor or the expected power output) as the chief criterion once land

eligibility constraints are met. This siting strategy has been a mainstay in the industry over the last decades, as can be observed for existing wind [61] or solar PV [62] developments. In addition, in the context of the recent European Commission plan of developing up to 450 GW of offshore wind across European Seas [63], the lion's share of this capacity is expected to be developed in a relatively limited area within the North Sea [64]. Such deployment strategies are expected to lead to complex integration issues given the variable nature of RES over both short- and long-term time frames. A familiar example of such an issue is the occurrence of sustained periods (i.e., days to weeks) of system-wide renewable generation shortage, also dubbed "dunkelflaute" [65]. With RES assets clustered in areas with similar weather regimes, a "dunkelflaute" event could easily render the entire power system dependent on fossil fuel-based generation and thus curb its decarbonisation attempts. In the opposite situation, during times with high RES-based generation levels, overproduction of these units needs to be shifted in time in order to avoid curtailment and ensure their economic profitability.

Several solutions have been proposed to alleviate these issues and foster the large-scale integration of RES units, e.g., investment in storage assets [66] or developing demand response capabilities [67]. An alternative to these solutions proposes to spatially distribute RES assets and take advantage of the different weather regimes available such that the variability of the aggregate output, as well as the residual demand are minimised [68]. This idea, empirically observed in the operation of power systems as a "smoothing effect" [69], has led to the concept and investigation of (spatiotemporal) complementarity of renewable resources [70]. It is worth specifying clearly at this stage that, throughout this thesis, locations are considered complementary if they experience simultaneous low-production events very rarely.

1.2 Thesis Structure and Contributions

From here on, the manuscript is structured as follows.

The topic of renewable resource complementarity is first discussed in Chapter 2. In this chapter, a **first application-related contribution** of this thesis is represented by a comparison of wind regimes in Western Europe and Greenland, respectively. The analysis is conducted by leveraging a regional atmospheric model with proven results in polar conditions and reveals that Southern Greenland local climate patterns exhibit specific characteristics that facilitate extensive wind generation levels at times of resource scarcity in Europe.

The **first methodological contribution** of this thesis is showcased in Chapter 3, where the critical time windows framework is introduced and then leveraged to site RES assets based on resource complementarity criteria. The usefulness of this method in identifying deployment patterns that maximise complementarity among

RES sites is shown in a case study with roughly 300 candidate wind locations in continental Western Europe and Southern Greenland and ten years of reanalysis data with hourly resolution. Deployment patterns maximising complementarity with and without deployment constraints are proposed and analysed before a comparison with more conventional siting strategies opting for the candidate locations with the highest average capacity factors is conducted.

Then, Chapter 4 begins by defining the **second application-related contribution** of the thesis, i.e., evaluating the impact of RES siting strategies on the design and economics of power systems. To this end, a two-stage method is developed as a **second methodological contribution** of the current work. In the first stage, a highly-granular siting problem is solved in order to identify a suitable subset of candidate sites where RES power plants could be deployed. Then, in the second stage, the subset of locations selected in the first stage is passed to a capacity expansion planning framework that sizes the power generation, transmission and storage assets that should be deployed in order to satisfy pre-specified electricity demand levels at minimum cost subject to technical and policy constraints. The proposed case study makes for a **third application-related contribution** of this thesis, as it investigates siting options and their associated impact on planning decisions for the large-scale deployment of offshore wind throughout European Seas in accordance with recent European Commission guidelines.

Chapter 5 builds upon the investigation proposed in Chapter 4 and provides a **fourth application-related contribution**. More specifically, a third stage formulated as a mixed-integer linear program accounting for unit commitment costs and constraints of relevant power generation assets is hereby leveraged to assess the impact of siting outcomes on the short-term operation of power systems. In addition, a set of modelling aspects leveraged in Chapter 4 are refined. For example, multiple renewable sources are considered in the siting stage (onshore *and* offshore wind), while a higher-resolution network representation, as well as an enhanced modelling of power flows in transmission lines are leveraged in the sizing stage.

Chapter 6 proposes a method to reduce the spatial dimension and decrease the computational requirements of capacity expansion planning problems while preserving a detailed representation of RES assets. This is presented as the **third methodological contribution** of the thesis and is achieved by leveraging a heuristic that can be described as follows. First, a linear program is used to screen a set of candidate sites and identify sites that have little impact on optimal system design, which are then discarded. Then, information about the remaining sites is used as input data in a capacity expansion planning framework that determines the installed capacities of generation, storage and transmission assets leading to a minimum-cost system configuration. The proposed method makes it possible to reduce the size of the capacity expansion planning problem, and therefore enables memory and computation time savings.

Chapter 7 concludes the manuscript and proposes future work avenues. A common **software-related contribution** across all chapters of this thesis is represented by the development of open-data, open-source tools for power system planning and operations purposes. These tools include a comprehensive data-preprocessing package [71], a module comprising the integer programming complementarity-based siting formulation, as well as a set of solution methods to tackle the problem [72] and a set of methods required for their integration in expansion planning studies [73]. Then, the curation and processing work leading to the datasets summarized in Appendix A represent **data-related contribution** fostering the analysis of realistic Europe-centred case studies across Chapters 4, 5 and 6 of this manuscript. Finally, the work gathered in Appendix B constitutes an additional **modelling contribution**, as it enables a highly-granular representation of the European hydro units within power system expansion planning, as well as operations models.

1.3 List of Publications

The following peer-reviewed publications gather the contributions and define the structure of the thesis as stated in the previous sections:

- **David-Constantin Radu**, Mathias Berger, Raphaël Fonteneau, Simon Hardy, Xavier Fettweis, Marc Le Du, Patrick Panciatici, Lucian Balea, Damien Ernst, "Complementarity Assessment of South Greenland Katabatic Flows and West Europe Wind Regimes", Energy 175, 393-401, 2019, https://doi.org/10.1016/j.energy.2019.03.048
- Mathias Berger[1], **David-Constantin Radu**[1], Raphaël Fonteneau, Robin Henry, Mevludin Glavic, Xavier Fettweis, Marc Le Du, Patrick Panciatici, Lucian Balea, Damien Ernst, "Critical Time Windows for Renewable Resource Complementarity Assessment", Energy 198, 117308, 2020, https://doi.org/10.1016/j.energy.2020.117308
- **David-Constantin Radu**, Mathias Berger, Antoine Dubois, Raphaël Fonteneau, Hrvoje Pandžić, Yury Dvorkin, Quentin Louveaux, Damien Ernst, "Assessing the Impact of Offshore Wind Siting Strategies on the Design of the European Power System", Applied Energy 305, 117700, 2022, https://doi.org/10.1016/j.aplen.2021.117700
- **David-Constantin Radu**, Antoine Dubois, Mathias Berger, Damien Ernst, "Model Reduction in Capacity Expansion Planning Problems via Renewable Generation Site Selection," 2021 IEEE Madrid PowerTech, 2021, pp. 1-6, https://doi.org/10.1109/PowerTech46648.2021.9495027
- Mathias Berger, **David-Constantin Radu**, Damien Ernst, "On the role of resource complementarity in siting renewable power plants and its impact on

[1]Equally contributing authors.

power system design and economics", in "Complementarity of variable renewable energy sources", Jakub Jurasz & Alexandre Beluco (Eds.), ISBN: 978-0-323-85527-3, April 2022

In addition, the following peer-reviewed publications have been published during the course of the doctoral studies, yet they are not included in the current thesis:

- Mathias Berger, **David-Constantin Radu**, Raphaël Fonteneau, Thierry Deschuyteneer, Ghislain Detienne, Damien Ernst, "Centralised Planning of National Integrated Energy System with Power-to-Gas and Gas Storages", accepted in 11th Mediterranean Conference on Power Generation, Transmission, Distribution and Energy Conversion (Medpower2018), Dubrovnik, Croatia, 2018, https://doi.org/10.1049/cp.2018.1912

  This paper proposes an optimisation-based framework to tackle long-term centralised planning problems of integrated energy systems with bi-directional electricity-gas carriers coupling under various policy constraints. The framework is leveraged to gain insight into possible configurations of the future Belgian energy system, and identify the cost-optimal energy mix as well as short and long-term storage requirements to satisfy CO_2 emissions reduction targets. Results shed light on the economics of a transition to a low-carbon energy system and reveal the potential of power-to-gas and gas storage to help achieve ambitious emissions reduction goals.

- Mathias Berger, **David-Constantin Radu**, Raphaël Fonteneau, Thierry Deschuyteneer, Ghislain Detienne, Damien Ernst, "The Role of Power-to-Gas and Carbon Capture Technologies in Cross-Sector Decarbonisation Strategies", Electric Power Systems Research 180, 106039, 2020, https://doi.org/10.1016/j.epsr.2019.106039

  This paper proposes an optimisation-based framework to tackle long-term centralised planning problems of multi-sector, integrated energy systems including electricity, hydrogen, natural gas, synthetic methane and carbon dioxide. The model selects and sizes the set of power generation, energy conversion and storage as well as carbon capture technologies minimising the cost of supplying energy demand in the form of electricity, hydrogen, natural gas or synthetic methane across the power, heating, transportation and industry sectors whilst accounting for policy drivers, such as energy independence, carbon dioxide emissions reduction targets, or support schemes. The usefulness of the model is illustrated by a case study evaluating the potential of sector coupling via power-to-gas and carbon capture technologies to achieve deep decarbonisation targets in Belgium. Results indicate that power-to-gas can only play a minor supporting role in cross-sector decarbonisation strategies in Belgium, as electrolysis plants are deployed in moderate quantities whilst methanation plants do not appear in any studied scenario. However, given the limited renewable potential, post-combustion and direct air carbon capture technologies clearly play an enabling role in any decarbonisation strategy, but may also exacerbate the dependence on fossil fuels.

- Mathias Berger, **David-Constantin Radu**, Thierry Deschuyteneer, Ghislain Detienne, Aurore Richel, Damien Ernst, "Remote Renewable Hubs for Carbon-Neutral Synthetic Fuel Production", Frontiers in Energy Research 9:671279, 2021, https://doi.org/10.3389/fenrg.2021.671279

  This paper studies the economics of carbon-neutral synthetic fuel production from renewable electricity in remote areas where high-quality renewable resources are abundant. To this end, a graph-based optimisation modelling framework directly applicable to the strategic planning of remote renewable energy supply chains is proposed. More precisely, a hypergraph abstraction of planning problems is introduced, wherein nodes can be viewed as optimisation subproblems with their own parameters, variables, constraints and local objective. Nodes typically represent a subsystem such as a technology, a plant or a process. Hyperedges, on the other hand, express the connectivity between subsystems. The framework is leveraged to study the economics of carbon-neutral synthetic methane production from solar and wind energy in North Africa and its delivery to Northwestern European markets. The full supply chain is modelled in an integrated fashion, which makes it possible to accurately capture the interaction between various technologies on an hourly time scale. Results suggest that the cost of synthetic methane production and delivery would be slightly under 150 €/MWh *(higher heating value) by 2030 for a system supplying* 10 TWh *annually and relying on a combination of solar photovoltaic and wind power plants, assuming a uniform weighted average cost of capital of 7%. A comprehensive sensitivity analysis is also carried out in order to assess the impact of various techno-economic parameters and assumptions on synthetic methane cost, including the availability of wind power plants, the investment costs of electrolysis, methanation and direct air capture plants, their operational flexibility, the energy consumption of direct air capture plants, and financing costs. The most expensive configuration (around* 200 €/MWh*) relies on solar photovoltaic power plants alone, while the cheapest configuration (around* 88 €/MWh*) makes use of a combination of solar PV and wind power plants and is obtained when financing costs are set to zero.*

- Priyanka Shinde, Ioannis Boukas, **David-Constantin Radu**, Miguel Manuel de Villena, Mikael Amelin, "Analyzing Trade in Continuous Intra-Day Electricity Market: An Agent-Based Modeling Approach", Energies 14(13), 2021, https://doi.org/10.3390/en14133860

  In this paper, we propose an agent-based modelling framework to analyse the behaviour and the interactions between renewable energy sources, consumers and thermal power plants in the European Continuous Intra-day (CID) market. Additionally, we propose a novel adaptive trading strategy that can be used by the agents that participate in CID market. The agents learn how to adapt their behaviour according to the arrival of new information and how to react to changing market conditions by updating their willingness to trade. A comparative analysis was performed to study the behaviour of agents when they adopt the proposed strategy as opposed to other benchmark strategies.

The effects of unexpected outages and information asymmetry on the market evolution and the market liquidity were also investigated.

- Mathias Berger, **David-Constantin Radu**, Antoine Dubois, Hrvoje Pandžić, Yury Dvorkin, Quentin Louveaux, Damien Ernst, "Siting Renewable Power Generation Assets with Combinatorial Optimization", Optimization Letters, 2021, https://doi.org/10.1007/s11590-021-01795-0

  This paper studies the problem of siting renewable power generation assets using large amounts of climatological data while accounting for their spatiotemporal complementarity. The problem is cast as a combinatorial optimisation problem selecting a pre-specified number of sites so as to minimise the number of simultaneous low electricity production events that they experience relative to a pre-specified reference production level. It is shown that the resulting model is closely related to submodular optimisation and can be interpreted as generalising the well-known maximum coverage problem. Both deterministic and randomised algorithms are discussed, including greedy, local search and relaxation-based heuristics as well as combinations of these algorithms. The usefulness of the model and methods is illustrated by a realistic case study inspired by the problem of siting onshore wind power plants in Europe, resulting in instances featuring over ten thousand candidate locations and ten years of hourly-sampled meteorological data. The proposed solution methods are benchmarked against a state-of-the-art mixed-integer programming solver and several algorithms are found to consistently produce better solutions at a fraction of the computational cost. The physical nature of solutions provided by the model is also investigated, and all deployment patterns are found to be unable to supply a constant share of the electricity demand at all times. Finally, a cross-validation analysis shows that, except for an edge case, the model can successfully and reliably identify deployment patterns that perform well on previously unseen climatological data from historical data spanning a small number of weather years.

Chapter 2

Quantifying the Complementarity of Renewable Resources

One promising solution for decarbonising economies worldwide consists in harnessing high-quality variable renewable energy resources (RES, e.g., wind or solar irradiation) in remote locations and using transmission infrastructure to send the power towards end-users. In this context, the current chapter proposes a comparison of wind regimes in Western Europe and Greenland, respectively. By leveraging a regional atmospheric model (Modèle Atmosphérique Régional) with proven results in polar conditions, Southern Greenland local climate patterns are found to exhibit specific characteristics that facilitate extensive wind generation levels. In addition, a methodology to assess how connecting remote locations to major demand centres would benefit the latter from a resource availability standpoint is introduced and leveraged to reveal complementary wind generation potential in Greenland with respect to selected European sites.

This chapter is a reprint of *David-Constantin Radu, Mathias Berger, Raphaël Fonteneau, Simon Hardy, Xavier Fettweis, Marc Le Du, Patrick Panciatici, Lucian Balea, Damien Ernst, "Complementarity Assessment of South Greenland Katabatic Flows and West Europe Wind Regimes", Energy 175, 393-401, 2019,* https://doi.org/10.1016/j.energy.2019.03.048. Reprinted with permission from the publisher.

2.1 Introduction

A current trend in the power system community addresses renewable energy harvesting in remote, yet resource-rich locations and their subsequent integration via large-scale interconnections. In a future power system context defined by dominant RES generation and increased shares of electrical loads, linking separate power systems offers benefits on various operational levels. From a generation standpoint, one may see the potential of RES harnessing in resourceful sites and subsequent delivery to major load centres via adequate transmission links. In addition, the negative impact that high RES generation intermittency has on the operation of power systems could be reduced effectively through complementary production profiles originated from different resource patterns arising from time zone difference (on various latitudes) and the timing of seasons (across different longitudes). From a load perspective, exploiting shifted consumption patterns between regions induced by the geographical positioning of the consumers at different longitudes and latitudes has the potential to level out aggregated load profiles. These would, in turn, lead towards a less challenging operation of power systems, reduction of operational and planning costs, and greenhouse gas emission level mitigation.

Coupling distinct power systems from a country, to a regional and ultimately an intercontinental level would result in a globally interconnected electricity network [56]. This idea was first proposed in [74], where the authors envision RES technologies as crucial in meeting the ever-increasing electricity demand, with high-capacity interconnections being the backbone of the corresponding transmission infrastructure. The same article also describes various operational opportunities emerging from such a large-scale project and it highlights regulatory hurdles likely to arise in such a complex set-up. A more comprehensive, yet still conceptual view on the topic is provided in [75]. The book provides a more detailed assessment of the motivation behind the development of a global grid before mapping specific regions for energy harvesting and routes for long-haul interconnections, and finally discussing the technical innovation required for the successful deployment of this project. Also, an economic dispatch model is the subject of ongoing work for a CIGRE Working Group [56] that is investigating the technical feasibility of a global grid, as well as its economic competitiveness by assessing the trade-off between the cost of interconnectors and the benefits associated with remote RES harvesting.

The scope of this chapter is to assess the wind resource complementarity between two geographically adjacent macro-regions, namely, Europe and Greenland. Wind availability in the former is sometimes an issue that leads to increased utilization of balancing units (usually fossil fuel-based generators) and storage capabilities. In this regard, seasonal patterns generally show inferior resource availability during summer time [76], while winter conditions could also display wind resource scarcity coupled with usually low solar irradiation. A resource-rich and load-free region

such as Greenland has the potential to provide wind energy to European users in times of local scarcity, while mitigating the balancing and storage requirements.

For the remainder of the chapter, Section 2.2 documents previous works related to remote RES harvesting and resource potential assessment. Section 2.3 introduces the sources of wind data and briefly discusses local features of wind regimes in Greenland (i.e., katabatic winds) that are favourable for extensive RES generation. Locations for wind power generation to be investigated are selected in Section 2.5. Section 2.4 details the methodology proposed to study the resource complementarity before results of the Europe-Greenland case study are presented in Section 2.6. Finally, Section 2.7 concludes the chapter and proposes related future research directions.

2.2 Related Works

Harnessing RES in remote locations to supply major load centres is not a novel approach, as the available literature reveals. One of the first projects of this kind is the DESERTEC initiative [77], which studies the supply of Mediterranean countries by RES-abundant North African and Middle Eastern (MENA) territories. The project emphasizes the vast potential of solar power in the MENA region that could account for 15% of the electricity demand in Europe by 2050. The same approach is followed in the Gobitec proposal [78]. This programme investigates the potential of harvesting RES in the resource-rich Gobi Desert and its subsequent delivery to major load centres in China, Japan, South Korea or Russia. The report estimates the cumulated potential of the Gobi Desert in terms of wind and PV installed capacity at 2.6 TW. A GIS-based analysis makes the topic of another study that investigates the technical potential of wind, PV and concentrated solar power (CSP) to cover the full electricity demand of Europe and North Africa by 2050 [79]. An IEA study [80] also documents the theoretical potential of solar power generation in various regions known for their characteristic high solar irradiation, while a more recent article investigates the potential for RES (e.g., wind and PV) harvesting in Australia to supply major demand centres in East and South-East Asia [81]. The references stated above are just a small subset of what has been investigated in the literature. For a more comprehensive view of relevant studies and projects, the reader is advised to look into Chapter 2 of [56].

On a more distinct note, Greenland has also been the subject of RES resource analysis for power generation. A first PhD thesis on this topic investigates the potential of wind power generation in Greenland by using a mesoscale atmospheric model to recreate local wind regimes [82]. Certain locations are selected for large-scale wind turbine (e.g., 3 MW units) deployment and the study concludes that, even though the site selection process is highly complex, there is undisputed potential for wind

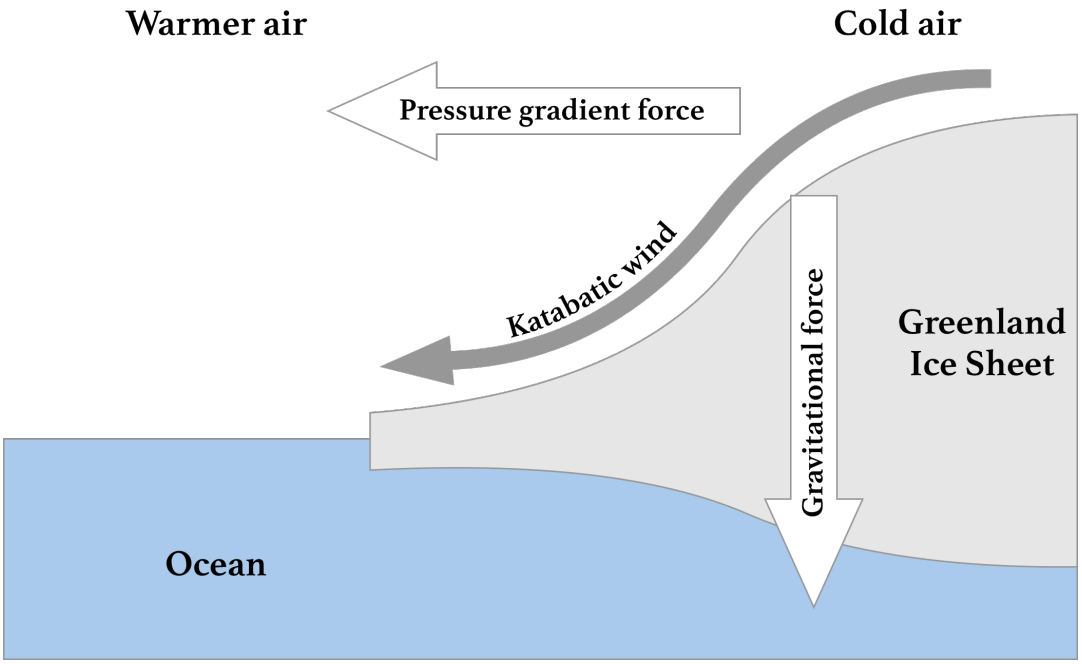

FIGURE 2.1: An illustration of katabatic winds in Greenland, carrying high-density air from a higher elevation down a slope under the force of gravity.

power generation in Greenland. A second PhD thesis on the same subject combines micro- and mesoscale climate modelling for an accurate representation of local wind circulation [83]. The conclusion of the study supports the resource potential of Greenland for wind generation, with specific features of local wind regimes (e.g., semi-permanent occurrence of katabatic flows) found to facilitate increased levels of electricity generation. A work authored by a Nordic consortium also studies the potential of renewable energy sources (e.g., hydro, wind, PV) in Greenland and different interconnection possibilities between the latter and northern Europe [84]. In addition, the author of [75] envisions Arctic regions (e.g., Greenland, Norwegian Sea, Barents Sea) as a next step of wind generation deployment in the North Sea, with a cumulated potential of electricity delivery to Europe and North America estimated at 1800 TWh per year.

In addition to assessing regional RES resources in terms of electricity generation potential, the current work provides a first account of quantifying complementarity between renewable resources in both space and time by means of a parametrised family of scalar indicators. Moreover, the wind resource assessment in Greenland is conducted via a mesoscale climate model proven to accurately replicate wind circulation in polar regions [85].

2.3 Reanalysis Data and Katabatic Winds

The process of wind resource assessment, as proposed in this chapter, starts with data acquisition. In this regard, collection of wind signals in Europe and Greenland at hourly resolution and covering the last ten years (i.e., 2008-2017) is achieved via two different sources. The first source, used for data collection in Europe, is the state-of-the-art ERA5 reanalysis [86] developed by the European Centre for Medium-Range Weather Forecasts (ECMWF) through the Copernicus Climate Change Service (C3S). It is an atmospheric reanalysis model[1] that incorporates in situ and satellite observations at high temporal (i.e., down to hourly) and spatial (i.e., $0.28^\circ \times 0.28^\circ$) resolution, at various pressure levels and currently covering the last ten years (i.e., 2008 - present). Within the scope of the current chapter, the ERA5 data used here is provided at a height of 100 meters above ground level and the hourly sampling rate chosen for wind potential assessment is achieved via linear interpolation from three-hourly output snapshots. Nevertheless, the limitations of reanalysis models in estimating wind energy potential are reported in the particular case of another reanalysis model (i.e., MERRA2) used in the European context, with significant spatial bias being identified for specific sub-regions [88], partly resulting from the coarse spatial resolution used to model the local or topography-induced winds. A comparison between the two reanalysis models [89] concludes that such tools are not recommended for estimating mean wind speeds for given locations due to their limitations in solving "local variations, especially in more complex terrain".

In order to overcome the limitations of the aforementioned tools when investigating the wind generation potential of Greenland, wind signals are retrieved from a second source, i.e., the regional MAR (*Modèle Atmosphérique Régional*) model. MAR is a climate model developed specifically for simulating climatic conditions of polar regions and has been repeatedly validated over Greenland [85]. MAR, as an atmospheric model[2], solves a set of dynamical equations over a limited integration domain by using reanalysis-based fields (here coming from ERA5) as lateral boundary conditions (e.g., temperature, wind, humidity, pressure at each vertical level of the MAR model). The choice of MAR for estimating Greenland's wind potential is based on its specific ability to accurately represent, at higher resolution (down to $5\,\text{km} \times 5\,\text{km}$), physical processes in Greenlandic regions, including the local, gravity-driven katabatic winds. For this work, MAR output at hourly resolution is generated at the same altitude level as ERA5 data (i.e., 100 meters above ground level).

The most promising, yet underestimated source of wind generation potential in Greenland stems from the existence of katabatic flows. These local atmospheric

[1] Reanalysis is the process of using a data assimilation system (i.e., a sequential procedure in which model states are updated on-line while previous forecasts are continuously compared to available measurements) providing "a consistent reprocessing of meteorological observations" [87].

[2] An atmospheric model is a mathematical model based on a set of dynamical equations governing atmospheric motions and using numerical methods to obtain approximate solutions of the studied system of coupled equations.

movements are the result of heat transfer processes between the cold ice cap and the warmer air mass above it. In brief, when the air mass temperature is higher than that of the ice sheet, the former is cooled down by radiation, thus the air density increases forcing it down the sloping terrain, as depicted in Figure 2.1. The flow of katabatic winds is driven by gravity, temperature gradient and inclination of the slope of the ice sheet [82]. This wind develops in the first tens of meters above surface (in the boundary layer) with a relatively constant direction down the slope of the terrain, is quasi-constant, but is strengthened when an atmospheric low-pressure area approaches the coast. Katabatic winds develop on a daily basis, regardless of the season, with a slight diurnal shift in their occurrence according to the season (i.e., arrival at the edge of the ice cap during early mornings throughout the winter, around noon during the summer). In addition, the highest intensity of katabatic winds is reported to occur on the south-eastern coast of Greenland, mainly due to steep slopes and flow-channelling conditions [83].

2.4 Methodological Framework

2.4.1 Preliminaries

In this manuscript, it is assumed that geographical areas are represented by a finite set of locations, and that simultaneously and uniformly sampled time series describing RES signals, e.g. wind speeds, are available at each location. Let $\mathcal{L}$ denote the set of all locations, while $L \subset \mathcal{L}$ and $l \in \mathcal{L}$ will be used to denote a subset of locations and an individual location, respectively. Then, let $\mathcal{T}$ stand for the discretised time horizon over which data is available, and let $t \in \mathcal{T}$ denote a time period.

It is hereby assumed in the following that a single RES type, e.g. wind or solar irradiance, can be harvested at a given location l. The associated resource signal will be denoted as $\mathbf{s}_l \in \mathbb{R}_+^{|\mathcal{T}|}$, with $|\mathcal{T}|$ the cardinality of $\mathcal{T}$. In a power systems context, working with capacity factors is more appropriate, as they directly express the amount of energy that may be recovered using a given technology. Hence, the raw signal time series $\mathbf{s}_l$ is converted into a capacity factor time series by means of an appropriate transfer function. Let $\boldsymbol{\pi}_l \in [0,1]^{|\mathcal{T}|}$ denote this capacity factor time series, while $\mathfrak{h}_l : \mathbb{R}_+^{|\mathcal{T}|} \mapsto [0,1]^{|\mathcal{T}|}$ stands for the transfer function of the candidate technology at location l, such that $\boldsymbol{\pi}_l = \mathfrak{h}_l(\mathbf{s}_l)$.

The selection of an appropriate transfer function $\mathfrak{h}_l$ is based on a multi-turbine power curve approach leveraged in [88] and introduced in [90]. In this regard, we make use of an aggregated transfer function modelled via a Gaussian filter (depicted in Figure 2.2) that emulates the dynamics of a wind farm comprised of identical individual units, while taking as input the wind signal of one single point within this farm.

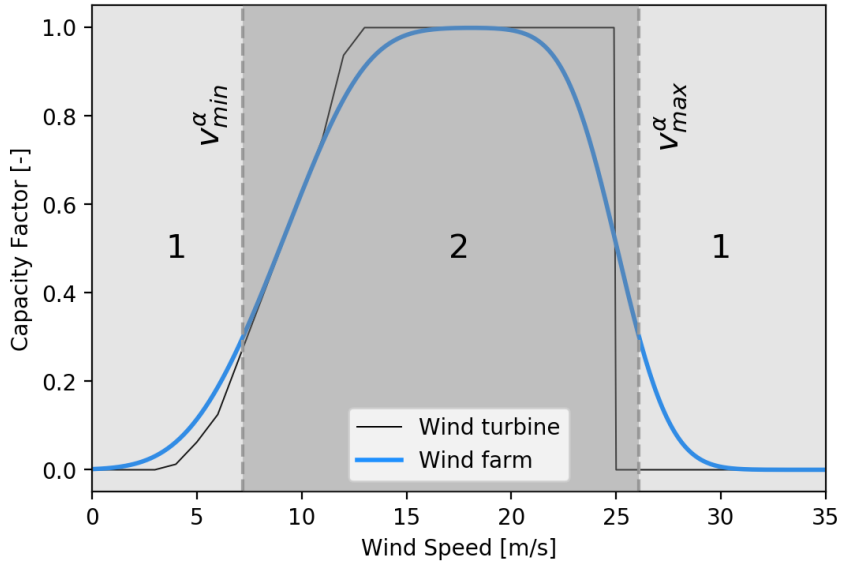

FIGURE 2.2: Single turbine and wind farm transfer functions. Example of wind farm aggregation based on multiple 8MW - aerodyn SCD 8.0/168 units. Wind regimes $(1, 2)$ associated with the two wind speed thresholds - $v^{med}_{low}, v^{high}_{med}$ - also displayed.

2.4.2 Spatiotemporal Complementarity Factors

Two wind speed thresholds are considered, such that v^{α}_{min} and v^{α}_{max} define the high-output operating regime of a generic wind farm, as shown in Figure 2.2. Let $\mathcal{Z} = \{1, 2\}$ be a set of labels denoting wind regimes and $\mathfrak{z} : \mathbb{R} \mapsto \mathcal{Z}$ be a mapping associating a wind speed class in $\mathcal{Z}$ to each resource sample s^{lt}, such that:

$$\mathfrak{z}(s_{lt}) = \begin{cases} 2, & s_{lt} \in [v^{\alpha}_{min}, v^{\alpha}_{max}) \\ 1, & otherwise\ . \end{cases}$$

According to this mapping, any wind time series $\mathbf{s}_l \in \mathbb{R}^T_+$ is clustered into two classes, depending on the relative position of each element (s_{lt}) with respect to the previously mentioned wind speed thresholds. Distribution of wind signals in two classes is suggested here as example, while the proposed clustering method is applicable for any other number of wind signal classes. In this particular case, the sectors correspond to wind regimes leading to i) little-to-no wind production (i.e., when wind speed is either too low or above the cut-out speed) and ii) to capacity factors above 25%. Furthermore, we define a family of mappings $\mathfrak{g}_{ij} : \mathcal{Z} \times \mathcal{Z} \mapsto \{0, 1\}$ associating a binary digit value to a pair of wind regime labels, such that:

$$\mathfrak{g}_{ij}(x, y) = \begin{cases} 1, & (x, y) = (i, j) \\ 0, & otherwise\ . \end{cases}$$

For any two locations $(l_1, l_2) \in \mathcal{L} \times \mathcal{L}$, we associate a $(|\mathcal{Z}| \times |\mathcal{Z}|)$-dimension matrix $M^{(l_1,l_2)}$ with entries:

$$m_{ij}^{(l_1,l_2)} = \frac{1}{T} \sum_{t=0}^{T-1} \mathfrak{g}_{ij} \left(\mathfrak{z}(s_{l_1 t}), \mathfrak{z}(s_{l_2 t}) \right) . \tag{2.1}$$

The coefficients m_{ij} that may be computed as given in Eq. 2.1 will be referred to as complementarity factors in what follows. Put simply, the complementarity factor m_{ij} quantifies how often the signal observed at location $l_1$takes values corresponding to class i, whilst the signal recorded at location l_2 takes values associated with class j. In general, one therefore has $m_{ij} \neq m_{ji}$. In the complementarity analysis proposed in this work, the underlying signal represents the hourly average capacity factors, while the associated classes correspond to low and high power generation regimes, respectively. It should be mentioned at this point that complementarity should not be understood in the usual sense of correlation (as computed on detrended signals via standard measures, such as Pearson, Spearman or Kendall correlation coefficients), but rather as the assessment of situations in which system-side, low-generation events occur, a detrimental feature of power systems characterized by high shares of RES generation. Roughly speaking, in terms of complementarity factors, such behaviour would translate into high m_{ij} values for classes i and j associated with low power generation regimes. Thus, in later developments, signals will be considered complementary if m_{ij} values associated with low production regimes are small.

2.5 Experimental Set-up

Site selection in Greenland relies on an a priori screening process of the local wind regimes. As seen in Figure 2.3, Greenland's southernmost region is the most promising from a wind resource perspective, therefore selection of the assessment point is constrained within the yellow and red-coloured areas plotted on the chart, ones with modelled average wind speeds above 13 m/s. In fact, availability of such high average wind speeds is the consequence of the common direction of the general circulation driven winds (as shown on the same chart) and the local katabatic winds that prevents the two atmospheric motions from cancelling each other out. Selection of an onshore point (i.e., $\texttt{GR}_{\text{on}}$) in this area of interest is further supported by year-long high temperatures (associated with low icing risks for the components of wind turbines - Figure 2.4) and the absence of a permanent ice sheet, as well as by the characteristic low elevation (Figure 2.5). In addition, an offshore location (i.e., $\texttt{GR}_{\text{off}}$), just south from the onshore one, will be assessed. The choice of the latter location is also supported by the bathymetry of Greenland's territorial waters, with depths up to 100 metres. The two sites are marked with a black cross in Figure 2.4.

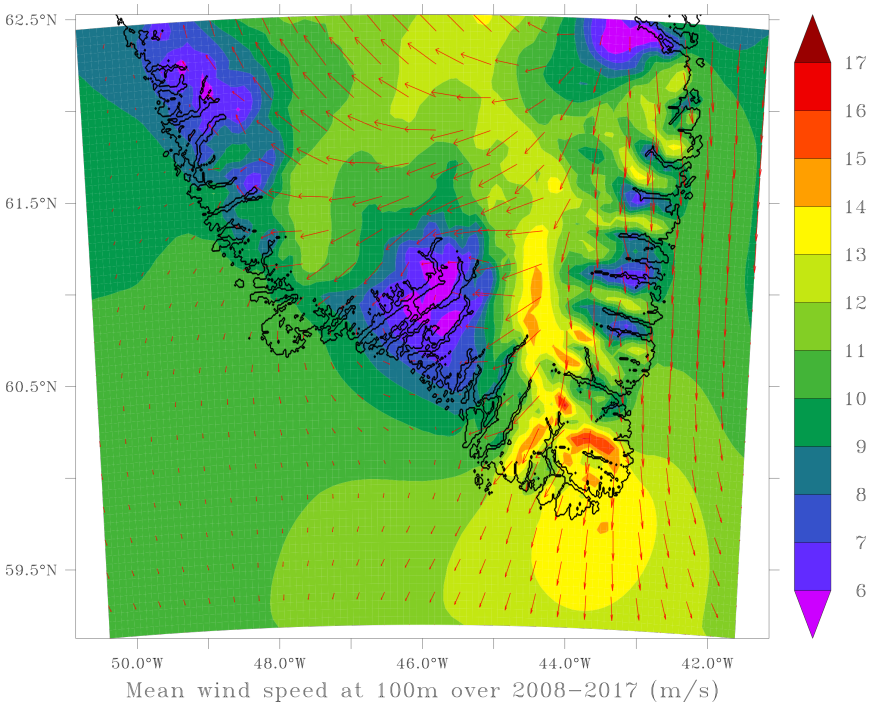

FIGURE 2.3: Greenland average wind speed magnitudes (m/s) as provided by MAR for 2008-2017. Underlying data represents average wind speeds at a 50 m height above ground level and a spatial resolution of 5 km×5 km.

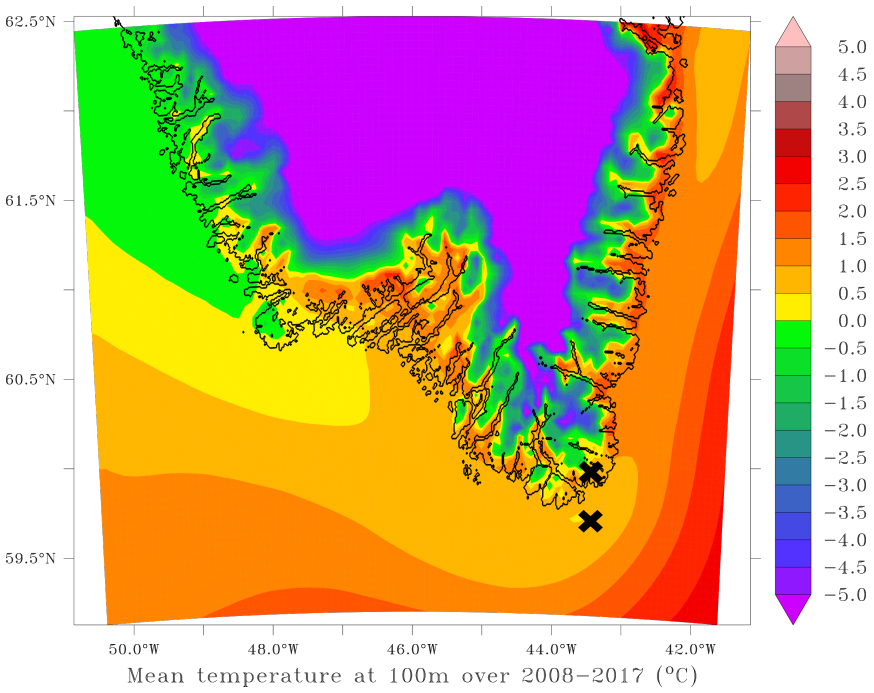

FIGURE 2.4: South Greenland average temperature profiles as computed via MAR for 2008-2017. Underlying data represents annual mean temperature in °C at 100 m above ground level, at a spatial resolution of 5 km×5 km.

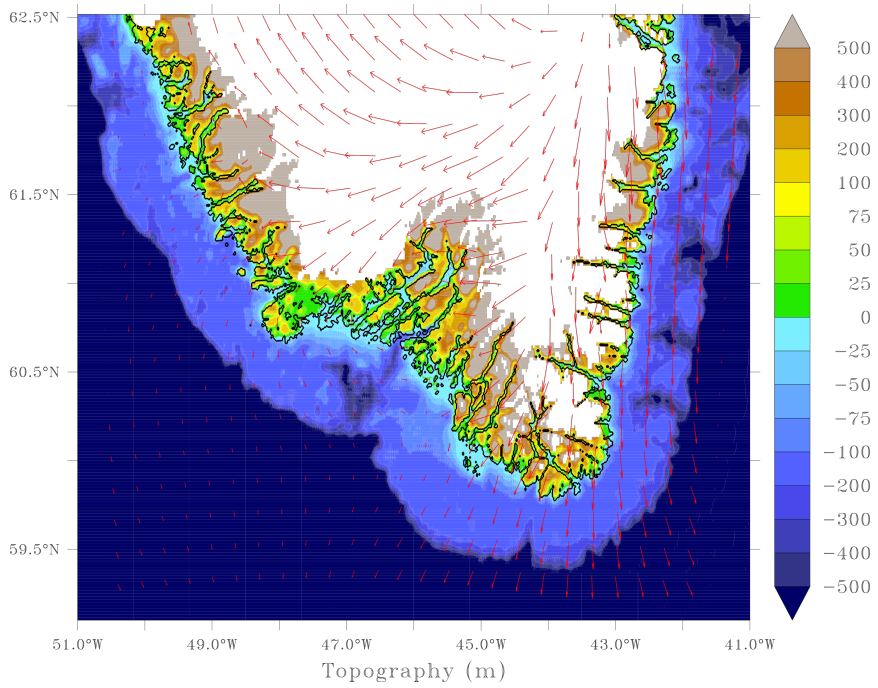

FIGURE 2.5: South Greenland topography superimposed over the land area not covered by permanent ice. Underlying data expressed in metres, at a spatial resolution of 1 km×1 km.

FIGURE 2.6: Location of the two European wind farms investigated.

Selection of the European generation sites to be compared with the locations in Greenland is initially bound to the region adjacent to or within the North Sea basin, one of the most productive areas on the continent [91]. Within these boundaries, two locations are selected based on the existence of operational wind farms. More specifically, the selected points coincide with the geographical coordinates of the *Horns Rev* (Danish offshore) - DK - and *Portes de Bretagne* (French onshore) - FR - wind farms. The location of the two wind farms is depicted with a blue cross in Figure 2.6.

2.6 Results

2.6.1 Wind Resource Assessment

The descriptive statistics of the wind time series associated with the studied locations are provided in Figure 2.7. The ten-year mean wind speed in both Greenland locations (i.e., around 14 m/s) is significantly higher than in both European sites (headed by the Danish offshore site, with an average wind speed of close to 10 m/s). In addition, a larger spread of modelled wind speeds in the Greenlandic regions can be observed. We note that, as reported in [92], a high standard deviation of the wind signals usually corresponds to increased turbulence intensity (i.e., short-term wind magnitude fluctuations relative to the mean velocity) that may negatively affect the performance of the wind farm. Nonetheless, it has been observed that larger standard deviation values corresponding to the sites in Greenland are not the result of intra-hourly variations of the underlying wind signal, but are rather due to the strong influence of seasonality of the local natural resource, and may therefore not be associated with high turbulence intensities.

Bivariate histograms of wind speed time series are displayed in Figure 2.8 as a first indicator of resource complementarity associated with selected pairs of locations. The first plot (Figure 2.8a) shows the approximate joint distribution of wind speeds in DK and FR (i.e., the European locations). Firstly, better wind resource at the former site is evident from the histogram, but high wind speeds (above 20 m/s) seldom occur in any of the two European locations. Then, a structured pattern featuring a very high concentration of data points between 5 and 10 m/s reveal a non-negligible degree of correlation between these sites. This analysis is further supported by a Pearson correlation coefficient value of 0.17, which, although modest, is much higher than that computed for pairs of remotely located sites, as discussed later. In Figure 2.8b, a clear linear pattern is observed in the histogram, suggesting a large degree of correlation between wind regimes at the two Greenlandic locations (an expected outcome considering the close geographical proximity of the two locations). This claim is further backed by a Pearson correlation coefficient score of 0.84, by far the largest among all considered cases. The same analysis for pairs of onshore (FR-GR_{on})and offshore (DK-GR_{off}) locations, respectively, is depicted in the last two subplots. The shape of the distribution in Figure 2.8c reveals significantly superior resource at the

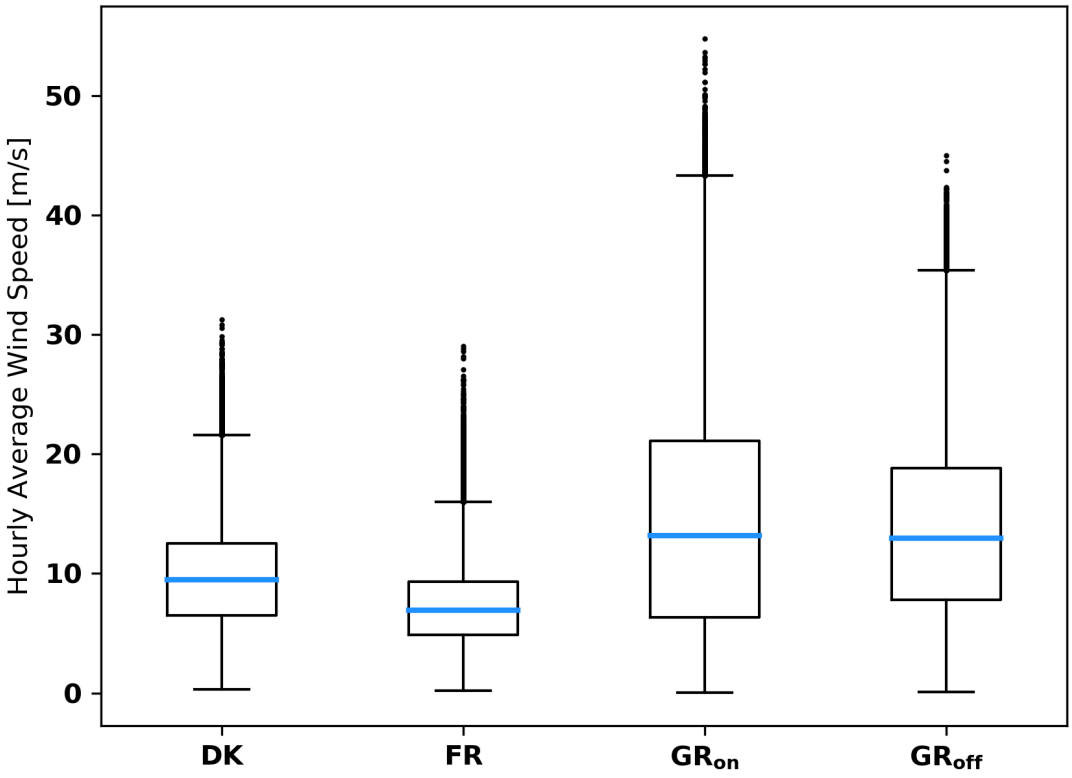

FIGURE 2.7: Box plots providing descriptive statistics of 100 m wind signals for the four locations under consideration. More specifically, the blue bar denotes the mean wind speed across the ten years investigated, while the box bounds define the first and third quartiles. In addition, outliers above the upper whisker (black round markers) represent data points outside the 95^{th} quantile.

Greenlandic onshore location compared to the European one, as well as very little correlation between wind signals (with an r score of 0.05). Regarding the offshore sites (Figure 2.8d), slightly superior resource is observed in Greenland compared to the European offshore location. Moreover,a relatively wide-spread and even distribution of data points,especially for wind speeds between 5 and 20 m/s, suggests lack of correlation between signals, a feature supported by the associated r index of 0.04.

2.6.2 Wind Farm Capacity Factor Comparison

Table 2.1 shows estimated values for average capacity factors computed as proposed in Section 2.4.1, assuming a 100% availability of the wind farm (no losses due to icing, down times, etc.). Compared to available operational data, the average capacity factor of the European sites is inflated by approximately 10%, assuming the currently in-use cut-out speed value of 25 m/s [93], [94]. These overestimates were expected considering the 100% availability assumption and the overestimation in reanalysis models of wind resource potential in northern and western Europe, as reported in [88]. Therefore, given the recurrent validation of MAR in accurately replicating wind conditions in polar regions [85], the differences between the capacity factors in the

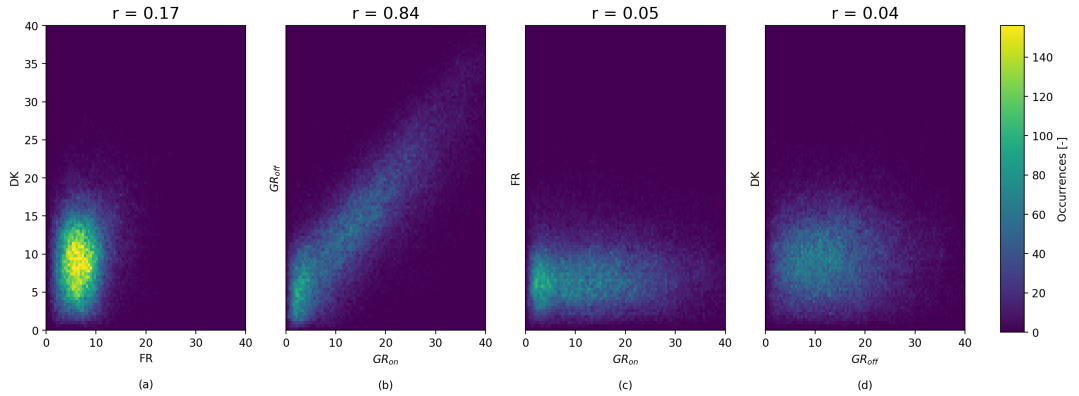

FIGURE 2.8: Bivariate histograms of wind signals for (a) the European, (b) Greenlandic, (c) the two onshore and (d) the two offshore locations. Each histogram bin corresponds to a 0.5×0.5 m/s square.

TABLE 2.1: Average capacity factors for the studied wind generation sites considering a transfer function associated with an aggregated wind farm for a single turbine (i) cut-out wind speed that is currently the state-of-the-art in the wind industry and (ii) an ideal cut-out wind speed superior to the maximum wind speed observed at different locations.

v_{cut}^{out} (m/s)	**DK**	**FR**	**GR$_{on}$**	**GR$_{off}$**
25	0.55	0.32	0.49	0.60
$\max_{l,t} s_t^l$	0.56	0.33	0.64	0.69

two Greenlandic locations and the ones associated with the European sites are even greater than those which can be inferred from Table 2.1. The second row of the same table shows the maximum theoretical capacity factor under the assumption that the individual units comprising a wind farm have a cut-out speed superior to any local wind speed to which they are exposed. In this case, while the average capacity factors of the European sites are barely affected (indicating very few occurrences of wind velocities above the current cut-out speeds), the same thing cannot be said about the locations in Greenland. There, under increased cut-out speed conditions, the onshore site would have the highest capacity factor gain (i.e., 15%), while an offshore wind farm could reach capacity factors of almost 70%.

These findings are supported by the duration curves depicted in Figure 2.9. On the one hand, overlapping curves in the two subplots at the top reflect marginal gains in terms of wind farm output for the European locations, when technological development (i.e., increased cut-out speeds of wind converters) is assumed. On the other hand, assuming availability of wind converters with cut-out speeds above the maximum wind speeds of each location results in massive output improvements in Greenland. In fact, for both locations, capacity factors of 90% or higher occur during more than half of the time. In this context, Figure 2.9 clearly shows the lost potential

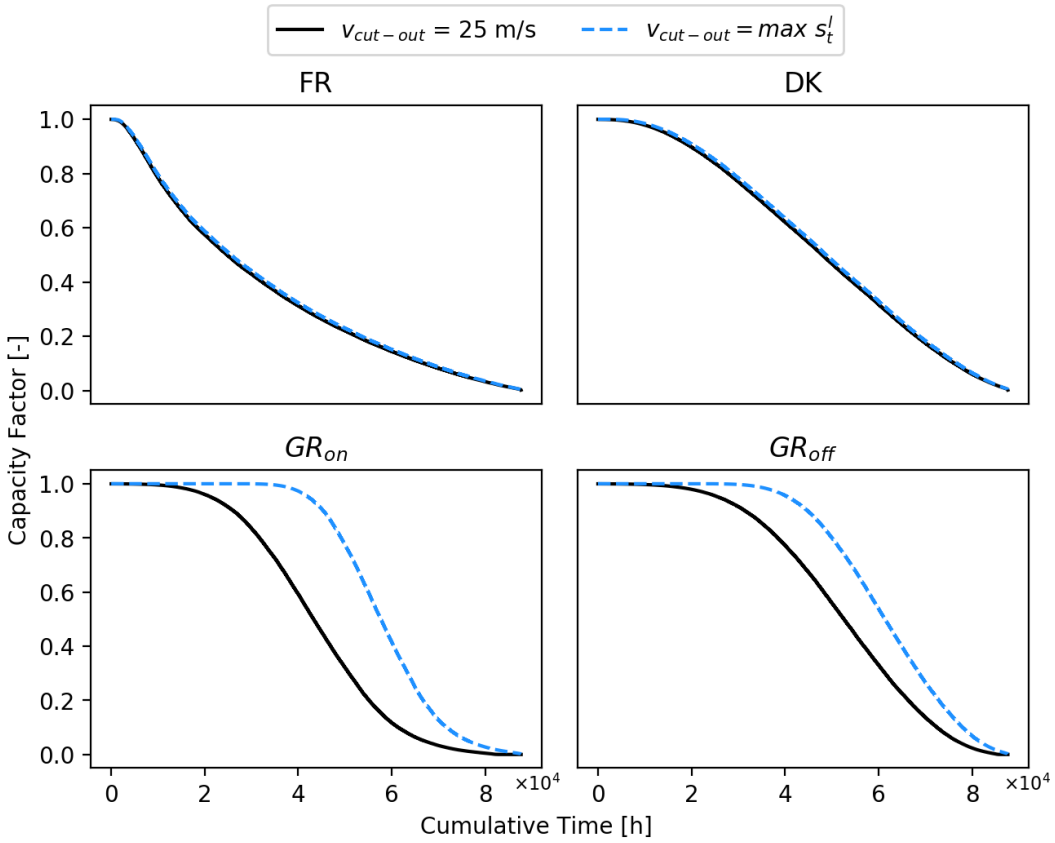

FIGURE 2.9: Duration curves of the four considered locations over the entire time horizon (2008-2017) assuming (i) a cut-out speed of individual wind converters of 25 m/s and (ii) an ideal cut-out speed superior to the maximum wind speed observed at each location.

of wind-based electricity generation in Greenland due to current technological limitations and indicates that novel wind turbine designs are required to fully harness the superior wind resource available in such regions.

2.6.3 Potential of Wind Generation Complementarity

In line with the previously detailed methodology, power output complementarity factors for selected pairs of locations will be evaluated in the upcoming section. Two classes representing a low-and a high-generation regime, respectively, are defined by wind speed values associated with a given capacity factor threshold, for a particular conversion technology. Figure 2.2 shows the separation of these classes via two wind speeds (v^{α}_{min} and v^{α}_{max}, respectively) for a capacity factor threshold (α) of 30% and assuming the conversion technology introduced in Section 2.4.1.

Power output complementarity factors for selected pairs of Greenlandic and European sites and for a capacity factor threshold of 30% are displayed in Table 2.2. Each cell in these tables corresponds to a pair of capacity factor classes (as depicted in Figure 2.2) and a pair of locations, and contains information simultaneously recorded at

each location and belonging to each corresponding class. Firstly, the aggregation of the two European locations (DK-FR) reveals a 17% (34%, respectively) probability of both sites yielding low (high, respectively) output, while the two locations complement each other for 49% of the time. Moreover, superior resource at DK is observed in the complementarity factors associated with different output regimes (the probability of high output at DK occurring simultaneously with low output at FR is 36%, while the opposite situation happens only 13% of the time). Secondly, considering the aggregation of both locations in Greenland (GR_{on}-GR_{off}), we observe a fairly high probability (74%) of both locations generating similar levels of output. Such a result was expected though, given the close geographical proximity of the two locations. In addition, using a conversion technology unable to harness frequently occurring high wind speeds in Greenland (due to relatively low cut-out speeds) can further justify increased proportions of simultaneously occurring low-output events in both Greenlandic locations compared to the all-European case, which is translated into a high value of the m_{11} coefficient. The two remaining cases assessing the effects of aggregating European and Greenlandic locations show contrasting results. Looking at the joint assessment of the two onshore generation sites (FR-GR_{on}), one sees a fairly even distribution of occurrences across the four possible bins and a rather high share of simultaneously low-output occurrences (22%) in both locations, an aspect that can be attributed to (i) the use of a sub-optimal conversion technology in Greenland and (ii) a relatively poor wind resource associated to the European location. In opposition, the aggregation of the two offshore locations (DK-GR_{off}) reveals a very good score for high output in at least one of the locations (91%), a result that supports the high quality wind potential suggested in Section 2.6.1, as well as the lack of correlation between wind regimes.

When defining the concept of complementarity, the emphasis was placed on the occurrence of detrimental low-generation events across systems. Indeed, when analysing complementarity factors as in Table 2.2, we are mostly interested in assessing simultaneous occurrences of low power output (that is, the m_{11} element of the complementarity matrices above) for a given location pair. In this regard, Figure 2.10 displays the evolution of the m_{11} score for each considered location pair against different capacity factor threshold values. First, for the aggregation of the two European locations (DK-FR), a linear increase in the proportion of low-output events is observed as the capacity factor threshold increases. Next, the close geographical proximity (and, thus, the highly correlated resource) of the two Greenlandic locations (GR_{on}-GR_{off}) results in relatively high m_{11} values for low capacity factor thresholds. For larger values of the latter, the influence of superior wind resource leads to a milder increase in low-generation events probability compared to the three other cases. Considering the FR-GR_{on} case, inferior resource associated with the European onshore node and a sub-optimal use of the conversion technology in the onshore Greenlandic location lead to higher shares of low-output events compared to the aggregation of European locations, for capacity factor thresholds smaller than 55%. Above this threshold, the

TABLE 2.2: Complementarity factors $m_{ij}^{(l_1,l_2)}$ for each pair (l_1, l_2) of considered locations, assuming a capacity factor threshold (α) of 30%. Two wind speed thresholds define two different classes for low - **1** - (below v_{min}^{α} and above v_{max}^{α}) and high - **2** - (between v_{min}^{α} and v_{max}^{α}) power output for a given conversion technology.

		FR	
		1	**2**
DK	**1**	0.17	0.13
	2	0.36	0.34

		GR$_{\text{off}}$	
		1	**2**
GR$_{\text{on}}$	**1**	0.23	0.19
	2	0.07	0.51

		GR$_{\text{off}}$	
		1	**2**
DK	**1**	0.09	0.21
	2	0.21	0.49

		GR$_{\text{on}}$	
		1	**2**
FR	**1**	0.22	0.31
	2	0.20	0.27

two curves intersect, driven mainly by superior wind resource in $\texttt{GR}_{\text{on}}$ with respect to FR. By far, the lowest occurrences of low-generation events for any capacity factor threshold considered is associated with the aggregation of the two offshore locations ($\texttt{DK-GR}_{\text{off}}$),which are characterized by high-quality and uncorrelated wind regimes.

2.7 Conclusion and Future Work

The current work evaluates Greenlandic wind resource quality through standard statistical metrics applied to raw wind data and to typical power generation proxies (i.e., capacity factors), as well as its complementarity with western European wind regimes via a systematic framework quantifying the occurrence of system-wide low-generation events. By leveraging a state-of-the-art regional climate model that has been repeatedly validated over polar regions, a promising area in southern Greenland is identified and found to exhibit vast wind power generation potential and possess complementary regimes with respect to European locations known for their high quality wind resource. These results lend further support to the claim that tapping into extensive renewable energy generation potential located in remote areas can prove beneficial for a secure and reliable supply of electricity in future power systems dominated by renewable energy sources. Another takeaway of this study pertains to the need for technological innovation in wind turbine design, a key aspect that could enable the achievement of even higher capacity factors in Greenlandic regions swept by high quality wind resource.

Regarding further research directions, analysis of wind regimes at different heights

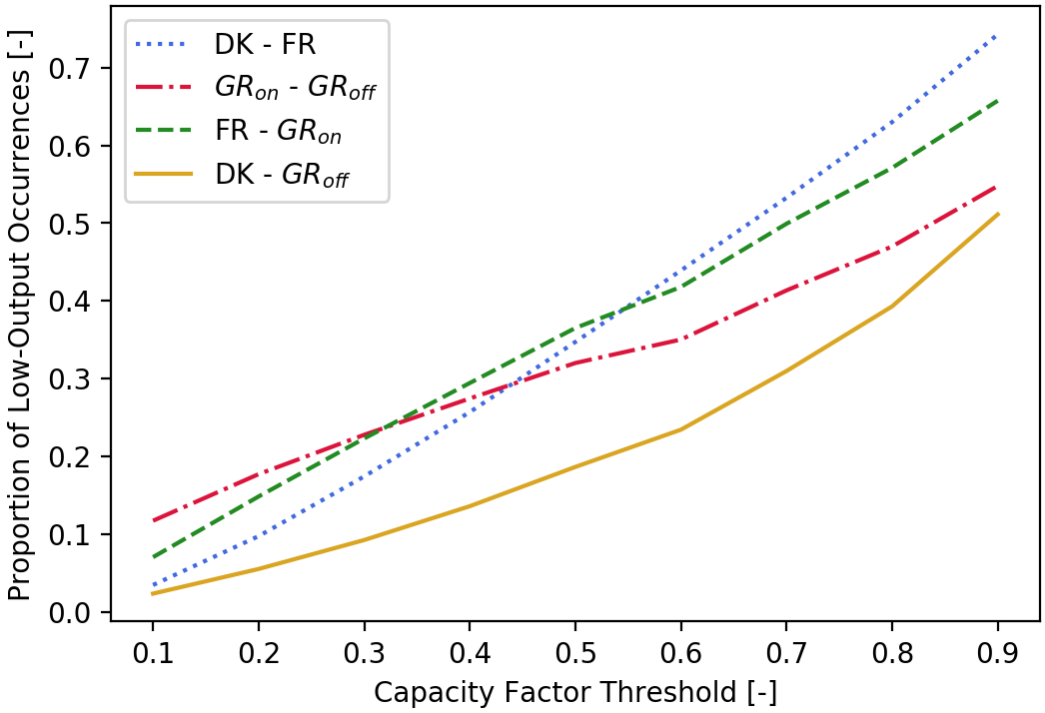

FIGURE 2.10: Proportion of low-output occurrences against various capacity factor thresholds (α) for a given conversion technology. For a capacity factor threshold of 30%, the values can be read in the upper left cell of the low-generation event assessment in Table 2.2.

above ground level is of considerable interest taking into account the particular features of Greenlandic katabatic flows. In this regard, increased average capacity factors are anticipated at lower elevations (e.g., 50 m above ground level), where the increased influence of topography and heat transfer processes bolsters a more frequent occurrence of semi-permanent katabatic flows, while the cut-out speeds of wind converters are reached less often. Another assessment path consists in developing a tailored analysis to quantify the potential benefits of a Greenlandic wind farm supplying Europe through an HVDC interconnection. In addition, devising a method able to quantify the spatiotemporal complementarity between RES sites on different time scales and spatial scopes could be paramount in properly understanding the role of complementarity in the design and operation of power systems dominated by renewable-based generation assets.

Chapter 3

Critical Time Windows for Renewable Resource Complementarity Assessment and Siting

This chapter proposes a framework to assess the complementarity between geographically dispersed variable renewable energy resources over arbitrary time scales. More precisely, the framework relies on the concept of critical time windows, which offers an accurate time-domain description of low probability power production events impacting power system operation and planning. A scalar criticality indicator is derived to quantify the spatiotemporal complementarity that renewable generation sites may exhibit, and it is leveraged to propose optimisation models seeking to identify deployment patterns with maximum complementarity. The usefulness of the framework is shown in a case study investigating the complementarity between wind regimes in continental western Europe and southern Greenland, using roughly 300 candidate locations and ten years of reanalysis and simulated data with hourly resolution. Besides showing that the occurrence of low wind power production events can be reduced on a regional scale by exploiting diversity in local wind patterns, results highlight the fact that aggregating wind power production sites located on different continents may result in a lower occurrence of system-wide low wind power production events.

This chapter is a reprint of *Mathias Berger, David-Constantin Radu, Raphaël Fonteneau, Robin Henry, Mevludin Glavic, Xavier Fettweis, Marc Le Du, Patrick Panciatici, Lucian Balea, Damien Ernst, "Critical Time Windows for Renewable Resource Complementarity Assessment", Energy 198, 117308, 2020,* https://doi.org/10.1016/j.energy.2020.117308. Reprinted with permission from the publisher.

3.1 Introduction

The large-scale deployment of technologies harnessing variable renewable energy sources (RES) for power generation has lead to novel challenges for power system operators and planners, mostly as a result of the intermittency of such resources. Several solutions have been envisaged to improve power system flexibility, including the deployment of additional storage capacity or the introduction of demand response programmes. An alternative solution, which seeks to smooth the variability of aggregate RES, consists in developing new electricity interconnections on a continental or global scale to take advantage of the diversity of resource types and profiles across vast geographical areas [68], [95], while exploiting time differences in production and consumption profiles in different regions [56], [74].

The topic of renewable energy resource (RES) complementarity has received increased interest in recent years [96]. More precisely, both the complementarity that may exist between different RES types and the spatiotemporal complementarity dispersed power plants harnessing the same RES may exhibit have been studied. In each of these contexts, a variety of definitions of complementarity have been proposed and different metrics have been developed to quantify it [96]. From a power systems perspective, however, an appropriate definition of complementarity should account for at least one key aspect of power systems operation and planning. Indeed, it should reflect the fact that simultaneous low power generation events are particularly detrimental to the power system, as back-up dispatchable capacity must be kept in the system to satisfy given adequacy criteria, possibly at a high cost. Interestingly, a vast proportion of complementarity studies rely on correlation analyses, e.g. [97] or [98], which fail to accurately capture such events, as they usually correspond to tail behaviour of the probability distribution of aggregate production signals. Comparatively few metrics embody such considerations, and, to the best of the authors' knowledge, very few of them have been applied to cases comprising hundreds of locations and several years of data with hourly resolution. Though this would provide a more robust complementarity assessment, the extent to which these methods scale up to tackle such cases is unclear.

To address these issues, this chapter leverages the *critical windows* framework, which allows to evaluate the spatiotemporal complementarity between a set of dispersed power plants harnessing various types of RES. In this framework, locations are considered complementary if they experience simultaneous low-production events very rarely. The spirit of the method can be described as follows. First, resource signal time series are divided into a set of time windows of fixed length, and, for each location considered, signal quality is evaluated over each time window via a given metric, e.g. the average signal value. A location is considered critical over a given window if the value produced by the metric is lower than a pre-specified threshold.

Then, the system-wide criticality is evaluated based on the number of critical locations over each time window, thereby producing a binary classification of time windows accurately capturing system-wide critical events. The approach is designed to exploit vast amounts of climatological data, e.g. retrieved from reanalysis databases [86], and can also be used as a basis to derive optimisation models addressing the RES siting problem while accounting for RES complementarity.

The methodology is illustrated on a case study focusing on western Europe and Greenland. More precisely, the framework is leveraged to evaluate the complementarity between the wind regimes in France and southern Greenland, in the context of the development of an interconnection between continental western Europe and Greenland. Then, optimisation problems are formulated to identify locations with the best complementarity within and between these regions. Finally, the framework is exploited to highlight the differences between wind power plants deployment schemes seeking to maximise complementarity and annual electricity output, respectively.

This chapter is structured as follows. Section 3.2 reviews related works and emphasises how this work contributes to the literature. Section 3.3 then introduces the framework of critical time windows and discusses how it may be leveraged in a RES siting context. Section 3.4 describes the case study illustrating the usefulness of the framework, and results are presented in section 3.5. Finally, section 3.6 concludes the chapter and formulates research questions to be addressed in future work.

3.2 Related Works

The complementarity between dispersed renewable production sites on different time scales has been studied extensively in recent years [70], [96]. Throughout the surveyed literature, two different definitions of renewable resources complementarity are used. On the one hand, RES complementarity refers to the output variability reduction effect incurred by the aggregation of spatially distributed variable resources (e.g., wind, solar). On the other hand, complementarity is defined as the synergy between two or more renewable resources (e.g., wind and solar). In the upcoming section, the physical implications of RES complementarity under both aforementioned definitions are briefly summarized before a detailed account of various methods employed to tackle it is provided.

An early investigation of wind resource spatial complementarity is provided by Giebel [68], who computes the cross-correlation coefficient between wind signals recorded at pairs of generation sites in Europe as a function of the distance separating the locations, revealing mitigated correlation levels with increasing distances between sites. Subsequently, the statistical properties of spatially averaged signals reveal the existence of a *smoothing effect*, whereby increasing the geographical scope

and the number of generation sites appears to decrease the variability of the aggregated wind output. In the same vein, Olauson et al. [99] investigate the correlation between pairs of wind signals in Europe on various time scales and aggregated at country levels. The paper concludes, in line with the previous study, that wind correlation decreases with increasing distance between regions. In another paper [100], the authors investigate the output variability of utility-scale solar PV plants in Gujarat (India) on multiple time scales and the results reveal diminishing marginal returns in variability reduction as more plants are aggregated within the state. In [101], Sterl et al. assess the synergy between wind and solar resources in West Africa and conclude that wind power has great potential for complementing solar resources over daily time frames. Likewise, Slusarewicz et al. [102] investigate the wind-solar synergies over pairs of generation sites in Texas (USA), revealing different degrees of complementarity depending on the site locations and time horizons considered.

The methods employed in resource complementarity analyses are manifold. Standard statistical tools have most often been invoked and correlation analysis have proved very popular in the literature. In particular, methods relying on various correlation coefficients, such as Pearson, Kendall, Spearman, exponential or sample coefficients, as well as cross-correlation coefficients have all been used to evaluate RES complementarity in various spatial settings, e.g., in Sweden [97], Britain [103], Europe [68], [104], Brazil [105], the United States [95], [102], China [106], or even between locations on different continents (Canada and Australia) [98]. Similarly, Jurasz et al. [107] use the Pearson correlation coefficient to investigate the resource complementarity within small-scale hybrid systems comprising wind and solar PV units and their load-matching capabilities. In [108], the authors evaluate wind-solar complementarity in Canada using descriptive statistics (percentile ranking). Montforti et al. [109] propose a Monte Carlo-based analysis of renewable resource complementarity across locations in Italy, where multiple randomly generated deployment patterns are investigated to retrieve the location set with the lowest associated Pearson coefficient. In [110], the authors assess the smoothing effect using frequency-domain analysis methods introduced in [111] instead of statistical tools, again highlighting the reduction in short-term variability as the geographical scope increases. Principal component analysis (PCA) has also been used to assess wind-solar complementarity in [112] and [113]. In particular, Li et al. [112] define a *complementarity index for wind and solar radiation* impacted by more than fifty variables (incl. terrain, precipitation, temperature or pressure levels) to investigate wind-solar complementarity across Oklahoma (USA). Lastly, methods relying on custom scalar indicators have also been proposed in the literature. For instance, Prasad et al. [114] investigate potential synergies between wind and solar resources at hourly time scales in Australia. To this end, the authors define wind-solar complementarity as the proportion of hours during which at least one of the two aforementioned resources is available above pre-defined power density thresholds. In [101], the authors assess

the complementarity between the same two renewable resources via a *stability coefficient* representing the variance reduction of capacity factors associated with a hybrid solar-wind system, relative to a solar-only set-up. In [115], Ren et al. evaluate complementarity of wind resources across neighbouring sites in China through a score computed from wind power densities across adjacent locations. Beluco et al. [116] tackle the assessment of complementarity between pairs of resources at one given location through a *complementarity index* incorporating correlation, resource quality and variation amplitude of any two resource signals.

Although the aforementioned studies have provided a better understanding of RES complementarity in various settings, the underlying methods appear to have been overwhelmingly geared towards the evaluation of complementarity in terms of the reduction in output variability that may be achieved by aggregating RES power plants. From a power systems operation and planning perspective, this approach makes sense but still fails to account for other key considerations. In particular, solely focussing on output variability overlooks the fact that simultaneous low RES production events are particularly detrimental, in that additional dispatchable backup capacity must be kept in the system or other flexibility options must be deployed to satisfy given adequacy criteria. Such simultaneous low production events typically correspond to tail behaviour of the underlying probability distributions and most methods invoked above are ill-suited to capture such phenomena. In addition, very few of the methods reviewed allow for the straightforward comparison and ranking of arbitrary deployment patterns, e.g. via a meaningful score quantifying the level of complementary displayed by the underlying locations and resources. Hence, applying such methods in a RES siting context seems particularly cumbersome. Finally, the extent to which the aforementioned methods can scale up to tackle problems featuring hundreds or thousands of locations and years of climatological data with temporal resolution is unclear. The methodology proposed in this chapter addresses these drawbacks, as detailed in the forthcoming sections.

3.3 Introducing the Time Windows Framework

Recall from Section 2.4.1 that, in this manuscript, it is assumed that geographical areas are represented by a finite set of locations, and that simultaneously and uniformly sampled time series describing RES signals, e.g. wind speeds, are available at each location. Let $\mathcal{L}$ denote the set of all locations, while $L \subset \mathcal{L}$ and $l \in \mathcal{L}$ will be used to denote a subset of locations and an individual location, respectively. Then, let $\mathcal{T}$ stand for the discretised time horizon over which data is available, and let $t \in \mathcal{T}$ denote a time period. In addition, a single RES type, e.g. wind or solar irradiance, can be harvested at a given location l. The associated resource signal will be denoted as $\mathbf{s}_l \in \mathbb{R}_+^{|\mathcal{T}|}$, while the corresponding capacity factor time series are expressed by $\boldsymbol{\pi}_l \in [0,1]^{|\mathcal{T}|}$, with $\mathfrak{h}_l : \mathbb{R}_+^{|\mathcal{T}|} \mapsto [0,1]^{|\mathcal{T}|}$, such that $\boldsymbol{\pi}_l = \mathfrak{h}_l(\mathbf{s}_l)$.

3.3.1 Time Windows

Let $\delta \in \mathbb{N}$ be the time window duration. Then, for time periods $t \in \mathcal{T}$ and $(t + \delta - 1) \in \mathcal{T}$, the time window w_t^δ spanning the time interval between these periods writes as $\mathrm{w}_t^\delta = [t, t + \delta - 1] \cap \mathbb{N}$. Then, let $\mathcal{W}$ be the set of time windows of length δ that may be extracted from the discretised time horizon, which is constructed as

$$\mathcal{W} = \{\mathrm{w}_t^\delta | t \in \mathcal{T}, (t + \delta - 1) \in \mathcal{T}\}. \tag{3.1}$$

A time window $\mathrm{w} \in \mathcal{W}$ can be seen as a subset $\mathcal{T}_\mathrm{w} \subseteq \mathcal{T}$ of δ successive time periods, and all time windows $\mathrm{w} \in \mathcal{W}$ have the same length δ. It is worth noting that given this definition, successive time windows overlap and have $\delta - 1$ periods in common.

Critical Locations

Once time series have been divided into time windows, the quality of renewable resource signals is measured at each location over the duration of each time window. If the resulting score is smaller than a pre-specified quality threshold, the location is labelled as *critical*. The opposite also holds, i.e., if the score is higher than the quality threshold, the location is deemed *non-critical*. Thus, for each window, this procedure allows to identify a set of (non-)critical locations, and repeating it for all time windows yields a complete picture of the *local criticality* properties of the area under consideration.

More formally, let $\mathfrak{q}_l : [0,1]^\delta \mapsto [0,1]$ be the metric used to evaluate local resource quality at candidate location l. This mapping essentially produces a score $\overline{\pi}_{l\mathrm{w}} = \mathfrak{q}_l(\{\pi_{lt}\}_{t \in \mathcal{T}_\mathrm{w}})$ capturing how well location l performs over window w. In particular, $\mathfrak{q}_l$ may compute an average value but other metrics, e.g., the median, can be readily employed in this framework. Then, let $\alpha_{lw} \in [0,1]$ be the *local criticality threshold*, which defines the condition under which individual locations are considered *critical* during window w. Note that this threshold can be defined independently for each location l and time window w. However, in the current chapter, α is assumed to be constant in time and space, i.e., $\alpha_{lw} = \alpha$ (e.g., a capacity factor threshold that applies to all locations and across all time windows). Therefore, for any window $\mathrm{w} \in \mathcal{W}$ and subregion $L \subseteq \mathcal{L}$, the subset of *non-critical locations* $\mathcal{J}_\mathrm{w}^L \subseteq L$ can be constructed as

$$\mathcal{J}_\mathrm{w}^L = \{l \in L | \overline{\pi}_{l\mathrm{w}} \geq \alpha\}. \tag{3.2}$$

Note that, for any window $\mathrm{w} \in \mathcal{W}$, the number of *non-critical locations* N_w^L is given by the cardinality of $\mathcal{J}_\mathrm{w}^L$, i.e., $\mathrm{N}_\mathrm{w}^L = |\mathcal{J}_\mathrm{w}^L| \leq |L|$.

Critical Windows

Recall that, in this manuscript, the spatiotemporal complementarity assessment relies on a binary classification of time windows capturing the occurrence of system-wide critical events, e.g., simultaneous low-production events recorded across most of the locations considered, and from which a *criticality indicator* is derived. Such a score can be computed for any subset $L \subseteq \mathcal{L}$, which therefore permits to evaluate the respective merits of different deployment patterns.

The classification of time windows is made possible by the introduction of the *global criticality threshold* parameter, which specifies the proportion of locations that should be (non-)critical for a time window to be counted as system-wide (non-)critical. Let $c \in \mathrm{N}$ denote this parameter. For a given deployment pattern $L \subseteq \mathcal{L}$, the set of *non-critical time windows* $\mathcal{W}_{\mathrm{C}}^{L}$ is constructed as

$$\mathcal{W}_{\mathrm{C}}^{L} = \{\mathrm{w} \in \mathcal{W} | \mathrm{N}_{\mathrm{w}}^{L} \geq c\}, \tag{3.3}$$

where c represents the number of locations that should be non-critical for a time window to be considered system-wide non-critical. The *criticality indicator* $\mathfrak{c}^{L} \in [0, 1]$ of a deployment pattern L is then simply computed as

$$\mathfrak{c}^{L} = 1 - \frac{|\mathcal{W}_{\mathrm{C}}^{L}|}{|\mathcal{W}|}, \tag{3.4}$$

i.e., it gives the proportion of critical time windows observed throughout the entire horizon $\mathcal{T}$. Hence, a value of $\mathfrak{c}^{L}$ close to 1 suggests that most time windows in the horizon considered are critical, which is indicative of poor complementarity between locations in L. By contrast, a low value of $\mathfrak{c}^{L}$ shows some level of complementarity between locations in L.

Even though the dependence of the criticality indicator upon the time window duration δ, local criticality threshold α and global criticality threshold c has been made implicit in prior developments, it must not be overlooked. Indeed, in reality $\mathfrak{c}^{L} = \mathfrak{c}^{L}(\delta, \alpha, c)$. In other words, for a given region L, different values of the criticality indicator can be produced by adjusting the values of the three aforementioned parameters. In particular, updating the value of δ will allow to assess criticality and complementarity on different time scales. Furthermore, the values of α and c can be modified to update the definition of criticality. For instance, α or c could be expressed as functions of exogenous quantities such as the electricity load in order to tailor the definition of criticality to one's needs.

Finally, a probabilistic interpretation of the criticality indicator is provided. Indeed, since c^{L} represents a proportion, it can also be interpreted as the likelihood of obtaining a critical time window when drawing uniformly at random from the set of time windows $\mathcal{W}$. With this in mind, sets of locations corresponding to higher values of

the criticality indicator can be understood to have a higher empirical probability of experiencing critical events.

3.3.2 Critical Windows for Siting of Renewable Generation Assets

Besides providing a way of evaluating the spatiotemporal complementarity between dispersed power plants harnessing RES, the machinery of the *critical windows* framework can be leveraged to formulate optimisation models seeking to deploy RES so as to maximise their complementarity. Indeed, such deployment patterns can be identified via optimisation models minimising the value of the criticality indicator.

More formally, let $\mathcal{P}(\mathcal{L})$ be the power set of $\mathcal{L}$, that is, the set of all subsets of $\mathcal{L}$. Then, let $\mathfrak{f}_C : \mathcal{P}(\mathcal{L}) \mapsto [0, 1]$ be a function associating its criticality indicator value to any set of locations $L \subset \mathcal{L}$, i.e., $\mathfrak{c}^L = \mathfrak{f}_C(L)$. Moreover, let $k \in \mathbb{N}$ be the number of locations which should be deployed. An optimisation problem seeking to deploy k power plants whilst maximising their complementarity then writes as

$$\begin{aligned} \min_{L \subset \mathcal{L}} \quad & \mathfrak{f}_C(L) \\ \text{s.t.} \quad & |L| = k, \end{aligned} \tag{3.5}$$

where the constraint $|L| = k$ enforces that exactly k sites are selected. This formulation can be readily extended to include geographical deployment constraints, e.g., deploying a pre-defined number of sites in subregions. In such a context, if $\mathcal{N}_B$ denotes the subregions, with $|\mathcal{N}_B| = B$, L would be replaced by a collection of (disjoint) locations sets $\{L_n\}_{n \in \mathcal{N}_B}$ such that $L = \cup_{n=1}^{B} L_n$ and $|L_n| = k_n$, with k_n the number of sites to deploy in subregion n. A greedy algorithm to solve problem (3.5) is hereafter proposed. For an un-partitioned case (i.e., $B = 1$), this algorithm works as follows. Starting from the full set of candidate sites $\mathcal{L}$, locations are removed from the incumbent solution as long as its cardinality is greater than $k \in \mathbb{N}$. At each iteration, sites whose removal from L would minimise the difference (in absolute value) between the criticality index values computed at consecutive steps are stored in set $l^\star$. If more than one site leads to the same difference between criticality indicators, the cardinality of $l^\star$ is greater than one and one location is sampled at random and added to the incumbent solution. These ideas are summarized in Algorithm 1.

3.4 Test Case

In this section, a particular application is proposed in order to illustrate the usefulness of the indicator defined in Section 3.3. More specifically, a wind regime analysis is conducted in South Greenland and France in the context of an electrical interconnection between Greenland and mainland Europe, as part of a broader global grid. At first, a general assessment of the spatiotemporal criticality observed

Algorithm 1 Backward Randomised Greedy Algorithm

Require: $\mathcal{L}$, k, $\mathfrak{f}_C$
  $L \leftarrow \mathcal{L}$
  while $|L| > k$ **do**
    $l^\star \leftarrow \arg\min_{l \in \mathcal{L} \setminus L} \mathfrak{f}_C(L \setminus \{l\})$
    $l \leftarrow$ one location sampled from $l^\star$ uniformly at random
    $L \leftarrow L \setminus \{l\}$
  end while
Ensure: $L, \mathfrak{f}_C(L)$

in wind signals across (i) Greenland, (ii) France and (iii) within their spatial aggregation is carried out via the proposed criticality indicator. Recall from the previous chapter that the critical window framework relies on a tuple of three parameters, i.e., (α, δ, c), defining the local criticality threshold, the time window length and the global criticality threshold, respectively. In this exercise, the value of α is constant across all candidate locations and time windows (i.e., $\alpha_{lw} = \alpha$), and the impact of different window lengths (δ) and c values is assessed. Then, the optimal distribution of wind generation sites within those geographical areas is analysed under various deployment constraints.

3.4.1 Data Acquisition

This subsection introduces the wind signal datasets used in the current work and briefly discusses the selection of geographical regions employed in the Section 3.5 analyses.

Two distinct data sources are used in the wind signal acquisition process for the geographical regions under consideration. Resource data within the boundaries of mainland France is acquired via the ERA5 climate reanalysis model. Set on a regular geodesic grid, hourly-sampled wind data at 100 meters above ground level is provided at a spatial resolution of $0.28^\circ \times 0.28^\circ$ [86]. Besides multiple features that have contributed to the success of such methods in energy-related applications [117], the shortcomings of these datasets in the context of wind power generation studies stem mainly from the relatively coarse spatial resolution of their underlying grids. More specifically, in complex terrain conditions, this latter aspect limits the accurate replication of local, topography-induced winds patterns [89].

A second source of data, the MAR regional atmospheric model, is leveraged to alleviate some of the previously mentioned limitations of reanalysis frameworks for wind data acquisition in Greenland. Repeatedly validated over the aforementioned island, MAR has been specifically developed for simulating atmospheric conditions over polar regions [118]. The main advantage of this tool lies in its ability to accurately reproduce, at refined spatial resolution (down to $5\,\text{km} \times 5\,\text{km}$), particular features of the atmospheric circulation over this region, including the local, semi-permanent katabatic flows that may enable high levels of wind power generation.

FIGURE 3.1: Locations considered for the wind resource assessment in France and South Greenland. The upper-left corner of the map displays the geographical points included in $\mathcal{L}_G$, while the locations superimposed over the French mainland territory comprise $\mathcal{L}_F$.

For this study, ERA5 fields (e.g., wind speeds, air temperature, humidity or pressure) are used as forcing at the spatial boundaries above Greenland to retrieve MAR-based hourly wind time series at 100 meters above ground level.

The selection of South Greenland as the focus of this analysis is done via a MAR-based visual inspection of the entire Greenlandic land mass that reveals vast wind resource, relatively high temperatures and favourable topography for the sub-region considered [119]. The locations sets used in the following analysis comprise geographical points which exist in both the ERA5 and MAR grids, respectively. In the following, the set of all locations in France is denoted by $\mathcal{L}_F$, while sites in South Greenland are grouped in $\mathcal{L}_G$. A third set, denoted by $\mathcal{L}_{FG}$, is defined as the union of the two location sets $\mathcal{L}_{FG} = \mathcal{L}_F \cup \mathcal{L}_G$. The total number of 294 candidate sites are depicted in Figure 3.1.

3.4.2 Defining the Conversion Technology

The mapping of wind speeds to hourly average capacity factors is performed via a transfer function mimicking the normalised power output of a wind farm comprising identical units which are geographically distributed in the direct vicinity of the site of interest. This approach is consistent with power system planning processes, where one is usually interested in developing wind farms rather than constructing a single turbine. As proposed in [88], such a transfer function is derived from the power curve of a representative wind turbine (the *aerodyn SCD 8.0/168*, in this particular case) by means of a Gaussian fit, where a 100% availability of the individual units is assumed (i.e., no down times due to maintenance, icing etc.). In addition, this specific wind energy converter is selected for illustration purposes only, regardless of its appropriateness for deployment at the locations considered. The result of

this approach leads to the same power curve as the one used in the previous chapter and displayed in Figure 2.2.

3.5 Results

This section presents a detailed discussion of results generated with the criticality indicator introduced in Section 3.3. Firstly, the values of the criticality indicator are examined for various instances of the (δ, α, c) triplet within the selected geographical areas. Then, the optimal deployment of generation sites in different geographical set-ups is discussed. Lastly, the current framework is leveraged to highlight potentially undesirable consequences of current power systems planning practices, which primarily favour electricity generation potential and disregard the complementarity in electricity production regimes when selecting wind farm deployment sites.

3.5.1 Spatiotemporal Complementarity Assessment

Initially, a comprehensive evaluation of wind resource complementarity in the available locations sets over a time period stretching the last ten years (2008-2017) is conducted using the criticality index. In the following example, as well as in all other applications subsequently proposed, the local criticality threshold (α) is set to 35%. That is, a given location l is considered to be critical during time window w if $\overline{\pi}_{l\mathrm{w}}$ falls below this value. This choice stems from it standing between the average capacity factors of the two regions, as computed from available data (i.e., 22% for French sites and 48% for the locations in Greenland). The process of mapping wind signals to normalised power output values is done using the methodology introduced in Section 3.4.2. Formally, $\mathfrak{f}_C(L)$ is computed for $L \in \{\mathcal{L}_F, \mathcal{L}_G, \mathcal{L}_{FG}\}$, $\alpha = 0.35$, for all window lengths $\delta \in \{1, 24, 72, 168\}$ and for all global criticality thresholds $c/|L| \in \{0.5, \ldots, 1.0\}$. The results of this analysis are shown in Figure 3.2. In this plot, the x-axis is defined as the ratio between the global criticality threshold c and the cardinality of candidate sites $|L|$. In this context, *criticality* is harder to achieve as the value of $c/|L|$ increases. For instance, for $c/|L| = 0.5$, a time window is *critical* if 50% of locations are *critical* across its duration. For $c/|L| = 1.0$, *all* locations must be *critical* for the window to be *critical*. In other words, a single *non-critical* location during a given time window renders the entire time window *non-critical*.

First, as can be observed in all subplots of Figure 3.2, the value of $\mathfrak{f}_C$ decreases as the $c/|L|$ increases, regardless of the time window length (δ) considered. This is happening since time window criticality is easier to achieve at lower $c/|L|$ values, where less locations are required to have insufficient generation in order for the time window to be critical. In addition, for all locations sets observed, it appears that considering $c/|L| = 1.0$ in the computation of $\mathfrak{f}_C$ leads to values of the criticality indicator close to zero, an aspect that highlights significant wind regime diversity even at regional scale.

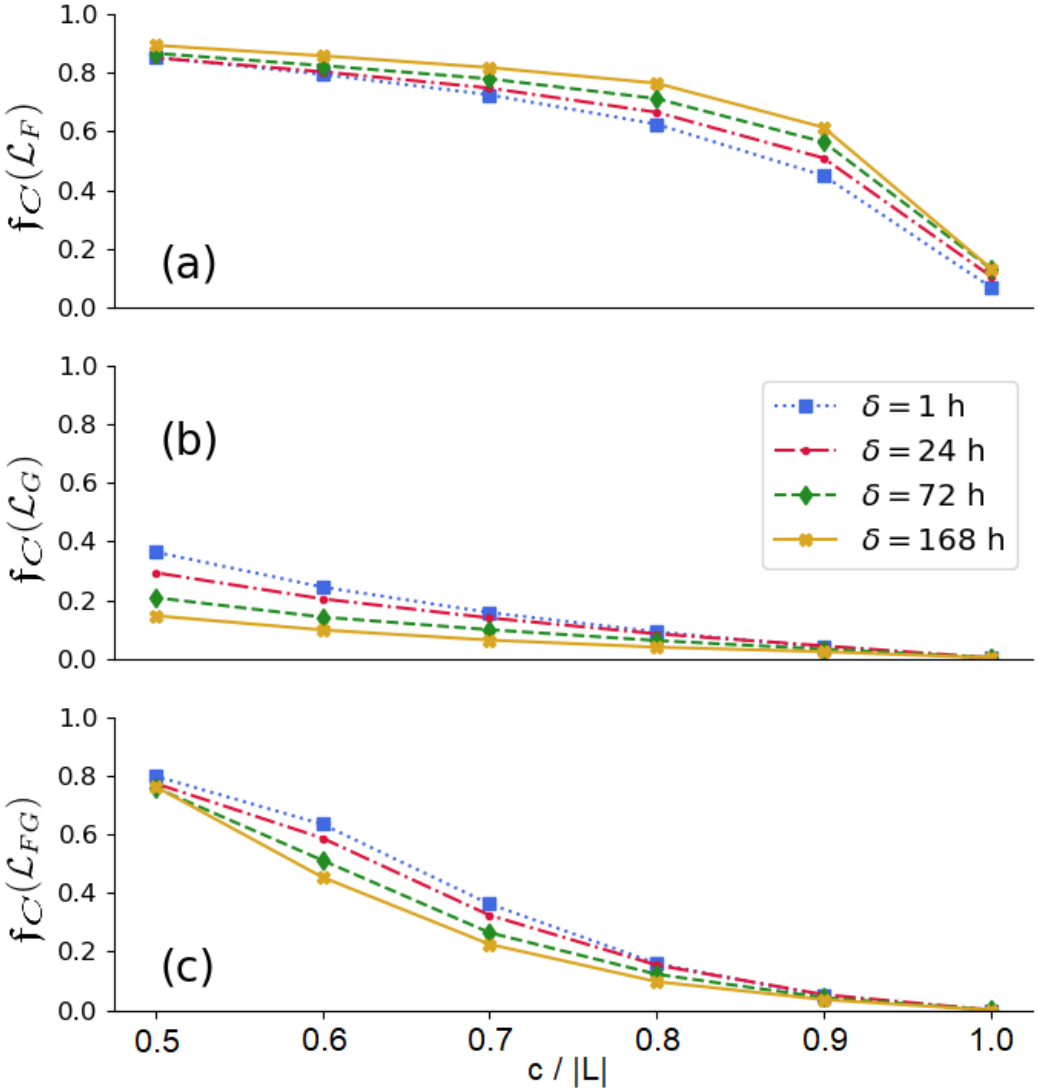

FIGURE 3.2: Criticality indicator $\mathfrak{f}_C$ values for a local criticality threshold (i.e., α) of 35% for all locations in (a) France ($\mathcal{L}_F$), (b) Greenland ($\mathcal{L}_G$) and (c) the aggregation of the two ($\mathcal{L}_{FG}$).

TABLE 3.1: Percent values of the criticality index $\mathfrak{f}_C$ for various global criticality threshold values (c) and for all considered locations sets, considering a local criticality threshold (α) of 35% and a window length (δ) of 24 hours.

$c/\lvert L\rvert$ / L	0.5	0.6	0.7	0.8	0.9	1.0
$\mathcal{L}_F$	85.1	80.4	74.8	66.6	50.9	10.6
$\mathcal{L}_G$	29.4	20.4	13.9	8.5	4.4	0.3
$\mathcal{L}_{FG}$	77.4	58.8	32.4	15.4	5.3	0.1

The change in criticality index values associated with the locations in France ($\mathcal{L}_F$) for different (δ, α, c) instances is depicted in Figure 3.2a. For a time window length of 24 hours, as the global criticality threshold decreases, the proportion of critical windows drops from 85.1% ($c/|L| = 0.5$) to 66.6% ($c/|L| = 0.8$) and, finally, to 10.6% if $c/|L| = 1.0$. The same decreasing trend applies for all other δ values, with the score of the $\mathfrak{f}_C$ index observed to be increasing as the window length is extended. Results corresponding to the available locations in Greenland are presented in Figure 3.2b. Superior resource quality in this region is evidenced by the range of the resulting criticality indices. For instance, in case of a δ value of 24 hours, a drop in the proportion of critical time windows from 29.4% (for $c/|L| = 0.5$) to 8.5% ($c/|L| = 0.8$) and 0.3%, when $c/|L| = 1.0$, can be seen. Contrary to the change in criticality index values for the locations in France, it can be observed that, for each global criticality threshold (c), the criticality index values in Greenland decrease as the length of the time window increases.

In this particular (δ, α, c) configuration, the opposing development of $\mathfrak{f}_C$ with respect to δ stems from (i) the positioning of α between the average capacity factors of the two regions and (ii) the utilisation of a resource quality mapping $\mathfrak{q}$ returning the mean signal over each time window. Under these assumptions, the following can be observed. On the one hand, the chosen α is greater than the average capacity factor observed in France (i.e., 22%). Given the resource quality mapping considered, the probability of a random time window sample being critical is greater for large values of δ since less frequent occurrences of high energy output in this region are averaged over the time window length (thus cancelling the extreme wind events and rendering the time window critical overall). On the other hand, α is smaller than the estimated average capacity factor in Greenland (i.e., 48%). In this case, the opposite of the aforementioned situation holds, with short time windows being more likely to turn out critical for a given (α, c) pair. This happens since, for a resource-rich area, low wind events have a greater impact (in terms of time window criticality) on short time horizons, while the effects of those same events are often annihilated when computing the resource quality mapping for larger δ values.

Lastly, the outcome of coupling the two regions ($\mathcal{L}_F$ and $\mathcal{L}_G$) is displayed in Figure

3.2c. As for Greenland, the criticality index decreases as the time window length (δ) increases. It should also be noted that, except for the $c/|L| = 1.0$ case, the criticality indices in Figure 3.2c are, for all (δ, c) configurations, smaller than the ones associated with the locations in France ($\mathcal{L}_F$) and greater than the ones corresponding to the sites in Greenland ($\mathcal{L}_G$). This can be explained by the fact that the influence of the inferior wind resource in France is more pronounced for lower values of $c/|L|$. Nevertheless, the impact of the high-quality wind resource of Greenland is observed in the shape of the plotted curves which, compared to the ones associated to France (Figure 3.2a), change curvature, leading to a steeper drop of the $\mathfrak{f}_C$ values as the c factor increases. Numerically, given a window length of 24 hours, the criticality index decreases from 77.4% ($c/|L| = 0.5$) to 15.4% ($c/|L| = 0.8$) and, to 0.1%, for a $c/|L|$ value of 1. These observations already give a clear indication of the benefits of harvesting wind energy in Greenland in order to complement the existing wind regimes in France. For the sake of clarity, the output values of the criticality indicator for different locations sets, global criticality threshold values and considering a 24-hour time-window length are summarised in Table 3.1.

3.5.2 Optimal Deployment of Generation Sites

This subsection details the results of the minimisation problem defined in Eq. (3.5). More specifically, the optimal deployment of n generation sites across B areas is assessed for different input regions (e.g., $\mathcal{L}_F, \mathcal{L}_G, \mathcal{L}_{FG}$), a given triplet (δ, α, c) and taking account of pre-defined constraints on the geographical repartition of wind farms throughout the B sub-regions. A time window length δ of 168 hours (one week), a local criticality threshold α of 35% and a global criticality threshold $c/|L|$ of 1 are considered for illustrative purposes in the following example. Algorithm 1 provides a suboptimal solution to the optimisation problem at hand, and results are shown in Figure 3.3.

The optimal deployment of five generation sites within the available locations in southern Greenland and continental France is shown in Figure 3.3a and Figure 3.3b, respectively. At first glance, it can be observed that the identified generation sites are evenly distributed over the regions of interest, again revealing (this time visually) the complementarity of wind regimes across dispersed locations even on the regional scale. Also, the actual wind farm locations in both cases can be explained via well-documented, prevailing local or regional wind regimes. For Greenland, the deployment of all but one wind farm is in line with the spatial occurrence of local katabatic flows [119]. Shifting to France, two wind farms are deployed in the resource-richer north, while the remaining ones are built in southern areas often swept by strong, local winds (the Mistral and Tramontane) [120]. Numerically, the five locations in France display a 15% probability of critical windows occurrence, while the superior wind resource in Greenland translates to an almost zero (0.4%) criticality index value.

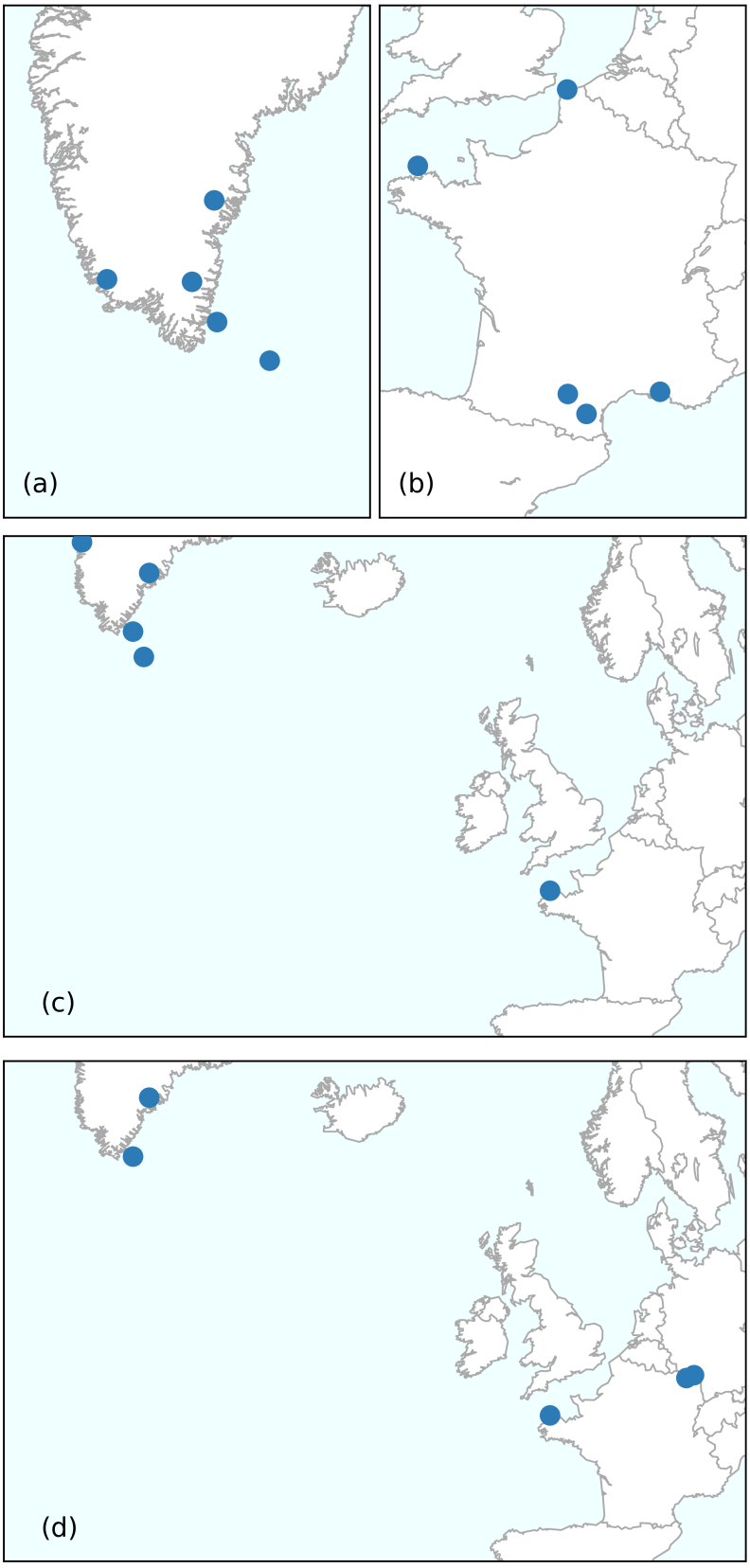

FIGURE 3.3: Visualisation of the optimal deployment of five wind farms in (a) Greenland, (b) France, (c) the aggregation of the two without and (d) with constraints on the geographical repartition. Results corresponding to a time window length (δ) of one week, a local criticality threshold (α) of 35% and a global criticality threshold ($c/|L|$) of 1.

The results of two variations on the same minimisation problem applied to the aggregated locations set ($\mathcal{L}_{FG}$) are discussed next. Figure 3.3c displays the optimal distribution of generation sites in France and Greenland without any deployment constraints. This variant corresponds to the case of a single, aggregated input region (i.e., $B = 1$). Numerically, the proportion of one-week-long time windows with generation levels under 35% capacity factor across all five sites is only 0.005% over the full time horizon. Nevertheless, constraints on the geographical repartition of the generation sites can play a decisive role, as can be observed in Figure 3.3d. This plot shows the optimal deployment of the five sites considering the number of wind farms to be developed in Greenland is limited to two, in which case the criticality index score increases to 0.06%.

3.5.3 Comparison with Average Capacity Factors as Primary Criterion

It is particularly insightful to compare the generation site selection according to different criteria. In particular, the usual criterion used for wind farm deployment is the generation potential (or the average capacity factor) of the site. A comparison between this indicator and the complementarity criterion proposed in this chapter is presented in Figure 3.4 for the case of France. In this plot, the red markers are associated with the solution of the minimisation problem (3.5). The yellow ones correspond to the five best locations in $\mathcal{L}_F$ (see Figure 3.1), strictly from a generation potential perspective (i.e., locations are ranked based on integrated capacity factor values over the available time horizon). The green point represents a generation site common to both solutions.

The minimisation problem returns a deployment pattern whose criticality indicator value stands at roughly 0.15, which corresponds to a 15% probability of observing simultaneous low-production events. The criticality indicator value associated with the five most productive sites is much higher (23.6%). In other words, for a capacity factor threshold of 35% and compared with the locations set identified through the minimisation problem, the likelihood of recording a 168-h long critical window across the five most productive sites is 60% higher. This increase stems from the geographical proximity of the locations, which makes them subject to very similar wind regimes. However, the improvement in criticality indicator value for the locations with highest complementarity comes at the expense of total annual output. While the five most productive wind farms boast an aggregated capacity factor value of 46% over the entire time horizon considered, the locations with highest complementarity only have an aggregated capacity factor value of 34%.

Overall, these results suggest that a trade-off exists between high production levels and a reduced occurrence of simultaneous low-production events, and such considerations should be accounted for in planning decisions and incentive schemes.

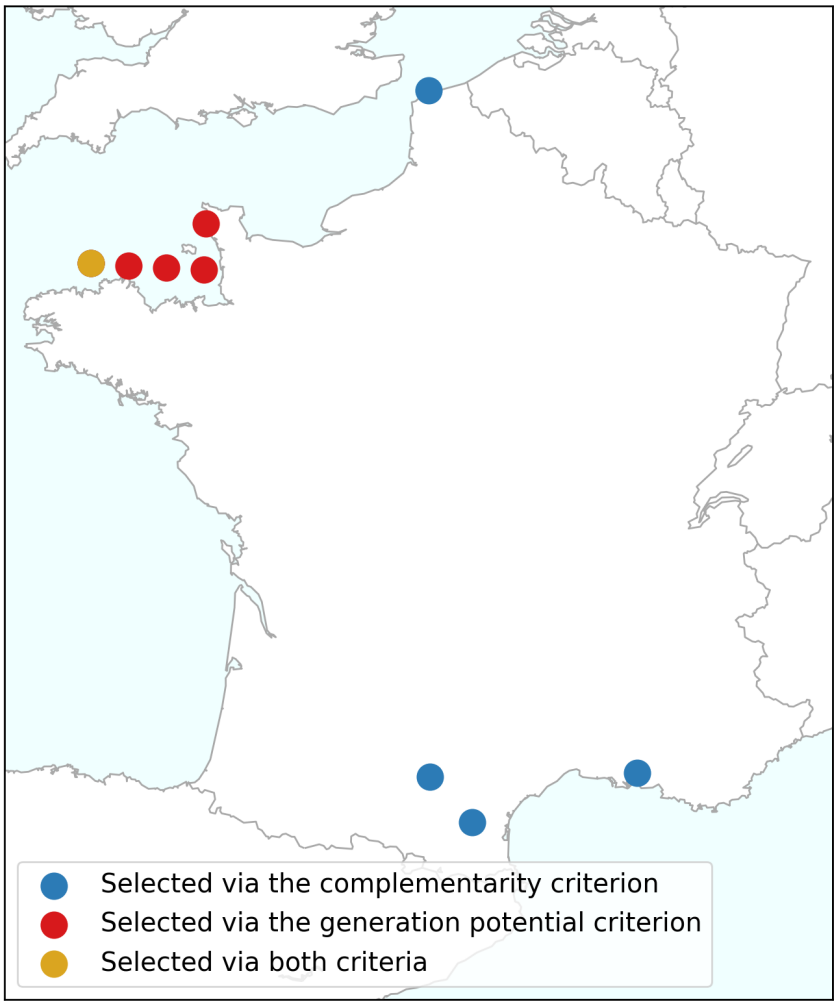

FIGURE 3.4: Comparison of criticality index-based (blue) and electricity yield-based (red) deployment of wind farms within a given subset of locations, based on the criticality indicator values. Example depicting the results for the subset of potential generation sites in France, $\mathcal{L}_F$.

TABLE 3.2: Influence of the local criticality threshold (α) on the trade-off between criticality index gain and average capacity factor loss in the context of deployment strategy comparison between (i) criticality index minimisation and (ii) average capacity factor as selection criterion. Numerical results displayed for one-week-long time windows ($\delta = 168$) and global criticality thresholds ($c/|L|$) of 1.

α	-	0.15	0.35	0.40	0.45	0.65
$\Delta \mathfrak{f}_C$	%	-99.6	-36.4	-27.6	-20.4	-1.9
$\Delta \tilde{\pi}$	%	-28.2	-26.0	-26.0	-26.0	-16.6

3.5.4 Discussion

A key factor impacting the accuracy of results presented in Section 3.5 is the accuracy of the raw data used throughout the analysis. In this respect, it has been previously shown that significant spatial bias can be identified in the ability of reanalysis models to recreate RES patterns in certain topographies [88]. This undesirable feature is also observed in the current study that uses ERA5 as reanalysis database. Comparing modelled average capacity factors (as computed from ERA5 resource data) with actual realisations of the regions where the generation sites in Figure 3.4 are located, non-negligible differences can be observed. On the one hand, for the locations in Southern France, the computed average capacity factor is close to 25%, a value which is just about the official statistics (27.4% in 2016) [94]. On the other hand, a clear positive bias of the reanalysis model can be observed for the six locations in Northern France. For these locations, a modelled average capacity factor of 45% is significantly higher than the reported 19-22% values associated with the corresponding French regions in 2016 [94] but it seems unlikely that the aforementioned bias alone leads to such a substantial difference. At any rate, the sole purpose of the wind database used in this work is to illustrate the mathematical framework proposed in Section 3.3 and the continuous improvement of reanalysis models over the years suggests that these tools could be used more reliably in such applications in the near future. Nevertheless,final decisions on wind farm site selection should be confirmed by extensive in-situ measurements.

One interesting implication of the proposed methodology stems from the results presented in Section 3.5.3, which suggest the existence of a trade-off between maximising energy volumes (and revenues, in current regulatory settings) and maximising continuity of supply (via the criticality index) in the planning process of RES generation. This aspect brings into question the regulatory frameworks favouring the former option and potential enhancements that can be addressed in this regard. In a regulatory set-up that incentivises producers to provide ancillary network services (e.g., contributing to a base load provision of electricity from renewable sources), novel business cases could emerge by optimally deploying (from a criticality indicator standpoint) production sites in power systems relying heavily on renewable energy generation.

Table 3.2 provides additional insight into how the local criticality threshold value influences the properties of the deployment patterns obtained via Eq. (3.5), and how these properties compare with those of the deployment pattern maximising annual electricity output. More precisely, each entry in the second row shows the relative difference in criticality indicator values between the deployment pattern maximising complementarity and the one maximising electricity output, respectively. Thus, each entry expresses the change in the number of critical time windows between deployment patterns, and a negative sign indicates that the pattern maximising complementarity has fewer critical time windows.Then, the third row gives the relative difference in average capacity factor values. A negative sign indicates that the power generation potential of the deployment pattern maximising complementarity is lower than that of the pattern maximising electricity output. Now, inspecting the second row reveals that the change in criticality indicator values becomes smaller as the value of the local criticality threshold increases. In other words, a deployment pattern produced by (3.5) for a high value of the local criticality threshold has a number of critical time windows roughly equal to that observed for the deployment pattern maximising electricity output. A similar trend is observed in the third row. It therefore appears that the deployment patterns produced by (3.5) converge towards the deployment pattern maximising electricity output as the local criticality threshold value increases. It is also worth noting that, in contrast to the differences in criticality indicator values, the differences in average capacity factor values remain constant over a range of α values. This observation suggests that deployment patterns displaying the same level of annual electricity output can exhibit different levels of complementarity. Hence, the method developed in this work also allows for the identification of deployment patterns maximising complementarity within a subset of locations with a pre-specified level of electricity output, which can be simply achieved by tuning the local criticality threshold parameter.

3.6 Conclusion and Future Work

A framework to systematically assess the complementarity of dispersed variable renewable energy resources over arbitrary time scales has been presented. The framework relies on the concept of critical time windows, which provide an accurate, time-domain description of low probability RES power generation events impacting power system operation and planning. A scalar indicator quantifying the complementarity dispersed RES generation sites may exhibit is derived, providing a practical tool to evaluate the respective merits of different RES deployment patterns. This indicator is also leveraged to formulate optimisation models seeking to identify deployment patterns with the smallest occurrence of low production events within a region of interest.

The usefulness of the proposed framework is illustrated by a case study investigating the complementarity between wind regimes within and between continental

France and southern Greenland. The analysis reveals that a significant reduction in the occurrence of system-wide low RES generation events can be achieved when the two areas are spatially aggregated, pointing to potential benefits of such intercontinental electrical interconnections. Moreover, the solutions to optimisation problems derived from the criticality indicator shows that the occurrence of low power production events can also be reduced on a regional scale by exploiting the diversity in local wind regimes. In essence, results confirm the intuition that deploying generation sites across continents makes it possible to simultaneously take advantage of high-quality resources and exploit the greater diversity in wind regimes in order to substantially reduce the occurrence of simultaneous low power generation events. The relevance of the proposed methodology in a power systems planning context is further supported by a comparison of two wind farm deployment strategies favouring complementarity and seeking to maximise annual electricity output, respectively. These two approaches, which were tested in continental France, yield starkly different deployment patterns, with implications for planning strategies in future power systems dominated by vast shares of renewable-based generation, where maintaining adequate levels of security of electricity supply may require a comprehensive assessment of renewable resource complementarity.

Several research avenues can be pursued in future work. For instance, a straightforward extension of the present analysis would consist in applying the framework to investigate the complementarity between different renewable resource types across much greater geographical areas, possibly spanning several continents simultaneously. From a computational standpoint, recasting the proposed optimisation problems in a more structured form would be beneficial, as it would enable the use of efficient off-the-shelf solvers, e.g. branch-and-bound, which would provide certificates of optimality. If such efforts prove fruitless, a comprehensive analysis and extension of the proposed heuristic to cases in which $c/|L| \neq 1.0$ would be needed. Finally, further exploring the trade-off between maximising complementarity and annual electricity output would be particularly useful for planning purposes. More precisely, quantifying the value of complementarity in economic terms would make it possible to identify whether transmission, dispatchable generation or storage capacity expansion strategies should be pursued to ensure adequacy in a power system with ever-increasing shares of variable renewable resources. In the same vein, updating the optimisation problems to include other constraints and costs, for instance reflecting a desired level of installed renewable generation capacity or the difficulty to connect to existing infrastructure, would allow for a more complete assessment of renewable generation deployment options.

Chapter 4

Evaluating the Impact of Siting Strategies on the Design of Power Systems

This chapter provides a detailed account of the impact of different offshore wind siting strategies on the design of the European power system. To this end, a two-stage method is proposed. In the first stage, a highly-granular siting problem identifies a suitable set of sites where offshore wind plants could be deployed according to a pre-specified criterion. Two siting schemes are analysed and compared within a realistic case study. These schemes essentially select a pre-specified number of sites so as to maximise their aggregate power output and their spatiotemporal complementarity, respectively. In addition, two variants of these siting schemes are provided, wherein the number of sites to be selected is specified on a country-by-country basis rather than Europe-wide. In the second stage, the subset of previously identified sites is passed to a capacity expansion planning framework that sizes the power generation, transmission and storage assets that should be deployed and operated in order to satisfy pre-specified electricity demand levels at minimum cost. Results show that the complementarity-based siting criterion leads to system designs which are up to 5% cheaper than the ones relying on the power output-based scheme when offshore wind plants are deployed with no consideration for country-based deployment targets. On the contrary, the power output-based scheme leads to system designs which are consistently 2% cheaper than the ones leveraging the complementarity-based siting strategy when such constraints are enforced. The robustness of the reported results is supported by a sensitivity analysis on offshore wind capital expenditure and inter-annual weather variability, respectively.

This chapter is a reprint of *David-Constantin Radu, Mathias Berger, Antoine Dubois, Raphaël Fonteneau, Hrvoje Pandžić, Yury Dvorkin, Quentin Louveaux, Damien Ernst, "Assessing the Impact of Offshore Wind Siting Strategies on the Design of the European Power System", Applied Energy 305, 117700, 2022,* https://doi.org/10.1016/j.aplen.2021.117700. Reprinted with permission from the publisher.

4.1 Introduction

The large-scale deployment of technologies harnessing renewable energy sources (RES) for electricity production has been a mainstay of climate and decarbonization policies. In Europe, solar photovoltaic and onshore wind power plants have formed the bulk of new renewable capacity additions for over a decade [121]. Nevertheless, in spite of the need for extra capacity deployments required to achieve ambitious decarbonization targets [3], the pace at which these technologies are deployed in a number of countries has remained sluggish of late [121], often as a result of social acceptance issues [122] and the phasing out of renewable support schemes. On the other hand, the economics of offshore wind power generation have greatly improved in recent years [123]. Offshore wind power plants are also located in unpopulated areas and are therefore less subject to social acceptance issues than onshore ones. Furthermore, the offshore wind resource is most often of much better quality than the onshore one [124]. Hence, the large-scale deployment of offshore wind power plants has increasingly been viewed as a key enabler of European decarbonization efforts [63], [91].

However, widely-available RES such as solar irradiance or offshore wind are inherently variable on time scales ranging from minutes to years and integrating them in power systems typically complicates planning and operational procedures [70]. Several solutions have been advocated to alleviate these issues, including the large-scale deployment of electricity storage systems [66], [125] or the implementation of demand response programs [67]. Alternatively, since RES are heterogeneously-distributed in space and time, it has been suggested that siting RES electricity production assets so as to exploit this diversity may reduce the aggregate output variability of RES power plants as well as the residual electricity load (i.e., total load minus renewable production) [68], [126]. The concept of RES complementarity formalises this idea [96].

From a modelling perspective, the interplay between investment (both siting and sizing) and operational decisions should be accounted for in order to evaluate the impact of siting strategies on system design and economics. Hence, ideally, models should perform both siting and sizing simultaneously, have a high spatiotemporal resolution as well as a high level of technical detail. Unfortunately, such models quickly become impractical (e.g., require tens of thousands of core-hours [52]) or intractable. Thus, the siting and sizing problems have traditionally been tackled separately in the literature, but the outcomes of siting models have rarely been leveraged in sizing models.

In this paper, the role that offshore wind power plants may play in the European power system is analysed, with a particular focus on the impact that plant siting strategies have on system design and economics. To this end, a two-stage method is developed. In the first stage, a highly-granular siting problem is solved in order to

identify a suitable subset of candidate sites where offshore wind power plants could be deployed. Then, in the second stage, the subset of locations selected in the first stage is passed to a capacity expansion planning framework that sizes the power generation, transmission and storage assets that should be deployed and operated in order to satisfy pre-specified electricity demand levels at minimum cost subject to technical and policy constraints. An open source tool implementing the two-stage method is also provided for the sake of transparency.

Two types of deployment schemes that select sites so as to maximise their aggregate power output and spatiotemporal complementarity are analysed. Roughly speaking, sites are considered complementary if they rarely experience simultaneous low electricity production events [127]. Two variants of these siting schemes are studied, wherein the number of sites to be selected is specified on a country-by-country basis rather than Europe-wide. A few hundred sites are identified using each scheme, by leveraging a high resolution grid and ten years of reanalysis data [86]. These sites are then passed to a capacity expansion planning framework relying on a stylised model of the European power system where each country corresponds to an electrical bus and including an array of power generation and storage technologies. The framework sizes gas-fired power plants, offshore wind power plants, battery storage and electricity transmission assets and operates the system so as to supply electricity demand levels consistent with current European electricity consumption at minimum cost while reducing carbon dioxide emissions from the power sector by 90% compared with 1990 levels and taking a broad range of legacy assets into account. A detailed sensitivity analysis is also performed in order to evaluate the impact of offshore wind cost assumptions and inter-annual weather variability on system design and economics.

This manuscript is organised as follows. Section 4.2 reviews the relevant studies in the literature. Section 4.3 presents the two-stage method used to evaluate the impact of RES siting strategies on power system design and economics. The case study is introduced in Section 4.4, while results are presented and analysed in Section 4.5. Section 4.6 concludes the chapter and discusses future work avenues.

4.2 Related Works

The precise estimation of required capacities and incurred costs in RES-dominated power systems relies heavily on the detailed modelling of RES assets [51]. In one of the first studies to quantify the impact of this modelling aspect, Krishnan and Cole [57] reveal that using 356 and 134 profiles to model the wind and solar resource, respectively, within the contiguous US leads to significantly different capacity outcomes compared to the case where the same resources are modelled via one single profile per state (i.e., 48 profiles per resource). For example, the solar PV capacity difference between the two set-ups exceeded 32 GW, or 10% of the total installed

capacity for this technology. In a more recent assessment, Frysztacki et al. [60] evaluate the role of high-resolution RES siting in a study focusing on the European power system. They confirm the findings of [57] regarding the considerable impact of RES representation on the installed capacity requirements and, in addition, point out that modelling RES via 1024 different profiles leads to 10.5% lower system costs compared to more simplified set-ups using only 37 distinct profiles (i.e., one per country) per renewable resource. In the following, the detailed representation of RES to produce an accurate (i.e., high-resolution) assessment of the most suitable locations for asset deployment will be referred to as *siting*. A set-up where the detailed RES representation is integrated in models whose outcomes include installed capacities and associated costs, will be referred to as *sizing*.

The siting of RES assets has been a growing research topic lately. The models tackling this problem typically put more emphasis on the representation of renewable resources at the expense of other modelling features such as network or time-coupling constraints. In addition, they use non-monetary objectives such as, e.g., residual load or resource variability minimization. For instance, Jerez et al. [128] propose a tool which enables the distribution of RES capacities, as well as their output estimation via several transfer functions, across a regular grid with a spatial resolution of 0.44°. The problem is tackled by first computing distribution keys that take into account resource quality, population density and the existence of protected areas and then leveraging them to spread pre-defined capacities of RES across the system. Becker and Thrän [129] propose a method that sites wind generators such that the correlation (estimated via the Pearson coefficient) of the underlying resource with that of existing assets is minimized. A heuristic is also designed to solve the problem. Then, Musselman et al. [130] tackle the wind farm siting problem via two different bi-objective models formulated as mixed-integer linear programs (MILP). The first model seeks to simultaneously minimize i) the average residual demand and ii) the average power output variability (measured as the absolute change in residual demand between consecutive periods), while the second model simultaneously minimizes i) the average residual demand and ii) the maximum increase in residual demand over a set of time periods of pre-specified length. Furthermore, Hu et al. [131] use linear programming and portfolio optimisation concepts to site RES assets such that the standard deviation of their aggregate feed-in (i.e., the portfolio volatility) is minimized. However, overlooking the electricity demand in this process brings into question the ability of some of these methods [129], [131] to achieve proper siting. A framework siting RES assets such that the occurrence of simultaneous, system-wide low-generation events is minimized has been recently proposed by Berger et al. [127]. The problem has since been cast as an integer program (IP) for which several solution methods have been proposed [132]. Although they offer a valuable overview of different siting criteria proposed in the literature, a common drawback of all these studies is that they fall short in evaluating the implications of the corresponding outcomes on the design and economics of power systems. Such a

feature usually surfaces once a sizing model reveals the configuration of the power system.

The sizing of renewable power generation plants has been traditionally achieved via capacity expansion planning (CEP) frameworks, a class of problems which has received a great deal of attention in recent years [19]. For example, Baringo and Conejo [133] have studied the strategic investment in wind power generation assets by making use of a bi-level formulation in which investment decisions (siting and sizing) define the upper level and market clearing forms the lower level problem. In addition, Munoz et al. [134] tackled the joint generation and transmission expansion planning via a MILP where investment decisions are done in two stages, such that corrective actions are possible once uncertainty is revealed. In theory, such models are capable of evaluating the implications of RES siting on the design and economics of power systems. However, owing to computational limitations, these models usually have relatively low spatial and temporal resolutions, an aspect that makes it difficult to accurately capture correlations between variable renewable resources and properly site RES assets. Several attempts to integrate spatially-resolved siting of RES assets have been made, yet a common drawback can be identified across all of them. On the one hand, in line with [133], [134] where purely economic criteria are optimised, a study by MacDonald et al. [52] leverages a CEP framework cast as a linear program (LP) to jointly optimise generation, transmission and storage capacities. The model is instantiated with hourly-sampled RES and demand data, while a 13 km regular grid is used for an accurate representation of renewable resources. However, the approach is reported to require thousands of core hours to solve large-scale instances, a feature which makes it difficult to reproduce and limits its use in practice. Another study making use of a cost-minimization CEP framework cast as an LP sites RES assets over a 0.75° regular grid [135]. This time, the formulation of the CEP problem relies on a highly simplified temporal representation of the renewable resource availability (i.e., the hourly resolution is replaced by a 144-step duration curve), an aspect that often limits the ability of the underlying model to accurately estimate system needs [136]. On the other hand, non-economic optimisation criteria have also been used in sizing set-ups. For instance, Wu et al. [137] propose an IP for siting and sizing wind generation at high spatial resolutions (e.g., 3.6 km used in their study) such that the need for peak conventional generation feed-in is minimised. Nevertheless, their formulation, which relies on a full coefficient matrix, is computationally inefficient and its scalability is limited to a few hundred locations and one year of data with hourly resolution. In a similar fashion, Zappa and van den Broek [138] minimize year-round residual demand through a linearly constrained quadratic program. In the proposed model, RES assets are sited over the same regular grid used in [135]. However, their method suffers from similar scalability issues as [137], which limits the scale of problems tackled to a few hundred of RES sites and one year with hourly resolution.

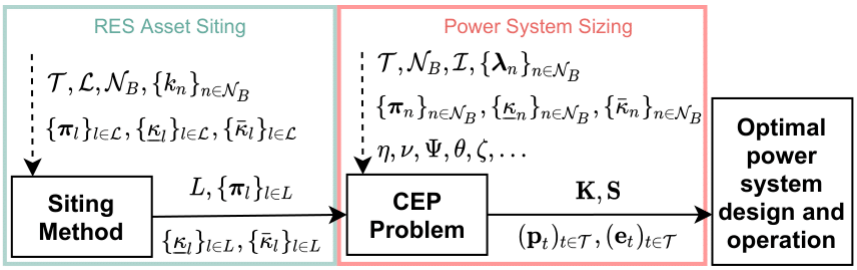

FIGURE 4.1: Workflow of the proposed two-stage method. Dotted arrows denote exogenous input streams, while full arrows represent output streams, respectively.

In this chapter, a method that enables the screening of thousands of candidate sites and tens of years of resources data is leveraged to evaluate the economic impact of different strategies for siting offshore wind across European Seas. To this end, a two-stage routine that bridges the gap between the streams of literature independently tackling the siting and sizing of RES assets in CEP frameworks is proposed. At first, siting of RES assets is addressed via an integer programming problem with a non-monetary objective. Then, linear programming is used to formulate a cost-minimization capacity expansion planning problem that unfolds some of the implications of siting RES assets according to predefined criteria.

4.3 Methodology

This section describes the two-stage method combining asset siting schemes and a capacity expansion planning model. Some basic notation used throughout this section is first introduced. The models and solution methods used in the siting stage are discussed next. Finally, the capacity expansion planning framework is presented. A visual representation of the proposed workflow is shown in Figure 4.1.

4.3.1 Preliminaries

A finite time horizon $T \in \mathbb{N}$ and associated set of time periods $\mathcal{T} = \{1, \ldots, T\}$ are considered. A geographical area is represented by a finite set of sites $\mathcal{L}, |\mathcal{L}| = L$, which may be partitioned into a collection of disjoint regions $\mathcal{L}_n \subseteq \mathcal{L}$, $\forall n \in \mathcal{N}_B$, where $\mathcal{N}_B, |\mathcal{N}_B| = B$, may for instance represent the set of electrical buses in a power system and $\mathcal{L}_n$ may represent a set of candidate RES sites that may be connected to bus $n \in \mathcal{N}_B$. Each location $l \in \mathcal{L}$ is assumed to have a fixed technical potential $\bar{\kappa}_l \in \mathbb{R}_+$, which represents the maximum capacity that may be deployed at this location. In addition, some legacy capacity $\underline{\kappa}_l \in \mathbb{R}_+$ may have already been deployed at sites $l \in \mathcal{L}_0 \subseteq \mathcal{L}$. A time series $\mathbf{s}_l = \left(s_{l1}, \ldots, s_{lT}\right) \in \mathbb{R}_+^T$ describing renewable resource data (e.g., wind speed, solar irradiation) over $\mathcal{T}$ is assumed to be available at each location $l \in \mathcal{L}$. Furthermore, the instantaneous power output

of location $l \in \mathcal{L}$ is estimated via a suitable transfer function $\mathfrak{h}_l$ that returns per-unit capacity factor values $\pi_{lt} = \mathfrak{h}_l(s_{lt}), \forall t \in \mathcal{T}$, which are stored in a time series $\boldsymbol{\pi}_l = \left(\pi_{l1}, \ldots, \pi_{lT}\right) \in \{0,1\}^T$. This transfer function may be that of a single RES power generation technology (e.g., a wind turbine or a solar PV module) or that of an entire power station (e.g., a wind farm or a PV power station).

4.3.2 Siting Schemes

The models and solution methods used in asset siting schemes are described in this section.

Models

Models that select a pre-specified number of suitable candidate sites so as to optimise a given criterion are introduced. Two different criteria are considered, leading to two different siting schemes. The first criterion measures the aggregate power output (*PROD*), while the second one measures the spatiotemporal complementarity that sites exhibit (*COMP*). Both siting problems are cast as integer programming models.

Aggregate Power Output This siting scheme selects a collection of disjoint subsets of locations so as to maximise their average capacity factor. More precisely, a pre-specified number of locations $k_n \in \mathbb{N}$ (including legacy locations) is selected in each region $\mathcal{L}_n$, and the total number of locations that must be deployed is $k = \sum_{n \in \mathcal{N}_B} k_n$. In order to formulate this problem as an IP, a set of binary variables is introduced. Indeed, a binary variable $x_l \in \{0,1\}$ is used to indicate whether location l is selected for deployment, that is, $x_l = 1$ if location l is selected for deployment and $x_l = 0$ otherwise. A binary matrix with entries $A_{nl} \in \{0,1\}$ is also used to indicate whether location l belongs to region $\mathcal{L}_n$, such that $A_{nl} = 1$ if this is the case and $A_{nl} = 0$ otherwise. Note that since regions are disjoint, each column of this matrix has exactly one nonzero entry, and we may assume without loss of generality that locations are ordered such that matrix A is block diagonal. The problem at hand then reads

$$\max_{x_l} \quad \frac{1}{k} \sum_{l \in \mathcal{L}} x_l \left[\frac{1}{T} \sum_{t \in \mathcal{T}} \pi_{lt} \right] \tag{4.1a}$$

$$\text{s.t.} \sum_{l \in \mathcal{L}} A_{nl} x_l = k_n, \ \forall n \in \mathcal{N}_B, \tag{4.1b}$$

$$x_l = 1, \ \forall l \in \mathcal{L}_0, \tag{4.1c}$$

$$x_l \in \{0,1\}, \ \forall l \in \mathcal{L}. \tag{4.1d}$$

The objective function (4.1a) computes the average capacity factor of the locations selected for deployment. The cardinality constraints (4.1b) ensure that exactly k_n

locations are selected in region $\mathcal{L}_n$, $\forall n \in \mathcal{N}_B$, while constraints (4.1c) guarantee that legacy assets are taken into account. Finally, constraints (4.1d) express the binary nature of location selection decisions.

Spatiotemporal Complementarity This siting scheme selects a collection of disjoint subsets of locations so as to maximise their spatiotemporal complementarity. Recall that, in this manuscript, locations are considered complementary if they rarely experience simultaneous low electricity production events (compared with a prespecified reference production level) [127], [132]. The framework that makes it possible to cast this problem as an IP is discussed next.

First, a set of time windows $\mathcal{W}$, $|\mathcal{W}| = W$, is constructed from the set of time periods $\mathcal{T}$. More precisely, a time window $\mathrm{w} \in \mathcal{W}$ can be seen as a subset $\mathcal{T}_\mathrm{w} \subseteq \mathcal{T}$ of δ successive time periods, and all time windows $\mathrm{w} \in \mathcal{W}$ have the same length δ. Note that successive time windows overlap and share exactly $\delta - 1$ time periods, while the union of all time windows covers the set of time periods $\mathcal{T}$. Then, the per-unit power generation level $\overline{\pi}_{l\mathrm{w}} \in [0,1]$ of each candidate site $l \in \mathcal{L}$ is evaluated over the duration of each time window $\mathrm{w} \in \mathcal{W}$ using a prescribed measure $\mathfrak{q}_l$, such that $\overline{\pi}_{l\mathrm{w}} = \mathfrak{q}_l(\{\pi_{lt}\}_{t\in\mathcal{T}_\mathrm{w}})$. This measure may for instance compute the average production level over each window $\mathrm{w} \in \mathcal{W}$. This would essentially be equivalent to applying a moving average-based filter to the original power production signal and result in a smoothed power output signal. The degree of smoothing would be controlled by δ, which makes it possible to study resource complementarity on different time scales. A local, time-dependent reference production level $\alpha_{l\mathrm{w}} \in \mathbb{R}_+$ is also specified at each candidate site $l \in \mathcal{L}$, and may for instance be proportional to the electricity demand. A location $l \in \mathcal{L}$ is considered productive enough over window w if $\overline{\pi}_{l\mathrm{w}} \geq \alpha_{l\mathrm{w}}$. Location l is then said to *cover* window w and be *non-critical*. Checking whether this condition is satisfied for all locations and time windows enables the construction of a binary matrix with entries $D_{l\mathrm{w}} \in \{0,1\}$, such that $D_{l\mathrm{w}} = 1$ if location l covers window w and $D_{l\mathrm{w}} = 0$ otherwise. In order to formalise the intuitive definition of resource complementarity introduced earlier, a threshold $c \in \mathbb{N}$ is specified, such that for any subset of candidate locations $L \subseteq \mathcal{L}$, a window $\mathrm{w} \in \mathcal{W}$ is said to be *c-covered* or *non-critical* if at least c locations cover it (i.e., produce enough electricity over its duration). More formally, window w is non-critical if $\sum_{l\in L} D_{l\mathrm{w}} \geq c$.

Using the notation introduced for the first siting scheme, formulating the integer programming problem only requires the definition of a set of additional binary variables. More precisely, for each window $\mathrm{w} \in \mathcal{W}$, a binary variable $y_\mathrm{w} \in \{0,1\}$ indicating whether window w is non-critical is introduced, such that $y_\mathrm{w} = 1$ if window w is non-critical and $y_\mathrm{w} = 0$ otherwise. The problem of siting renewable power plants so as to maximise their spatiotemporal complementarity then reads

$$\max_{x_l, y_w} \quad \sum_{w \in \mathcal{W}} y_w \tag{4.2a}$$

$$\text{s.t.} \quad \sum_{l \in \mathcal{L}} D_{lw} x_l \geq c y_w, \ \forall w \in \mathcal{W}, \tag{4.2b}$$

$$\sum_{l \in \mathcal{L}} A_{nl} x_l = k_n, \ \forall n \in \mathcal{N}_B, \tag{4.2c}$$

$$x_l = 1, \ \forall l \in \mathcal{L}_0, \tag{4.2d}$$

$$x_l \in \{0, 1\}, \ \forall l \in \mathcal{L}, \tag{4.2e}$$

$$y_w \in \{0, 1\}, \ \forall w \in \mathcal{W}. \tag{4.2f}$$

The objective function (4.2a) simply computes the number of non-critical time windows observed over the time horizon of interest. Dividing the objective by the total number of time windows shows that it can be interpreted as quantifying the empirical probability of having sufficient levels of electricity production across at least c locations simultaneously. A low objective value therefore implies that simultaneous low electricity production events occur often, which indicates poor complementarity between locations. Note that this interpretation is opposite to the definition of $\mathfrak{c}$ in Chapter 2, however a simple re-formulation of (4.2a-4.2f) as a minimisation problem would level the definitions. Constraints (4.2b) define the binary classification of time windows and express the fact that a time window $w \in \mathcal{W}$ is non-critical if at least c locations selected for deployment cover it. The cardinality constraints (4.2c) ensure that exactly k_n locations are selected in region $\mathcal{L}_n$, $\forall n \in \mathcal{N}_B$, while constraints (4.2d) guarantee that legacy assets are accounted for in siting decisions. Finally, constraints (4.2e-4.2f) express the binary nature of location selection decisions and time window criticality, respectively.

Solution Methods

The solution methods used to tackle problems (4.1) and (4.2) are discussed next.

Aggregate Power Output Since the objective function (4.1a) is separable and the coefficient matrix in Eq. (4.1b) is block diagonal, problem (4.1a-4.1d) is straightforward to decompose and solve. More precisely, the k_n most productive locations can be selected independently in each region $\mathcal{L}_n$, $\forall n \in \mathcal{N}_B$. In each region $\mathcal{L}_n$, this can be achieved by successively i) computing the average capacity factor of each location $\tilde{\pi}_l = (1/T) \sum_{t \in \mathcal{T}} \pi_{lt}$, $\forall l \in \mathcal{L}_n$, ii) sorting locations based on their average capacity factor $\tilde{\pi}_l$, iii) adding the locations with the highest average capacity factors to a set $L_n \subseteq \mathcal{L}_n$ that initially contains the legacy locations belonging to region n, until $|L_n| = k_n$. The solution L to problem (4.1) is then obtained by taking the union of these sets, $L = \bigcup_{n \in \mathcal{N}_B} L_n$.

Spatiotemporal Complementarity An approximate solution method relying on a mixed-integer relaxation of problem (4.2) followed by a local search algorithm inspired by the simulated annealing algorithm [139] is used to tackle (4.2a-4.2f) [132]. The mixed-integer relaxation is formed by relaxing the integrality constraint (4.2f) of the time window variables. The key advantage of this approach lies in the fact that the siting variables $x_l, \forall l \in \mathcal{L}$, remain integer in the solution and subsets of locations $L_n \subseteq \mathcal{L}_n$, $\forall n \in \mathcal{N}_B$, can be directly extracted from them. The number of non-critical windows associated with this collection of subsets $L = \bigcup_{n \in \mathcal{N}_B} L_n$ can be computed via a function $\mathfrak{f}_C$ such that

$$\mathfrak{f}_C(L) = \left| \left\{ \mathrm{w} \in \mathcal{W} \middle| \sum_{l \in L} D_{\mathrm{w}l} \geq c \right\} \right|. \tag{4.3}$$

The local search algorithm starts from a subset of locations $L_0 \subseteq \mathcal{L}$ obtained by solving the mixed-integer relaxation of problem (4.2). Note that by construction, L_0 includes legacy locations and satisfies the cardinality constraints (4.2c). Since legacy locations cannot change, they are first removed from L_0 in order to initialise the incumbent solution $L \subseteq \mathcal{L}$. Likewise, legacy locations are removed from the set of candidate sites that may be selected in each region $\mathcal{L}_n$, $\forall n \in \mathcal{N}_B$. Then, the algorithm performs a fixed number of iterations $I \in \mathbb{N}$ in the hope of improving the incumbent solution. More specifically, in each iteration, a fixed number $N \in \mathbb{N}$ of neighbouring solutions or radius $r \in \mathbb{N}, r \leq k$ is drawn at random from the neighbourhood of the incumbent solution. This neighbourhood is formed by solutions that satisfy the cardinality constraints (4.2c) and share exactly $k - r$ locations with the incumbent solution. A neighbouring solution $\hat{L}$ can be constructed from the incumbent solution as follows. For each region $\mathcal{L}_n$, $\mathbf{s}(n)$ different locations are sampled uniformly at random from both $\mathcal{L}_n \setminus L$ and $\mathcal{L}_n \cap L$, and these locations are swapped. The numbers of locations sampled in different regions are chosen at random such that the cardinality constraints (4.2c) remain satisfied and $\sum_{n \in \mathcal{N}_B} \mathbf{s}(n) = r$. Then, each of the N neighbouring solutions is tested against the incumbent solution and stored in a temporary candidate solution $\tilde{L}$ if it is found to outperform previously-explored neighbouring solutions. Their performance is evaluated via the difference $\tilde{\Delta}$ between the objectives achieved by the neighbouring and incumbent solutions. Once N neighbouring solutions have been explored, the candidate solution corresponds to a neighbouring solution that maximises $\tilde{\Delta}$ among all sampled solutions. Note that $\tilde{\Delta}$ may be negative (i.e., if the algorithm does not manage to improve on the incumbent). If $\tilde{\Delta} > 0$, the candidate solution becomes the new incumbent solution. By contrast, if $\tilde{\Delta} < 0$, whether the candidate solution becomes the new incumbent solution depends on the outcome b of a random variable drawn from a Bernoulli distribution with parameter p. This parameter depends on both $\tilde{\Delta}$ and the so-called *annealing temperature* $T(i)$. Roughly speaking, the temperature controls the extent to which the search space is explored in an attempt to find better solutions and exit local optima. The temperature is specified by a *temperature schedule* that provides a

Algorithm 2 Local Search Algorithm

Require: L_0, $\mathcal{L}_0$, $\mathcal{N}_B$, $\{\mathcal{L}_n\}_{n\in\mathcal{N}_B}$, I, N, r, $T(i)$, $\mathfrak{f}_C$

$L \leftarrow L_0 \setminus \mathcal{L}_0$
for $n \in \mathcal{N}_B$ **do**
    $\mathcal{L}_n \leftarrow \mathcal{L}_n \setminus \mathcal{L}_0$
end for
$i \leftarrow 0$
while $i < I$ **do**
    $\tilde{\Delta} \leftarrow -\infty$
    $j \leftarrow 0$
    while $j < N$ **do**
        $\hat{L} \leftarrow L$
        $\mathbf{s} \leftarrow$ vector storing the number of locations to sample per region
        for $n \in \mathcal{N}_B$ **do**
            $S_+ \leftarrow \mathbf{s}(n)$ locations sampled from $\mathcal{L}_n \setminus L$ uniformly at random
            $S_- \leftarrow \mathbf{s}(n)$ locations sampled from $\mathcal{L}_n \cap L$ uniformly at random
            $\hat{L} \leftarrow (\hat{L} \setminus S_-) \cup S_+$
        end for
        $\hat{\Delta} \leftarrow \mathfrak{f}_C(\hat{L} \cup \mathcal{L}_0) - \mathfrak{f}_C(L \cup \mathcal{L}_0)$
        if $\hat{\Delta} > \tilde{\Delta}$ **then**
            $\tilde{L} \leftarrow \hat{L}$
            $\tilde{\Delta} \leftarrow \hat{\Delta}$
        end if
        $j \leftarrow j + 1$
    end while
    if $\tilde{\Delta} > 0$ **then**
        $L \leftarrow \tilde{L}$
    else
        $p \leftarrow \exp(\tilde{\Delta}/T(i))$
        draw b from Bernoulli distribution with parameter p
        if $b = 1$ **then**
            $L \leftarrow \tilde{L}$
        end if
    end if
    $i \leftarrow i + 1$
end while
$L \leftarrow L \cup \mathcal{L}_0$

Ensure: $L, \mathfrak{f}_C(L)$

temperature $T(i)$ for each iteration i. This procedure is repeated until the maximum number of iterations I is reached. Algorithm 2 summarises these ideas.

4.3.3 Capacity Expansion Planning Framework

Upon retrieving a suitable subset of locations $L \subseteq \mathcal{L}$ from the siting stage, the associated capacity factor time series $\{\boldsymbol{\pi}_l\}_{l\in L}$, legacy capacities $\{\underline{\kappa}_l\}_{l\in L}$ and technical potentials $\{\overline{\kappa}_l\}_{l\in L}$ are passed as input data to a capacity expansion planning (CEP) framework that determines the optimal power system design. More precisely, the CEP model described in (4.4a-4.4s) selects and sizes the power generation, transmission and storage assets that should be deployed and operated in order to satisfy pre-specified electricity demand levels across Europe at minimum cost subject to a set of technical and environmental constraints. In the formulation below, Latin letters denote optimization variables, while Greek characters represent problem parameters.

A set of working assumptions characterize the capacity expansion planning framework used in the current study. First, investment decisions in power system assets are made by a central planner that also operates the system, has perfect foresight, and whose goal is to minimise total system cost in a purely deterministic set-up. A static investment horizon is considered and the investment and operation problems are solved concurrently. Investment decisions are made once (at the beginning at the optimisation horizon), while operational decisions are taken on an hourly basis. Second, investments in generation, transmission or storage capacities are continuous variables and transmission expansion is limited to the reinforcement of existing corridors. Third, the network is represented by i) a set of existing nodes, which represent an aggregation of real electrical nodes and ii) a set of existing transmission corridors, which connect the aforementioned nodes. Legacy generation assets at existing nodes are taken into account. Additional dispatchable capacity (e.g., gas-fired power plants) may be added at those nodes, while additional RES generation capacity may also be built at existing nodes, provided that the local renewable potential is not fully exploited. Finally, as seen in (4.4a-4.4s), no unit commitment constraints are considered and the full operating range of dispatchable power plants is assumed stable.

The objective (4.4a) includes the capacity-dependent investment and fixed operation and maintenance (O&M) costs and the output-dependent variable O&M expenditures[1]. In addition, an economic penalty is enforced on electricity demand shedding. Then, the electricity supply and demand balance is enforced via (4.4b).

[1]Note that the VOM, as defined here, include the plan-specific variable operation and maintenance costs, fuel costs, as well as CO_2-related expenses.

$$\min_{\mathbf{K},\mathbf{S},(\mathbf{p}_t)_{t\in\mathcal{T}},(\mathbf{e}_t)_{t\in\mathcal{T}}} \sum_{\substack{n\in\mathcal{N}_B\\ l\in L_n}} (\zeta^l+\theta^l_f)K_l + \sum_{\substack{n\in\mathcal{N}_B\\ j\in\mathcal{G}\cup\mathcal{R}\cup\mathcal{S}}} (\zeta^j+\theta^j_f)K_{nj} + \sum_{\substack{n\in\mathcal{N}_B\\ s\in\mathcal{S}}} \zeta^s_S S_{ns} + \sum_{i\in\mathcal{I}} (\zeta^i+\theta^i_f)K_c$$
$$+ \sum_{t\in\mathcal{T}} \omega_t \Big[\sum_{\substack{n\in\mathcal{N}_B\\ l\in L_n}} \theta^l_v p_{lt} + \sum_{\substack{n\in\mathcal{N}_B\\ g\in\mathcal{G}\cup\mathcal{R}}} \theta^g_v p_{ngt} + \sum_{\substack{n\in\mathcal{N}_B\\ s\in\mathcal{S}}} \theta^s_v (p^C_{nst}+p^D_{nst}) + \sum_{i\in\mathcal{I}} \theta^i_v |p_{it}| + \sum_{n\in\mathcal{N}_B} \theta^{ens} p^{ens}_{nt} \Big] \tag{4.4a}$$

$$\text{s.t.} \sum_{\substack{n\in\mathcal{N}_B\\ l\in L_n}} p_{lt} + \sum_{g\in\mathcal{G}\cup\mathcal{R}} p_{ngt} + \sum_{s\in\mathcal{S}} p^D_{nst} + \sum_{i\in\mathcal{I}^+_n} p_{it} + p^{ens}_{nt} = \lambda_{nt} + \sum_{s\in\mathcal{S}} p^C_{nst} + \sum_{i\in\mathcal{I}^-_n} p_{it},$$
$$\forall n\in\mathcal{N}_B, \forall t\in\mathcal{T} \tag{4.4b}$$

The operation and deployment of the RES units whose locations are determined by leveraging the siting models in Section 4.3.2 are constrained by (4.4c) and (4.4d), respectively. The next six equations model the operation and sizing of the remaining generation units, including RES technologies that are not sited. More specifically, modelling aspects such as instantaneous in-feed (4.4e), ramp rates (4.4f-4.4g), minimum operating levels (4.4h), CO_2 emission levels (4.4i) or technical potential limitations (4.4j) are considered.

$$p_{lt} \leq \pi_{lt}(\underline{\kappa}_l + K_l),\ \forall l\in L_n, \forall n\in\mathcal{N}_B, \forall t\in\mathcal{T} \tag{4.4c}$$
$$\underline{\kappa}_l + K_l \leq \overline{\kappa}_l,\ \forall l\in L_n, \forall n\in\mathcal{N}_B \tag{4.4d}$$
$$p_{ngt} \leq \pi_{nt}(\underline{\kappa}_{ng} + K_{ng}),\ \forall n\in\mathcal{N}_B, \forall g\in\mathcal{G}, \forall t\in\mathcal{T} \tag{4.4e}$$
$$p_{ngt} - p_{ng(t-1)} \leq \Delta^+_g(\underline{\kappa}_{ng} + K_{ng}),\ \forall n\in\mathcal{N}_B, \forall g\in\mathcal{G}, \forall t\in\mathcal{T}\setminus\{0\} \tag{4.4f}$$
$$p_{ngt} - p_{ng(t-1)} \geq -\Delta^-_g(\underline{\kappa}_{ng} + K_{ng}),\ \forall n\in\mathcal{N}_B, \forall g\in\mathcal{G}, \forall t\in\mathcal{T}\setminus\{0\} \tag{4.4g}$$
$$\mu_g(\underline{\kappa}_{ng} + K_{ng}) \leq p_{ngt},\ \forall n\in\mathcal{N}_B, \forall g\in\mathcal{G}, \forall t\in\mathcal{T} \tag{4.4h}$$
$$q^{CO_2}_{ngt} = \nu^{CO_2}_g p_{ngt}/\eta_g,\ \forall n\in\mathcal{N}_B, \forall g\in\mathcal{G}, \forall t\in\mathcal{T} \tag{4.4i}$$
$$\underline{\kappa}_{ng} + K_{ng} \leq \overline{\kappa}_{ng},\ \forall n\in\mathcal{N}_B, \forall g\in\mathcal{G} \tag{4.4j}$$

It is worth mentioning the two most common situations in which the latter six constraints are enforced. On the one hand, if dispatchable units are modelled (e.g., gas-fired power plants), the time-dependent availability π_{nt} in Eq. (4.4e) is set to one across the entire optimisation horizon. On the other hand, if a RES technology not sited via the models in Section 4.3.2 is addressed, the aforementioned parameter is instantiated with a per-unit capacity factor time series that is aggregated at the spatial resolution represented by bus $n\in\mathcal{N}_B$. Furthermore, the per-unit ramp rates Δ^+_g and Δ^-_g in Eq. (4.4f-4.4g) are set to one, while the must-run and the specific CO_2 emission levels μ_g and $\nu^{CO_2}_g$, respectively, are set to zero.

$$p^D_{nst} \leq K_{ns},\ \forall n\in\mathcal{N}_B, \forall s\in\mathcal{S}, \forall t\in\mathcal{T} \tag{4.4k}$$
$$p^C_{nst} \leq \phi_s K_{ns},\ \forall n\in\mathcal{N}_B, \forall s\in\mathcal{S}, \forall t\in\mathcal{T} \tag{4.4l}$$

$$e_{nst} = \eta_s^{SD} e_{ns(t-1)} + \omega_s \eta_s^C p_{nst}^C - \omega_s \frac{1}{\eta_s^D} p_{nst}^D, \ \forall n \in \mathcal{N}_B, \forall s \in \mathcal{S}, \forall t \in \mathcal{T} \tag{4.4m}$$

$$\mu_s S_{ns} \leq e_{nst} \leq S_{ns}, \forall n \in \mathcal{N}_B, \forall s \in \mathcal{S}, \forall t \in \mathcal{T} \tag{4.4n}$$

$$\underline{\kappa}_{ns} \leq S_{ns} \leq \overline{\kappa}_{ns}, \ \forall n \in \mathcal{N}_B, \forall s \in \mathcal{S} \tag{4.4o}$$

Storage units are modelled via (4.4k) to (4.4o), assuming independent energy and power ratings and asymmetric charge and discharge rates, while constraints (4.4p) and (4.4q) define the transportation model governing the flow in transmission assets.

$$|p_{it}| \leq (\underline{\kappa}_i + K_i), \ \forall i \in \mathcal{I}, \forall t \in \mathcal{T} \tag{4.4p}$$

$$\underline{\kappa}_i + K_i \leq \overline{\kappa}_i, \ \forall i \in \mathcal{I} \tag{4.4q}$$

$$\sum_{\substack{n \in \mathcal{N}_B \\ g \in \mathcal{G} \\ t \in \mathcal{T}}} \omega_t q_{ngt}^{CO_2} \leq \Psi^{CO_2} \tag{4.4r}$$

$$\sum_{d \in \mathcal{D}} K_{nd} + \sum_{r \in \mathcal{R}} \Pi_{nr} K_{nr} + \sum_{l \in L_n} \Pi_l K_l \geq (1 + \Phi_n) \hat{\lambda}_n, \ \forall n \in \mathcal{N}_B \tag{4.4s}$$

A system-wide CO_2 budget is enforced via (4.4r). Then, a system adequacy constraint is enforced via (4.4s) following the definition provided in [140], according to which a system is adequate in the long-term by ensuring that the amount of firm capacity exceeds the peak demand by a planning reserve margin. According to Eq. (4.4s), this constraint is enforced at every bus $n \in \mathcal{N}_B$ and the corresponding peak demands and reserve margins are defined by $\hat{\lambda}_n$ and Φ_n, respectively. There are two main sources providing firm capacity. On the one hand, set $\mathcal{D}$ in the first term on the left-hand side gathers dispatchable power generation technologies. On the other hand, RES assets also contribute to the provision of firm capacity and their participation is proportional to their capacity credit, as defined in [141]. To this end, two sets of RES technologies are defined. The one in the second term of (4.4s) gathers the subset of RES technologies which are not sited, while L_n defines, for every $n \in \mathcal{N}_B$ the collection of sites obtained from the previous siting stage.

4.3.4 Implementation

With the exception of the siting algorithm (detailed in Section 4.3.2) which was implemented in Julia 1.4, the implementation of the proposed framework is based on Python 3.7. All simulations were run on a workstation running under CentOS, with an 18-core Intel Xeon Gold 6140 CPU clocking at 2.3 GHz and 256 GB RAM. The sizing problem (4.4a-4.4s) is implemented in PyPSA 0.17 [32]. Gurobi 9.1 was used to solve the MIR of (4.2a-4.2f), as well as (4.4a-4.4s).

4.4 Case Study

The upcoming section describes the case study used to investigate i) the outcome of siting offshore wind plants within European borders by leveraging the two siting

strategies introduced in Section 4.3.2 and ii) the impact these siting strategies have on the resulting power system configurations. First, the realistic set-up used in the siting stage is presented. Then, the main features of the CEP framework are introduced. Recall that, in this exercise, offshore wind is the only renewable resource for which siting decisions are analysed, while the other RES technologies (i.e., onshore wind, utility-scale and distributed PV) are modelled via aggregate, per-country profiles obtained from the *renewables.ninja* data platform [142], [143].

4.4.1 Offshore Wind Siting

Renewable Resource Data For this analysis, ten years (i.e., 2010 to 2019) of hourly-sampled wind speed data at a spatial resolution of 0.25° are obtained from the ERA5 reanalysis dataset [86]. The time series are then re-sampled by preserving the mean of each consecutive subset of three hours across the entire time horizon, yielding $T = 29216$ time periods. The conversion of raw resource data into capacity factor time series (a step required in both siting strategies introduced in Section 4.3.2) is achieved by applying the transfer function of a wind farm to the time series of wind speeds. Determining the appropriate wind farm transfer function for each candidate site involves a two-step process. First, the ten-year average wind speed is computed and the relevant IEC wind class is determined [144]. Once the wind class is known, an appropriate wind turbine is selected (in this exercise, two wind turbines are available, i.e., the Vestas V90 and V164 models) and the corresponding farm-specific transfer function is determined via a power curve smoothing procedure inspired from [90].

Deployment Targets Initially, an a priori filtering of candidate offshore wind locations is performed in order to discard sites where it would be impractical to deploy wind power plants. To this end, the following criteria are considered. First, a latitude threshold of 70° N is considered and all candidate locations beyond that limit are discarded. Second, sites with an average depth (i.e., the water depth across the entire reanalysis grid cell associated with the site) beyond 999 m are also discarded. Third, only candidate sites situated between 12 nm and 120 nm (i.e., nautical miles) from the shore are further considered [145]. Finally, sites where operational or already planned offshore wind farms exist [61] are added back to the set of candidate locations, in case they were discarded following the application of the aforementioned filters. As a result, a total of $L = 2472$ candidate offshore sites (whose distribution per EEZ can be seen in the $|\mathcal{L}_n|$ column of Table 4.1) are available in the siting stage. A visualization of the set of candidate sites is provided in Appendix A.1.

In order to compute the number of sites k that should be considered for deployment, the siting stage assumes the need for up to 450 GW of offshore wind across 19 Exclusive Economic Zones (EEZ) within Europe, in line with a recent study published under the aegis of the European Commission [91]. The conversion of the capacity

requirements within each EEZ (κ_n) into the cardinality constraints (k_n) required in (4.1a-4.1d) and (4.2a-4.2f) is achieved through Eq. (4.5), where $\lceil \cdot \rceil$ denotes the ceiling function, ρ_r denotes the power density of the RES technology $r \in \mathcal{R}$ (expressed in MW/km^2), σ_{site} represents the surface area of a (generic) candidate location (expressed in km^2) and ϵ_{site} denotes the dimensionless cell surface utilisation factor (since only a share of the cell surface area can be exploited for RES deployment purposes due to competing land uses). Given that, at this stage, the geo-positioning of the k sites to be identified is not known, average values for the last two parameters are considered. In particular, an offshore power density of 6 MW/km^2 (consistent recent developments in the North Sea basin [146]), a candidate site surface area of 442.5 km^2 (corresponding to a 0.25°-resolution cell at a latitude of 55° N) and a cell surface utilization factor of 50% were considered. In consequence, a total of 350 sites (whose per-country distribution can be seen in column $\tilde{k}_n$ of Table 4.1) are required to accommodate the targeted 450 GW of offshore wind.

$$\tilde{k}_n = \left\lceil \frac{\kappa_n}{\rho_r \times \sigma_{site} \times \epsilon_{site}} \right\rceil, \forall n \in \mathcal{N}_B \tag{4.5}$$

According to a recent survey [61], around 99 GW of offshore wind capacity are currently in operation or in various stages of planning (e.g., construction, permitting, etc.) within European borders. When siting RES assets, taking into account the existence of legacy installations has a significant impact on the final outcome, as their location (and the corresponding generation patterns) influences the resulting deployment schemes. In the exercise at hand, the exact geo-positioning of the available legacy wind installations (retrieved from [61]) is mapped to the reanalysis grid used to perform the siting exercise, such that each wind farm is associated with an ERA5 grid point. This procedure reveals that, among the $L = 2472$ candidate sites, $|\mathcal{L}_0| = 135$ of them (whose distribution per country is given in column $|\mathcal{L}_{0,n}|$ of Table 4.1) have at least 100 MW of legacy wind installations. At this point, a final adjustment is required to determine the values of k_n. This adjustment is necessary in two particular cases, i.e, i) when the number of legacy sites exceeds the previously computed $\tilde{k}_n$ or ii) when the number of candidate sites does not suffice to accommodate the required capacity under the aforementioned $(\rho_r, \sigma_{site}, \epsilon_{site})$ assumptions, and is enforced via Eq. (4.6). As a result of this final adjustment, three additional sites (i.e., all of them associated with the EEZ of Greece) are added to the sets of required deployments and candidate locations, respectively. The resulting values for k_n are gathered under the column with the same name in Table 4.1. Throughout the analysis, both partitioned (i.e., $B = 19$, where offshore wind sites are deployed whilst respecting the k_n values per EEZ specified in Table 4.1) and un-partitioned (i.e, $B = 1$, where the $k = \sum_{n \in \mathcal{N}_B} k_n$ sites are freely deployed across the European Seas) siting strategies will be investigated.

TABLE 4.1: Capacity requirements and cardinalities of various locations sets for the 19 European countries included in this study. Table entries sorted in descending order based on the capacity requirements per EEZ.

EEZ	κ_n [GW]	$\lvert\mathcal{L}_n\rvert$ [sites]	$\lvert\mathcal{L}_{0,n}\rvert$ [sites]	$\tilde{k}_n$ [sites]	k_n [sites]
UK	80	700	39	61	61
NL	60	102	8	46	46
FR	57	231	7	43	43
DE	36	81	17	28	28
DK	35	119	15	27	27
NO	30	187	1	23	23
PL	28	51	10	22	22
IE	22	219	5	17	17
IT	20	112	2	16	16
SE	20	254	9	16	16
FI	15	128	5	12	12
ES	13	77	0	10	10
GR	10	39	11	8	11
PT	9	17	1	7	7
BE	6	4	2	5	4
LV	4	8	1	4	4
LT	3	49	0	3	3
EE	1	47	2	1	2
HR	1	47	0	1	1

$$k_n = \min\{|\mathcal{L}_n|, \max\{|\mathcal{L}_{0,n}|, \tilde{k}_n\}\},\ \forall n \in \mathcal{N}_B \tag{4.6}$$

COMP Siting Set-Up The *COMP* siting strategy is carried out for a time window length δ of one time period (i.e., three hours). Then, a location $l \in \mathcal{L}$ is considered non-critical during time window w if its maximum theoretical generation potential exceeds a pre-defined share of the system-wide electricity demand. By expressing the former as the product between the technical potential $\overline{\kappa}_l$ and the capacity factor $\overline{\pi}_{l\mathrm{w}}$, this condition can be written as

$$\overline{\kappa}_l \overline{\pi}_{l\mathrm{w}} \geq \frac{\varsigma \overline{\lambda}_{\mathrm{w}}}{k}\,, \tag{4.7}$$

where ς represents the proportion of the electricity demand during window w (i.e, $\overline{\lambda}_{\mathrm{w}}$) to be covered by offshore wind plants (which in this exercise is uniformly set to 30%, as suggested in [147]) and k denotes the number of system-wide offshore wind deployments, whose per-partition distribution is detailed in Table 4.1. Dividing both

sides of Eq. (4.7) by $\overline{\kappa}_l$ yields the local criticality definition introduced in Section 4.3.2, where the reference production level $\alpha_{lw} = \varsigma\overline{\lambda}_w/\overline{\kappa}_l k$. Furthermore, threshold c in Eq. (4.2b) is set such that at least half of the locations must cover any time window for it to be labeled non-critical. In order to retrieve the *COMP* set of sites, Algorithm 2 is run thirty times and the solution with the highest objective function (i.e., the highest number of non-critical windows) is retrieved and passed to the subsequent CEP stage. With respect to the algorithm parameters, a neighbourhood radius r of 1, an initial temperature T of 100 and an exponential temperature schedule $T(i) = 100 \times \exp(-10 \times i/I)$ were considered. Additionally, $I = 5000$ iterations with $N = 500$ neighbouring solutions each are considered for each run of the algorithm.

4.4.2 Capacity Expansion Problem

Network Topology The set of countries considered in the sizing stage includes, aside from the ones listed in Table 4.1, Austria, Hungary, The Czech Republic, Slovakia, Switzerland (as landlocked territories), Bulgaria, Romania and Slovenia (with no offshore wind capacity mentioned in [91]). It should be noted that $L_n = \emptyset$ for the subset of countries previously mentioned (i.e., no offshore wind sites available). Each country is modelled as one node, while the network topology is based upon that used for the 2018 version of the *TYNDP* [55]. A map of the topology is provided in in Figure 4.2. It is hereby assumed that all interconnections crossing bodies of water are developed as DC cables, while the remainder are AC cables. As mentioned previously, transmission expansion decisions are limited to the reinforcement of existing corridors. The connection costs of offshore sites to the associated onshore buses depend on the capacity of the generation unit (representing a 20% share of the capital expenditure [148]), but not on the distance to shore. Hourly-sampled demand data covering the same ten years used in the siting stage (i.e., 2010 to 2019) is retrieved from [149]. Then, as in the previous siting stage, time series are resampled at three-hourly resolution by preserving the mean of each consecutive subset of three hours across the entire time horizon.

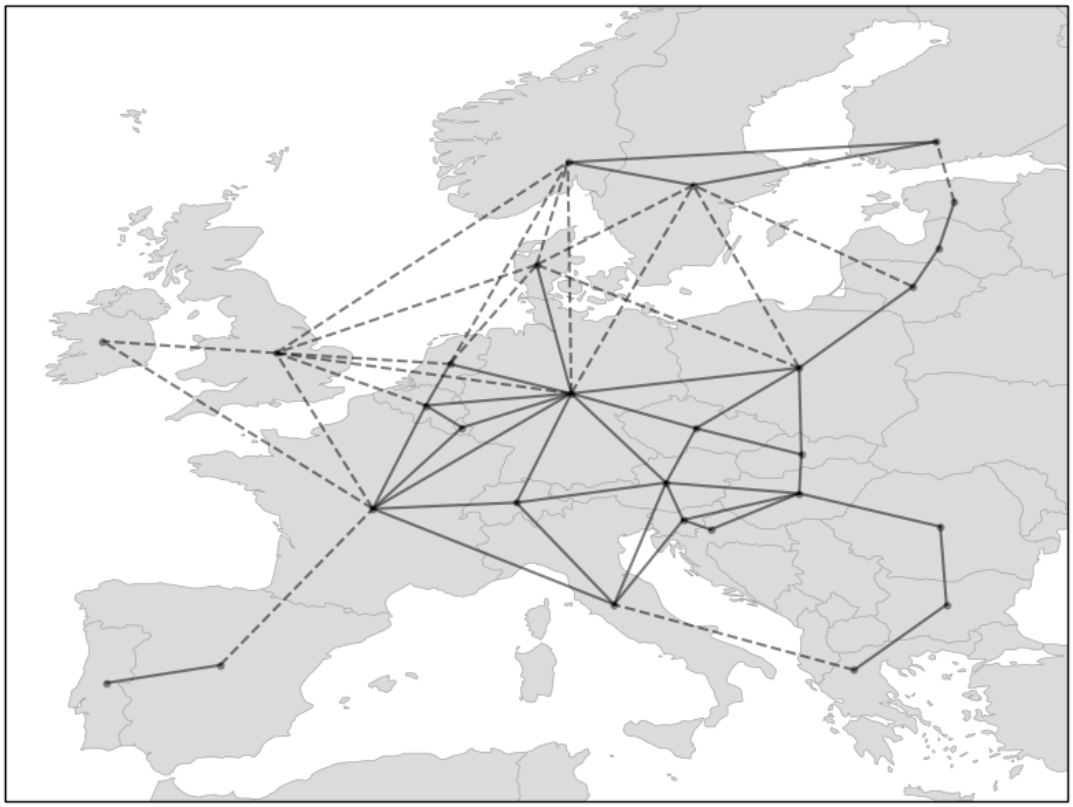

FIGURE 4.2: Network topology used in the capacity expansion planning stage.

TABLE 4.2: Summary of techno-economic parameters used to instantiate the CEP problem. N/A values denote either i) the lack of a capacity upper bound or ii) economic information which is irrelevant for the purpose of this study. Data sources are provided in Appendix A.1.

Technology	$\underline{\kappa}$ GW(h)	$\overline{\kappa}$ GW(h)	CAPEX M€/GW(h)	FOM M€/GW(h)-yr	VOM M€/GWh	Lifetime yrs
Onshore Wind	160.51	160.51	N/A	29.47	0.00	25
Offshore Wind	99.14	≈450.00[1]	1881.08	49.11	0.00	25
Utility-Scale PV	45.52	45.52	N/A	7.14	0.00	25
Distributed PV	77.69	77.69	N/A	5.36	0.00	25
OCGT	0.0	N/A	838.87	3.03	0.0076	30
CCGT	0.0	N/A	1005.27	7.58	0.0053	30
Nuclear	61.55	61.55	N/A	106.25	0.0018	N/A
Run-of-River Hydro	33.52	33.52	N/A	0.00	0.0119	N/A
Reservoir Hydro	98.12	98.12	N/A	0.00	0.0152	N/A
Pumped-Hydro	54.54	54.54	N/A	14.20	0.0002	N/A
Battery Storage[2]	0.00	N/A	100.00 / 94.00	0.54	0.0017	10
HVAC	100.61	N/A	2.22	0.017	0.00	40
HVDC	31.07	N/A	1.76	0.021	0.00	40

[1] Value to be interpreted as a lower bound on the real value which depends on the outcome of the sizing stage (as the potential of each site is proportional to its corresponding surface area which, in turn, depends on the latitude).

[2] For battery storage (Li-ion), the values before and after the slash sign under the CAPEX header express the capital expenses for power and energy components. Moreover, the FOM is expressed in M€/GW and applies to the power component, while the VOM is expressed in M€/GWh and applies to the energy component.

Electricity Generation Assets There are nine technologies available for electricity generation, i.e., offshore and onshore wind, utility-scale and distributed solar PV, run-of-river and reservoir-based hydro, nuclear plants, open- and combined-cycle gas turbines (OCGT and CCGT, respectively). Only a subset of these technologies (i.e., the offshore wind and the gas-fired units) are sized, while installed capacities of onshore wind, solar PV, hydro and nuclear power plants remain fixed throughout the optimisation. Recall that the technical potentials of the offshore wind sites are inputs from the siting stage. By contrast, those of the remaining generation technologies to be sized in the CEP framework (i.e., OCGT and CCGT) are assumed to be unconstrained. All generation technologies except the gas-fired power plants are assumed to have non-zero installed capacities at the beginning of the optimisation exercise. More specifically, 61.5 GW of nuclear power capacity, 33.5 GW of run-of-river hydro power capacity and 98.1 GW of reservoir-based hydro power capacity are available throughout the selected European countries [150], [151][2]. Existing wind capacity is obtained from [61], where 99.1 GW of offshore wind and 160.5 GW of onshore wind capacity in various development stages are reported across Europe. Utility-scale solar PV capacity data is retrieved from [62], where a legacy capacity of 45.5 GW is reported throughout Europe. Finally, country-aggregated capacities for distributed PV installations are retrieved from [152], where the existence of 77.7 GW of such installations is reported within European borders.

Electricity Storage Assets Two technologies are available for storing electricity, namely, pumped-hydro (PHS) and battery storage (Li-Ion). It is assumed that no legacy capacity is available in Europe for the latter. Pumped-hydro units are not sized within the CEP framework at hand and the power ratings of existing plants are retrieved from [151], where a total of 54.5 GW / 1950 GWh of PHS units are reported[3]. A summary of the techno-economic data used to instantiate the CEP problem is provided in Table 4.2.

Policy Constraints A set of policy-related constraints are enforced in the CEP problem. One of the main constraints driving the design of power systems under deep decarbonization targets is the CO_2 budget. In the current exercise, this budget is enforced system-wide and its value imposes a 90% reduction in carbon dioxide emissions throughout the optimisation horizon relative to 1990 levels. Then, a planning reserve margin of 20% is considered at each bus $n \in \mathcal{N}_B$ via Eq. (4.4s). The set $\mathcal{D}$ gathering dispatchable generation units providing firm capacity includes OCGT, CCGT, nuclear and reservoir-based hydro power plants. Furthermore, at each bus $n \in \mathcal{N}_B$, the capacity credit of RES sites is computed during the top 5% time instants of peak electricity demand.

[2]The modelling of run-of-river capacity factors and of inflows into the water storage of reservoir-based plants is detailed in Appendix B.

[3]The specific durations of these units is estimated on a unit-by-unit basis via a procedure that is detailed in Appendix B.

A detailed account of the techno-economic assumptions considered in this study is provided in Appendix A.1. The input data used to set-up the siting and sizing models is available at [153]. The code used to run both models is available at [154] and [155], respectively.

4.5 Results

In this section, a series of experiments that compare the implications of the proposed siting schemes on the design and economics of power systems is conducted. In particular, the impact of two variants (i.e., partitioned and un-partitioned) of *PROD* and *COMP* on the siting of roughly 350 offshore wind power plants in the European power system is discussed.

4.5.1 Impact of Siting Decisions on Offshore Production and Residual Load

The first set of results provides insight into the impact of the two siting strategies on the aggregate offshore wind and residual demand signals. To this end, an un-partitioned set-up is used (i.e., where sites are deployed with no consideration for territorial constraints), whose outcome can be seen in Figure 4.3 for both *PROD* and *COMP* schemes, where green markers depict the 135 legacy offshore wind sites. In the left-hand side figure, the *PROD* strategy concentrates all remaining sites to be deployed in two of the most productive areas within the European Seas (i.e., the Atlantic region offshore the British Isles and the North Sea area between Denmark and Norway) [124]. By contrast, the right-hand side subplot shows that the *COMP* strategy distributes sites across several distinct areas found within European EEZ. More specifically, offshore wind deployments under this strategy seem to follow two directions. On the one hand, resource-rich sites in the Atlantic region are still exploited, though to a lesser extent considering that the very good resource in the North Sea basin is already well represented in the set of legacy sites. On the other hand, a significant share of the sites picked by *COMP* are spread in two regions (i.e., Iberia and Southeastern Europe) that are known to have distinct and complementary wind regimes to the ones in Northern Europe, as pointed out in [156], [157].

The effects of offshore wind power plant siting decisions on the aggregate offshore wind and residual load signals can be seen in Figures 4.4 and 4.5. More specifically, Figure 4.4 displays the aggregate offshore wind signal (top subplot) as well as the aggregate residual demand signal (bottom subplot). The signal shown in the top subplot is obtained by spatially averaging the capacity factor time series of the 353 locations selected by the two siting schemes under consideration, while the aggregate residual demand signal is calculated as follows i) the technology power density and site area assumptions considered in Section 4.4.1 are preserved and ii) the demand signals of every country in Table 4.1 are summed to yield a single EU-wide

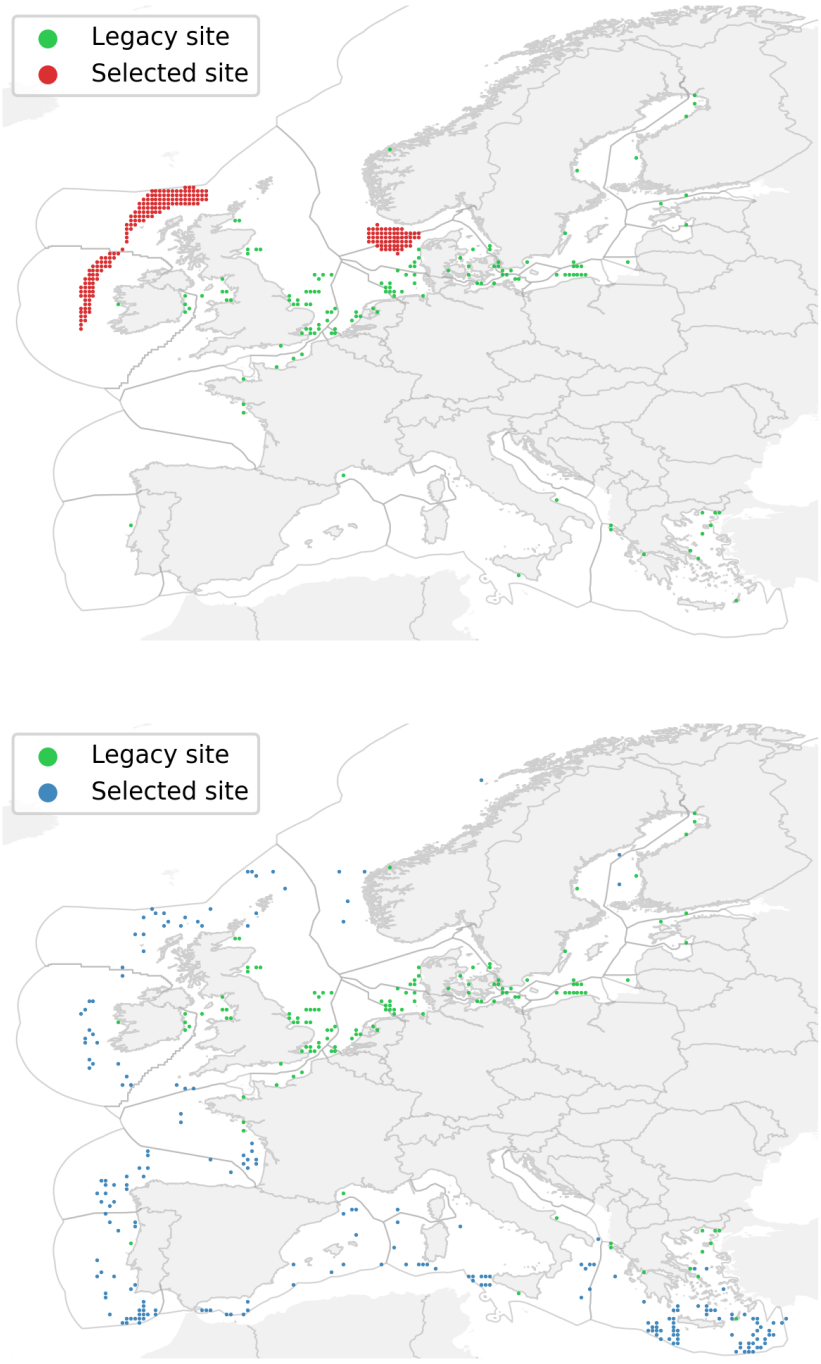

FIGURE 4.3: Deployment patterns for the *PROD* (left) and *COMP* (right) siting schemes for the unpartitioned ($B = 1$) case. In both plots, legacy locations are displayed in green. Exclusive Economic Areas depicted by the grey contours outside the European land mass.

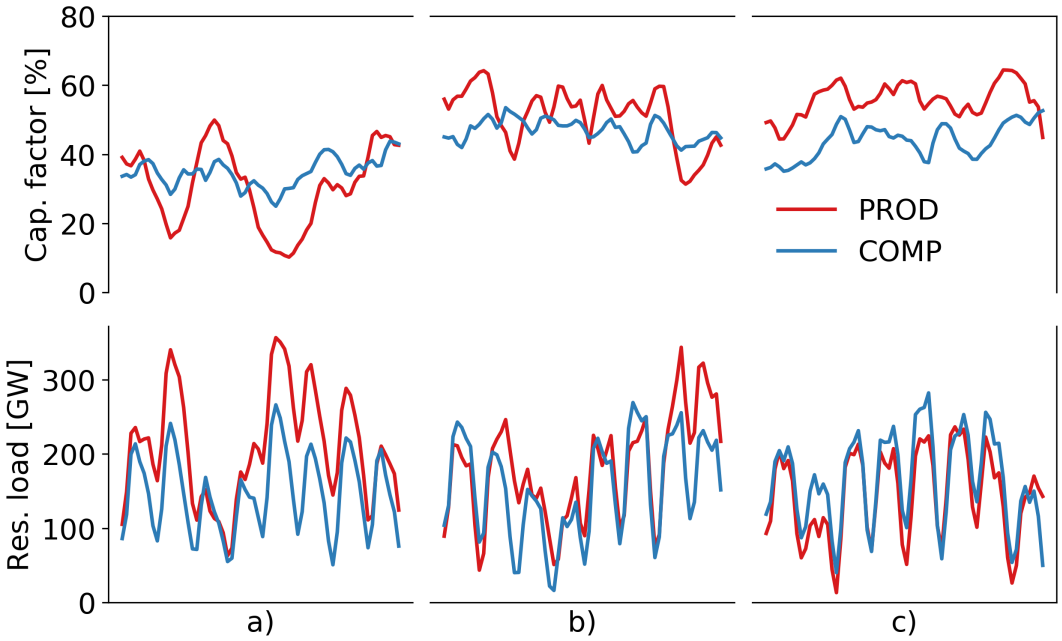

FIGURE 4.4: Visual examples of aggregate offshore wind (top) and residual demand (bottom) signals for the unpartitioned ($B = 1$) *PROD* and *COMP* schemes.

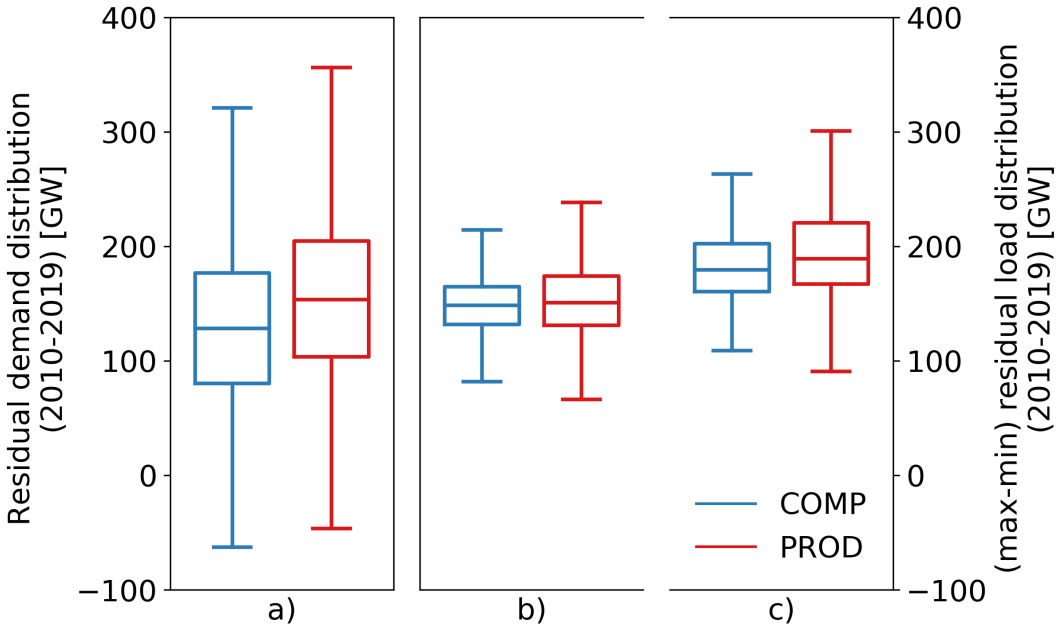

FIGURE 4.5: Statistical distribution of the residual demand under the unpartitioned ($B = 1$) *PROD* and *COMP* siting schemes (left). Statistical distribution of the (max-min) spread for 12-hourly and daily disjoint intervals of the residual demand time series under the unpartitioned ($B = 1$) *PROD* and *COMP* siting schemes (right). Boxes depicting the first quartile, median and third quartile of time series, respectively.

profile from which the aggregate offshore wind feed-in is subtracted. Figure 4.5, on the other hand, shows the statistical distribution of the residual demand (4.5a) as well as the statistical distribution of the spread between the maximum and minimum residual demand for 12-hourly and daily (disjoint) time periods (4.5b and 4.5c). All distributions are constructed using data from ten weather years (2010-2019).

Figure 4.4 suggests that the *COMP* scheme is indeed able to select sites with fewer periods of simultaneous low electricity production than the *PROD*. More precisely, aggregate capacity factor values stay between (roughly) 30% and 60% for the *COMP* scheme while the range of capacity factor values covered by the *PROD* scheme is much broader. This observation is consistent with the fact that the *COMP* deployment pattern covers 29031 time windows (out of 29218), while the *PROD* pattern covers 27147 time windows (around 6.5% fewer than *COMP*), which also implies that instances of high residual load are more frequent in the *PROD* pattern. This claim is supported by Figure 4.5a, which shows that the *COMP* scheme leads to an overall reduction in residual demand. Indeed, the first quartile, the median, the third quartile and the maximum of the *COMP* scheme all correspond to significantly lower residual demand values than those of the *PROD* scheme. Furthermore, Figure 4.4 suggests that some degree of aggregate output variability reduction on time scales ranging from hours to days may be obtained as a by-product of the *COMP* scheme. This intuition is also supported by the box plots in Figures 4.5b and 4.5c, which indicate that both the full and interquartile ranges of siting patterns produced by the *COMP* scheme are narrower than those obtained by the *PROD* scheme. Finally, in Figure 4.4c, it can be seen that the *COMP* scheme sometimes produces less than *PROD* for a few days in a row, which can partly be attributed to the fact that the *PROD* scheme maximises the average capacity factor.

Variants of the *PROD* and *COMP* siting schemes that select locations while satisfying country-based deployment targets ($B = 19$, as shown in Table 4.1) are analyzed next. The associated *PROD* and *COMP* deployment patterns are shown in Figure 4.6, where green markers depict legacy locations. In this context, the *PROD* scheme (left-hand side map) yields a set of clusters of locations, which correspond to the most productive areas of each EEZ. Hence, the resulting deployment pattern is much more scattered than the one observed in the unpartitioned set-up and benefits from much more diverse wind regimes, as suggested by Grams et al. [156]. The *COMP* pattern (right-hand side map) is even more scattered than the *PROD* one. Legacy locations are common to both schemes and about 19% of non-legacy locations selected by the *COMP* scheme are also selected by the *PROD* scheme, up from 6% in the unpartitioned set-up. The partitioned *PROD* and *COMP* patterns therefore share a total of 176 locations (i.e., roughly 50% of all selected locations). Furthermore, in several countries, the number of candidate locations available is only slightly greater than the number of locations that must be deployed there. Hence, even though locations selected in these countries by the *PROD* and *COMP* schemes may not be

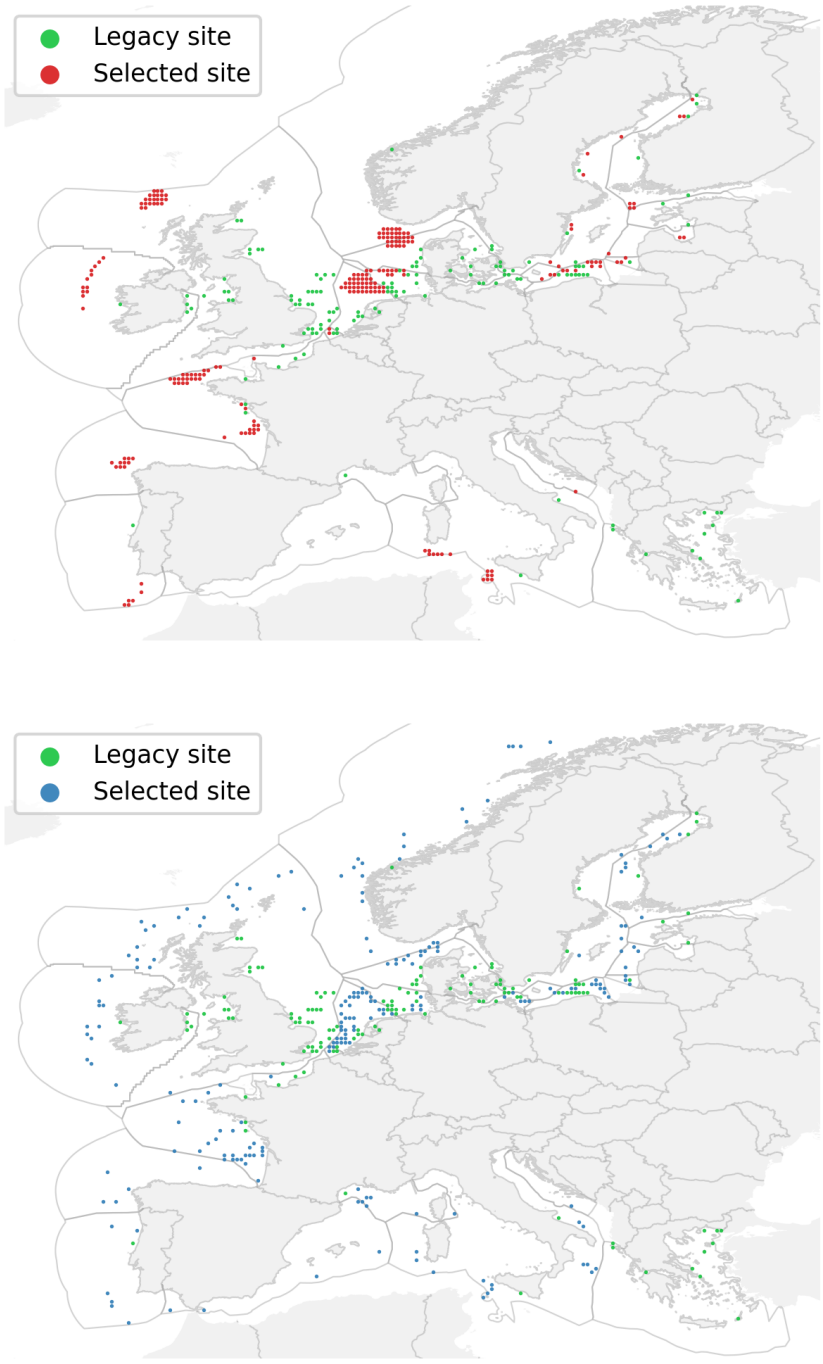

FIGURE 4.6: Deployment patterns for the *PROD* (left) and *COMP* (right) siting schemes for the unpartitioned ($B = 19$) case. In both plots, legacy locations are displayed in green. Exclusive Economic Areas depicted by the grey contours outside the European land mass.

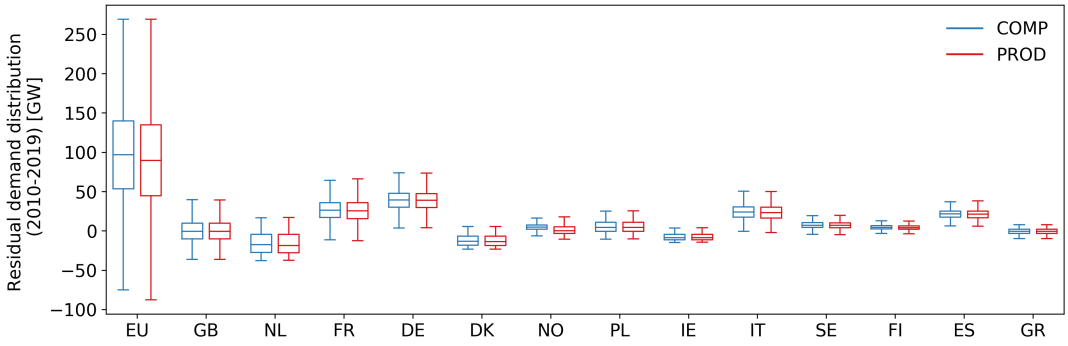

FIGURE 4.7: Statistical distributions of residual demand time series i) aggregated across Europe and ii) in countries with more than $k_n = 10$ deployments under the partitioned ($B = 19$) *PROD* and *COMP* siting schemes.

exactly identical, they nevertheless end up being in the direct vicinity of one another and therefore experience very similar wind regimes. This is especially true in the Baltic Sea and in countries like Denmark or the Netherlands. This also happens in countries such as France and Ireland, though to a lesser extent, in spite of the fact that the numbers of candidate locations available far exceed the numbers of locations that must be deployed there.

Overall, this analysis suggests that the two siting schemes are likely to yield deployment patterns whose performance are comparable. Inspecting the *COMP* siting objectives achieved by both deployment patterns confirms this intuition. More precisely, the *COMP* pattern covers 27981 windows, while the *PROD* pattern covers 27688 windows. In other words, there is only a 1% difference between them. In addition, Figure 4.7 shows the distributions of residual demand aggregated across Europe and on a country-by-country basis. At the notable exception of Norway, where the median residual load of the *COMP* scheme is slightly higher than that of the *PROD* scheme, the residual demand distributions that both schemes yield are virtually identical. Interestingly, the first quartile, median and third quartile of the EU-wide *COMP* distribution correspond to residual demand levels that are slightly higher than those observed for the *PROD* distribution, while maximum residual levels are virtually identical for both schemes. Hence, these results suggest that enforcing country-based deployment targets and selecting locations in the most productive areas is enough to take advantage of the diversity that exists in European offshore wind regimes.

4.5.2 Impact of Siting Decisions on Capacity Expansion Planning Outcomes

In this section, the impact of different siting schemes on the outcomes of the capacity expansion planning set-up described in Section 4.3.3 are investigated. To this end, the outcomes of the two variants of the two siting schemes introduced in Section

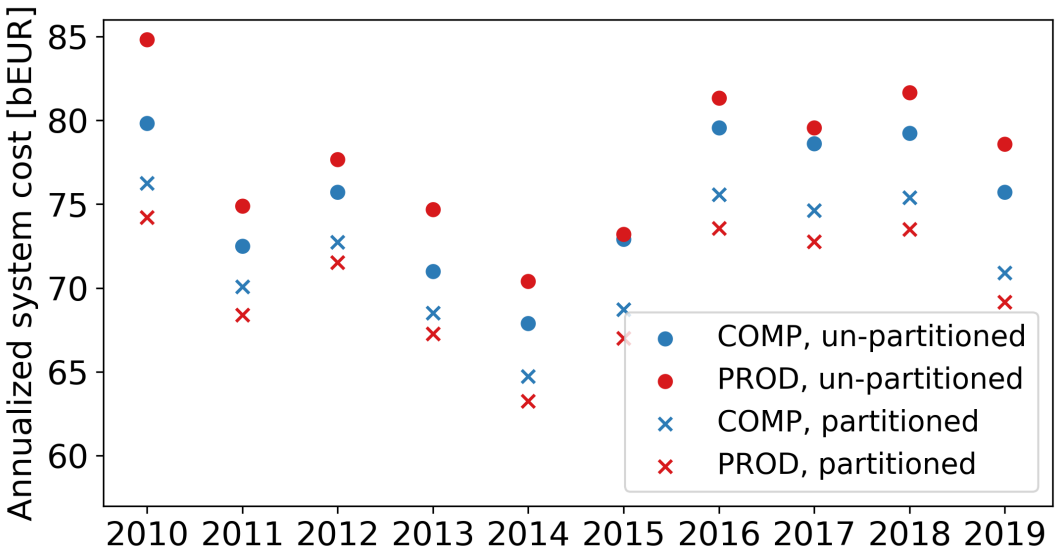

FIGURE 4.8: Capacity expansion objectives of single-year set-ups instantiated with the outcomes of partitioned ($B = 19$) and unpartitioned ($B = 1$) *PROD* and *COMP* siting schemes.

4.3.2 (four in total, i.e., $B = 1$ vs $B = 19$ for both *PROD* and *COMP*) are used to run the CEP stage over the ten individual weather years included in the siting optimization problem (i.e., 2010 to 2019).

Impact on Power System Economics

Figure 4.8 gathers the objectives (i.e., annualized system costs) achieved in the forty aforementioned runs. First, the scatter plot shows distinct trends across partitioned and unpartitioned siting schemes, respectively. On the one hand, *COMP* seems to outperform *PROD* consistently (i.e., by 0.4% to 5.9% depending on the weather year considered) across the ten weather years when partitioning constraints are not enforced ($B = 1$). By contrast, when country-based deployment targets ($B = 19$) are accounted for in the siting of offshore wind power plants, the *PROD* scheme leads to annualized system costs that are between 1.2% and 2.8% lower than those achieved by the *COMP* scheme, depending on the weather year considered. In addition, this plot shows a great deal of variability in the sizing objectives achieved by different siting schemes and for different weather years (e.g., differences of up to 20% between the partitioned and unpartitioned *PROD* schemes). This suggests that both siting decisions and inter-annual weather variability can have a substantial impact on the economics of power systems relying heavily on weather-dependent renewable generation assets such as offshore wind power plants. Unless otherwise stated, the analyses carried out in the next sections focus on the two extreme weather years (i.e., 2010 and 2014) in order to gain a better understanding of how siting decisions affect power system design.

Impact on Power System Design

A summary of relevant system design indicators is provided in Table 4.3, where the CEP outcomes of eight different runs (i.e., two weather years, two siting strategies, two deployment set-ups) are reported.

The first half of Table 4.3 gathers results obtained for CEP instances constructed using unpartitioned deployment patterns ($B = 1$, depicted in Figure 4.3). A number of observations can be made. First, higher offshore wind capacities are observed in *COMP*-based configurations. This is due to the fact that the average capacity factors (41.5% and 41.6% for 2010 and 2014, respectively) are lower than the ones of the set of sites corresponding to *PROD* (43.0% and 45.0% for 2010 and 2014, respectively), an aspect which inherently leads to higher installed capacities in the former scheme (considering that both *PROD* and *COMP* are required to meet the same electricity demand profile). More installed capacity leads to more electricity generation from these units in the 2010 instance and also to a significant reduction of curtailment volumes in both weather years considered. Moreover, maybe the most notable effect of deploying sites based on *COMP* is a reduction in dispatchable capacity requirements. Recall that *COMP* is designed to minimize the occurrence of system-wide resource scarcity events, such as the one depicted in Figure 4.4a. As a result, the corresponding sizing instances consistently reveal smaller capacities for dispatchable generation units. More specifically, OCGT and CCGT capacities are reduced by up to 18.2% and 49.8% compared to the corresponding *PROD* runs. This also translates into considerably smaller generation volumes from these units, with the exception of OCGT in the 2014 run, where the additional 2.4 TWh are used to replace the generation deficit brought up by offshore wind. Furthermore, Li-Ion does not seem to play a significant role in the design of the resulting systems (an aspect that holds across all subsequent runs). This outcome has two main causes. First, considerable pumped-hydro storage capabilities exist as legacy installations in the system under study. Second, the time resolution used in this exercise (i.e., three-hourly) does not capture short-term balancing events for which Li-Ion storage is particularly appealing. With respect to transmission capacities, it appears that *COMP* is on par with *PROD* in the 2010 instance (though a 15.7% increase in flows leads to a more efficient utilization of the infrastructure), while a reduction of 16.4% is observed in the 2014 run. Put together, these outcomes lead to total system cost reductions under the *COMP* scheme of 5.9% (for 2010) and 3.6% (for 2014). It is worth pointing out that cost savings achieved by a reduction in dispatchable capacity deployment and use are partly offset by an increase in offshore wind capacity deployment, which is comparatively much more expensive per unit capacity.

Results pertaining to CEP instances constructed from partitioned deployment patterns ($B = 19$, shown in Figure 4.6) are provided in the second half of Table 4.3. To begin with, the number of non-critical windows obtained for these set-ups reveal a much tighter difference between the two deployment schemes, i.e., 94.71% (or

TABLE 4.3: Comparison of annualized system costs and installed capacities for various technologies sized in the CEP framework. The analysis is conducted for the partitioned ($B = 1$) and un-partitioned ($B = 19$) variants of the *PROD* and *COMP* siting schemes and for a weather year with inferior (i.e., 2010) and superior (i.e., 2014) wind quality, respectively.

	Weather Year	2010				2014			
	Siting Scheme	*PROD*		*COMP*		*PROD*		*COMP*	
	Indicator	K[1]	p[2]	K	p	K	p	K	p
un-partitioned ($B = 1$)	W_{off}[3]	416.4	1532.4	463.8	1679.2	397.0	1517.9	411.3	1514.1
			(29.7)		(25.4)		(41.3)		(15.7)
	OCGT	298.6	5.3	286.2	4.7	308.6	7.1	252.4	9.5
	CCGT	73.7	179.2	36.9	56.8	25.0	24.7	20.3	21.4
	Li-Ion	0.01		0.01	N/A	0.01	N/A	0.01	N/A
	Transm.[4]	189.0	1802.5	188.9	2085.3	188.8	2015.9	157.8	1839.67
	ASC[5]	84.8		79.8		70.4		67.9	
partitioned ($B = 19$)	W_{off}	464.3	1696.3	478.8	1687.9	400.8	1521.3	412.4	1519.4
			(38.4)		(39.7)		(22.4)		(23.7)
	OCGT	268.0	7.7	267.1	7.8	230.5	9.6	226.1	9.8
	CCGT	34.3	46.6	32.9	51.4	24.7	23.4	25.5	26.0
	Li-Ion	0.0	N/A	0.0	N/A	0.01	N/A	0.0	N/A
	Transm.	124.3	1359.3	124.4	1371.7	116.3	1319.6	115.8	1306.9
	ASC	74.2		76.3		63.3		64.7	

[1] K denotes the system-wide capacity of a given technology (incl. legacy capacity), as resulted from the optimisation exercise and it is expressed in energy units. For instance, capacities of generation technologies (e.g., offshore wind, OCGT, CCGT) are reported in GW. For lithium-ion storage (Li-Ion), the same quantity it is expressed in GWh, while transmission capacities are expressed in TWkm.

[2] p denotes the amount of electricity produced (for generation technologies) or transported (for transmission technologies) across over a full year. Values are expressed in TWh.

[3] Values in parentheses represent offshore wind curtailment volumes (expressed in the same units as p).

[4] In this table, both electricity transmission technologies (i.e., AC and DC) are aggregated into one term.

[5] ASC stands for "annualized (total) system cost", is expressed in billion € and represents the objective function of the expansion planning stage.

27688) and 95.77% (or 27981) for *PROD* and *COMP*, respectively. In terms of system costs, partitioned *PROD* regularly out-performs partitioned *COMP*, as already revealed in Figure 4.8. Specifically, the latter scheme leading to system configurations which are 2.8% (for the 2010 instance) and 2.3% (for the 2014 case) more expensive than the corresponding *PROD*-based runs. This outcome can be explained as follows. Regardless of the weather year considered, the *COMP*-based runs deploy more offshore wind capacity (additional 3.1% and 2.9% in the 2010 and 2014 runs, respectively), which translates into higher capital expenditures. Nevertheless, the associated generation levels are slightly inferior to those of the *PROD*-specific instances due to the differences between the capacity factors of the sets of sites associated with the two siting schemes (recall that *PROD* is by design selecting the locations with the highest capacity factors in all $B = 19$ regions). More specifically, the average capacity factors for the *PROD* set of $k = 353$ sites are 42.3% and 43.8% (2010 and 2014, respectively), compared to 40.9% (during 2010) and 42.3% (during 2014) for the *COMP* set of locations. This time, however, the *PROD* deployment pattern also exploits a great deal of resource diversity itself, which leads to significantly mitigated dispatchable capacity and generation requirements compared to the un-partitioned *PROD* case. The *COMP* siting scheme enables, even in these conditions, an overall capacity reduction of dispatchable units (i.e., of 2.4 GW and 3.6 GW in 2010 and 2014, respectively) compared to *PROD*, which indicates that the complementarity-based siting method still manages to provide a set of sites that decreases the peak residual demand across the system. However, power generation from VOM-intensive dispatchable power plants is now used to cover for the offshore wind feed-in deficit, thus resulting in increased O&M expenditures compounding the additional capital costs due to wind offshore deployments. Finally, no significant differences can be seen in terms of transmission capacity or transited volumes. These results suggest that, as opposed to the un-partitioned scenario, *COMP* slightly under-performs compared to a siting strategy that assumes the deployment of the most productive offshore sites across the 19 Exclusive Economic Zones.

4.5.3 Sensitivity Analysis

In this section, a sensitivity analysis is performed in order to evaluate the robustness of results obtained for the partitioned deployment patterns with respect to offshore wind cost assumptions and inter-annual weather variability.

Impact of Offshore Wind Cost Assumptions

In view of recent offshore wind cost projections suggesting that costs are likely to decrease substantially by 2050 [158] and considering the small difference between annualized system costs reported in Table 4.3 for the *PROD* and *COMP* schemes (especially for the partitioned set-ups), evaluating the sensitivity of these results to the economic assumptions laid out in Table 4.2 is warranted. More precisely, the

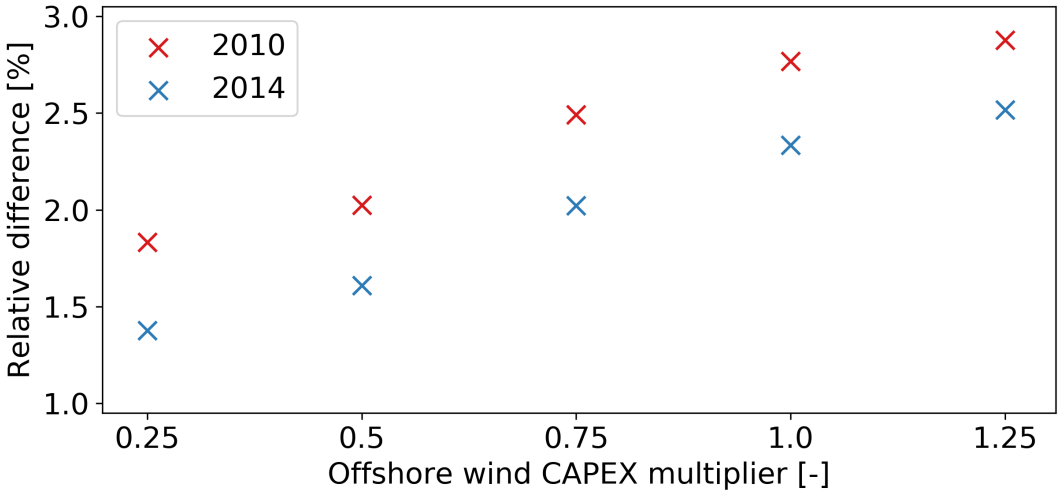

FIGURE 4.9: Relative differences in annualized system costs achieved by expansion planning instances using the outcomes of partitioned ($B = 19$) *COMP* and *PROD* siting schemes, for different offshore wind CAPEX multiplicative factors. The analysis is carried out for two weather years (i.e., 2010 and 2014).

outcomes of the partitioned *PROD* and *COMP* schemes are used in CEP set-ups where the capital expenditure of offshore wind is varied between 25% and 125% of the reference cost, by increments of 25%. The results of this experiment are gathered in Figure 4.9, where the red and blue markers represent the relative difference (in percentage points) between the objectives of *PROD*- and *COMP*-based runs (a positive value indicates higher costs for the latter) for the 2010 and 2014 weather years, respectively.

It is clear from Figure 4.9 that *COMP*-based power system designs are consistently more expensive than their *PROD* counterparts, regardless of the offshore wind cost. The relative difference between the sizing objectives decreases steadily as the value of the cost multiplier decreases and falls below 2% for both weather years considered, when offshore wind CAPEX is assumed to be only 25% of the reference value. Overall, the *COMP* schemes lead to system designs that are 1.37% to 2.51% and 1.83% to 2.88% more expensive than their *PROD* counterparts for the 2014 and 2010 weather years, respectively. The main reason behind *PROD* consistently leading to cheaper system configurations is the fact that, regardless of the offshore wind cost, the total cost of *COMP*-based system designs is offset by additional offshore wind capacity deployments. As already discussed in Section 4.5.2, this outcome is driven by lower average capacity factors for the *COMP* sites compared to the ones corresponding to the *PROD* sets of locations.

Impact of Inter-Annual Weather Variability

The variance in the sizing outcomes obtained for problem instances with a time horizon of one year (shown in Figure 4.8) supports previous findings suggesting

TABLE 4.4: Breakdown of installed capacities and costs per technology for the partitioned *PROD*- and *COMP*-based system designs obtained for a sizing problem instance with a time horizon of ten years (corresponding to the ten weather years used in the siting stage, namely 2010-2019).

Scheme	ASC		OCGT	CCGT	W_{off}	Transm.
PROD	722.68 (b€)	K (GW/TWkm)	291.3	36.4	435.7	129.4
		CAPEX (b€)	106.6	17.4	420.6	41.7
		p (TWh)	88.0	590.6	16512.5	14270.5
		OPEX (b€)	8.2	41.1	0.0	0.0
COMP	740.22 (b€)	K (GW/TWkm)	288.4	36.6	444.3	129.4
		CAPEX (b€)	105.6	17.5	431.4	41.7
		p (TWh)	80.4	696.3	16334.0	14147.4
		OPEX (b€)	7.5	48.4	0.0	0.0

that inter-annual weather variability may have a substantial impact on the cost of operating power systems with high shares of RES-based generation [159]. Consequently, this experiment seeks to evaluate the performance of power system designs obtained with the partitioned *PROD* and *COMP* schemes when the full time series of weather data leveraged in the siting stage (i.e., 2010-2019) is used to instantiate the CEP problem that sizes the system.

The figures in Table 4.4 indicate that the intuition provided by the sizing runs relying on extreme weather years (see Section 4.5.2) still holds when the inter-annual variability of the offshore wind resource is properly accounted for. More specifically, the system configuration based on the *COMP* siting strategy is 2.4% more expensive than the one relying on the *PROD* deployment scheme. Two main factors are behind this cost difference. First, the partitioned *PROD* siting scheme naturally yields a collection of very productive offshore wind sites. Indeed, a ten-year average capacity factor of 43.2% is achieved across the 353 sites. Moreover, as previously reported in Section 4.5.2, the partitioned *PROD* deployment pattern achieves a *COMP* siting objective that is only 1% lower than that of the *COMP* deployment pattern. On the other hand, the average capacity factor of the 353 *COMP* sites is around 41.9%. This drives the investment in an additional 8.6 GW of offshore wind capacity in the *COMP* system, which represents more than half of the annualized system cost difference between *PROD* and *COMP* in Table 4.4. Second, although the *COMP* siting scheme leads to a system design with more offshore wind capacity, the slightly inferior capacity factors lead to a generation deficit of 178 TWh across the ten-year optimisation horizon. Legacy generation units, e.g., run-of-river or reservoir-based hydro plants, with non-zero operating costs (as opposed to offshore wind generation) and CCGT power plants (with high O&M costs) are used to cover the aforementioned shortfall. In total, the additional operating costs incurred by this shift from offshore wind to other generation technologies make up for the remainder of

the total cost difference observed between the *PROD*- and *COMP*-based configurations in Table 4.4.

4.5.4 Discussion

It is worth pointing out that, even in the most extreme of situations (represented in Figure 4.8 by the 2010 un-partitioned set-up), the relative cost difference between system designs using *PROD* or *COMP* siting outcomes does not exceed 6%. The reasons for this limited difference are twofold. First, the case study proposed in this chapter investigates solely the siting of offshore wind sites. In the ten-year runs detailed in Section 4.5.3, offshore wind represents 38.7% and 45.4% of the Europe-wide total installed capacity and generation volumes, respectively (values for the *COMP*-based run), while the remainder corresponds to power generation, storage and transmission technologies which are modelled in an identical fashion in both *PROD*- and *COMP*-based CEP set-ups. Therefore, the system cost differences identified throughout Section 4.5.2 should be interpreted accordingly as the economic impact of one offshore wind siting strategy or the other on the design of the power system. Second, it should be emphasized that 135 out of a total of $k = 353$ sited offshore locations (i.e., a share of 38%) belong to the subset of legacy sites. This aspect further explains the relatively limited differences in total system costs as, in practice, only 218 offshore wind locations are being sited via the investigated siting strategies. In other words, at most 218 offshore wind resource profiles can differ between the outcomes of *COMP* and *PROD*.

An observation consistently made throughout the results section is that *COMP* outperforms *PROD* as long as the latter does not fully exploit the resource diversity available across European EEZs (i.e., the un-partitioned set-ups). This suggests that concentrating offshore wind installations in rich, but relatively limited geographical scopes (e.g., the North Sea [64]), while deferring their deployment in regions swept by distinct wind regimes (e.g., the Baltic or Mediterranean areas) could lead to undesirable outcomes. One example of such an outcome would be the heavy deployment of thermal dispatchable capacity that would be required to guarantee system adequacy which, considering the duration of investment cycles in the power sector and unless carbon-neutral fuels can be used, would lead to investment decisions that are not consistent with the pathways enabling the achievement of ambitious climate targets by 2050 [3].

Another finding in Section 4.5.2 concerns the differences observed between the system configurations leveraging the un-partitioned and partitioned siting schemes, respectively. In particular, the two *COMP* schemes will be discussed. On the one hand, as the un-partitioned set-up is a relaxation of the partitioned case, the former outperforms the latter in terms of siting scores. Specifically, the $B = 1$ case yields a set of locations covering 99.36% of the time windows, while 95.77% of the time windows are non-critical under the $B = 19$ set-up. Interestingly, the superior siting score

of the unpartitioned scheme does not translate into a cheaper system configuration, as observed in Figure 4.8, where **x** markers fall below the **o** markers, regardless of the weather year considered.

This outcome can be partly explained by the workings of the system adequacy constraint (4.4s) of the CEP framework, according to which offshore wind (as any other RES technology) can contribute to the provision of firm capacity. More precisely, this constraint is such that system adequacy must be ensured at country-level in order to avoid situations where certain countries excessively depend on electricity imports. Thus, in the partitioned set-up, offshore wind contributes to the provision of firm capacity in all $B = 19$ countries across Europe where capacity could be deployed [91]. On the contrary, ignoring the partitioning constraints (i.e., $B = 1$) results in some countries having less (e.g., Germany, the Netherlands, Norway, etc.) wind deployments compared with the partitioned set-up, as seen in Figure 4.3. For those countries, the offshore wind potential (which is proportional to the number of deployed sites) becomes lower than in the partitioned set-up (where more sites were deployed) and, in turn, cannot contribute as much to system adequacy. The two dispatchable power generation technologies sized in the CEP problem (i.e., OCGT and CCGT) become the alternatives for firm capacity (since other RES are not sized in the CEP) and the optimiser ends up deploying additional OCGT capacity due to its lower cost per unit capacity, thus augmenting the total system cost of the unpartitioned set-up.

Another explanation for the partitioned cases outperforming the un-partitioned ones in terms of system cost pertains to the limited amount of system-related information that is made available to the siting stage, irrespective of the siting strategy considered. An example of such information whose implications are relatively easy to gauge are the network constraints. Recall that the siting stage relies solely on renewable resource and electricity demand data and that the classification of time windows is oblivious to limits on transmission capacity between regions. In consequence, even though the unpartitioned *COMP* siting scheme leads to a higher siting score than the partitioned case, the CEP stage does not manage to take full advantage of the offshore sites identified in the $B = 1$ set-up. Indeed, on average (across the ten single-year *COMP* runs reported in Figure 4.8), the capacities deployed at 92.2% of the 218 offshore sites selected by the partitioned *COMP* scheme (excluding legacy sites) exceed 100 MW, while only 73.4% of them exceed the same capacity threshold in the CEP set-up based on the unpartitioned *COMP* outcome. Most of the unexploited sites in the $B = 1$ scheme are located in the densely deployed areas of Southwestern and Southeastern Europe. From a siting perspective, the wind regimes of these regions are particularly appealing, since they differ from the ones that prevail in the Northern half of the continent [156]. Nevertheless, in this case, the benefits of resource diversity cannot be reaped due to the limited options for electricity transmission between the Iberian peninsula and Central-Western Europe,

and between Greece and Central Europe.

4.6 Conclusion

In this chapter, a realistic case study evaluating the role that offshore wind power plants may play in the European power system is proposed, with a particular focus on the impact that plant siting strategies have on system design and economics. The chapter builds upon a method that combines a siting stage selecting a subset of promising locations for deployment and a capacity expansion framework identifying the power system design that supplies pre-specified demand levels at minimum cost while satisfying technical and policy constraints. In the interest of transparency, an open source tool implementing the two-stage method is also made available.

Two types of deployment schemes that select sites so as to maximise their aggregate power output (*PROD*) and spatiotemporal complementarity (*COMP*) are analysed. Two variants of these siting schemes are also considered, wherein the number of sites to be selected is specified on a country-by-country basis rather than Europe-wide. A few hundred sites are identified by each scheme using a high resolution grid and ten years of reanalysis data, and these sites are then passed to a capacity expansion planning framework in order to assess the impact of siting decisions on power system design and economics. The framework relies on a stylised model of the European power system where each country corresponds to an electrical bus and includes an array of power generation and storage technologies. The framework seeks to size gas-fired power plants, offshore wind power plants, battery storage and electricity transmission assets and operate the system in order to supply electricity demand levels consistent with current European electricity consumption at minimum cost while reducing carbon dioxide emissions from the power sector by 90% compared with 1990 levels and taking a broad range of legacy assets into account. A detailed sensitivity analysis is also performed in order to evaluate the impact of offshore wind cost assumptions and inter-annual weather variability on system design and economics.

Results show that the *COMP* scheme yields deployment patterns that have both a much steadier aggregate power output and much lower residual load levels than the *PROD* scheme if sites are selected without enforcing country-based deployment targets. However, when such constraints are enforced, the siting schemes produce deployment patterns that lead to similar levels of residual load. This suggests that systematically deploying offshore wind sites in the most productive areas of most European countries makes it possible to take full advantage of the diverse wind regimes available in European seas. In addition, power system designs obtained using *COMP* deployment patterns consistently feature more offshore wind capacity and less dispatchable capacity than *PROD*-based designs. This difference does not always translate into power systems that are cheaper for either of the siting schemes.

More precisely, the *COMP* scheme leads to system designs that are up to 5% cheaper than *PROD*-based ones when sites are selected without enforcing country-based deployment targets. When such targets are enforced, however, the *PROD* scheme leads to system designs that are consistently 2% cheaper than *COMP*-based ones. These results are shown to hold under a broad range of offshore wind cost assumptions and are not affected by inter-annual weather variability.

In future work, several directions can be envisioned for refining the analysis. First, integrating the siting of other RES technologies (e.g., onshore wind, solar PV) into the proposed two-stage method would be of interest to evaluate their synergies in supplying European demand at minimal cost. Then, enhancing the network modelling by i) using a higher spatial resolution and a refined topology, ii) relying on a better approximation of network flows (e.g., a DC-OPF model) would improve the accuracy of the analysis. Evaluating the impact of unit commitment costs and constraints on system designs obtained for different siting schemes would also be of interest. Finally, representing the effect of short-term RES uncertainty in dispatch decisions could also provide some insight into the benefits that different siting schemes may bring about.

Chapter 5

Assessing the Impact of Siting Strategies on the Design and Operation of Power Systems: A Refined Analysis

In this chapter, the impact of two siting strategies for wind assets on the design and operation of the Continental European power system is investigated. A three-stage routine is leveraged to this end. In the first stage, a highly-granular siting problem identifies a suitable set of sites where wind assets could be deployed according to a pre-specified criterion. Two siting schemes are analysed and compared in a realistic case study. These schemes essentially select a pre-specified number of sites so as to maximise their aggregate power output and their spatiotemporal complementarity, respectively. In the second stage, the subset of previously identified sites is passed to a capacity expansion planning framework that sizes the power generation, transmission and storage assets that should be deployed and operated in order to satisfy pre-specified electricity demand levels at minimum cost. Once the capacities of these assets are known, a third stage, formulated as a unit commitment and economic dispatch problem, is leveraged to investigate the impact of the aforementioned wind siting strategies on the short-term operation of the power system. Results seem to confirm the findings from the previous section. More specifically, deploying wind sites in the most productive areas throughout Europe already captures a significant degree of spatiotemporal resource complementarity and thus leads to lower costs for the design and operation of the power system compared to a deployment strategy where resource complementarity is explicitly leveraged as siting criterion.

5.1 Motivation

The results of the analysis proposed in Chapter 4 revealed that different Europe-wide offshore wind siting criteria lead to very similar system costs, albeit fairly distinct power system configurations. It was thus suggested that further work has to be conducted and the underlying models to be refined in order to improve the accuracy of investment decisions in different siting scenarios.

A first modelling aspect that was identified as potentially relevant in a follow-up analysis consisted of including multiple RES technologies in the siting stage. Such a modelling feature was particularly interesting due to the interplay different renewable resources manifest in planning ventures [160]. Then, relying on a more refined grid topology improves the representation of transmission bottlenecks and, thus, of system costs [60]. In addition, leveraging a more accurate model of power flows in transmission lines further enhances the representation of bottlenecks in transmission infrastructure, particularly in highly-meshed grids [161]. Finally, accounting for unit commitment costs and constraints in the operation of dispatchable generators may also play an important role when assessing the economic value of a complementarity-based siting strategy that minimizes the occurrence of low-generation RES states.

However, accounting for all these features within a model that also sizes the system (i.e., a CEP framework) quickly leads to impractical solving times or even intractable instances. Thus, modellers have usually resorted to various solution methods to tackle such problems [162]. For instance, the frameworks proposed in [38], [163], [164] include most of these features in a single model that tackles both the design and operation of the underlying system. However, owing to the resulting computational complexity of such instances, unit commitment constraints are usually discarded or stylized, while power flows in transmission infrastructure are modelled via a simplified transportation model. In order to overcome the aforementioned downsides, a first solution modellers have resorted to is represented by the unidirectional soft-linking, where the outcome of the planning model is given as input to the operational model without any feedback from the latter to the former. Examples of such studies include works by Lew et al. [165], Deane et al. [166], Poncelet et al. [167] or Kiviluoma et al. [168]. Their solution methods enable the consideration of unit commitment constraints, as well as of linearized power flow equations yet, with no feedback between the planning and operational stages, investment decisions are likely to be sub-optimal [162]. One straightforward way to tackle this issue proposes a bidirectional link between the planning and operational models. In such a set-up, feedback from the operational model is available to the planning stage and the two stages are run for a pre-specified number of iterations until convergence (e.g., of objective function value or installed capacities across consecutive iterations) is reached. Studies by Mills and Wiser [169] or Pina et al. [170] leverage such a solution method.

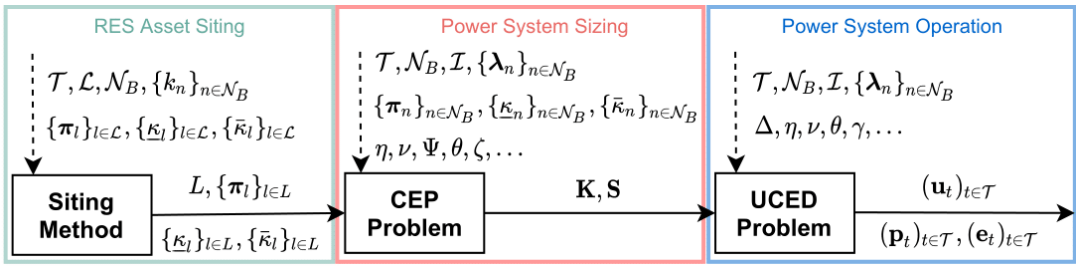

FIGURE 5.1: Workflow of the proposed three-stage method. Dotted arrows denote exogenous input streams, while full arrows represent output streams, respectively.

A fourth approach to embed all the aforementioned modelling features consists of co-optimising investment and operational decisions. Typically, this approach leverages the decomposable structure of the co-optimisation problem at hand and uses decomposition techniques (e.g., Benders or Danzig-Wolfe) to alleviate the associated computational burden. For example, in a classic Benders-like algorithm, the operational model produces optimality cuts that are included in the planning problem at each iteration until convergence is reached. This approach is employed in studies by Pudjianto et al. [171], Koltsaklis and Georgiadis [172], Palmintier and Webster [173] or Flores-Quiroz et al. [174].

In this chapter, a method to assess the impact of different siting criteria for both on- and offshore wind assets on the planning and operation of the European power system is proposed. To this end, a unidirectional soft-linking approach is pursued [162]. At first, two RES deployment schemes that select sites so as to maximise their aggregate power output and spatiotemporal complementarity, respectively, are analysed. Once the most appropriate sites for RES deployment are identified, they are passed to a capacity expansion planning framework which sizes gas-fired power plants, RES assets, battery storage and electricity transmission infrastructure. Upon retrieving the optimal capacities of the aforementioned power system technologies, they are passed as input to a unit commitment and economic dispatch problem that provides detailed information with respect to their short-term operation.

From here on, the chapter is structured as follows. Section 5.2 describes the method used to investigate the impact of siting criteria on the design and operation of power systems. Then, Section 5.3 detail the proposed case study and modelling set-ups, respectively, before results are reported in Section 5.4. Section 5.5 concludes the chapter and proposes future work avenues.

5.2 Method

In this section, the models at the core of the proposed three-stage method are described. The proposed workflow is depicted in Figure 5.1.

5.2.1 Siting Models

The models and solution methods for RES assets siting described in Sections 4.3.2 and 4.3.2 of this manuscript, respectively, are used without any modification to identify the sets of sites that maximise their aggregate power output (i.e., *PROD*) and spatiotemporal complementarity (i.e., *COMP*), respectively. As seen in Figure 5.1, inputs to this problem include the time horizon $\mathcal{T}$, the set of candidate locations $\mathcal{L}$ and a vector of partition-based deployment constraints $\{k_n\}_{n\in\mathcal{N}_B}$. In addition, for each candidate location $l \in \mathcal{L}$, renewable resource time series covering the entire time horizon (i.e., $\{\boldsymbol{\pi}_l\}_{l\in\mathcal{L}}$), the technical potential (i.e., $\{\overline{\kappa}_l\}_{l\in\mathcal{L}}$) and the corresponding legacy capacity (i.e., $\{\underline{\kappa}_l\}_{l\in\mathcal{L}}$) are made available. Upon solving the model, the same last three quantities are returned for every selected location $l \in L$, with $L \subseteq \mathcal{L}$.

5.2.2 Capacity Expansion Planning Framework

Once the subset of selected RES sites $L \subseteq \mathcal{L}$ is known, $\{\boldsymbol{\pi}_l\}_{l\in L}$, $\{\overline{\kappa}_l\}_{l\in L}$ and $\{\underline{\kappa}_l\}_{l\in L}$ are passed as input data to a CEP framework that determines the cost-optimal power system design and whose mathematical formulation differs from the one proposed in Section 4.3.3 of this manuscript in way power flows are modelled. More specifically, in this chapter, a linearized optimal power flow (i.e., a dc-opf) formulation is employed. In consequence, the CEP framework leveraged in this section writes as

$$\min \quad (4.4a) \tag{5.1a}$$

$$\text{s.t.} \quad (4.4b) - (4.4s) \tag{5.1b}$$

$$\sum_{i\in\mathcal{I}_{ac}} C_{ic} x_i p_{it} = 0, \ \forall c \in \mathcal{C}, \forall t \in \mathcal{T} \tag{5.1c}$$

Note that the additional constraint (5.1c) represents the cycle-based Kirchhoff Voltage Law [175] and is applied solely on the power flows across the subset of non-controllable transmission assets, i.e., $\mathcal{I}^{ac}$.

5.2.3 Unit Commitment and Economic Dispatch Problem

Let κ^* and σ^* denote the optimal installed capacities (incl. legacy capacity) of generation, storage and transmission assets identified in the expansion planning stage (5.1a-5.1c). The unit commitment and economic dispatch (UCED) problem enabling the evaluation of the impact of siting strategies on the operation of power systems is thus formulated via (5.2a-5.2o). The objective function of this problem (5.2a) minimizes the VOM, start-up and shut-down costs of dispatchable generation units[1], the

[1]Note that the VOM of generation assets, as defined here, include the plan-specific variable operation and maintenance costs, fuel costs, as well as CO_2-related expenses.

VOM of RES assets, storage units and transmission assets, as well as the economic penalties associated with unserved demand.

$$\min_{(\mathbf{u}_t)_{t\in\mathcal{T}},(\mathbf{p}_t)_{t\in\mathcal{T}},(\mathbf{e}_t)_{t\in\mathcal{T}}} \sum_{t\in\mathcal{T}} \omega_t \Big[\sum_{\substack{n\in\mathcal{N}_B \\ g\in\mathcal{G}\cup\mathcal{R}}} \theta_v^g p_{ngt} + \sum_{\substack{n\in\mathcal{N}_B \\ g\in\mathcal{G}}} \theta_{SU}^g u_{ngt}^U + \sum_{\substack{n\in\mathcal{N}_B \\ g\in\mathcal{G}}} \theta_{SD}^g u_{ngt}^D$$
$$+ \sum_{\substack{n\in\mathcal{N}_B \\ l\in L_n}} \theta_v^l p_{lt} + \sum_{\substack{n\in\mathcal{N}_B \\ s\in\mathcal{S}}} \theta_v^s (p_{nst}^C + p_{nst}^D) + \sum_{i\in\mathcal{I}} \theta_v^i |p_{it}| + \sum_{n\in\mathcal{N}_B} \theta^{ens} p_{nt}^{ens} \Big] \tag{5.2a}$$

The energy balance constraint (5.2b) ensures that supply matches demand at every node and time step $t \in \mathcal{T}$. The feasibility of this constraint is ensured via the slack variable p_{nt}^{ens}, whose associated cost is the value of lost load also featuring in the objective function. Furthermore, the operation of RES assets belonging to technologies sited in the Section 5.2.1 is modelled via Eq. (5.2c), which simply limits the output of the corresponding units to their maximum production capabilities.

$$\text{s.t.} \sum_{\substack{n\in\mathcal{N}_B \\ l\in L_n}} p_{lt} + \sum_{g\in\mathcal{G}\cup\mathcal{R}} p_{ngt} + \sum_{s\in\mathcal{S}} p_{nst}^D + \sum_{i\in\mathcal{I}_n^+} p_{it} + p_{nt}^{ens} = \lambda_{nt} + \sum_{s\in\mathcal{S}} p_{nst}^C + \sum_{i\in\mathcal{I}_n^-} p_{it},$$
$$\forall n \in \mathcal{N}_B, \forall t \in \mathcal{T} \tag{5.2b}$$

$$p_{lt} \leq \pi_{lt}\kappa_l^*, \ \forall l \in L_n, \forall n \in \mathcal{N}_B, \forall t \in \mathcal{T} \tag{5.2c}$$

The operation of the remaining generation units, i.e., dispatchable assets and RES units not sited via Section 5.2.1, is modelled via Eqs. (5.2d-5.2i). More specifically, Eq. (5.2d) defines the feed-in from such units, taking into account minimum operational levels (μ_{ngt}), maximum availabilities (π_{ngt}) and unit commitment decisions (u_{ngt}). Then, Eq. (5.2e) defines the unit commitment logic, thus enabling the accounting of start-ups and shut-downs, while Eqs. (5.2f-5.2g) bounds the ramp rates of dispatchable units to pre-specified ramping capabilities. The last set of constraints (5.2h-5.2i) enforce the minimum up and down times for these generators, respectively.

$$u_{ngt}\mu_{ngt}\kappa_{ng}^* \leq p_{ngt} \leq u_{ngt}\pi_{ngt}\kappa_{ng}^*, \ \forall n \in \mathcal{N}_B, \forall g \in \mathcal{G}, \forall t \in \mathcal{T} \tag{5.2d}$$

$$u_{ngt} = u_{ngt-1} + u_{ngt}^{SU} - u_{ngt}^{SD}, \ \forall n \in \mathcal{N}_B, \forall g \in \mathcal{G}, \forall t \in \mathcal{T} \tag{5.2e}$$

$$p_{ngt} - p_{ng(t-1)} \leq \Delta_g^+ \kappa_{ng}^*, \ \forall n \in \mathcal{N}_B, \forall g \in \mathcal{G}, \forall t \in \mathcal{T} \setminus \{0\} \tag{5.2f}$$

$$p_{ngt} - p_{ng(t-1)} \geq -\Delta_g^- \kappa_{ng}^*, \ \forall n \in \mathcal{N}_B, \forall g \in \mathcal{G}, \forall t \in \mathcal{T} \setminus \{0\} \tag{5.2g}$$

$$\sum_{\tau=t}^{t+\delta_g^{mut}} u_{ng\tau} \geq \delta_g^{mut}(u_{ngt} - u_{ng(\tau-1)}), \ \forall n \in \mathcal{N}_B, \forall g \in \mathcal{G}, \forall t \in \mathcal{T} \tag{5.2h}$$

$$\sum_{\tau=t}^{t+\delta_g^{mdt}} (1 - u_{ng\tau}) \geq \delta_g^{mdt}(u_{ng(\tau-1)} - u_{ngt}), \ \forall n \in \mathcal{N}_B, \forall g \in \mathcal{G}, \forall t \in \mathcal{T} \tag{5.2i}$$

It should be noted that, when RES assets are modelled via (5.2d-5.2i), the minimum operational level μ_{ngt} is set to zero, the ramp rates (i.e., Δ_g^- and Δ_g^+) are set to one, while the mininum up and down times (i.e., δ_g^{mut} and δ_g^{mdt}) are set to the working time resolution. In addition, it is assumed these assets are non-controllable, thus u_{ngt} is also set to one. On the other hand, when (5.2d-5.2i) are leveraged to model the operation of dispatchable generators, the maximum availability π_{ngt} is set to one, while the remainder of technology-dependent parameters are set exogeneously.

$$p^D_{nst} \leq \kappa^*_{ns}, \ \forall n \in \mathcal{N}_B, \forall s \in \mathcal{S}, \forall t \in \mathcal{T} \tag{5.2j}$$

$$p^C_{nst} \leq \phi_s \kappa^*_{ns}, \ \forall n \in \mathcal{N}_B, \forall s \in \mathcal{S}, \forall t \in \mathcal{T} \tag{5.2k}$$

$$e_{nst} = \eta^{SD}_s e_{ns(t-1)} + \omega_s \eta^C_s p^C_{nst} - \omega_s \frac{1}{\eta^D_s} p^D_{nst}, \ \forall n \in \mathcal{N}_B, \forall s \in \mathcal{S}, \forall t \in \mathcal{T} \tag{5.2l}$$

$$\mu_s \sigma^*_{ns} \leq e_{nst} \leq \sigma^*_{ns}, \forall n \in \mathcal{N}_B, \forall s \in \mathcal{S}, \forall t \in \mathcal{T} \tag{5.2m}$$

Then, Eqs. (5.2j-5.2m) define the operation of storage units, which are modelled with asymmetrical charge-to-discharge rates. Constraints (5.2n-5.2o) model the power flows in trasnsmission assets.

$$|p_{it}| \leq \kappa^*_i, \ \forall i \in \mathcal{I}, \forall t \in \mathcal{T} \tag{5.2n}$$

$$\sum_{i \in \mathcal{I}_{ac}} C_{ic} x_i p_{it} = 0, \ \forall c \in \mathcal{C}, \forall t \in \mathcal{T} \tag{5.2o}$$

It should be emphasized here, as in the previous section, that constraint 5.2o (i.e., the cycle-based Kirchhoff Voltage Law) is enforced solely on the subset of non-controllable transmission assets, i.e., the ones developed as HVAC corridors.

5.2.4 Implementation

As in the previous chapter, with the exception of the siting algorithm (detailed in Section 4.3.2) which was implemented in Julia 1.4, the implementation of the proposed framework is based on Python 3.7. All simulations were run on a workstation running under CentOS, with an 18-core Intel Xeon Gold 6140 CPU clocking at 2.3 GHz and 256 GB RAM. Problems (5.1a-5.1c), as well as (5.2a-5.2o) are implemented in PyPSA 0.18 [32]. Gurobi 9.1 was used to solve the mixed-integer relaxation of the siting algorithm described in Section 4.3.2, as well as problems (5.1a-5.1c) and (5.2a-5.2o).

5.3 Experimental Set-up

This section describes the case study used to investigate the impact of the two siting strategies on the design and operation of power systems, as well as the modelling set-ups leveraged to this end. Throughout the proposed analysis solely wind (both onshore and offshore) generation assets are sited via the models discussed in Section 4.3.2. Solar-based technologies, on the other hand, are modelled via one profile per

bus, i.e., the capacity factor time series corresponding to a given bus is derived from the solar irradiance profile associated with the closest reanalysis grid point to the bus itself). It should be mentioned that the current analysis is limited to twelve European countries within Continental Europe, namely, Austria (AT), Belgium (BE), Czechia (CZ), Denmark (DK), France (FR), Germany (DE), Italy (IT), Luxembourg (LU), the Netherlands (NL), Portugal (PT), Spain (ES) and Switzerland (CH)[2]. Lastly, it should be noted that the upcoming exercise investigates solely partitioned siting instances (i.e., where sites are deployed taking into account the territorial boundaries of the $B = 12$ previously listed countries), unlike the test case proposed in the previous chapter that also analysed un-partitioned schemes (i.e., where siting of RES assets did not account for territorial boundaries).

5.3.1 Siting RES Assets

Renewable Resource Data As was the case in Chapter 4, ten years (i.e., 2010 to 2019) of hourly-sampled wind speed data at a spatial resolution of 0.25° are used in this analysis [86]. Unlike the set-up proposed in the previous chapter, time series are not re-sampled to a coarser temporal resolution. The conversion of resource data into capacity factor time series is managed via the transfer function of a wind farm comprising appropriate (based on the IEC61400 classification [144]) wind turbines for the renewable resource regimes found at each individual location [90]. The available wind turbines for wind deployment include the Vestas V90, V110, V117 and V164 models, each suitable for particular wind regimes [176].

Candidate Sites The set of candidate locations for onshore and offshore wind deployment, respectively, is determined via a filtering procedure that discards the reanalysis grid points where the installation of such technologies would be impractical. With respect to the onshore wind deployments, three distinct filters are applied. More specifically, all reanalysis grid points with an average population density above 200 inhabitants/km^2 are discarded. Then, grid points whose average terrain slope is greater than 3% or whose forestry cover is above 80% are also removed. A single filter is applied for offshore wind deployments, i.e., distance to shore. In particular, offshore wind deployments are possible in a band between 12 nm and 120 nm from the shore, in accordance with the considerations suggested in [145]. As a result of this filtering procedure, a total of 4573 onshore and offshore points (seen in Figure A.3) are available for deployment across the territories of the twelve European countries under investigation.

Deployment Targets The estimation of the country-specific cardinality constraints in 4.1c and 4.2d, respectively, starts from the outcome of two previous studies quantifying the pan-European requirements for wind power capacity to achieve deep

[2]The main reason for limiting the analysis to these twelve countries is the availability of reliable, highly-granular topology data for the British Isles and South-Eastern Europe.

decarbonisation targets in the electricity system by 2050 [91], [177]. According to these studies, up to 450 GW of offshore wind would be needed to supply 30% of the European electricity demand, while additional 253 GW of onshore wind capacity would contribute to an augmentation of 20% of the aforementioned supply target. It is hereby assumed that the capacity targets (on- and offshore) of the twelve countries considered in this exercise lead to the same system-wide wind-based electricity supply share of 50%. In other words, the current analysis envisions the deployment of 236 GW of offshore wind and 179 GW of onshore wind capacity, respectively.

Converting these capacity targets to cardinality constraints k_n necessitates yet another set of assumptions with respect to i) the area of a grid cell, ii) the power density of the underlying generation technology and iii) the land utilization factor, according to Eq. (4.5). In this regard, the assumptions considered in Section 4.4.1 are still valid for offshore wind deployment, whereas a site surface area of 442.5 km^2 (corresponding to a 0.25°-resolution cell at a latitude of 55° N), a power density of 5 MW/km^2 and a land utilization factor of 30% are assumed for onshore wind installations. Put together with the capacity targets in Eq. (4.5), these assumptions yield a total of $k = 452$ deployments to host the 415 GW of wind installations. Among these 452 sites, 180 are offshore locations while the remainder (i.e., 272) are onshore deployments. The distribution of these sites per country and technology is provided in Table 5.1.

COMP Siting Set-up The parameters of the *COMP* siting set-up (e.g., time window length δ, global criticality threshold c, local search algorithm parameters) are identical to the ones used to instantiate the exercise proposed in Chapter 4 with the exception of i) ς in Eq. (4.7), which is set to 50%, in line with the estimations provided in [91], [177] and ii) the global criticality threshold c which is set such that 10% of the locations must cover any time window for it to be labeled non-critical.

5.3.2 Capacity Expansion Planning Framework

Network Topology The network topology leveraged in this exercise is based on the interactive ENTSOE map [178]. In order to reduce the computational complexity of the problem, the sets of electrical buses and transmission lines provided by [178] were aggregated at a spatial resolution defined by the NUTS2 administrative regions [179] via the clustering procedure proposed in [59]. The resulting topology can be observed in Figure 5.2. It is hereby assumed, as in the exercise proposed in Chapter 4, that transmission expansion is limited to the reinforcement of existing corridors, while development of new transmission corridors is not taken into account at this stage.

Electricity Demand Ten years of electricity demand time series covering the twelve countries previously mentioned and simultaneously sampled with the resource data

TABLE 5.1: Capacity requirements and cardinalities of various locations sets for the twelve European countries included in this study. Table entries sorted in descending order based on the wind (onshore and offshore) capacity requirements per country.

Country	Technology [-]	κ_n [GW]	$\lvert\mathcal{L}_n\rvert$ [sites]	k_n [sites]
DE	W_{on}	70	449	53
	W_{off}	36	78	14
FR	W_{on}	36	804	28
	W_{off}	57	392	22
NL	W_{on}	8	10	7
	W_{off}	60	98	23
ES	W_{on}	35	629	27
	W_{off}	13	646	5
DK	W_{on}	5	86	4
	W_{off}	35	110	14
IT	W_{on}	14	197	11
	W_{off}	20	691	8
PT	W_{on}	7	123	6
	W_{off}	9	235	4
BE	W_{on}	4	22	4
	W_{off}	6	3	3
AT	W_{on}	0[1]	0	0
	W_{off}	N/A[2]	N/A	N/A
CH	W_{on}	0	0	0
	W_{off}	N/A	N/A	N/A
CZ	W_{on}	0	0	0
	W_{off}	N/A	N/A	N/A
LU	W_{on}	0	0	0
	W_{off}	N/A	N/A	N/A

[1] Values of zero justified by limited capacity targets, as provided in [177], for Czechia, Luxembourg and Switzerland. For Austria, it represents a modelling assumption.

[2] N/A stands for "Not Applicable" and applies to landlocked countries, e.g., Austria, Czechia, Luxembourg or Switzerland.

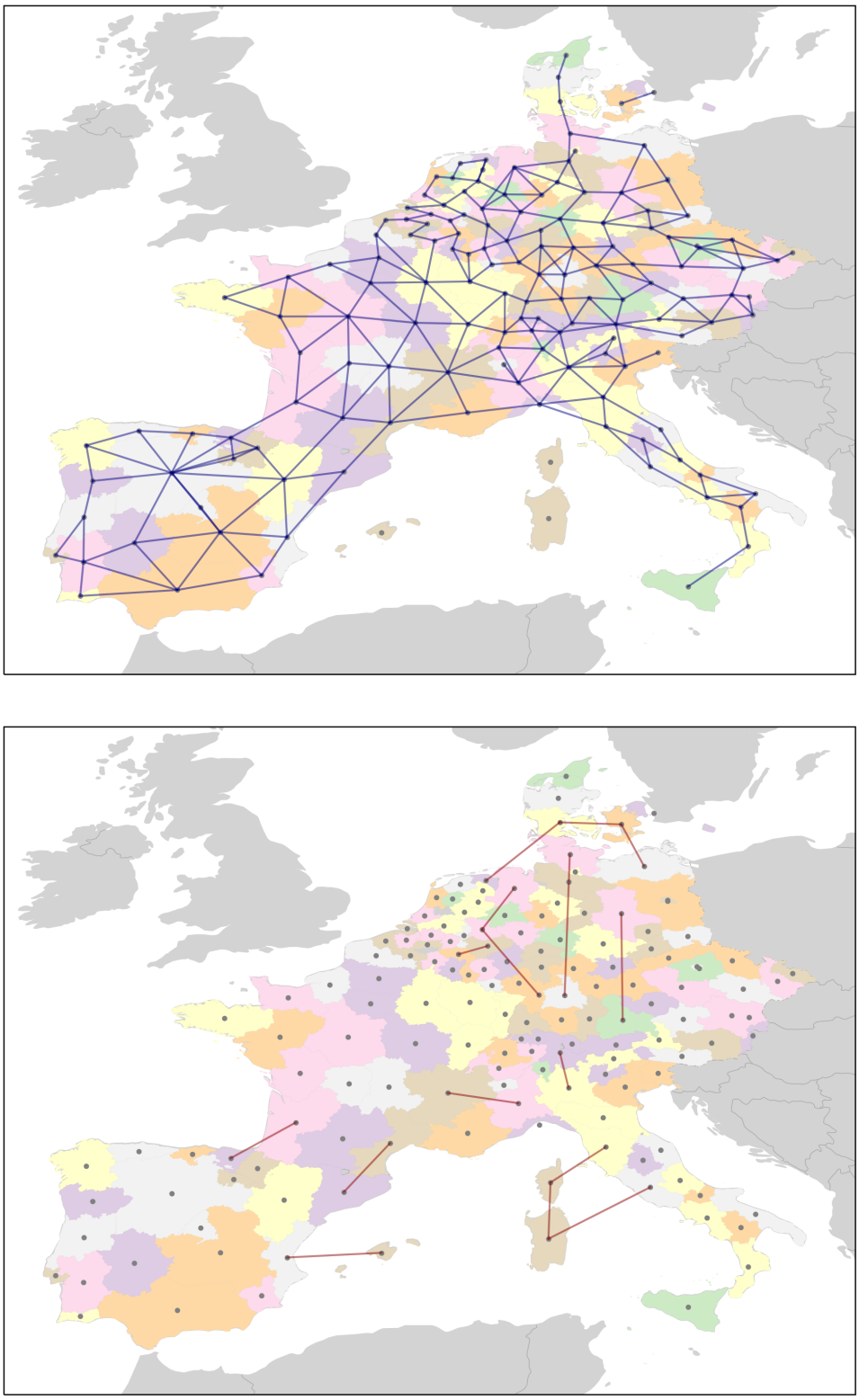

FIGURE 5.2: Network topology based on the NUTS2 administrative regions. AC transmission corridors are shown on top while DC links are depicted in the bottom subplot.

leveraged in the siting stage are retrieved from [149]. The distribution of electricity demand across the NUTS2 regions is carried out by taking into account the population density [180] and the gross domestic product [181], respectively, of the regions in the corresponding countries.

Electricity Generation Technologies There are nine technologies available for electricity generation, i.e., offshore and onshore wind, utility-scale and distributed solar PV, run-of-river and reservoir-based hydro, nuclear plants, open- and combined-cycle gas turbines (OCGT and CCGT, respectively). Only a subset of these technologies (i.e., the wind-based and gas-fired units, respectively) are sized, while installed capacities of solar-, hydro- and nuclear power plants remain fixed throughout the optimisation. All generation technologies except the wind-based and gas-fired power plants are assumed to have non-zero installed capacities at the beginning of the optimisation exercise. More specifically, 44.5 GW of nuclear power capacity, 24.8 GW of run-of-river hydro power capacity and 37.3 GW of reservoir-based hydro power capacity are available throughout the selected European countries [150], [151]. Utility-scale solar PV capacity data is retrieved from [62], where a legacy capacity of 33.9 GW is reported throughout Europe. Finally, country-aggregated capacities for distributed PV installations are retrieved from [152], where the existence of 68.8 GW of such installations is reported within European borders. Recall that the technical potentials of wind-based technologies are inputs from the siting stage. The technical potentials of the remaining generation technologies to be sized in the expansion planning framework (i.e., OCGT and CCGT) are assumed to be unconstrained.

Electricity Storage Technologies Two technologies are available for storing electricity, namely, pumped-hydro (PHS) and battery storage (Li-Ion). It is assumed that no legacy capacity is available in Europe for the latter. Pumped-hydro units are not sized within the CEP framework at hand and the power ratings of existing plants are retrieved from [151], where a total of 43.1 GW/1236 GWh of PHS units are reported. A summary of the techno-economic data used to instantiate the CEP problem is provided in Table A.1.

Policy Considerations The expansion planning problem (5.1a-5.1c) contains the same two policy constraints featured in Chapter 4. More specifically, a CO_2 reduction of 90% compared to 1990 levels is enforced system-wide (i.e., not on a country by country basis), while a 20% planning reserve margin is considered in the definition of the system adequacy constraint.

Solution Method Solving the CEP problem (5.1a-5.1c) is a daunting computational task, given the temporal resolution and horizon proposed by this instance (i.e., 1 h and ten years, respectively) and the spatial resolution chosen to model RES assets

(with more than 450 sizing variables for wind sites only), as well as dispatchable generation units or transmission infrastructure. In order to mitigate the computational burden brought by these modelling features, two simplifying techniques are hereby leveraged.

First, a temporal reduction technique based on the selection of typical periods is employed to reduce the temporal dimension of the underlying instance [53]. In particular, the ten-year planning horizon with hourly resolution was reduced to seventy unlinked representative days[3] with hourly intra-daily resolution. In other words, $\omega_s = 1$ in Eq. (4.4m), while ω_t in Eqs. (4.4a) and (4.4r) is equal to the number of days associated to each of the seventy representative periods [183]. Second, since transmission lines are expanded in the proposed CEP, their series reactance x_i in Eq. (5.1c) would also decrease and would thus introduce a bilinear term with the variable denoting the power flows (namely, p_{it}). In order to keep the CEP formulation continuous linear, the following iterative solution method inspired from the works of Hagspiel et al. [184] is proposed. According to this method, the CEP problem is run with the series reactance of all non-controllable lines as parameters. Once the solution of the problem is retrieved, reactances are updated[4] and the process is repeated until the relative difference between consecutive iterations falls below 3%. A list of solver parameters whose values were tuned for the purpose of this CEP exercise is provided in Table A.5.

5.3.3 Unit Commitment and Economic Dispatch Problem

Electricity Generation Technologies There are three electricity generation technologies whose unit commitment costs and constraints are modelled, namely, nuclear, OCGT and CCGT units. In particular, the following modelling aspects are taken into account for these three technologies: start-up costs, ramp rates and minimum operating levels, as well as minimum up- and down-times. The values assumed for these parameters are gathered in Table A.4.

Solution Method In order to solve the UCED problem stated in (5.2a-5.2o), two simplifying assumptions are made. First, the generation technologies whose unit commitment costs and constraints are modelled do not represent individual units, but aggregation of multiple units per electrical bus. In other words, a CCGT plant at a particular bus represented in Figure 5.2 can represent multiple individual units with identical techno-economic parameters and operating regimes. The second assumption made to mitigate the computational requirements of the UCED problem at hand relates to splitting the ten-year time horizon in 3653 daily blocks with hourly resolution that are tackled independently by the solver. Put differently, $|\mathcal{T}| = 24, \omega_t =$

[3] The details and modelling implications of using unlinked typical periods in CEP frameworks are addressed in a recent article by Gonzato et al. [182]

[4] The procedure for updating line characteristics in the proposed iterative method are detailed in [185].

1 and $\omega_s = 1$ for each UCED instance modelled via (5.2a-5.2o). It should also be noted that the proposed solution method does not consider a rolling horizon[5], however it accounts for the inter-daily coupling of storage units (i.e., the state of charge of storage units is passed from the end of one day to the beginning of the next one). The solver parameters whose values were tuned in the context of the current UCED problem are summarized in Table A.6.

5.4 Results

In this section, a series of experiments that compare the implications of the proposed siting schemes on the design and operation of power systems is conducted. In particular, the impact of siting of roughly 450 wind power plants in the continental European power system according to deployment criteria that maximise their aggregate power output - *PROD* - and spatiotemporal complementarity - *COMP* -, respectively, is discussed.

5.4.1 Siting of Renewable Generation Assets

The outcome of siting wind power plants across continental Europe according to the two proposed siting criteria is displayed in Figure 5.3. In this plot, the set union of red and yellow markers denote the sites associated with the *PROD* scheme, while the union of blue and yellow markers depicts the *COMP* deployment pattern. A number of 256 onshore and offshore wind sites (or 56% of the total number of deployments) are common across the two siting schemes. For the remainder, significant differences are observed between *PROD* and *COMP*. For instance, while the former strategy deploys virtually all German onshore wind sites in the Northern regions (swept by high quality winds [124]), the *COMP* scheme deploys a considerable share of these sites in the Eastern, South-Western and Southern part of the country. In a similar fashion, yet to a lesser extent, sites in Northern France are re-located via *COMP* in the Mediterranean region, as already revealed in the analysis proposed in Chapter 3. Significant differences in onshore wind deployments are also observed in Italy (where a number of sites deployed by *PROD* in Sardinia are re-located by *COMP* in Sicily and the South-Eastern regions of the country) or Spain (where some sites in the Atlantic region are deployed by *COMP* in Andalusia). However, more striking differences between the two siting schemes are observed for the offshore deployments. For example, under the *COMP* scheme, the Dutch and Danish offshore deployments cover a larger surface in the North Sea, while some of the German sites in the same area are re-located in the Baltic Sea. In addition, *PROD*-based French and Spanish deployments in the Atlantic region are re-located to the Mediterranean,

[5]The decision to discard the rolling horizon method from the proposed UCED implementation is supported by the lack of two modelling features that would justify its utilization and the associated increase in computational complexity, i.e., the availability and update of RES forecasts on intra-day time horizons and the availability of power plant outage rates.

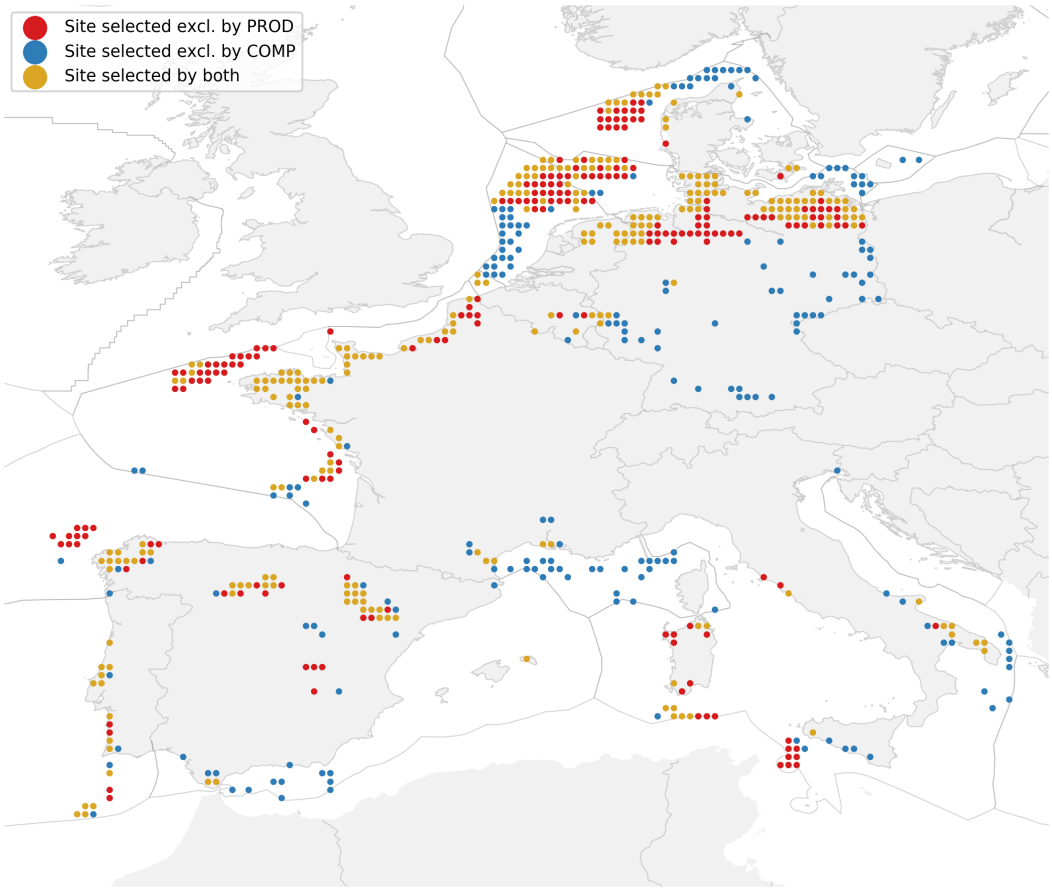

FIGURE 5.3: Sets of sites deployed via the *PROD* and *COMP* schemes, respectively. The red markers show sites that are exclusively selected by *PROD*, while the blue markers denote sites chosen by the *COMP* scheme. Yellow markers show common sites across the two siting schemes.

a region with distinct wind regimes [159]. Moreover, differences between *PROD* and *COMP* in the deployment of offshore sites can also be seen in Italy. Around ten locations located south of Sicily and Sardinia in the former scheme are found in the Adriatic region under the latter strategy. Overall, in terms of siting objective, these differences lead to 74786 non-critical windows (or 85.3% of the total number of time windows) for the *PROD* scheme and 76066 non-critical windows (or 86.8% of the total number of windows) for the *COMP* strategy, respectively.

5.4.2 Cost-Optimal System Design

Before analysing the results of the sizing stage, i.e., capacities and costs of power system assets, a closer look into the outcome of the temporal reduction technique employed within this problem is provided. To this end, Figure 5.4 summarizes some relevant information with respect to how the seventy representative days are selected within the capacity expansion problems leveraging the *PROD* (red) and *COMP* (blue) siting schemes, respectively. In this figure, the top subplot shows the

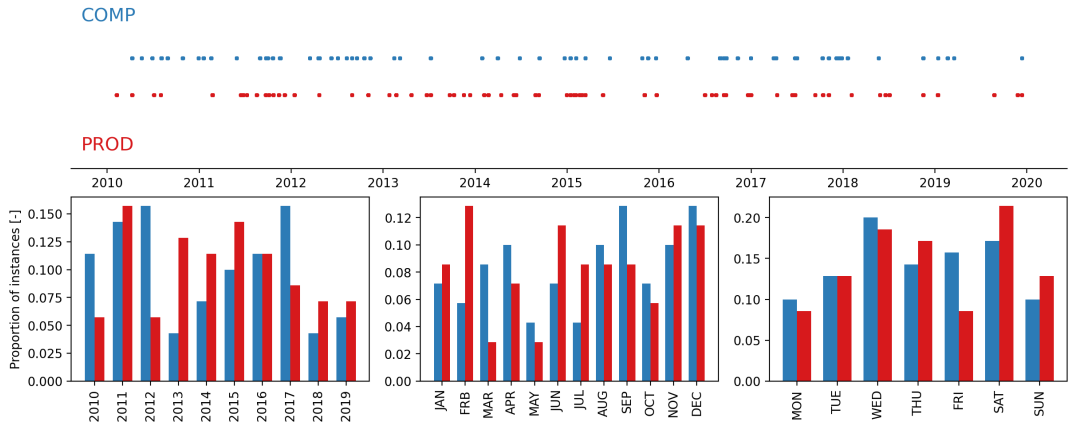

FIGURE 5.4: Representative day selection for the two expansion planning problems, i.e., *COMP* and *PROD* (top). The subplots below depict histograms of the selected time steps per year (left), month (middle) and day of week (right), respectively.

sequence of the seventy selected days (among a total of 3652 days between January 1, 2010 and December 31, 2019) for the two expansion planning problems. In this plot, each unitary segment represents one full day, or 24 h, and they are ordered chronologically. This subplot is accompanied by the three bottom figures, which show histograms of representative day selection per year (left), month (middle) and day of week (right), for each of the two sizing problems. At a first glance, these histograms reveal a fairly balanced choice of representative periods between the two instances. For instance, the years of 2011, 2015, 2016, 2018 or 2019 have fairly similar weights in the two cases. The same applies for the months of January, May, August, October, November or December, as well as for all days of week except for Fridays.

This result is supported by the figures in Table 5.2, where a series of relevant metrics in the two expansion planning problems are summarized. More specifically, these metrics include peak and total demand, as well as average and standard deviation values for PV and ROR capacity factors and inflows in reservoir-based hydro units, respectively. It can be seen in this table that all but one metric, namely, the standard deviation of hydro inflows, are virtually equal across the two sizing problems. This points out the balanced selection of representative days across the two CEP problems and, thus, enables a fair comparison between the two siting schemes in terms of system design and costs within the same problem.

Table 5.3 gathers installed capacities and associated costs for the technologies which are sized in the *PROD*- and *COMP*-based CEP problems. In general, the outcomes reported in this table support the findings of Chapter 4. First, the total cost (i.e., CAPEX and VOM of generation, storage and transmission units) of the system leveraging the *COMP* siting scheme for wind assets is 2.1% more expensive than the *PROD* counterpart. Second, Li-Ion storage does not play a significant role in the system design for the same reasons stated in Section 4.5.2. Third, the *COMP* siting

TABLE 5.2: Comparative view of time series statistics across the two capacity expansion planning instances considered. Values reflecting peak demand, total demand, average and standard deviation of PV capacity factors, run-of-river hydro capacity factors and reservoir-based hydro inflows, respectively.

	$\hat{\lambda}$ [GW]	$\sum\lambda$ [TWh]	$\bar{\pi}_{PV}$ [-]	σ_{PV} [-]	$\bar{\pi}_{ROR}$ [-]	σ_{ROR} [-]	$\bar{\pi}_{STO}$ [-]	σ_{STO} [-]
PROD	311.87	376.99	0.122	0.185	0.441	0.324	0.307	0.600
COMP	311.19	377.18	0.122	0.184	0.437	0.330	0.306	0.669

strategy seems to lead to reduced installed capacities, yet a more pronounced utilization of natural gas-fired power plants compared to the sizing instance leveraging the *PROD* siting scheme. More specifically, the former leads to a total of 243 GW, while the latter scheme leads to a total of 270 GW of OCGT and CCGT units across the studied system. In contrast, 871 TWh are produced via the natural gas-based units in the *COMP* instance, while only 580 TWh are generated by the same installations in the *PROD* instance. This difference of over 290 TWh is required under the former scheme to make up for most of the deficit in wind feed-in, which has two main causes. On the one hand, *PROD* deploys less offshore wind capacity than *COMP*, which results in annual cost savings of 5.5 b€. However, the superior capacity factors at the *PROD*-specific sites (47.2% compared to only 44.2% for the *COMP* sites) enables a production from these units which is 152 TWh greater than the one associated with the *COMP* sites. On the other hand, an additional 7 GW of onshore wind are deployed in the *PROD* instance (mainly because of the better trade-off between upfront costs and average capacity factors). This aspect, corroborated by the fact that the average capacity factor of *PROD*-based onshore wind units is 1.2% higher than the one of the *COMP* onshore wind sites (i.e., 33.8% for the former against 32.4% for the latter) leads to an additional 254 TWh of wind feed-in deficit for the *COMP* based instance. In total, 406 TWh of *missing* wind feed-in are thus supplied via natural gas power plants, as well as (in a smaller proportion) by hydro power units. Overall, the *COMP* strategy leads to marginal cost savings from wind investments, i.e., 0.16 b€. Nonetheless, roughly 10 b€worth of savings each year result from transmission investments, with results showing 35% less additional AC capacity and 40% less additional DC capacity needed in this instance. However, these savings turn out to be insufficient to cover for the VOM-intensive operation of OCGT and CCGT units required to make up for the deficit in onshore and offshore wind feed-in across the system.

Another interesting result in Table 5.3 relates to the fact that onshore wind capacity targets are (almost) fully met, while offshore capacity requirements stated in Section 5.3.1 are covered in a proportion of 76% and 78% for the *PROD* and *COMP*-based instances, respectively. An aspect worth mentioning at this stage is that the total

TABLE 5.3: Comparison of additional (excl. legacy) installed capacities, electricity volumes and associated costs for various technologies sized in the CEP framework according to the two siting strategies. Even if Li-Ion storage is sized in the current exercise, it plays a limited role and thus is not reported in this table. CAPEX include FOM costs, as well.

		Technology	OCGT	CCGT	W_{on}	W_{off}	AC	DC
PROD	K	[GW/TWkm]	232.06	38.01	181.04	180.53	35.92	8.29
	p	[TWh]	59.08	520.24	5318.49	7252.75		
	CAPEX	[b€]	84.94	18.18	132.22	224.61	26.04	5.39
	VOM	[b€]	5.49	36.42	0.00	0.00	N/A	N/A
COMP	K	[GW/TWkm]	196.95	46.25	173.80	184.90	23.88	5.04
	p	[TWh]	87.75	783.28	5064.09	7099.47		
	CAPEX	[b€]	72.09	22.12	126.94	230.05	17.31	3.28
	VOM	[b€]	8.16	54.83	0.00	0.00	N/A	N/A

capacity of onshore wind deployed under the *PROD* scheme seems to be greater than the 179 GW targeted in Section 5.3.1. This is a result of the assumption made in Eq. (4.5) with respect to the area of each grid cell, whose value was assumed to represent the surface of a grid cell at 55° N. However, once wind locations are known, their capacity potential is computed ex-post based on the surface area of the corresponding grid cell and used as input data in the capacity expansion planning problem. Wind sites located South of the aforementioned reference point have larger surface areas and, thus, more capacity potential that the initial estimate (while the opposite is valid for sites North of the reference point). In consequence, the aggregate deployment of onshore and/or offshore wind may be greater than 179 GW and 236 GW, respectively.

Further on, Figure 5.5 provides a more detailed view of how wind capacities are deployed across the 472 sites in the two CEP instances. In this figure, the plots on the left show the site-specific installed capacity of onshore deployments, while the right hand-side plots depict the site-by-site capacities of offshore farms selected via the two siting criteria. In all these four subplots, wind sites represented by dark red markers denote locations whose installed capacity in the sizing problem is below 50 MW (and are thus considered under-developed considering their total potential of over 800 MW or 1750 MW, respectively). The onshore wind deployments associated with the *PROD* siting scheme are fully developed in the sizing problem in all but two countries, namely, Germany (North and North-East) and Italy (Sardinia and Sicily). With respect to the offshore sites, it is mainly Dutch and French sites that are not exploited in the CEP instance. For the *COMP*-based instance, things are slightly different. On the one hand, onshore sites are not developed in South and South-West Germany, South-East Italy, as well as North and North-West Spain

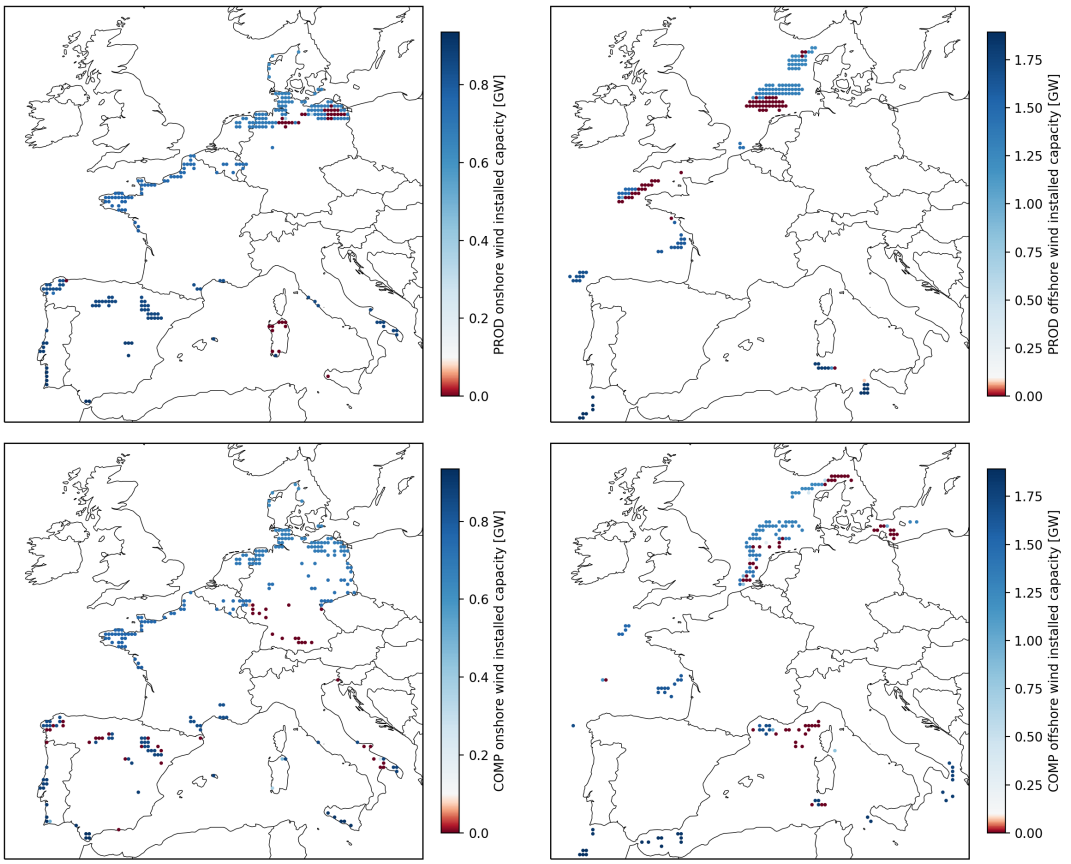

FIGURE 5.5: Installed capacity across the 472 wind locations identified by the capacity expansion planning problem. The two plots on the top (bottom) show the installed capacities of onshore and offshore installations whose locations were identified via the *PROD* (*COMP*) siting algorithms.

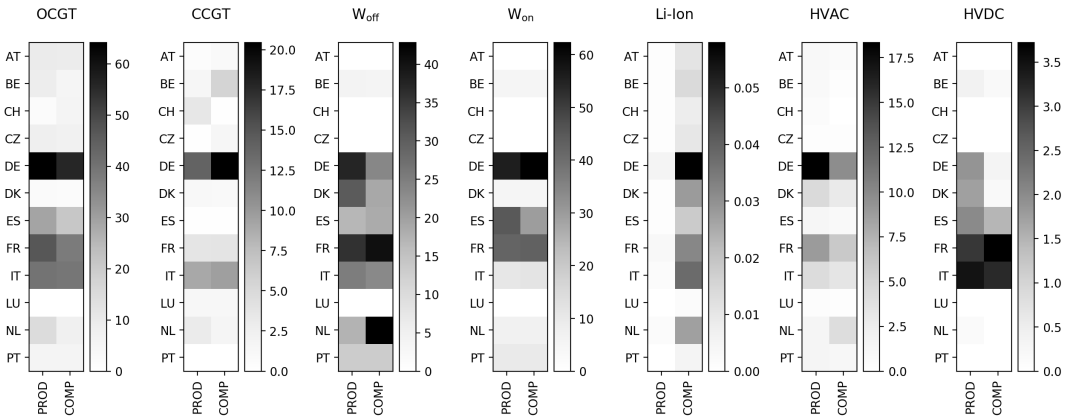

FIGURE 5.6: Breakdown of additional (excl. legacy capacities) installed capacities of different technologies sized within the capacity expansion planning problem per country and siting strategy. Values expressed in GW, GWh and TW $\times$ km for generation, storage and transmission technologies, respectively. For transmission assets, capacity is assigned to both ends of the interconnector. Therefore, an additional 1 GW of capacity for an AC interconnection between a bus in DE and another one in BE will be reflected in both the DE and BE squares in the heatmap above.

(additional offshore wind in this country under the *COMP* scheme replaces onshore wind generation). Offshore sites, on the other hand, are less exploited in Denmark, Germany (the Baltic area), but also Italy (North of Corsica, as well as South of Sicily) and, to a lesser extent, the Netherlands. More details about these changes in the generation fleet of specific countries are provided in the following paragraph based on observations from Figure 5.6.

Figure 5.6 gathers installed capacities for different classes of power system assets sized in the CEP instances, namely, OCGT and CCGT units, onshore and offshore wind farms, Li-Ion battery storage systems, AC and DC transmission links. A couple of interesting outcomes that support the previous findings can be observed in this plot. First, the Netherlands and France deploy significantly more offshore wind capacity under the *COMP* scheme at the expense of less deployments in Denmark and Germany. Slightly more offshore wind capacity in Spain is compensated by less onshore wind in the same country. Otherwise, onshore wind deployments are fairly consistent across the two siting strategies, with the exception of Germany, where an additional 6 GW are installed under the *COMP*-based instance. In the same sizing instance, OCGT deployments decrease across most of the twelve countries compared to *PROD*, again indicating a less stringent need for peak dispatchable capacity. As seen in Table 5.3, the overall CCGT capacity increases by 20% in the *COMP* set-up compared to the *PROD* one, mainly to cover for the wind feed-in deficit in the former scheme. This difference of 20% is largely attributed to Germany (going from 14 GW in the *PROD* instance to 19 GW in the *COMP* one), Italy and Belgium. Storage (i.e., Li-Ion) capacity is greater in the *COMP* scheme, yet limited to 250 MWh system-wide. Then, in terms of transmission expansion, the sizing instance based on the *COMP* siting scheme leads to lower installed capacities with very few exceptions. For instance, HVAC ties are less needed across the entire twelve countries investigated, except in the Netherlands where additional capacity is required to evacuate all the surplus electricity produced by offshore wind capacity (relative to *PROD*) discussed earlier. Similarly, HVDC connections are less required in the *COMP* scheme. The sole exception are the connections of Spain and Italy to France, which are reinforced more than in the *PROD* scheme in order to supply the South European countries with power from generators located in Central-Western Europe.

5.4.3 Impact on the Operation of Power Systems

In this section, the results of the UCED problems (5.2a-5.2o) instantiated with the *COMP*- and *PROD*-based sizing outcomes and, in particular, the costs of operating the underlying power systems are discussed. Figure 5.7 depicts overlapping (normed) histograms of daily operating system costs throughout the ten year horizon considered in the study (i.e., a total of 3653 samples per histogram). Some important outcomes should be emphasized here. First, as can be seen in the zoomed area within the plot, it appears that the *COMP* siting scheme leads to a reduction of

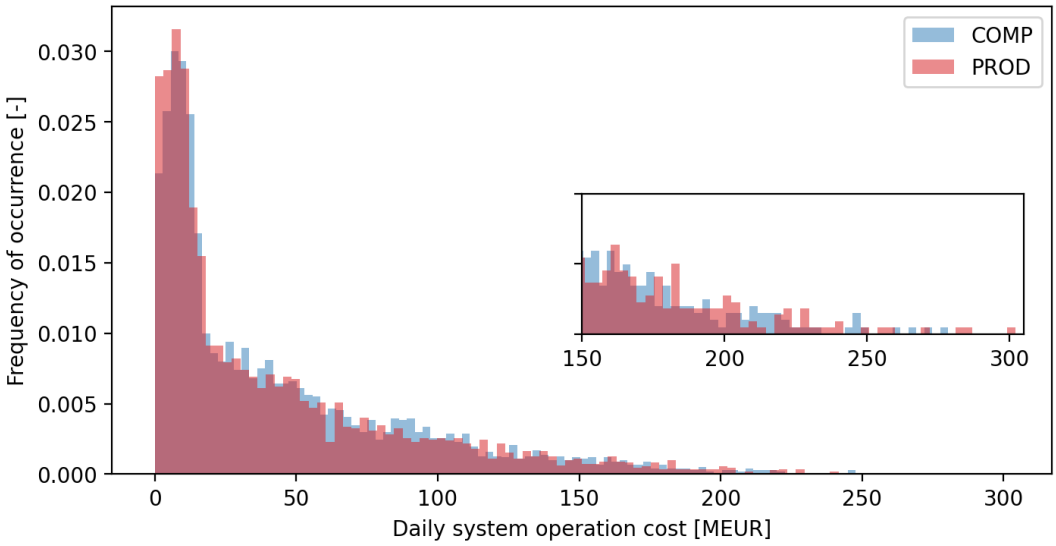

FIGURE 5.7: Distribution of daily system operation costs [M€] resulting from running the UCED problem with the sizing outcomes of the *COMP* (blue) and *PROD* (red) instances, respectively. A total of one hundred bins are used to generate each of the two histograms.

the spread in the daily operating costs. In other words, the complementarity-based strategy for wind asset deployment manages to reduce the maximum daily operational cost by roughly 10%. However, a second outcome worth discussing is the fact that *PROD* still leads to lower operating costs than *COMP* across the full horizon of 3653 days. More specifically, the total operating costs resulting from the *PROD* siting strategy are 3.7% lower than the costs of operating the system with the *COMP* deployment pattern (153.7 b€ under the former scheme and 159.5 b€under the latter). This difference supports the findings from the previous sections and can mainly be explained by the more frequent occurrence of days with very low operating costs (i.e., dominated by RES feed-in) under the scheme maximizing capacity factors of wind assets, as can be seen in the top left area of Figure 5.7.

A day-by-day comparison of operating costs provides further insight into the two instances. To this end, Figure 5.8 shows the cumulative distribution of the operating cost differences between pairs of days, resulting from the UCED problems instantiated with *COMP* and *PROD* sizing outcomes, respectively. In this plot, negative values reflect cheaper operating costs for *COMP* compared to *PROD*, for a given day. Two interesting aspects are worth mentioning here. Even though *PROD* leads to overall lower costs for operation, the *COMP* siting scheme leads to cheaper daily operating cost more than 60% of the time. In addition, one can observe that the underlying cumulative distribution function grows steeply in the [-25, 25] interval, which represents less than 10% of the full range of variation. In other words, the daily operating costs of the *COMP*- and *PROD*-based systems are very close most of the time. This points to the sensitivity of this comparison to the economic assumptions made to instantiate the UCED problems and hints at the potential for an

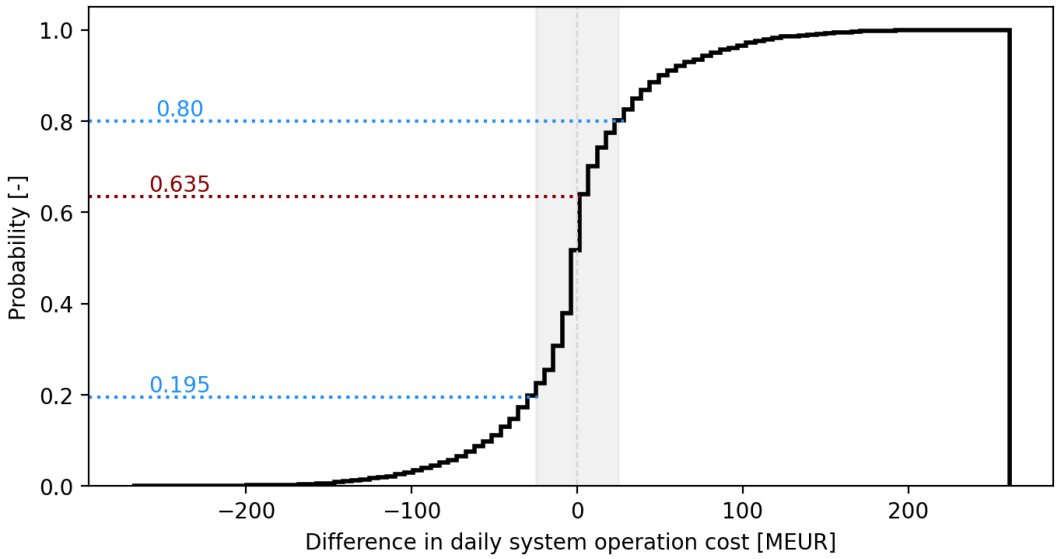

FIGURE 5.8: Cumulative distribution of the difference in daily system operation costs [M€] between *COMP*- and *PROD*-based UCED instances. A negative (positive) value indicates a lower daily operating cost for the *COMP*-based (*PROD*-based) instance.

in-depth analysis that takes into account the techno-economic development of the flexible technologies considered in this study.

Figure 5.9 further contributes to this analysis by providing a more detailed view of how the total operating costs of power generation assets whose unit commitment constraints were considered in the corresponding *COMP*- and *PROD*-based UCED instances are split between different categories (e.g., variable cost of operation, start-up cost, ramping cost) and technologies, respectively. The plot on top shows the break-down of costs (associated with OCGT, CCGT and nuclear units) per type of expense and reveals that the VOM (incl. fuel and CO_2-related, shown in light yellow) fraction takes the lion's share of the operating expenses for any of the two UCED instances. Start-up costs (shown in dark yellow) also make a visible, yet limited (around 5%) contribution to the total, while ramping costs (not visible in this plot) account for under 0.1% of the total cost of operating these units. Overall, it can be observed in this subplot that most of the 3.4% difference revealed in one of the previous paragraphs is attributed to the higher VOM of generation units under the *COMP* instance, which simply stem from their more frequent utilisation.

Then, the three plots in the lower half of Figure 5.9 reveal further information about how these costs are split among technologies and how they compare between the two UCED instances investigated. To begin with, the costs of OCGT units are consistently higher under the *PROD* scheme. Higher installed capacities (see Table 5.3) corroborated by higher average capacity factors (see Figure 5.10) lead to greater VOM costs, as see in the bottom left subplot of Figure 5.9. These peaking units are also started-up and ramped more often under the *PROD* scheme, an aspect which

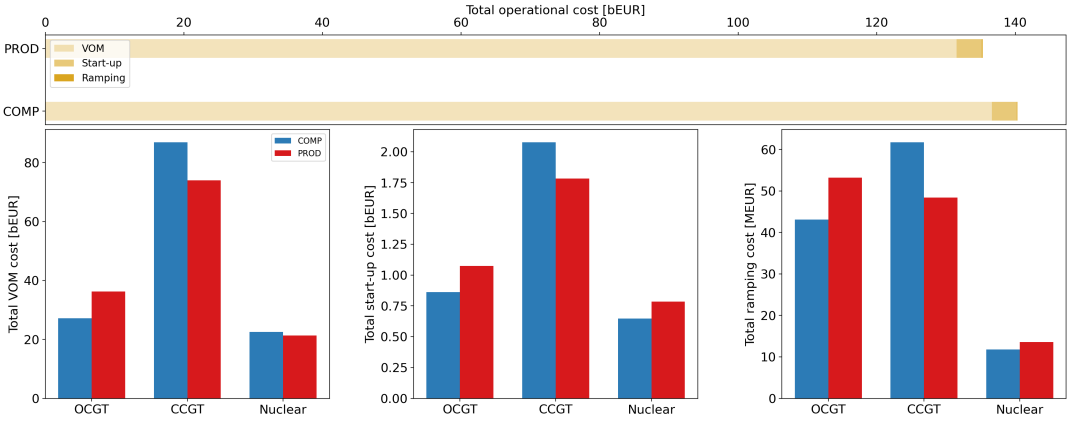

FIGURE 5.9: Unit commitment and economic dispatch costs associated with the three technologies with such constraints modelled in the UCED problem (i.e., OCGT, CCGT, nuclear) and the two siting strategies considered (i.e., *COMP* and *PROD*). On top, the break-down of operating expenses per type (e.g., VOM, start-up, ramping), expressed in M€. Below, break-down per technology for each individual type of operational cost, namely, VOM (left), start-up (middle), ramping (right), and the two siting strategies investigated. Ramping costs are estimated ex-post, based on cost assumptions from [186].

hints at the ability of the proposed complementarity-based siting scheme to avoid system-wide RES scarcity events. Then, according to Figure 5.10, nuclear units (with equal installed capacity across the two UCED instances) have higher capacity factors under the *COMP* scheme, which translates into higher VOM costs. However, this deployment scheme for wind assets also enables a more steady operation of such units, which experience fewer start-ups and fewer ramping events, according to the middle and right subplots of Figure 5.9. Lastly, the increased costs of CCGT units under the *COMP* scheme can be explained as follows. As already discussed in the section describing the results of the CEP stage, the wind feed-in deficit associated with the complementarity-based siting scheme leads to a more sustained utilization of the higher-efficiency dispatchable option. This outcome persists in the UCED stage and translates into higher VOM costs for CCGT generators. More specifically, a 340 TWh deficit of wind feed-in corresponding to the *COMP* scheme is covered partially by a more efficient utilization of hydro and nuclear units (as seen in Figure 5.10), but also by ramping up CCGT generation by a total of 184 TWh across the ten year horizon. The higher start-up costs for this technology under the *COMP* instance are mainly due to the associated increases in installed capacities across Belgium, Germany and Switzerland (see Figure 5.6). Finally, the higher ramping costs for CCGT units under the *COMP* scheme compared to the *PROD*-based one are a by-product of their increased utilization, considering that they are used in a load-following mode for most of the time they are generating electricity.

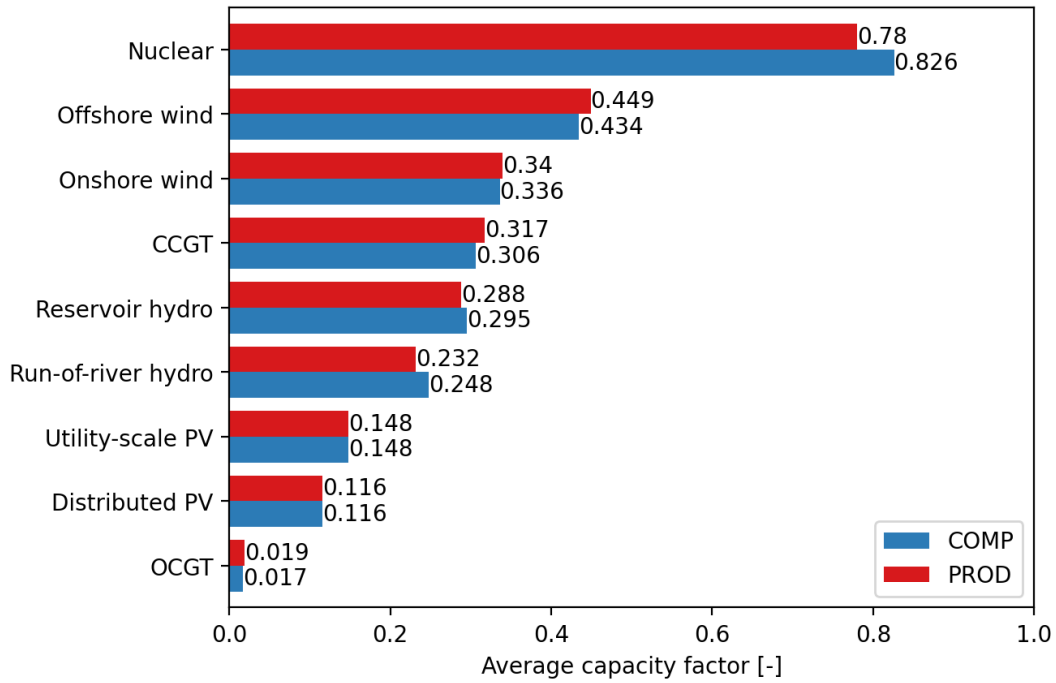

FIGURE 5.10: Ten-year average capacity factors for various generation technologies considered in the UCED problems. In blue, values associated with the *COMP*-based instance. In red, outcomes derived from the *PROD*-based model. Labels sorted in descending order based on the *COMP* value.

5.5 Conclusion

In this chapter, the impact of two siting strategies for wind assets on the design and operation of the Continental European power system is investigated. A three-stage routine is leveraged to this end. In the first stage, a highly-granular siting problem identifies a suitable set of sites where wind assets could be deployed according to a pre-specified criterion. Two siting schemes are analysed and compared in a realistic case study. These schemes essentially select a pre-specified number of sites so as to maximise their aggregate power output and their spatiotemporal complementarity, respectively. In the second stage, the subset of previously identified sites is passed to a capacity expansion planning framework that sizes the power generation, transmission and storage assets that should be deployed and operated in order to satisfy pre-specified electricity demand levels at minimum cost. Once the capacities of these assets are known, a third stage, formulated as a unit commitment and economic dispatch problem, is leveraged to investigate the impact of the aforementioned wind siting strategies on the short-term operation of the power system.

Results seem to support the findings of the analysis proposed in the previous chapter, in that the *COMP* siting scheme leads to a system design that is roughly 2% more expensive than the *PROD* counterpart. This suggests that leveraging a more refined network topology and relying on a better approximation of network flows does not

lead to a more appealing case for the complementarity-based wind asset siting strategy. From an operational standpoint, results are similar. On the one hand, the unit commitment and economic dispatch problem proposed in this chapter revealed that the *COMP* siting strategy leads to lower daily system operating costs in almost two thirds of the over 3653 days included in the study. However, a view across the full ten year horizon revealed that the *PROD* siting strategy leads to overall lower (i.e., 3.7%) operating costs mainly due to the less sustained utilization of CCGT units for load following purposes.

Chapter 6

Model Reduction in Capacity Expansion Planning Problems via Renewable Generation Site Selection

The accurate representation of variable renewable generation (RES, e.g., wind, solar PV) assets in capacity expansion planning (CEP) studies is paramount to capture spatial and temporal correlations that may exist between sites and impact both power system design and operation. However, it typically has a high computational cost. This paper proposes a method to reduce the spatial dimension of CEP problems while preserving an accurate representation of renewable energy sources. A two-stage approach is proposed to this end. In the first stage, relevant sites are identified via a screening routine that discards the locations with little impact on system design. In the second stage, the subset of relevant RES sites previously identified is used in a CEP problem to determine the optimal configuration of the power system. The proposed method is tested on a realistic EU case study and its performance is benchmarked against a CEP set-up in which the entire set of candidate RES sites is available. The method shows great promise, with the screening stage consistently identifying 90% of the optimal RES sites while discarding up to 54% of the total number of candidate locations. This leads to a peak memory reduction of up to 41% and solver runtime gains between 31% and 46%, depending on the weather year considered.

This chapter is a reprint of *David-Constantin Radu, Antoine Dubois, Mathias Berger, Damien Ernst, "Model Reduction in Capacity Expansion Planning Problems via Renewable Generation Site Selection," 2021 IEEE Madrid PowerTech, 2021, pp. 1-6,* https://doi.org/10.1109/PowerTech46648.2021.9495027.

6.1 Introduction

Capacity expansion planning (CEP) problems are powerful tools for the design, analysis and implementation of energy system decarbonisation policies. In such frameworks, the accurate spatiotemporal representation of variable renewable energy generation (RES, e.g., wind, solar PV) is paramount for the precise estimation of capacity requirements [51]. However, the detailed modelling of RES comes at a high computational cost and ways to mitigate this issue in order to strike the right balance between accuracy and computational effort when solving such problems are necessary, yet seldom proposed. For example, a highly detailed representation of RES within a CEP set-up cast as a linear program (LP) is proposed by MacDonald et al. [52], yet the reported runtimes (thousands of core hours for large-scale instances) limit its use in practice and its reproducibility. Wu et al. [137] also propose an LP-cast CEP framework in which high-resolution RES modelling is made possible via a GIS-based resource assessment tool. Nonetheless, the coefficient matrix stores hourly capacity factor values at each location and is therefore full, which limits the scalability of the proposed method to a few hundreds of candidate RES sites only, thus rendering it unsuitable for large-scale applications.

Although plenty of work has been carried out in recent years to develop temporal reduction techniques for RES in CEP settings [53], studies tackling the issue of spatial model reduction are scarce. Cohen et al. [187] suggest the aggregation of RES in resource regions, with wind and solar PV resources over the contiguous United States being modelled via 356 and 134 profiles, respectively. In a similar vein, Hörsch and Brown [59] leverage a CEP framework formulated as an LP to assess the impact of spatial resolution on the outcomes of co-optimizing generation and transmission assets across Europe. A network reduction process based on k-means clustering is incorporated in their method and the resulting topology serves as the basis for modelling renewable resources. More precisely, Europe-wide RES are represented via 37 to 362 different aggregate profiles, depending on the desired number of network clusters. While spatial aggregation approaches, as the ones proposed in [59], [187], partly mitigate the aforementioned computational issues [52], [137], the limited number of RES profiles considered hinders their ability to exploit the benefits of resource diversity which, in turn, can lead to system cost overestimation [58].

This chapter proposes a method to reduce the spatial dimension and decrease the computational requirements of CEP problems while preserving a detailed representation of RES assets. This is achieved by leveraging a two-stage heuristic that can be described as follows. The first stage, which is cast as an LP, is used to screen a set of candidate sites and identify sites that have little impact on optimal system design, which are then discarded. In the second stage, information (geo-positioning and capacity factors time series) about the remaining sites is used as input data in a CEP framework that determines the installed capacities of generation, storage and

transmission assets leading to a minimum-cost system configuration. Thus, the proposed method makes it possible to reduce the size of the CEP problem, and therefore enables memory and computation time savings.

The chapter is structured as follows. Section 6.2 details the methods at the core of the proposed two-stage approach. Then, Section 6.3 briefly describes the case study used to showcase the applicability of the suggested approach before results are reported in Section 6.4. Section 6.5 concludes the chapter and discusses future work avenues.

6.2 Method

The proposed solution method (or SM) is introduced in this section. Firstly, the standard CEP framework (from hereon, the FLP) is formulated. In the remainder of this chapter, the FLP denotes the CEP set-up that simultaneously tackles the siting and sizing of RES assets, as well as the sizing of other power system (e.g., generation, storage or transmission) technologies. Then, the screening method for candidate RES sites (SITE) that enables the formulation of a reduced-size CEP framework (from hereon, the RLP) is described. The SITE-RLP sequence will hereafter be referred to as the SM.

6.2.1 Capacity Expansion Planning Framework

Let $\mathcal{N}_B$ and $\mathcal{I}$ be the sets of existing buses and transmission corridors, respectively. Let L_n be a set of candidate RES sites that are connected to buses $n \in \mathcal{N}_B$, which is partitioned into disjoint subsets L_n^r, with r denoting a given renewable technology $\in \mathcal{R}$. Therefore, note that a single RES technology $r \in \mathcal{R}$ is associated with each site $l \in L_n$. The static CEP formulation reads

$$\min_{\mathbf{K},(\mathbf{p}_t)_{t\in\mathcal{T}}} \sum_{\substack{n\in\mathcal{N}_B \\ l\in L_n}} \left(\zeta^l + \theta_f^l\right) K_l + \sum_{\substack{n\in\mathcal{N}_B \\ j\in\mathcal{G}\cup\mathcal{S}}} \left(\zeta^j + \theta_f^j\right) K_{nj} + \sum_{i\in\mathcal{I}} \left(\zeta^i + \theta_f^i\right) K_i$$
$$+ \sum_{t\in\mathcal{T}} \left[\sum_{i\in\mathcal{I}} \theta_v^i |p_{it}| + \sum_{\substack{n\in\mathcal{N}_B \\ l\in L_n}} \theta_v^l p_{lt} + \sum_{\substack{n\in\mathcal{N}_B \\ j\in\mathcal{G}\cup\mathcal{S}}} \theta_v^j |p_{njt}| + \sum_{n\in\mathcal{N}_B} \theta^{ens} p_{nt}^{ens} \right] \tag{6.1a}$$

$$\text{s.t.} \sum_{l\in L_n} p_{lt} + \sum_{g\in\mathcal{G}} p_{ngt} + \sum_{s\in\mathcal{S}} p_{nst}^D + \sum_{i\in\mathcal{I}_n^+} p_{it} + p_{nt}^{ens} = \lambda_{nt} + \sum_{s\in\mathcal{S}} p_{nst}^C + \sum_{i\in\mathcal{I}_n^-} p_{it},$$
$$\forall n \in \mathcal{N}_B, \forall t \in \mathcal{T} \tag{6.1b}$$

$$p_{lt} \leq \pi_{lt}(\underline{\kappa}_l + K_l), \ \forall n \in \mathcal{N}_B, \forall l \in L_n, \forall t \in \mathcal{T} \tag{6.1c}$$

$$\underline{\kappa}_l + K_l \leq \overline{\kappa}_l, \ \forall n \in \mathcal{N}_B, \forall l \in L_n \tag{6.1d}$$

$$p_{ngt} \leq \underline{\kappa}_{ng} + K_{ng}, \ \forall n \in \mathcal{N}_B, \forall g \in \mathcal{G}, \forall t \in \mathcal{T} \tag{6.1e}$$

$$\underline{\kappa}_{ng} + K_{ng} \leq \overline{\kappa}_{ng}, \ \forall n \in \mathcal{N}_B, \forall g \in \mathcal{G} \tag{6.1f}$$

$$p_{nst} = -p^C_{nst} + p^D_{nst}, \forall n \in \mathcal{N}_B, \forall s \in \mathcal{S}, \forall t \in \mathcal{T} \tag{6.1g}$$

$$|p_{nst}| \leq \phi^{EP}_s(\underline{\kappa}_{ns} + K_{ns}), \forall n \in \mathcal{N}_B, \forall s \in \mathcal{S}, \forall t \in \mathcal{T} \tag{6.1h}$$

$$e_{nst} \leq \underline{\kappa}_{ns} + K_{ns}, \forall n \in \mathcal{N}_B, \forall s \in \mathcal{S}, \forall t \in \mathcal{T} \tag{6.1i}$$

$$e_{nst} = \eta^{SD}_s e_{ns(t-1)} + \eta^C_s p^C_{nst} - p^D_{nst}/\eta^D_s, \ \forall n \in \mathcal{N}_B, \forall s \in \mathcal{S}, \forall t \in \mathcal{T} \tag{6.1j}$$

$$\underline{\kappa}_{ns} + K_{ns} \leq \overline{\kappa}_{ns}, \ \forall n \in \mathcal{N}_B, \forall s \in \mathcal{S} \tag{6.1k}$$

$$|p_{it}| \leq \underline{\kappa}_i + K_i, \ \forall i \in \mathcal{I}, \forall t \in \mathcal{T} \tag{6.1l}$$

$$\underline{\kappa}_i + K_i \leq \overline{\kappa}_i, \ \forall i \in \mathcal{I} \tag{6.1m}$$

The problem described in (6.1a-6.1m) minimizes total annualized system cost subject to a set of constraints of the underlying assets[1]. The objective function (6.1a) comprises capital expenditure, fixed and variable operating costs[2] of the generation, storage and transmission assets, as well as the economic penalties associated with unserved demand. Constraint (6.1b) enforces the energy balance at each bus, while the operation and sizing of RES assets is modelled via (6.1c-6.1d). Then, conventional generators are modelled via (6.1e-6.1f) and the operation and sizing of storage units follows (6.1g-6.1k). Finally, constraints (6.1l-6.1m) encode the transportation model governing the power flows in transmission links. It is worth noting that, although the absolute values in Eqs. (6.1a), (6.1h) or (6.1l) render the CEP problem described in (1a-m) non-linear, it can be cast as an LP using standard reformulation techniques.

6.2.2 Renewable Sites Selection Method

The proposed `SM` works by decoupling the siting and sizing of RES assets. At first, the `SITE` stage is leveraged to screen the sets of candidate RES locations and identify those sites that play a role in the optimal system design, while discarding the rest. To this end, the siting problem is formulated by i) discarding some complicating variables and approximating a subset of complicating constraints (i.e., the ones associated with dispatchable power generation, storage systems and power flows in transmission lines) and ii) relaxing and taking linear combinations, as well as scaling the right-hand site coefficients of certain equality constraints (i.e., the power balance equations). The objective function (6.2a) is obtained by preserving the terms related to the costs of deploying and operating RES technologies and the economic penalty associated with unserved demand. Then, the constraints discarded from (6.1a-6.1m) are approximated via two parameters found in (6.2b). More formally, let $\mathcal{T}$ be the set of time periods, let $\mathcal{T}_\tau \subseteq \mathcal{T}$, $|\mathcal{T}_\tau| = \delta\tau$, $\tau = 1, \ldots, T$, be a collection of disjoint

[1]Note that the current formulation holds for a static representation of the CEP with a time horizon of one year. A more generic formulation would require the addition of a weighting factor in the CAPEX side of the objective function, such that the length of the time horizon is properly accounted for in the estimation of fixed costs.

[2]Note that the VOM, as defined here, include the plan-specific variable operation and maintenance costs, fuel costs, as well as CO_2-related expenses.

subsets forming a partition of $\mathcal{T}$ into time slices of length $\delta\tau$. More precisely, $\delta\tau$ represents the length of a time slice (e.g., one hour, one day) over which the energy balance in (6.2b) is enforced and its role is to emulate the behavior of storage assets shifting RES supply in time. Furthermore, let $\xi_\tau^n \in \mathbb{R}_+$ denote regional minimum RES feed-in targets enforced over every time slice $\mathcal{T}_\tau$, $\tau = 1, \ldots, T$. This parameter enforces a minimum level of local power production from renewable sources which i) mirrors the effect of transmission constraints and ii) accounts for low-carbon legacy generation capacity that would offset the country-specific RES requirements. Constraints (6.1c-6.1d) are preserved as such and the siting problem thus reads

$$\min_{\mathbf{K},(\mathbf{p}_t)_{t\in\mathcal{T}}} \quad \sum_{\substack{n\in\mathcal{N}_B \\ l\in L_n}} (\zeta^l + \theta_f^l) K_l \; + \sum_{t\in\mathcal{T}} \Big[\sum_{\substack{n\in\mathcal{N}_B \\ l\in L_n}} \theta_v^l p_{lt} + \sum_{n\in\mathcal{N}_B} \theta^{ens} p_{nt}^{ens} \Big] \tag{6.2a}$$

$$\text{s.t.} \sum_{t\in\mathcal{T}_\tau} \Big[\sum_{l\in L_n} p_{lt} + p_{nt}^{ens} \Big] \geq \xi_\tau^n \sum_{t\in\mathcal{T}_\tau} \lambda_{nt}, \; \forall n \in \mathcal{N}_B, \; \forall \tau \in \{1, \ldots, T\} \tag{6.2b}$$

$$p_{lt} \leq \pi_{lt}(\underline{\kappa}_l + K_l), \; \forall n \in \mathcal{N}_B, \forall l \in L_n, \forall t \in \mathcal{T} \tag{6.2c}$$

$$\underline{\kappa}_l + K_l \leq \overline{\kappa}_l, \; \forall n \in \mathcal{N}_B, \forall l \in L_n \tag{6.2d}$$

For every $n \in \mathcal{N}_B$, the problem returns the set of candidate RES sites identified as relevant (i.e., with an installed capacity above 1 MW) in the optimal system design, i.e. $L_n^{\texttt{SITE}}$. Then, the RLP is built by replacing L_n with $L_n^{\texttt{SITE}}$ in constraints (6.1a-6.1d) of the CEP problem.

6.3 Case Study

6.3.1 Input Data

The analysis is conducted for three individual weather years (i.e., 2016, '17 and '18) and over 33 countries within the ENTSOE system. The siting stage relies on hourly-sampled resource data obtained from the ERA5 reanalysis database [86] at a spatial resolution of 1.0°. The mapping of resource data to capacity factors time series is achieved via the transfer functions of appropriate conversion equipment for each individual technology. More precisely, a site-specific selection of wind generators is carried out based on the IEC 61400 standard [144] and four different converters are available for deployment (i.e., the *Vestas V110, V90, V117* and *V164*), each of them suitable for specific wind regimes. The selection of solar energy converters is done on a technology basis, with the *TrinaSolar DEG15MC* module available for utility-scale PV deployment and the *TrinaSolar DD06M* array available for distributed PV generation. A greenfield approach is adopted, i.e., no legacy capacity of RES assets is considered, while the technical potential is estimated via a land eligibility assessment framework [188] that yields eligible surface areas for RES deployment for a

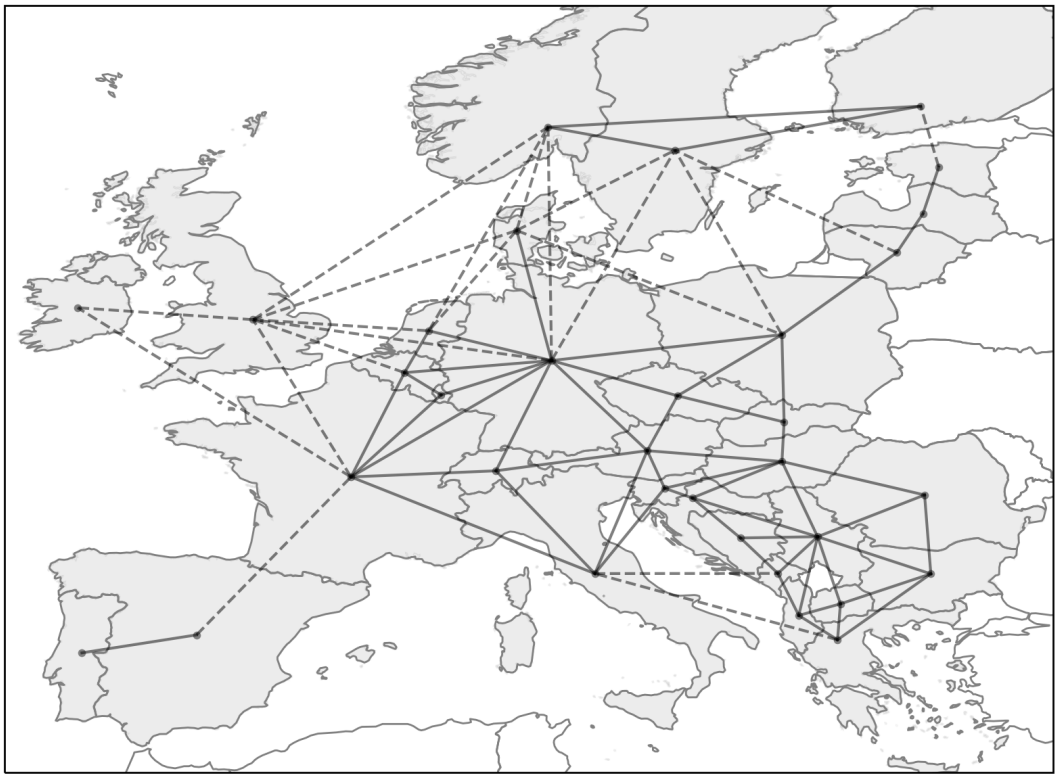

FIGURE 6.1: System topology in the capacity expansion planning framework. AC connections displayed in full lines, DC links shown in dotted lines.

set of 1740 candidate sites. A set of assumptions pertaining to the power densities of different generation technologies are then made to map surface areas into maximum allowable installed capacities, i.e., technical potentials. Specifically, a density of 5 MW/km^2 is considered for wind deployments [91]. With respect to solar PV units, power densities of 40 MW/km^2 and 16 MW/km^2 are considered for utility-scale and residential installations, respectively [189]. Electricity demand time series for all considered countries are retrieved from the *OPSD* platform [190].

The CEP frameworks (i.e., both the FLP and RLP) follow a centralized planning approach and build upon the 2018 TYNDP dataset, where each European country is modelled as one node [55]. The resulting network topology is displayed in Figure 6.1. In this exercise, the expansion of the transmission network is limited to the reinforcement of existing links. Furthermore, the total capacity of each link may not exceed twice the 2040 capacity estimated for this link in the TYNDP. Besides the four RES technologies sited in the previous stage, three more generation technologies are available for power generation, namely run-of-river (ROR) and reservoir-based (STO) hydro, as well as combined-cycle gas turbines (CCGT), with the latter being the only of the three that is also sized in (6.1a-6.1m). The existing capacities of the other two are retrieved from [151], where the existence of 34 GW of ROR and 98 GW of STO installations is reported. Then, two technologies are available

for electricity storage, namely pumped-hydro (PHS) units and Li-Ion batteries. The latter is the only one being sized in (6.1a-6.1m) and a fixed energy-to-power ratio of 4 h is assumed. The legacy capacity of the former is retrieved from [151], where 55 GW/1950 GWh of PHS storage is reported. The CEP problem is implemented in PyPSA 0.17 [32], while the techno-economic assumptions are gathered in [191].

6.3.2 Parametrization of the SITE Stage

The two parameters of (6.2a-6.2d) are defined as follows. First, the slicing period $\delta\tau$ is considered to be equal to 24 h, which corresponds to the nonzero frequency component of the aggregate EU-wide RES capacity factor time series with the largest amplitude (i.e., as provided by a discrete Fourier transform). Then, the country-dependent ξ_τ^n values are assumed not to be time-dependent and their estimation proceeds as follows. First, the residual demand (i.e., the difference between demand and generation potential of legacy dispachable units) is computed at peak load conditions. Then, the RES generation potential during the same time instants is determined. For each country, if RES potential exceeds the electricity demand for at least half the time steps in the optimization horizon, its potential transmission capabilities (i.e., 2040 TYNDP capacity limits times the length of slicing period $\delta\tau$) are added to the residual demand, as the country is a potential exporter of electricity in the EU-wide system. Conversely, if the electricity demand is higher than the RES potential most of the time, the transmission capabilities of that country are subtracted from the residual demand, as cross-border exchanges will oftentimes be used to cover for the domestic electricity needs. Finally, the ξ_τ^n values are determined as the ratio between the RES potential and the transmission capacity-adjusted residual demand, respectively.

6.3.3 Implementation

The SM, as well as the FLP are implemented in Python 3.7 and the proposed instances are run on a workstation running under CentOS, with an 18-core Intel Xeon Gold 6140 CPU clocking at 2.3 GHz and 256 GB RAM. Gurobi 9.0 was used to solve both (6.1a-6.1m) and (6.2a-6.2d). The dataset and code used in these simulations are available at [191] and [155].

6.4 Results

The results of a set of experiments evaluating the performance of the SM against the FLP are detailed in this section.

Table 6.1 summarizes the performance of the siting stage by means of two indicators. First, the technology-specific spatial reduction share (γ_r) denotes the proportion of initial candidate RES sites discarded via SITE. Then, the screening accuracy (β_r) measures the ability of the method to identify the relevant candidate RES sites.

More formally, if $\mathcal{R}$ is the set of renewable technologies, let L_n^r be the subset of sites with technology $r \in \mathcal{R}$ (these subsets are disjoint for different r and form a partition of L_n). Note that for the purpose of this exercise, offshore and onshore wind are considered as different resources. In addition, let $L_r^{\texttt{FLP}}$ and $L_r^{\texttt{SITE}}$ be the subsets of L_n^r selected by FLP and SITE where at least 1 MW of capacity is deployed, respectively. Then, the screening accuracy is defined as

$$\beta_r = \frac{|L_r^{\texttt{SITE}} \cap L_r^{\texttt{FLP}}|}{|L_r^{\texttt{FLP}}|}, \ \forall r \in \mathcal{R}, \tag{6.3}$$

where $|\cdot|$ denotes the cardinality of a given set. First, in this table, it can be seen that the relative reduction achieved by SITE varies from 6% for utility-scale PV to 62% for distributed PV installations in the 2017 instance, with an average reduction in onshore and offshore wind sites of 38% and 54%, respectively. Furthermore, an overall reduction of the number of selected RES sites of up to 54% is observed across the three considered instances. In other words, less than half of the candidate RES sites are found to be relevant in the optimal system configuration by SITE and subsequently passed to the RLP. With respect to the ability of SITE to identify relevant RES locations, only the distributed PV sites have a selection accuracy score below 85%. However, the limited deployment of this technology in the solution of the proposed CEP instances enables the screening stage to properly identify over 90% of the relevant RES sites (i.e., the ones appearing in the FLP solution), irrespective of the weather year considered.

However, not all candidate RES sites found in the FLP solution are identified by SITE which selects different locations instead. For instance, when the latter is run with 2016 weather data, it fails to identify a total of 45 sites (14 onshore wind, 12 offshore wind and 19 distributed PV locations, respectively) out of 418 identified in the benchmark. Investigating how far these locations are from the ones selected by the FLP provides a first insight into how different the system designs associated with the two methods are. If the distances between the locations selected via SITE and FLP were found to be small, one would expect the effect of misidentifying sites to be limited, as RES patterns are usually comparable at neighboring sites. Conversely, large

TABLE 6.1: Technology-specific sites reduction (γ_r) and screening accuracy (β_r) of SITE. Number of candidate sites used in the FLP specified in parantheses.

	W_{on} (590)		W_{off} (417)		PV_u (128)		PV_d (605)	
	γ_r	β_r	γ_r	β_r	γ_r	β_r	γ_r	β_r
2016	0.40	0.94	0.55	0.85	0.10	1.00	0.57	0.54
2017	0.37	0.94	0.55	0.86	0.06	1.00	0.62	0.83
2018	0.36	0.93	0.52	0.85	0.16	1.00	0.59	0.59

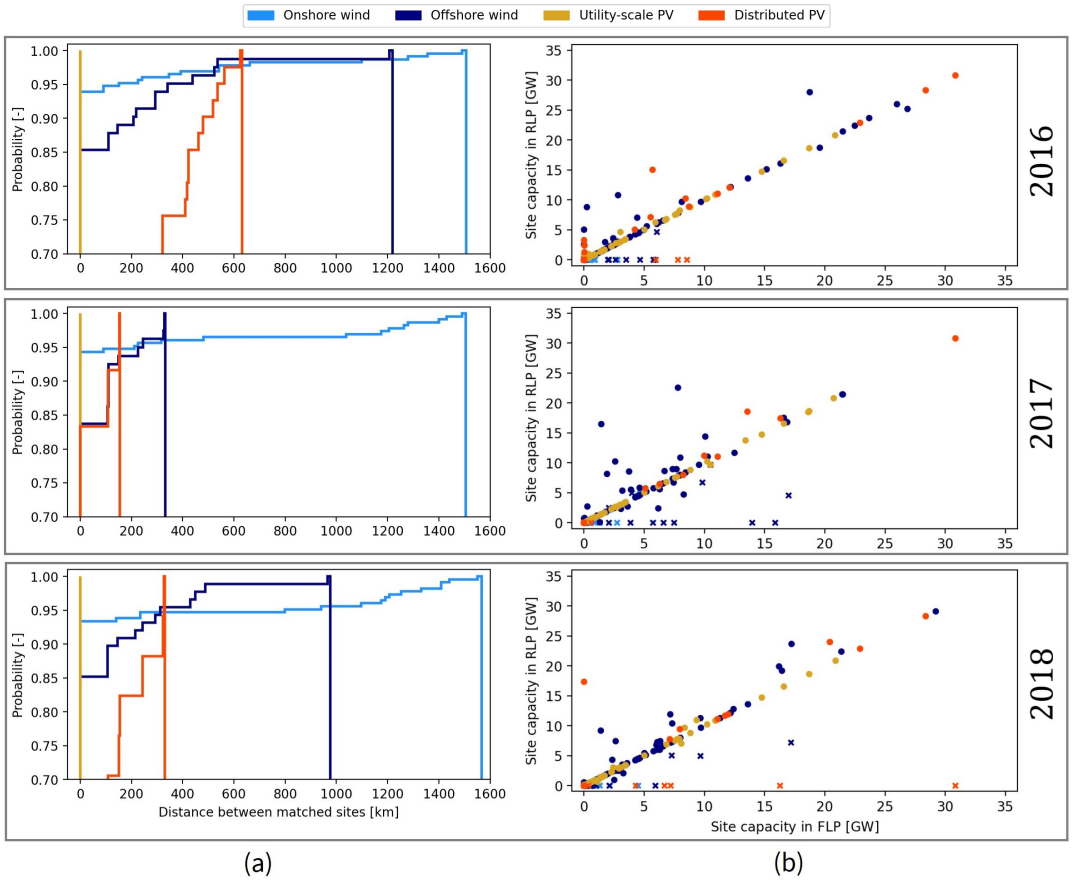

FIGURE 6.2: (a) Distribution of geographical distances between pairs of sites identified via SITE and the FLP. (b) Site-specific installed capacity correlation between the RLP and the FLP.

distances between sites identified via the two methods would often imply distinct RES patterns and could thus lead to substantial differences in the way the technologies are sized. The result of this analysis is shown in Figure 6.2a. These plots depict, for each technology and weather year, the distribution of distances (expressed in kilometres) between pairs of sites selected via the `FLP` and `SITE`, respectively. The procedure used to generate these curves is as follows. First, distances of zero are associated to the pairs of sites found by both methods (β_r shares in Table 6.1). Then, each unidentified site in the `FLP` solution is matched with the geographically closest (based on the geodesic distance) location in the set of `SITE`-exclusive locations. Once two sites are paired, none of them can be subsequently matched with another. Upon pairing all unidentified sites in the `FLP` with a counterpart in `SITE`, a cumulative distribution function of technology-specific distances is plotted. It can be observed in these three plots that, without exception, the 95^{th} percentile of the matching distance for any of the four RES technologies falls below 500 km. In a European context, it has been previously shown that country-aggregated wind output (usually more spatially heterogeneous than PV generation) is remarkably correlated at distances below the aforementioned threshold, especially in the North Sea basin where most onshore and offshore sites are deployed in the studied instances [192]. Furthermore, a maximum distance between matched sites of under 1600 km is reported for all technologies and weather years, with the largest discrepancies being consistently observed for onshore wind locations.

TABLE 6.2: Differences in system-wide capacities between FLP and RLP for various technologies and weather years. A positive value reflects more capacity installed (or higher TSCE) in the RLP, while a negative value indicates more capacity in the FLP.

Year	W_{on} [GW]	W_{off} [GW]	PV_u [GW]	PV_d [GW]	CCGT [GW]	AC [TWkm]	DC [TWkm]	Li-Ion [GWh]	TSCE [b€]
2016	-7.38	6.06	3.86	-1.63	0.10	-0.03	-0.05	0.51	0.36
	(-16.31%)	(1.48%)	(1.92%)	(-1.01%)	(0.11%)	(-0.04%)	(0.10%)	(1.99%)	(0.40%)
2017	-7.94	4.96	0.60	7.51	1.01	-2.33	-0.16	1.18	0.44
	(-12.84%)	(1.17%)	(0.29%)	(7.36%)	(2.30%)	(-2.90%)	(-0.29%)	(4.07%)	(0.52%)
2018	-13.73	12.19	2.51	-5.60	1.03	0.57	-0.04	-1.53	0.42
	(-23.34%)	(2.97%)	(1.21%)	(-2.99%)	(2.54%)	(0.65%)	(-0.07%)	(-3.63%)	(0.48%)

TABLE 6.3: Computational performance assessment of the SM. Numerical values represent reductions associated with the SM expressed in relative terms (%) with respect to the FLP.

Year	Variables	Constraints	Non-Zeros	PMR	SRT
2016	34.54	34.67	33.48	41.37	36.56
2017	33.31	33.39	32.22	40.11	30.90
2018	33.72	33.82	32.67	39.28	46.57

Upon screening the candidate RES locations via SITE, the RLP is run in order to retrieve, among others, the associated installed capacities. Figure 6.2b shows, for each weather year, the correlation between installed capacities of i) the sites identified in the FLP and ii) the sites identified by SITE and sized via RLP. In this plot, round markers (o) denote data points associated with locations that are common to FLP and SITE, while crosses (x) represent data points corresponding to the pairs of sites matched according to the procedure described in the previous paragraph. The first remark in these plots is that in 76% (for 2016) to 79% (for 2018) of the cases, the installed capacities of FLP and RLP sites are matched to MW-order precision. Then, it can be observed that most of the (x) markers are situated on the bottom of the corresponding subplots. A complementary analysis of the resource signals associated with these data points suggests the existence of high-quality RES sites exploited by the FLP, but whose SITE counterparts (determined via the distance-based pairing algorithm) exhibit inferior resource quality and thus end up not being part of the RLP solution. In such a situation, the missing capacity, i.e., FLP capacity of the (x) data points in the lower part of the plot, is compensated in the RLP by superior power ratings at (o) sites above the trend line in Figure 6.2b.

Table 6.2 reports, for different data years and for various technologies sized within the CEP stage, the difference between the system-wide installed capacities obtained by the FLP and RLP models, respectively (positive values indicate more capacity in the latter). In the last column, it can be seen that the relative objective function difference (i.e., the TSCE) between the two CEP set-ups does not exceed 0.52%, irrespective of the weather year considered. However, as suggested in a recent study by Neumann and Brown [160], rather small differences in total system costs can translate into fairly distinct system configurations. In this exercise, differences of 23.3%, 2.9%, 1.9% and 7.3% are reported for onshore wind, offshore wind, utility-scale and distributed PV, respectively, between the RLP and the FLP. A closer look at the breakdown of capacities per country reveals the reasons behind such differences, as the large majority of the discrepancies observed in Table 6.2 are associated to a handful of resource-rich countries (e.g., Ireland, Italy, Spain or the UK). For instance, in 2017 and 2018, the FLP over-sizes onshore wind (and, thus, selects more sites) in Ireland and the UK, and uses it to supply Central Europe. Under the proposed $(\delta\tau, \xi_\tau^n)$ set-up of the SITE stage, a subset of these locations are not identified (see discussion

on the (x) markers in Figure 6.2a) and the associated capacity in the FLP is replaced in the RLP by a mix of offshore wind and distributed PV. Further on in Table 6.2, transmission capacities vary within 2.9% of the FLP outcome, while a maximum of 4.1% Li-Ion storage capacity difference can be observed during the same year where distributed PV differed the most from the benchmark (i.e., 2017).

Finally, Table 6.3 summarizes the computational performance gains (relative to the FLP) achieved by leveraging the SM. More specifically, the reductions in i) the CEP problem size (number of variables, constraints and non-zeros), ii) the peak memory requirements (PMR) and iii) the solver runtime (or SRT, taking into account the solver runtime of both the SITE and RLP stages of the SM) are reported. In this table, it can be observed that the proposed SM leads to an average CEP problem size reduction of 33% which, in turn, enables an average PMR reduction of 40% and runtime savings between 31% and 46% across the studied instances.

6.5 Conclusion

This chapter proposes a method to reduce the spatial dimension of CEP frameworks while preserving an accurate representation of renewable energy sources. This is achieved via a two-stage heuristic. First, a screening stage is used to identify the most relevant sites for RES deployment among a pool of candidate locations and discard the rest. Then, the subset of RES sites identified in the first stage is used in a CEP problem to determine the optimal power system configuration. The proposed method is tested on a realistic EU case study and its performance is assessed against a CEP set-up in which the entire set of candidate RES sites is available. The method shows great promise and manages to consistently identify more than 90% of the optimal sites while reducing peak memory consumption and solver runtime by up to 41% and 46%, respectively.

Capacity differences between the solutions provided by the proposed method and the benchmark observed for some weather years suggest that further work on the selection of parameters used in the first-stage siting routine would be useful. Moreover, re-casting the proposed heuristic into a more structured form, e.g., where the siting and sizing of RES assets are used as stages in a Benders-like decomposition framework, is also envisaged as a promising development avenue.

Chapter 7

Conclusion

This chapter concludes the work and proposes future research avenues that could improve the methods and analysis proposed in the current manuscript.

This thesis seeks to assess whether the spatiotemporal complementarity of variable renewable resources has an economic value for power systems. In order to answer this research question, a series of methods and analyses are proposed. From the offset, a custom definition of spatiotemporal complementarity of renewable resources is proposed, such that it aligns with the current challenges of power system planners and operators. More specifically, renewable resources are considered complementary in this thesis if they rarely lead to system-wide low production events. With this definition, a means to quantify RES complementarity on arbitrary spatial and temporal scopes is proposed and an optimisation problem identifying subset of sites with maximum complementarity is devised. Once a way of leveraging the spatiotemporal RES complementarity in siting decisions was available, a comprehensive analysis assessing its value for power systems follows. In addition, the impact of such screening methods on the computational complexity of CEP problems is also analysed.

In Chapter 2, the spatiotemporal complementarity of the wind resource between remote locations is evaluated via a systematic framework quantifying the occurrence of system-wide low-generation events. Results reveal complementary wind regimes in the investigated regions and support the idea according to which distributing renewable generation assets in space can prove beneficial for a secure and reliable supply of electricity in future power systems dominated by renewable energy sources. Then, in Chapter 3, the time windows framework is presented. This framework provides an accurate, time-domain description of low probability RES power generation events impacting power system operation and planning and enables the definition of a scalar indicator quantifying the complementarity of renewable resources on arbitrary spatial and temporal scopes. This indicator is then leveraged to formulate optimisation models seeking to identify deployment patterns with maximum complementarity within a region of interest. The solutions to optimisation problems derived from the criticality indicator shows that the occurrence of low production events can be reduced on a regional scale by exploiting the diversity in local wind regimes. The relevance of the proposed methodology in a power systems planning context is further supported by a comparison between two wind farm deployment strategies favouring the spatiotemporal complementarity between RES and seeking to maximise annual average capacity factors, respectively. These two approaches, which were tested at country level, yield starkly different deployment patterns, with implications for planning strategies in future power systems dominated by vast shares of renewable-based generation.

Chapter 4 then leverages the aforementioned siting schemes in a realistic case study evaluating the role that offshore wind power plants may play in the European power system, with a particular focus on the impact that plant siting strategies have on system design and economics. The chapter builds upon a method that combines a siting stage selecting a subset of promising locations for deployment and a CEP framework identifying the power system design that supplies pre-specified demand

levels at minimum cost while satisfying technical and policy constraints. Results show that the complementarity-based siting schemes yields deployment patterns that have both a much steadier aggregate power output and much lower residual load levels than the capacity factor-maximizing scheme if sites are selected without enforcing country-based deployment targets. However, when such constraints are enforced, the two siting schemes produce deployment patterns that lead to similar levels of residual load. In economic terms, the complementarity-based scheme leads to system designs that are up to 5% cheaper than capacity factor-based ones when sites are selected without enforcing country-based deployment targets. When such targets are enforced, however, the capacity factor-based scheme leads to system designs that are consistently 2% cheaper than complementarity-based ones. These results are shown to hold under a broad range of offshore wind cost assumptions and are not affected by inter-annual weather variability. Chapter 5 builds upon the two-stage method previously proposed and considers an additional UCED stage in order to properly model the limited flexibility of thermal units and thus more accurately approximate the cost of operating the system. A similar case study is proposed, where the economic impact of the two aforementioned siting strategies for onshore and offshore wind assets across twelve countries within the continental European synchronous grid is investigated. Results show that deploying wind assets based on the proposed definition of sptatiotemporal complementarity leads to a system design which is 2% more expensive than the system where wind assets are located in the most productive locations. In other words, the findings in Chapter 4 seem to hold even for more refined set-ups that take into account i) more detailed network topologies, ii) a more accurate representation of network flows and iii) the unit commitment constraints of dispatchable units. Furthermore, it is shown that deploying wind assets based on capacity factor criteria leads to total system operating costs which are 3.7% lower than the costs of operating a system where wind generation assets are deployed based on the proposed complementarity criterion. It is revealed that this difference is mostly attributed to the need of more gas-based electricity generation via CCGT units to compensate for the wind feed-in deficit brought by the lower average capacity factors associated with the deployment patterns leveraging resource complementarity.

Lastly, Chapter 6 contributes to the literature by proposing a method to reduce the computational complexity of CEP frameworks while preserving an accurate representation of RES in space and time. This is achieved via a two-stage method that works as follows. Initially, a screening stage is used to identify the most relevant sites for RES deployment among a pool of candidate locations and discard the rest. The complementarity-based siting criterion leveraged throughout the previous chapters of the manuscript could be seen as such a screening stage. Then, the subset of RES sites identified in the first stage is used in a CEP problem to determine the optimal power system configuration. The proposed method is tested on a realistic Europe-based case study and its performance is assessed against a CEP set-up in which the

entire set of candidate RES sites is available. The method shows great promise and manages to consistently identify a large share (i.e., more than 90%) of the optimal sites while almost halving peak memory consumption and solver runtime.

In times of a climate crisis doubled down by an energy crisis in Europe and beyond, this thesis addresses a timely topic for the development of future power systems, namely, evaluating the impact of different siting strategies for RES assets. With the expected evolution of variable renewable generation into the chief contributor to the electricity supply in Europe, the next decades of power system planning must be well-informed with respect to the economic and technical implications of different siting strategies for such assets in both planning and operational time frames. It is thus the author's hope that the contributions included in this manuscript will be of use to future research and policy-making by broadening the search space of potential solutions for power system decarbonisation.

7.1 Future Work

As for future work, a list of promising research avenues that could potentially enhance the methods and analysis proposed in this manuscript are discussed in the following. These propositions are grouped in two main categories, namely, *methodological and algorithmic enhancements* (i.e., improvements to the methods and algorithms chosen to study the underlying problems) and *modelling improvements* (i.e., aspects mainly pertaining to the modelling choices).

Methodological and Algorithmic Enhancements

The current manuscript proposes a means to site RES assets based on criteria relying on a pre-specified spatiotemporal complementarity definition. It would be of great interest to compare the results of this deployment scheme with others trying to achieve similar outcomes. For instance, the works of Wu et al. [137], Musselman et al. [130] or Paz et al. [193] propose methods to deploy RES assets such that their aggregate output has desirable properties from a power system planning and operation standpoint. Although the notion of spatiotemporal complementarity is not explicitly addressed in these articles, the resulting siting schemes are expected to lead to insightful deployment patterns when compared to the strategy proposed in this document. A methodological improvement that could potentially impact the outcomes of the proposed analysis refers to the integration of the multiple stages proposed in Chapters 4, 5 or 6 into a single problem with decomposable structure. Solving such an problem would require tailored solution methods (e.g., a Benders decomposition scheme), yet would lead to more accurate outcomes in the planning and operational stages [162]. Another aspect not taken into account in the routines

proposed in this thesis relates to the consideration of uncertainties in both short- (induced by, e.g., renewable resource variability) and long-term (driven by, e.g., technology costs, policy implementation, demand growth). On the one hand, short-term uncertainties, such that the realization of renewable generators or loads, could be embedded in the proposed models via, e.g., stochastic programming or robust optimisation [194]. The same techniques have also been used in the representation of long-term uncertainties within energy systems models. Nevertheless, the MGA (modelling to generate alternatives) technique [195], is hereby seen as a promising research avenue in this direction for two reasons. First, it enables the mapping of a plethora of configurations for RES-dominated power systems, some of which being more appealing than others from different considerations than the techno-economic feasibility of a given solution (e.g., social acceptance of a technology, policy drivers). Second, this technique could also enable the development of a solution space rich enough to accurately identify the system set-ups where siting RES assets based on spatiotemporal complementarity criteria actually leads to cost savings in the planning and/or operational stages of the underlying power system.

Modelling Aspects

A set of modelling aspects should also be pursued in order to improve the underlying analyses. First of all, taking into account solar-based generation in the siting schemes could play a significant role in showcasing the value of complementarity for power systems, given the documented synergies between the two resources at regional and continental scales [101]. Second, one could argue that the spatial and temporal resolutions utilized in this manuscript for wind resource assessment are rather coarse. Indeed, a visual inspection of the Global Wind Atlas (a tool with a spatial resolution of 250 m) [124] reveals numerous local regimes that are not captured in a reanalysis dataset with a spatial resolution of 0.25°. In addition, a recent study by Pichault et al. [196] revealed significant intra-hourly variations in the power output of representative wind farms. Both these caveats could play a considerable role in selecting the location of power generation assets fuelled by variable renewable resources. Therefore, more refined spatial and temporal resolutions could be of high interest in the context of the proposed topic. A couple of additions to the sizing stages proposed in Chapters 4, 5 or 6 would also be of interest. For instance, taking into account operating reserve requirements in the planning stage of power system design has a substantial impact on installed capacities and resulting costs [197]. Then, having a better representation of the connection costs for RES assets to the corresponding network bus is also of high interest, as it leads to a more accurate representation of system costs [60]. Still on the transmission assets topic, a valuable addition to the sizing models considers the development of novel transmission corridors between subsets of network buses. Such a feature would support a more comprehensive comparison of the proposed siting schemes and their value for power systems. Furthermore, a deeper look into the temporal reduction techniques

leveraged in the expansion planning stage could be of use in order to have a more accurate approximation storage utilization on intra- and inter-period time frames [198]. In the unit commitment and economic dispatch problem, one straightforward improvement relates to accounting for dispatchable generation ramping costs [186] in the objective function of the underlying problem. In addition, extending the operational analysis to the entire European power network could also be of interest, as it enables the user to leverage the continent-wide spatiotemporal complementarity of renewable resources.

Appendix A

Modelling Assumptions

A.1 Chapter 4 - Evaluating the Impact of Siting Strategies on the Design of Power Systems

This section lists the main techno-economic assumptions used in Chapter 4 of the current manuscript.

This section gathers information which is relevant for instantiating the siting and sizing stages of the method proposed in Chapter 4. The document is split in two sections, similar to the sequential structure of the proposed method. First, a mapping of all candidate sites available for offshore wind deployment within European Seas is presented in Section A.1.1. Furthermore, a set of relevant expansion planning features are discussed. First, the simplified network topology is revealed in Section A.1.2. Then, Sections A.1.3 and A.1.4 gathers all techno-economic assumptions used to instantiate the capacity expansion planning model determining the cost-optimal design of the European power system.

A.1.1 Candidate Sites

The set of candidate sites for offshore wind deployment is shown in Figure A.1. In this plot, it can be easily seen that the latitude and distance-to-shore filters are the ones mainly driving the selection of candidate sites. In addition, candidate sites within several Exclusive Economic Zones (EEZ) are not included in this study for different reasons. First, as Albania, Bosnia and Herzegovina, as well as Montenegro are not considered in this study, their EEZs and the corresponding candidate offshore wind sites are not shown in Figure A.1. Second, the EEZ of the Russian exclave of Kaliningrad is not considered for similar reasons. In addition, the territorial waters around the British dependencies of Jersey and Guersney are not included, as they are not officially part of the EEZ of Great Britain.

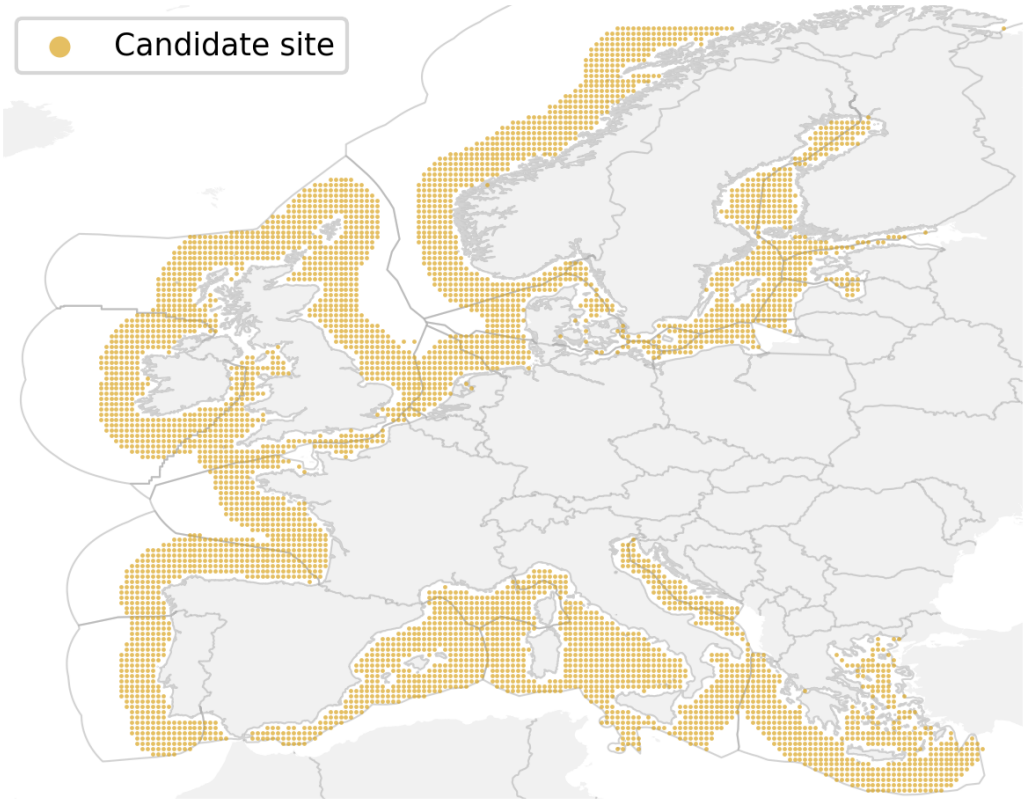

FIGURE A.1: Set of candidate locations for offshore wind deployment (in yellow).

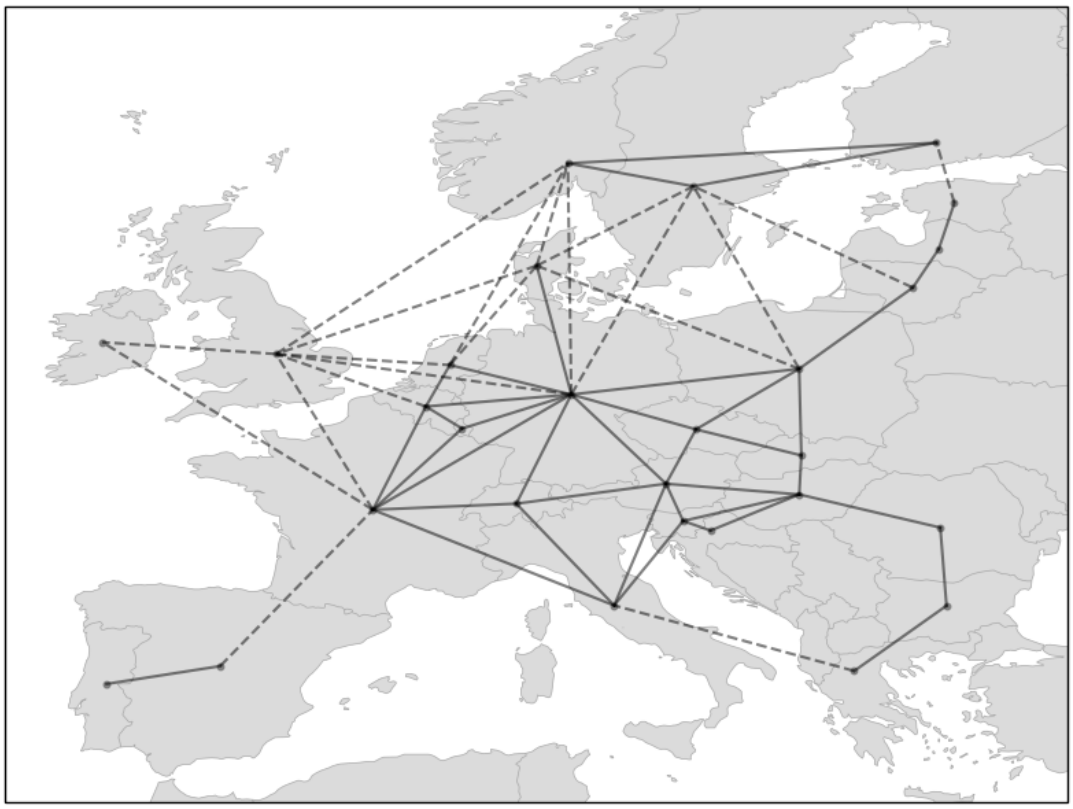

FIGURE A.2: Network topology used in the capacity expansion planning stage.

A.1.2 Network Topology

The power system topology used in the capacity expansion planning stage is based on the 2018 version of the Ten Year Network Development Plan of ENTSO-E [55]. More specifically, each country is represented by one node (to which demand and generation signals are attached) and a copper plate assumption is made for power flows within its borders. The links between countries represent aggregations of the total cross-border capacities projected in 2027. For costing purposes, all interconnectors crossing bodies of water are assumed to be developed as DC cables, while the remainder are assumed to be built as AC underground cables. These assumptions can be visualized in Figure A.2.

A.1.3 Economic Parameters

Economic parameters of every generation, storage or transmission technology are displayed in Table A.1. USD/EUR conversions are made assuming a conversion rate of 0.8929 EUR per USD. Then, GBP/EUR conversions are made assuming a conversion rate of 1.1405 EUR per GBP. Similarly, a AUD/EUR conversion rate of 0.6209 EUR per AUD is considered.

Plant	CAPEX M€/GW(h)	FOM M€/GW × yr	VOM M€/GWh	Lifetime years	Source
Onshore wind	1088.16	29.47	0.00	25	[199]
Offshore wind	1881.08	49.11	0.00	25	[199]
Utility-scale PV	687.79	7.14	0.00	25	[199]
Distributed PV	858.00	5.36	0.00	25	[199]
OCGT	838.87	3.03	0.0076	30	[200]
CCGT	1005.27	7.58	0.0053	30	[200]
Nuclear	N/A	106.25	0.0018	N/A	[199]
Run-of-river hydro	N/A	0.00	0.0119	N/A	[201]
Reservoir hydro	N/A	0.00	0.0152	N/A	[201]
Li-Ion (power)	100	0.54	N/A	10[1]	[202]
Li-Ion (energy)	94	N/A	0.0017	10[1]	[202]
PHS	N/A	14.20	0.0002	N/A	[203]
HVAC	2.22[2]	0.017	N/A	40[1]	[204]
HVDC	1.76[3]	0.021	N/A	40[1]	[204]

[1] Assumed value.
[2] Expressed per km and derived from a single circuit 1000 MVA, 400 kV cable.
[3] Expressed per km and derived from a 1100 MW, 350 kV underground DC cable pair.

TABLE A.1: Economic parameters of generation, storage and transmission technologies.

A.1.4 Technical Parameters

For generation technologies, efficiencies represent the ratio between primary energy input and electricity output. For storage technologies, three efficiencies are provided, i.e. for the discharging (D) and charging (S) states, as well as the self-discharge (SD) efficiency (i.e., one minus this value corresponds to the state-of-charge internal losses). For transmission technologies, the efficiency is provided per 1000 km. Besides efficiency values, some technologies are modelled with hourly ramp rates (up- and down-regulation), as well as with minimum must-run levels. At this stage the only technology with such constraints is the nuclear power generator, i.e., those generators can ramp their production up or down by a maximum of 10% per hour and must always output power at a minimum of 80% of their capacity. All values are centralized in Table A.2.

Some technologies (OCGT and CCGT) are using fuels which release CO_2 when burnt. Specific CO_2 emissions and associated feedstock costs of different fuels are collected in Table A.3.

The capacity expansion framework includes a carbon budget constraint reflecting the total amount of CO_2 that can be emitted by the underlying power system over one year. In line with the latest climate agreements, this budget is enforced as a share of the EU-wide 1990 emission levels. Data collection for yearly emission levels relies

Plant	Efficiency			Ramp rates[1]		Must-run[1]
	D [%]	S [%]	SD [%]	Up [%/hr]	Down [%/hr]	[%]
OCGT	41.0[2]					
CCGT	58.0[2]					
Nuclear	36.0[3]			10.0	10.0	80.0
Run-of-river hydro	85.0[1]					
Reservoir hydro	85.0[1]					
Pumped-hydro storage	90.0[4]	90.0[4]	100.0[1]			
Li-Ion storage	93.0[5]	93.0[5]	99.5[1]			

[1] Assumed values.
[2] Retrieved from [200].
[3] Retrieved from [199].
[4] Retrieved from [205].
[5] Retrieved from [203].
[6] Retrieved from [206].

TABLE A.2: Generation, storage and transmission technologies operational parameters.

Plant	Fuel	Fuel Cost €/MWh$_{th}$	CO_2 ton/MWh$_{th}$
OCGT	gas	26.5[1]	0.225[2]
CCGT	gas	26.5[1]	0.225[2]
Nuclear	uranium	1.7[1]	0.0

[1] Values are obtained from the TYNDP2020 Scenario Report, reference year 2040 [207].
[2] Values for stationary combustion from the IPCC Emissions Factor Database [208].

TABLE A.3: Fuels and associated costs and specific emissions.

on carbon intensity information released by the Europe Environment Agency (EEA) [209] and on yearly electricity generation data from the International Energy Agency (IEA) [210]. The baseline cost of CO_2 is set to 41.85 €/tCO_2 and it reflects its price on the EU ETS on March 30, 2021.

A.2 Chapter 5 - Assessing the Impact of Siting Strategies on the Design and Operation of Power Systems: A Refined Analysis

A.2.1 Candidate Sites

The current study takes into account the deployment of wind generation assets (both on- and offshore) in twelve European countries, namely, Austria (AT), Belgium (BE), Czechia (CZ), Denmark (DK), France (FR), Germany (DE), Italy (IT), Luxembourg (LU), the Netherlands (NL), Portugal (PT), Spain (ES) and Switzerland (CH). The set of candidate locations for onshore and offshore wind deployment, respectively, is determined via a filtering procedure that discards the reanalysis grid points where the installation of such technologies would be impractical. With respect to the onshore wind deployments, three distinct filters are applied. More specifically, all reanalysis grid points with an average population density above 200 inhabitants/km^2 are discarded. Then, grid points whose average terrain slope is greater than 3% or whose forestry cover is above 80% are also removed. A single filter is applied for offshore wind deployments, i.e., distance to shore. In particular, offshore wind deployments are possible in a band between 12 nm and 120 nm from the shore, in accordance with the considerations suggested in [145]. As a result of this filtering procedure, a total of 4573 onshore and offshore points (seen in Figure A.3) are available for deployment across the territories of the twelve European countries under investigation. It should be noted that the absence of candidate onshore points in Austria and Switzerland is justified by the lack of capacity deployments in these countries.

A.2.2 Unit Commitment Parameters

There are three electricity generation technologies whose unit commitment costs and constraints are modelled, namely, nuclear, OCGT and CCGT units. In particular, the following modelling aspects are taken into account for these three technologies: start-up costs, ramp rates and minimum operating levels, as well as minimum up- and down-times. The values assumed for these parameters are centralized in Table A.4.

A.2.3 Solver Parameters

A list of solver parameters whose values were tuned in the context of the current planning exercise is provided in Table A.5. Furthermore, a list of solver parameters whose values were tuned in the context of the unit commitment and economic dispatch problem tackled in Chapter 5 is provided in Table A.6.

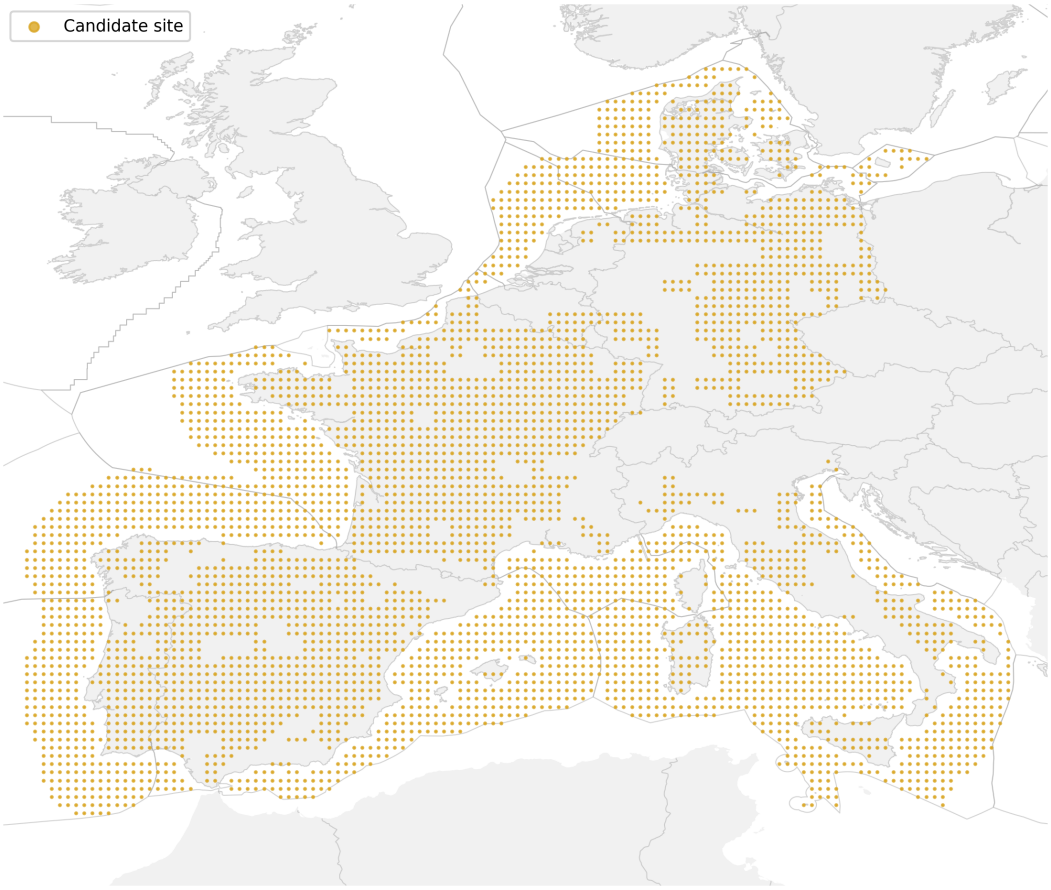

FIGURE A.3: Set of candidate sites for onshore and offshore wind deployment, respectively.

TABLE A.4: Unit commitment techno-economic assumptions.

	μ [%]	Δ^-/Δ^+ [%]	δ^{mdt} [h]	δ^{mut} [h]	θ_{SD}[1] [€/MW]	θ_{SU}[2] [€/MW]	Source
Nuclear	0.5	0.1	24	12	0.0	3.5	[211]
OCGT	0.48	1.0	6	1	0.0	42.3	[186]
CCGT	0.48	0.5	6	2	0.0	46.8	[186]

[1] Assumed values.
[2] Typical warm start data from [186].

TABLE A.5: Solver parameters used in the capacity expansion planning problem [212].

Parameter	Meaning	Default	Value
Threads	Number of parallel threads to use	0	15
Method	Algorithm used to solve continuous models	-1	2
Crossover	Barrier crossover strategy	-1	0
BarConvTol	Barrier convergence tolerance	10^{-8}	10^{-5}
FeasibilityTol	Primal feasibility tolerance	10^{-9}	10^{-6}
AggFill	Allowed fill during presolve aggregation	-1	0
PreDual	Presolve dualization	-1	0

TABLE A.6: Solver parameters used in the unit commitment and economic dispatch planning problem [212].

Parameter	Meaning	Default	Value
Threads	Number of parallel threads to use	0	15
Method	Algorithm used to solve continuous models	-1	2
Crossover	Barrier crossover strategy	-1	0
NodeMethod	Method used to solve MIP node relaxations	-1	2
MIPGap	Relative MIP optimality gap	10^{-4}	0.03
MIPFocus	Set the focus of the MIP solver	0	3
Heuristics	Turn MIP heuristics up or down	0.05	0.8

A.3 Chapter 6 - Model Reduction in Capacity Expansion Planning Problems via Renewable Generation Site Selection

This section lists the main techno-economic assumptions used in Chapter 6 of the current manuscript.

A.3.1 Economic parameters

Economic parameters of every generation, storage or transmission technology are displayed in Table A.7. All USD-EUR conversions are made assuming a conversion rate of 0.8928 EUR per USD. All GBP-EUR conversions are made assuming a conversion rate of 1.1405 EUR per GBP. All AUD-EUR conversions are made assuming a conversion rate of 0.6209 AUD per EUR.

TABLE A.7: Generation, storage and transmission technologies costs.

Plant	Type	CAPEX €/kW k(€/MW*km)	FOM €/kW*y (k€/MW*km*y)	VOM €/MWh-e	Lifetime years	Ref. Year	Source
NGPP	CCGT[1]	1005.27	7.58	7.6	25	2030	[200]
Wind	Onshore	1088.16	29.47	0.0	25	2050	[199]
Wind	Offshore	1881.08	49.11	0.0	25	2050	[199]
PV	Utility	614.12	8.0	0.0	25	2050	[199]
PV	Residential	766.09	6.0	0.0	25	2050	[199]
Hydro	Reservoir[2]	N/A	0.0	6.0	N/A	2015	[213]
Hydro	Run-of-river[2]	N/A	0.0	8.1	N/A	2015	[213]
Storage	Pumped-hydro[3]	N/A	14.20	0.2	50	2020	[203]
Storage	Li-ion[4]	382.00	0.54	1.7	10	2025	[214]
Transmission	HVAC[5]	2.22	0.0167	0.0	40	2015	[215]
Transmission	HVDC[6]	1.76	0.0205	0.0	40	2015	[215]

[1] Projected costs of future projects.
[2] Data retrieved as VOM average of large, operating hydro projects.
[3] Data retrieved from Appendix B.4.1 of the report, assuming greenfield project.
[4] Data for a 4h duration, Li-Ion battery.
[5] Data derived from single circuit 1000 MVA, 400 kV cable.
[6] Data derived from 1100 MW, 350 kV underground DC cable pair.

A.3.2 Technical parameters

For generation technologies, efficiencies represent the ratio between primary energy input and electricity output. For storage technologies, three efficiencies are provided, i.e. for the discharging (D) and charging (S) states, as well as the self-discharge (SD) efficiency (i.e., one minus this value corresponds to the state-of-charge internal losses). For transmission technologies, the efficiency is provided per 1000 km. All values are centralized in Table A.8.

TABLE A.8: Generation, storage and transmission technologies operational parameters.

Plant	Type	Efficiency		
		D [%]	S [%]	SD [%]
NGPP	CCGT	58.0[1]		
Hydro	Reservoir	85.0[2]		
Hydro	Run-of-river	85.0[2]		
Storage	Pumped-hydro	90.0[3]	90.0[3]	100.0[4]
Storage	Li-ion	93.0[5]	93.0[5]	99.5[6]
Transmission	HVAC	93.0[7]		
Transmission	HVDC	97.0[7]		

[1] Average efficiency values from [148].
[2] Assumed values.
[3] Values from Appendix B.4.1 of [205].
[4] Assumed value.
[5] Values for Li-Ion battery from [203].
[6] Assumed value.
[7] Values from [206].

Some technologies (only CCGT at this stage) are using fuels which release CO_2 when burnt. The cost of CO_2 is set to 40 €/tCO_2 and is based on the Global Ambitions scenario (reference year 2030) of the 2020 TYNDP [207]. Specific CO_2 emissions and associated feedstock costs of different fuels are collected in Table A.9.

TABLE A.9: Fuels and associated costs and specific emissions.

Plant	Type	Fuel	Fuel Cost €/MWh$_{th}$	CO_2[1] ton/MWh$_{th}$
NGPP	CCGT	gas	26.5[2]	0.225

[1] Values for stationary combustion from the IPCC Emissions Factor Database [208].
[2] From [207].

Appendix B

Modelling Hydro Inflows and Capacities

Hydro power plants modelling requires specific attention, as their operation is inherently constrained by resource- and design-related aspects, e.g., reservoir size, water inflows. The current assessment is hereby explained for a network topology where each country represents one equivalent electrical bus. However, the proposed workflow remains unchanged even if more granular network topologies are pursued (e.g., see Chapter 5). The first step in the workflow constitutes the mapping of individual power plants to their corresponding countries. To this end, geo-location data of hydro units is provided in [150], [151]. The result of this mapping is shown in Figure B.1 for run-of-river (ROR), reservoir-based (STO) and pumped-hydro storage units (PHS), respectively.

B.1 Run-of-River Hydro Power Plant Inflows

In modelling the ROR units, inspiration is drawn from the operation of variable RES technologies (e.g., wind, solar PV). Indeed, these former class of plants relies on the availability of water flows to operate, as they do not have significant storage capabilities to regulate their operation. Therefore, after distributing the 33.5 GW of ROR capacity across the 28 countries (based on their geo-location), these plants are modelled as non-dispatchable, aggregated installations whose per-unit, hourly capacity factors are assumed proportional to the runoff[1] available in the country where the aggregate ROR capacity is located.

More specifically, let $\mathcal{C}$ be the set of all countries and $\mathcal{T}$ be the time horizon under investigation. For any country $c \in \mathcal{C}$, the runoff associated with all reanalysis data points (sampled on a regular grid at, e.g., 0.25deg spatial resolution in both coordinate directions) found within its borders is first spatially aggregated into a single runoff time series (B.1a). Then, the resulting time series is normalized (B.1b) and

[1] Surface and sub-surface water draining away from precipitation, snow melting, etc. Hourly runoff time series covering the studied temporal horizon (2010 to 2019) are obtained from the same reanalysis dataset as wind speeds and solar irradiation data [86].

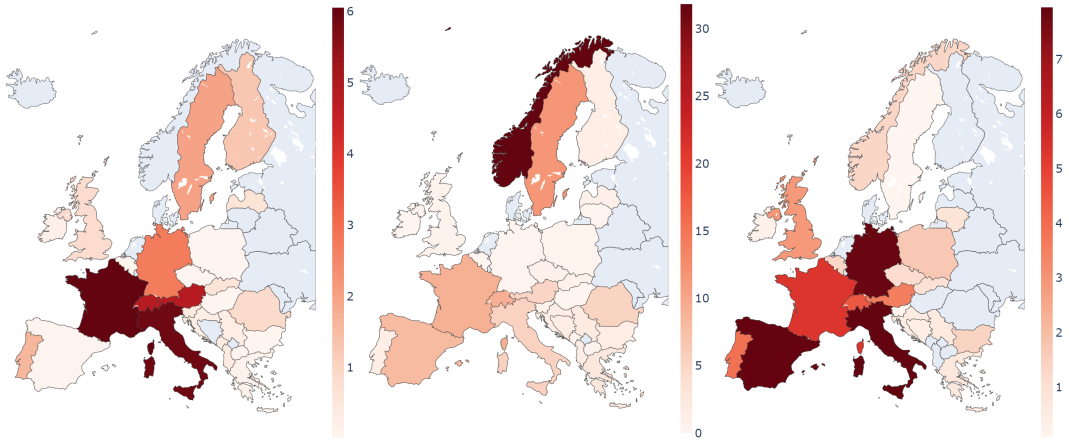

FIGURE B.1: Installed capacities (in GW) of run-of-river (left), reservoir-based (middle) and pumped-hydro units (right) across European countries. Each subplot is accompanied by its own colorbar.

data outliers (i.e., in this case, flood-related events during which the runoff spikes for short periods of time) are removed. The latter processing step is tackled via (B.1c) by defining a country-specific, dimensionless *flood event threshold*. In this equation, f_c denotes the aforementioned threshold, while $q_{f_c}(\overline{\mathbf{ro}}_c)$ denotes the $f_c{}^{\text{th}}$ quantile of the runoff vector in country c. The values of this threshold (listed in Table B.1) are set such that the yearly average ROR capacity factors reaches 50% across all countries[2]. Finally, the hourly availability of ROR plants can be obtained via (B.1d), where K_c^{ROR} denotes the ROR installed capacity in country c.

$$ro_{c,t} = \sum_{cell \in c} ro_{cell,t}, \quad \forall c \in \mathcal{C} \tag{B.1a}$$

$$\overline{ro}_{c,t} = \frac{ro_{c,t}}{max(\mathbf{ro}_c)}, \quad \forall c \in \mathcal{C}, \forall t \in \mathcal{T} \tag{B.1b}$$

$$\tilde{ro}_{c,t} = min(\overline{ro}_{c,t}, q_{f_c}(\overline{\mathbf{ro}}_c)), \quad \forall c \in \mathcal{C}, \forall t \in \mathcal{T} \tag{B.1c}$$

$$p_{c,t}^{ROR} = \tilde{ro}_{c,t} K_c^{ROR}, \quad \forall c \in \mathcal{C}, \forall t \in \mathcal{T} \tag{B.1d}$$

B.2 Reservoir-based Hydro Power Plant Inflows

Reservoir-based hydro power plants (STO) are modelled as dispatchable units with limited generation capabilities, as their feed-in is usually limited by two aspects, i.e.,

[2]Considering a *flood event threshold* of 0.9, the aggregate runoff time series within a region is clipped to its 90$^{\text{th}}$ percentile. From a ROR plant design standpoint, this is equivalent to considering that a given plant is designed for a rated flow of *p90* of the historical flow duration curve, a usual approach in the design of such units.

TABLE B.1: Hydro run-of-river (ROR) flood event threshold values (p.u.) for various countries in Europe.

ISO2	f_c	**ISO2**	f_c	**ISO2**	f_c
AT	0.9	GB	0.85	NO	0.9
BE	0.8	GR	0.9	PL	0.9
BG	0.9	HR	0.9	PT	0.9
CH	0.9	HU	0.9	RO	0.9
CZ	0.9	IE	0.85	RS	0.9
DE	0.7	IT	0.9	SE	0.9
ES	0.9	LT	0.9	SI	0.9
FI	0.9	LU	0.9	SK	0.9
FR	0.9	LV	0.9		

water inflow availability and storage capabilities. At first, as unit-specific STO reservoir capacity data is scarce in the literature [151], a procedure to approximate water retention capabilities of such units on a country-by-country basis is employed. Subsequently, inflow estimation in the form of hourly time series is pursued. The accurate estimation of these two parameters prove fundamental in replicating the generation patterns of STO installations, which are often driven by seasonal fluctuations.

The assessment of country-based reservoir capacities develops in three steps. First, the results of a peer-reviewed hydropower modelling framework [216] are queried. In case STO reservoir data is not available at this source for a specific country, information is sought for on the ENTSOE Transparency Platform [217], within time series of historical (i.e., 2014 to 2019) water reservoir levels. In this case, it is assumed that the maximum reported value for a country across the five available years coincides with its STO storage capabilities. Finally, if data is not found in any of the two aforementioned sources, the another database that stores more generic reservoir-specific data (that is, water storage capacities in reservoirs that also serve other purposes than hydro power generation) [218] is queried. More explicitly, the STO storage capabilities of a given country are assumed equal to the sum of the capacities of all reservoirs in that country whose main usage is linked to hydroelectricity. Upon using the three aforementioned data sources, 189 TWh of storage capacity for reservoir-based plants are found within the European countries of interest. The distribution of STO capacity is shown in the left subplot of Figure B.2.

The estimation of country-based inflows in STO reservoirs relies on reanalysis-based runoff time series [86]. However, instead of being expressed as per-unit values, the STO inflows are expressed in energy units (e.g., GWh). In this regard, let $\mathcal{G}$ denote the set of all reanalysis grid cells for which the inflow is computed. For each reanalysis grid cell $cell \in \mathcal{G}$, the product between the runoff and the corresponding grid

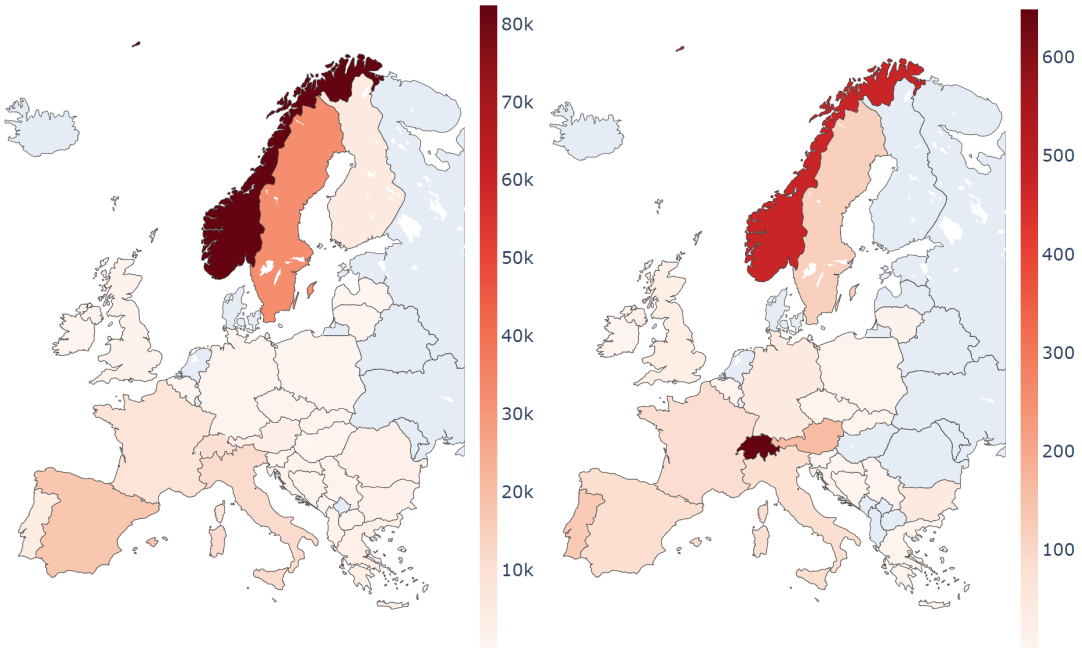

FIGURE B.2: Energy storage capacities (in GWh) of reservoir-based (left) and pumped-hydro units (right) across European countries. Each subplot is accompanied by its own colorbar.

cell surface area (α_{cell}) is computed, as seen in (B.2a). Given the fact that the runoff is natively expressed in meters[3], the product returns the equivalent volume of water available in each cell per unit time (i.e., water flow). Subsequently, the resulting time series are aggregated on a country basis, thus taking into account the grid cell geo-positioning with respect to country borders (as per (B.2b)) and converted into an energy-based inflow via (B.2c). In the latter equation, ρ_{H_2O} represents the water density (assumed 1000 km/m^3 and g stands for the gravitational constant (i.e., 9.81 m/s^2). Additionally, h_c stands for the the country-average water head (assumed unitary in a first stage).

$$q_{cell,t} = ro_{cell,t}\ \alpha_{cell}, \quad \forall cell \in \mathcal{G}, \forall t \in \mathcal{T} \tag{B.2a}$$

$$q_{c,t} = \sum_{cell \in c} q_{cell,t}, \quad \forall c \in \mathcal{C}, \forall t \in \mathcal{T} \tag{B.2b}$$

$$i_{c,t}^{STO,init} = q_{c,t}\ \rho_{H_2O}\ g\ h_c, \quad \forall c \in \mathcal{C}, \forall t \in \mathcal{T} \tag{B.2c}$$

$$E_c^{STO} = E_c^{HYDRO} - \sum_{t \in T} p_{c,t}^{ROR}, \quad \forall c \in \mathcal{C} \tag{B.2d}$$

$$fm_c = \frac{E_c^{STO}}{\sum_{t \in T} i_{c,t}^{STO,init}}, \quad \forall c \in \mathcal{C} \tag{B.2e}$$

$$i_{c,t}^{STO} = i_{c,t}^{STO,init}\ fm_c, \quad \forall c \in \mathcal{C}, \forall t \in \mathcal{T} \tag{B.2f}$$

[3]The runoff variable in use expresses "the depth the water would have if it were spread evenly over the grid box" [219].

TABLE B.2: Reservoir-based hydro (STO) flow multiplier values (expressed in metres) for various countries in Europe.

ISO2	fm_c	**ISO2**	fm_c	**ISO2**	fm_c
AT	114.3	GB	9.8	NO	279.3
BE	64.3	GR	82.7	PL	33.9
BG	116.9	HR	123.9	PT	194.5
CH	191.3	HU	11.3	RO	168.1
CZ	96.3	IE	0.07	RS	392.6
DE	48.7	IT	83.9	SE	159.9
ES	279.2	LT	44.4	SI	103.1
FI	22.7	LU	499.1	SK	129.5
FR	118.9	LV	3.6		

At this stage, the modelled STO water inflows are expressed in energy units, yet a brief comparison with historical yearly generation volumes reveals significant differences in favour of the latter. Indeed, on the one hand, a unitary water head is assumed in (B.2c), while the actual values of this parameter for individual plants vary between tens and hundreds of metres. On the other hand, it has been assumed that the entirety of the modelled inflows are used for hydroelectricity generation, whereas this is expected to be an unrealistic assumption, as e.g., part of the runoff is draining into the ground, part of it flows unconstrained through dam gates for environmental purposes, etc. In order to take these two factors (i.e., water head and the retain factor) into account in the definition of the STO inflow, a country-specific *flow multiplier* or fm_c is derived. For each country, yearly integrated ROR production data (whose estimation has been previously discussed) is subtracted from the total hydroelectricity generation volumes (E_c^{HYDRO} obtained from [220]) and the remainder is attributed to reservoir-based plants, as described by (B.2d). The ratio (B.2e) between the expected generation and the yearly integrated STO inflows assuming a unitary water head defines the flow multiplier mentioned above and centralized in Table B.2. The corrected STO inflow time series are therefore obtained by multiplying their initial values with this country-specific scalar, as seen in Eq. (B.2f).

B.3 Pumped-Hydro Storage Capacities

In the exercise at hand, pumped-hydro storage (PHS) is modelled as storage technology without the possibility of expansion. PHS units are modelled without natural inflows (i.e., closed-loop schemes) and with a unitary self-discharge efficiency (e.g., evaporation losses are not taken into account). Additionally, it is assumed that, for all PHS units, both turbine and pumping modes have identical rated powers and efficiencies. Installed capacities of such units are retrieved from [151] yet, as for STO

TABLE B.3: Pumped-hydro storage (PHS) power and energy capacities for various countries in Europe.

ISO2	K_c [GW]	S_c [GWh]	**ISO2**	K_c [GW]	S_c [GWh]	**ISO2**	K_c [GW]	S_c [GWh]
AT	3.6	159.4	GB	2.9	26.7	NO	1.3	472.6
BE	1.3	5.7	GR	0.7	5.1	PL	1.7	7.3
BG	1.4	41.1	HR	0.5	4.4	PT	3.9	130.7
CH	4.5	648.5	HU			RO		
CZ	1.2	5.57	IE	0.3	1.8	RS	0.6	3.6
DE	7.8	45.6	IT	7.9	81.0	SE	0.1	116.5
ES	7.9	83.1	LT	0.9	10.8	SI	0.2	0.5
FI			LU			SK	1.0	4.6
FR	5.3	85.6	LV					

units, information regarding to their storage capabilities is scarce. However, an accurate assessment of such information is paramount for an accurate modelling of PHS plants which, with over 54 GW of installed capacity, have a significant impact in the integration of RES throughout Europe. In this regard, the following unit-based approach is proposed. At first, storage capabilities data is sought for each individual plant obtained from [151] within a peer-reviewed database [125]. If for a given plant, unit-specific data does not exist, but country-specific duration (i.e., energy-to-power ratio) data is available, the latter is used to approximate storage capacities starting from the installed capacities in each individual country (i.e., if the specific duration for a PHS plant in France is not available, yet the country-specific parameter is provided and equal to 4 h, that PHS plant will have a specific duration of 4 h). In case country- and plant-specific data is missing, a default specific duration of 6 h is used to derive pumped-hydro storage capabilities for the remainder of the units. This procedure results in a total European pumped-hydro storage potential of 1930 GWh whose distribution is presented in Table B.3, as well as on the right subplot of Figure B.2.

Bibliography

[1] V. Masson-Delmotte, P. Zhai, A. Pirani, *et al.*, "Climate Change 2021: The Physical Science Basis. Contribution of Working Group I to the Sixth Assessment Report of the Intergovernmental Panel on Climate Change," 2021. [Online]. Available: https://www.ipcc.ch/report/ar6/wg1/.

[2] United Nations Framework Convention on Climate Change - UNFCCC, "The Paris Agreement - the Conference of the Parties on its twenty-first session," 2015. [Online]. Available: https://unfccc.int/process/conferences/pastconferences/paris-climate-change-conference-november-2015/paris-agreement.

[3] "Net Zero by 2050 - A Roadmap for the Global Energy Sector," International Energy Agency, Tech. Rep., 2021. [Online]. Available: https://www.iea.org/reports/net-zero-by-2050.

[4] International Renewable Energy Agency (IRENA), "World Energy Transitions Outlook: 1.5°C Pathway," 2021. [Online]. Available: https://www.irena.org/publications/2021/Jun/World-Energy-Transitions-Outlook.

[5] E. Larson, C. Greig, J. Jenkins, *et al.*, "Net-Zero America: Potential Pathways, Infrastructure, and Impacts," 2020. [Online]. Available: https://netzeroamerica.princeton.edu/.

[6] S. Mallapaty, *How China could be carbon neutral by mid-century*, published in Nature 586, 482-483, 2020. DOI: 10.1038/d41586-020-02927-9. [Online]. Available: https://www.nature.com/articles/d41586-020-02927-9.

[7] S. Zhang, J. Liu, G. Yin, Y. Bi, J. Qiao, and Y. Ji, "China Nationally Determined Contribution (NDC) and Domestic 14th Power Five-Year-Plan (FYP)," 2020. [Online]. Available: https://energyandcleanair.org/publication/china-nationally-determined-contribution-ndc-and-domestic-14th-power-five-year-plan-fyp/.

[8] "Clean energy for all Europeans package," European Commission, Tech. Rep., 2019. [Online]. Available: https://ec.europa.eu/energy/topics/energy-strategy/clean-energy-all-europeans_en.

[9] "A European Green Deal," European Commission, Tech. Rep., 2021. [Online]. Available: https://ec.europa.eu/info/strategy/priorities-2019-2024/european-green-deal_en.

[10] V. Masson-Delmotte, P. Zhai, H.-O. Pörtner, *et al.*, "Global Warming of 1.5°C. An IPCC Special Report on the impacts of global warming of 1.5°C above

pre-industrial levels and related global greenhouse gas emission pathways, in the context of strengthening the global response to the threat of climate change, sustainable development, and efforts to eradicate poverty," World Meteorological Organization, 2018.

[11] The International Energy Agency, *World Energy Balances: Overview*, 2020. [Online]. Available: https://www.iea.org/reports/world-energy-balances-overview.

[12] ——, *Renewables 2020 Data Explorer*, 2020. [Online]. Available: https://www.iea.org/articles/renewables-2020-data-explorer.

[13] S. G. Yalew, M. T. H. van Vliet, D. E. H. J. Gernaat, *et al.*, "Impacts of climate change on energy systems in global and regional scenarios," *Nature Energy*, vol. 5, pp. 794–802, 2020. DOI: https://doi.org/10.1038/s41560-020-0664-z.

[14] Energy Realpolitik, *South Africa's Blackouts Demonstrate Need for Distributed Energy Resources*, 2019. [Online]. Available: https://www.cfr.org/blog/south-africas-blackouts-demonstrate-need-distributed-energy-resources.

[15] J. W. Busby, K. Baker, M. D. Bazilian, *et al.*, "Cascading risks: Understanding the 2021 winter blackout in Texas," *Energy Research & Social Science*, vol. 77, p. 102 106, 2021, ISSN: 2214-6296. DOI: https://doi.org/10.1016/j.erss.2021.102106. [Online]. Available: https://www.sciencedirect.com/science/article/pii/S2214629621001997.

[16] Vanessa Dezem (for Bloomberg Green), *Thousands left in the dark in Germany as floods cut power supply*, 2021. [Online]. Available: https://www.bloomberg.com/news/articles/2021-07-16/thousands-left-in-the-dark-in-germany-as-floods-cut-power-supply.

[17] D. E. H. J. Gernaat, H. S. de Boer, V. Daioglou, S. G. Yalew, C. Müller, and D. P. van Vuuren, "Climate change impacts on renewable energy supply," *Nature Climate Change*, vol. 11, pp. 119–125, 2021. DOI: https://doi.org/10.1038/s41558-020-00949-9.

[18] A. Conejo, L. Baringo, S. Kazempour, and A. Siddiqui, "Investment in generation and transmission facilities," in *Investment in Electricity Generation and Transmission*, 2nd ed. Springer, 2016, ch. 1. DOI: 10.1007/978-3-319-29501-5_1.

[19] N. E. Koltsaklis and A. S. Dagoumas, "State-of-the-art generation expansion planning: A review," *Applied Energy*, vol. 230, 2018. DOI: doi:10.1016/j.apenergy.2018.08.087.

[20] M. Mahdavi, C. Sabillon Antunez, M. Ajalli, and R. Romero, "Transmission expansion planning: Literature review and classification," *IEEE Systems Journal*, vol. 13, no. 3, pp. 3129–3140, 2019. DOI: 10.1109/JSYST.2018.2871793.

[21] V. Krishnan, J. Ho, B. F. Hobbs, *et al.*, "Co-optimization of electricity transmission and generation resources for planning and policy analysis: Review

of concepts and modeling approaches," *Energy Systems*, vol. 7, pp. 297–332, 2016. DOI: 10.1007/s12667-015-0158-4.

[22] A. Botterud, M. Ilic, and I. Wangensteen, "Optimal investments in power generation under centralized and decentralized decision making," *IEEE Transactions on Power Systems*, vol. 20, no. 1, pp. 254–263, 2005. DOI: 10.1109/TPWRS.2004.841217.

[23] R. Loulou and U. Remne and A. Kanudia and A. Lehtila and G. Goldstein, *Documentation for the TIMES Model - PART I*, 2005. [Online]. Available: https://iea-etsap.org/index.php/etsap-tools/model-generators/times.

[24] The International Energy Agency, *Energy Technology Systems Analysis Program (ETSAP)*, 2021. [Online]. Available: https://iea-etsap.org/index.php/applications.

[25] F. Wiese, R. Bramstoft, H. Koduvere, *et al.*, "Balmorel open source energy system model," *Energy Strategy Reviews*, vol. 20, pp. 26–34, 2018, ISSN: 2211-467X. DOI: https://doi.org/10.1016/j.esr.2018.01.003. [Online]. Available: https://www.sciencedirect.com/science/article/pii/S2211467X18300038.

[26] C. Barragán-Beaud, A. Pizarro-Alonso, M. Xylia, S. Syri, and S. Silveira, "Carbon tax or emissions trading? An analysis of economic and political feasibility of policy mechanisms for greenhouse gas emissions reduction in the Mexican power sector," *Energy Policy*, vol. 122, pp. 287–299, 2018, ISSN: 0301-4215. DOI: https://doi.org/10.1016/j.enpol.2018.07.010. [Online]. Available: https://www.sciencedirect.com/science/article/pii/S0301421518304579.

[27] J. Gea-Bermúdez, L.-L. Pade, M. J. Koivisto, and H. Ravn, "Optimal generation and transmission development of the North Sea region: Impact of grid architecture and planning horizon," *Energy*, vol. 191, p. 116 512, 2020, ISSN: 0360-5442. DOI: https://doi.org/10.1016/j.energy.2019.116512. [Online]. Available: https://www.sciencedirect.com/science/article/pii/S0360544219322078.

[28] P. Meibom and K. Karlsson, "Role of hydrogen in future North European power system in 2060," *International Journal of Hydrogen Energy*, vol. 35, no. 5, pp. 1853–1863, 2010, ISSN: 0360-3199. DOI: https://doi.org/10.1016/j.ijhydene.2009.12.161. [Online]. Available: https://www.sciencedirect.com/science/article/pii/S036031990902120X.

[29] M. Howells, H. Rogner, N. Strachan, *et al.*, "OSeMOSYS: The open source energy modeling system: An introduction to its ethos, structure and development," *Energy Policy*, vol. 39, pp. 5850–5870, 2011. DOI: 10.1016/j.enpol.2011.06.033.

[30] H. Henke, *The Open Source energy Modelling Base for Europe (OSeMBE)*, 2019. [Online]. Available: https://kth.diva-portal.org/smash/get/diva2:1135883/FULLTEXT01.pdf.

[31] K. Löffler, K. Hainsch, T. Burandt, P.-Y. Oei, C. Kemfert, and C. Von Hirschhausen, "Designing a model for the global energy system—genesys-mod: An application of the open-source energy modeling system (osemosys)," *Energies*, vol. 10, no. 10, 2017, ISSN: 1996-1073. DOI: 10.3390/en10101468. [Online]. Available: https://www.mdpi.com/1996-1073/10/10/1468.

[32] T. Brown, J. Hörsch, and D. Schlachtberger, "PyPSA: Python for Power System Analysis," *Journal of Open Research Software*, vol. 6, 1 2018. DOI: 10.5334/jors.188. eprint: 1707.09913. [Online]. Available: https://doi.org/10.5334/jors.188.

[33] J. Hörsch, F. Hofmann, D. Schlachtberger, and T. Brown, "PyPSA-Eur: An open optimisation model of the European transmission system," *Energy Strategy Reviews*, vol. 22, pp. 207–215, 2018, ISSN: 2211-467X. DOI: https://doi.org/10.1016/j.esr.2018.08.012. [Online]. Available: https://www.sciencedirect.com/science/article/pii/S2211467X18300804.

[34] T. Brown, D. Schlachtberger, A. Kies, S. Schramm, and M. Greiner, "Synergies of sector coupling and transmission reinforcement in a cost-optimised, highly renewable European energy system," *Energy*, vol. 160, pp. 720–739, 2018, ISSN: 0360-5442. DOI: https://doi.org/10.1016/j.energy.2018.06.222. [Online]. Available: https://www.sciencedirect.com/science/article/pii/S036054421831288X.

[35] H. Liu, T. Brown, G. B. Andresen, D. P. Schlachtberger, and M. Greiner, "The role of hydro power, storage and transmission in the decarbonization of the Chinese power system," *Applied Energy*, vol. 239, 1308–1321, 2019, ISSN: 0306-2619. DOI: 10.1016/j.apenergy.2019.02.009. [Online]. Available: http://dx.doi.org/10.1016/j.apenergy.2019.02.009.

[36] Maximilian Parzen, *PyPSA meets Africa*, 2021. [Online]. Available: https://pypsa-meets-africa.github.io/.

[37] Thomas Spence and Neshwin Rodrigues and Raghav Pachouri and Shubham Thakre, *A model-based assessment of variable renewable grid integration costs in India*, 2021. [Online]. Available: https://www.teriin.org/sites/default/files/2021-02/A_Modal-Based_Assessment_Report_0.pdf.

[38] S. Pfenninger and B. Pickering, "Calliope: A multi-scale energy systems modelling framework," *Journal of Open Source Software*, 2018. DOI: 10.21105/joss.00825.

[39] T. Tröndle, J. Lilliestam, S. Marelli, and S. Pfenninger, "Trade-offs between geographic scale, cost, and infrastructure requirements for fully renewable electricity in Europe," *Joule*, vol. 4, no. 9, pp. 1929–1948, 2020, ISSN: 2542-4351. DOI: https://doi.org/10.1016/j.joule.2020.07.018. [Online]. Available: https://www.sciencedirect.com/science/article/pii/S2542435120303366.

[40] S. Pfenninger and J. Keirstead, "Comparing concentrating solar and nuclear power as baseload providers using the example of South Africa," *Energy*,

vol. 87, pp. 303–314, 2015, ISSN: 0360-5442. DOI: https://doi.org/10.1016/j.energy.2015.04.077. [Online]. Available: https://www.sciencedirect.com/science/article/pii/S0360544215005320.

[41] C. D. Pero, F. Leonforte, F. Lombardi, *et al.*, "Modelling of an integrated multi-energy system for a nearly zero energy smart district," in *2019 International Conference on Clean Electrical Power (ICCEP)*, 2019, pp. 246–252. DOI: 10.1109/ICCEP.2019.8890129.

[42] Jesse D. Jenkins and Nestor A. Sepulveda andDharik Mallapragada and Sambuddha Chakrabati and Jack Morris and Neha Patankar and Aaron Schwartz and Qingyu Xu, *GenX, a new tool for investment planning in the power sector*, 2021. [Online]. Available: https://energy.mit.edu/genx/.

[43] M. Schulthoff, I. Rudnick, A. Bose, and E. Gençer, "Role of hydrogen in a low-carbon electric power system: A case study," *Frontiers in Energy Research*, vol. 8, p. 344, 2021, ISSN: 2296-598X. DOI: 10.3389/fenrg.2020.585461. [Online]. Available: https://www.frontiersin.org/article/10.3389/fenrg.2020.585461.

[44] Breakthrough Energy Sciences, *REISE - Renewable Energy Integration Simulation Engine*, 2021. [Online]. Available: https://breakthrough-energy.github.io/docs/index.html.

[45] Y. Xu, N. Myhrvold, D. Sivam, *et al.*, *U.S. Test System with High Spatial and Temporal Resolution for Renewable Integration Studies*, 2020. arXiv: 2002.06155.

[46] I. H. Gonzales and S. Q. A. Zucker, "Dispa-SET 2.0: unit commitment and power dispatch model," *Publications Office of the European Union*, 2014. DOI: http://dx.doi.org/10.2790/967448.

[47] C. Coffrin, R. Bent, K. Sundar, Y. Ng, and M. Lubin, "Powermodels.jl: An open-source framework for exploring power flow formulations," in *2018 Power Systems Computation Conference (PSCC)*, 2018, pp. 1–8. DOI: 10.23919/PSCC.2018.8442948.

[48] H.-K. Ringkjøb, P. M. Haugan, and I. M. Solbrekke, "A review of modelling tools for energy and electricity systems with large shares of variable renewables," *Renewable and Sustainable Energy Reviews*, vol. 96, pp. 440–459, 2018, ISSN: 1364-0321. DOI: https://doi.org/10.1016/j.rser.2018.08.002. [Online]. Available: https://www.sciencedirect.com/science/article/pii/S1364032118305690.

[49] H.-K. Ringkjøb, P. M. Haugan, P. Seljom, A. Lind, F. Wagner, and S. Mesfun, "Short-term solar and wind variability in long-term energy system models - a European case study," *Energy*, vol. 209, p. 118 377, 2020, ISSN: 0360-5442. DOI: https://doi.org/10.1016/j.energy.2020.118377. [Online]. Available: https://www.sciencedirect.com/science/article/pii/S0360544220314845.

[50] J. Wohland, D. Brayshaw, and S. Pfenninger, "Mitigating a century of european renewable variability with transmission and informed siting," *Environmental Research Letters*, vol. 16, no. 6, p. 064 026, 2021. DOI: 10.1088/1748-9326/abff89. [Online]. Available: https://doi.org/10.1088/1748-9326/abff89.

[51] S. Pfenninger, A. Hawkes, and J. Keirstead, "Energy systems modeling for twenty-first century energy challenges," *Renewable and Sustainable Energy Reviews*, vol. 33, pp. 74 –86, 2014, ISSN: 1364-0321. DOI: https://doi.org/10.1016/j.rser.2014.02.003. [Online]. Available: http://www.sciencedirect.com/science/article/pii/S1364032114000872.

[52] A. MacDonald, C. Clack, A. Alexander, A. Dunbar, J. Wilczak, and Y. Xie, "Future cost-competitive electricity systems and their impact on US CO_2 emissions," *Nature Climate Change*, vol. 6, 2016. DOI: doi:10.1038/NCLIMATE2921.

[53] M. Hoffmann, L. Kotzur, D. Stolten, and M. Robinius, "A review on time series aggregation methods for energy system models," *Energies*, vol. 13, no. 3, 2020. DOI: 10.3390/en13030641.

[54] D. Schlachtberger, T. Brown, S. Schramm, and M. Greiner, "The benefits of cooperation in a highly renewable European electricity network," *Energy*, vol. 134, pp. 469–481, 2017, ISSN: 0360-5442. DOI: https://doi.org/10.1016/j.energy.2017.06.004. [Online]. Available: https://www.sciencedirect.com/science/article/pii/S0360544217309969.

[55] ENTSO-E, *Maps & Data: TYNDP2018*, 2018. [Online]. Available: https://tyndp.entsoe.eu/maps-data.

[56] J. Yu, G. Sanchis, K. Bakic, *et al.*, "Global Electricity Network Feasibility Study," CIGRE, Tech. Rep. 775, 2019.

[57] V. Krishnan and W. Cole, "Evaluating the value of high spatial resolution in national Capacity Expansion Models using ReEDS," *2016 IEEE PES General Meeting*, 2016.

[58] B. A. Frew and M. Z. Jacobson, "Temporal and spatial tradeoffs in power system modeling with assumptions about storage: An application of the POWER model," *Energy*, vol. 117, pp. 198 –213, 2016, ISSN: 0360-5442. DOI: https://doi.org/10.1016/j.energy.2016.10.074. [Online]. Available: http://www.sciencedirect.com/science/article/pii/S0360544216315110.

[59] J. Hörsch and T. Brown, "The role of spatial scale in joint optimisations of generation and transmission for European highly renewable scenarios," *2017 14th Intl. Conf. on the European Energy Market (EEM)*, 2017.

[60] M. M. Frysztacki, J. Hörsch, V. Hagenmeyer, and T. Brown, "The strong effect of network resolution on electricity system models with high shares of wind and solar," *Applied Energy*, vol. 291, p. 116 726, 2021, ISSN: 0306-2619. DOI: https://doi.org/10.1016/j.apenergy.2021.116726. [Online]. Available: https://www.sciencedirect.com/science/article/pii/S0306261921002439.

[61] M. Pierrot, *The Wind Power - Wind Energy Market Intelligence*, 2020. [Online]. Available: https://www.thewindpower.net/store_continent_en.php?id_zone=1001.

[62] P. Wolfe, *Wiki Solar - The authority on utility-scale solar power*, 2020. [Online]. Available: https://www.wiki-solar.org/data/index.html.

[63] "A Clean Planet for all - A European strategic long-term vision for a prosperous, modern, competitive and climate neutral economy," European Commission, Tech. Rep., 2018. [Online]. Available: https://ec.europa.eu/clima/policies/strategies/2050_en.

[64] "Towards the first hub-and-spoke project," North Sea Wind Power Hub Consortium, Tech. Rep., 2021. [Online]. Available: https://northseawindpowerhub.eu/knowledge/towards-the-first-hub-and-spoke-project.

[65] B. Li, S. Basu, S. J. Watson, and H. W. J. Russchenberg, "Mesoscale modeling of a "dunkelflaute" event," *Wind Energy*, vol. 24, no. 1, pp. 5–23, 2021. DOI: https://doi.org/10.1002/we.2554. eprint: https://onlinelibrary.wiley.com/doi/pdf/10.1002/we.2554. [Online]. Available: https://onlinelibrary.wiley.com/doi/abs/10.1002/we.2554.

[66] D. Stenclik, P. Denholm, and B. Chalamala, "Maintaining Balance: The Increasing Role of Energy Storage for Renewable Integration," *IEEE Power and Energy Magazine*, vol. 15, no. 6, pp. 31–39, 2017. DOI: https://doi.org/10.1109/MPE.2017.2729098.

[67] N. O'Connell, P. Pinson, H. Madsen, and M. O'Malley, "Benefits and Challenges of Electrical Demand Response: A Critical Review," *Renewable and Sustainable Energy Reviews*, vol. 39, pp. 686–699, 2014, ISSN: 1364-0321. DOI: https://doi.org/10.1016/j.rser.2014.07.098.

[68] G. Giebel, "On the benefits of distributed generation of wind energy in Europe," PhD thesis, University of Oldenburg, Germany, 2001.

[69] International Energy Agency (IEA), *Getting Wind and Solar onto the Grid*, 2017. [Online]. Available: https://www.iea.org/reports/getting-wind-and-solar-onto-the-grid.

[70] K. Engeland, M. Borga, J.-D. Creutin, B. François, M.-H. Ramos, and J.-P. Vidal, "Space-time variability of climate variables and intermittent renewable electricity production – a review," *Renewable and Sustainable Energy Reviews*, vol. 79, pp. 600 –617, 2017, ISSN: 1364-0321. DOI: https://doi.org/10.1016/j.rser.2017.05.046.

[71] A. Dubois and D. Radu, *EPIPPy - Input Pre-processing for Expansion Planning in Python*, 2020. [Online]. Available: https://github.com/montefesp/EPIPPy.

[72] D. Radu and M. Berger, *Resite - a framework for RES siting leveraging resource complementarity*, 2021. [Online]. Available: https://github.com/dcradu/resite_ip/.

[73] A. Dubois, D. Radu, and M. Berger, *Replan - a framework for bulk energy systems planning and analysis*, 2020. [Online]. Available: https://github.com/montefesp/replan.

[74] S. Chatzivasileiadis, D. Ernst, and G. Andersson, "The global grid," *Renewable Energy*, vol. 57, pp. 372–383, 2013. DOI: 10.1016/j.renene.2013.01.032.

[75] Z. Liu, *Global electricity interconnection*. Academic Press, 2016.

[76] G. Ingeborg and M. Korpås, "Variability characteristics of European wind and solar power resources - A review," *Energies*, vol. 9, no. 6, 2016. DOI: 10.3390/en9060449.

[77] S. Erdle, "The DESERTEC initiative: powering the development perspectives of Southern Mediterranean countries?" German Development Institute / Deutsches Institut für Entwicklungspolitik (DIE), Discussion Papers 12/2010, 2010. [Online]. Available: https://ideas.repec.org/p/zbw/diedps/122010.html.

[78] S. Mano, B. Ovgor, Z. Samadov, *et al.*, "Gobitec and Asian Super Grid for renewable energies in Northeast Asia," 2014. [Online]. Available: https://www.energycharter.org/fileadmin/DocumentsMedia/Thematic/Gobitec_and_the_Asian_Supergrid_2014_en.pdf.

[79] W. Platzer, I. Bole, A. Vogel, N. Tham, and P. Bretschneider, "Supergrid study - Approach for the integration of renewable energy in Europe and North Africa," 2016. [Online]. Available: https://www.ise.fraunhofer.de/en/publications/studies/supergrid.html.

[80] K. Komoto, T. Ehara, H. Xu, *et al.*, "Energy from the desert: Very large scale PV power plants for shifting to renewable energy future," 2015.

[81] A. Gulagi, D. Bogdanov, M. Fasihi, and C. Breyer, "Can Australia power the energy-hungry Asia with renewable energy?" *Sustainability*, vol. 9, no. 2, 2017, ISSN: 2071-1050. DOI: 10.3390/su9020233.

[82] J. P. da Silva Soares, "Wind energy utilization in the Arctic climate," Ph.D. dissertation, Uppsala University, 2016. [Online]. Available: https://www.diva-portal.org/smash/get/diva2:1046990/FULLTEXT01.pdf.

[83] K. R. Jakobsen, "Renewable energy potential of Greenland with emphasis on wind resource assessment," Ph.D. dissertation, DTU, 2016. [Online]. Available: https://orbit.dtu.dk/en/publications/renewable-energy-potential-of-greenland-with-emphasis-on-wind-res.

[84] Orkustofnun, Norges Arktiske Universitet, Energy Styrlesen, Jardfeingi, Shetland Islands Council, and Greenland Innovation Centre, "North Atlantic Energy Network," 2016. [Online]. Available: https://orkustofnun.is/gogn/Skyrslur/OS-2016/North-Atlantic-Energy-Network-Report.pdf.

[85] X. Fettweis, J. E. Box, C. Agosta, *et al.*, "Reconstructions of the 1900–2015 Greenland ice sheet surface mass balance using the regional climate MAR model," *The Cryosphere*, vol. 11, pp. 1015–1033, 2 2017. DOI: 10.5194/tc-11-1015-2017. [Online]. Available: https://tc.copernicus.org/articles/11/1015/2017/.

[86] European Centre for Medium-Range Weather Forecasts - ECMWF, *ERA5 data documentation*, https://confluence.ecmwf.int//display/CKB/, 2018.

[87] R. Gelaro, W. McCarty, M. J. Suárez, *et al.*, "The modern-era retrospective analysis for research and applications, version 2 (MERRA-2)," *Journal of Climate*, vol. 30, no. 14, pp. 5419–5454, 2017. DOI: 10.1175/JCLI-D-16-0758.1.

[88] I. Staffell and S. Pfenninger, "Using bias-corrected reanalysis to simulate current and future wind power output," *Energy*, vol. 114, pp. 1224–1239, 2016, ISSN: 0360-5442. DOI: 10.1016/j.energy.2016.08.068. [Online]. Available: https://www.sciencedirect.com/science/article/pii/S0360544216311811.

[89] J. Olauson, "ERA5: The new champion of wind power modelling?" *Renewable Energy*, vol. 126, pp. 322–331, 2018. DOI: 10.1016/j.renene.2018.03.056.

[90] P. Norgaard and H. Holttinen, "A multi-turbine power curve approach," 2004.

[91] K. Freeman, C. Frost, G. Hundleby, *et al.*, "Our energy, our future - How offshore wind will help Europe to go carbon-neutral," WindEurope, Tech. Rep., 2019. [Online]. Available: https://windeurope.org/wp-content/uploads/files/about-wind/reports/WindEurope-Our-Energy-Our-Future.pdf.

[92] L. J. L. Stival, A. K. Guetter, and F. O. de Andrade, "The impact of wind shear and turbulence intensity on wind turbine power performance," *Espaço Energia*, pp. 11–20, 27 2017.

[93] Danish Energy Agency, "Overview of the energy sector - Master data register of wind turbines," 2018. [Online]. Available: https://ens.dk/en/our-services/statistics-data-key-figures-and-energy-maps/overview-energy-sector.

[94] RTE, "Bilan électrique et perspectives - Bretagne," 2016. [Online]. Available: https://www.rte-france.com/analyses-tendances-et-prospectives/bilans-electriques-nationaux-et-regionaux.

[95] H. Louie, "Correlation and statistical characteristics of aggregate wind power in large transcontinental systems," *Wind Energy*, vol. 17, no. 6, pp. 793–810, 2013. DOI: 10.1002/we.1597.

[96] J. Jurasz, F. Canales, A. Kies, M. Guezgouz, and A. Beluco, "A Review on the Complementarity of Renewable Energy Sources: Concept, Metrics, Application and Future Research Directions," *Solar Energy*, vol. 195, pp. 703–724, 2020. DOI: https://doi.org/10.1016/j.solener.2019.11.087.

[97] J. Widen, "Correlations between large-scale solar and wind power in a future scenario for Sweden," *IEEE Transactions on Sustainable Energy*, vol. 2, no. 2, pp. 177–184, 2011, ISSN: 1949-3029. DOI: 10.1109/TSTE.2010.2101620.

[98] C. M. S. Martin, J. K. Lundquist, and M. A. Handschy, "Variability of interconnected wind plants: Correlation length and its dependence on variability time scale," *Environmental Research Letters*, vol. 10, no. 4, 2015. DOI: 10.1088/1748-9326/10/4/044004.

[99] J. Olauson and M. Bergkvist, "Correlation between wind power generation in the European countries," *Energy*, vol. 114, pp. 663 –670, 2016, ISSN: 0360-5442. DOI: https://doi.org/10.1016/j.energy.2016.08.036.

[100] K. Klima and J. Apt, "Geographic smoothing of solar PV: Results from Gujarat," *Environmental Research Letters*, vol. 10, no. 10, p. 104 001, 2015. DOI: 10.1088/1748-9326/10/10/104001.

[101] S. Sterl, S. Liersch, H. Koch, N. P. M. van Lipzig, and W. Thiery, "A new approach for assessing synergies of solar and wind power: Implications for west africa," *Environmental Research Letters*, vol. 13, no. 9, 2018. DOI: 10.1088/1748-9326/aad8f6.

[102] J. H. Slusarewicz and D. S. Cohan, "Assessing solar and wind complementarity in texas," *Renewables: Wind, Water, and Solar*, vol. 5, no. 1, p. 7, 2018, ISSN: 2198-994X. DOI: 10.1186/s40807-018-0054-3.

[103] P. E. Bett and H. E. Thornton, "The climatological relationships between wind and solar energy supply in Britain," *Renewable Energy*, vol. 87, pp. 96 –110, 2016, ISSN: 0960-1481. DOI: https://doi.org/10.1016/j.renene.2015.10.006.

[104] M. M. Miglietta, T. Huld, and F. Monforti-Ferrario, "Local complementarity of wind and solar energy resources over europe: An assessment study from a meteorological perspective," *Journal of Applied Meteorology and Climatology*, vol. 56, no. 1, pp. 217–234, 2017. DOI: 10.1175/JAMC-D-16-0031.1.

[105] P. S. dos Anjos, A. S. A. da Silva, B. Stosic, and T. Stosic, "Long-term correlations and cross-correlations in wind speed and solar radiation temporal series from Fernando de Noronha Island, Brazil," *Physica A: Statistical Mechanics and its Applications*, vol. 424, pp. 90 –96, 2015, ISSN: 0378-4371. DOI: https://doi.org/10.1016/j.physa.2015.01.003.

[106] G. Ren, J. Wan, J. Liu, and D. Yu, "Spatial and temporal assessments of complementarity for renewable energy resources in china," *Energy*, vol. 177, pp. 262 –275, 2019, ISSN: 0360-5442. DOI: https://doi.org/10.1016/j.energy.2019.04.023.

[107] J. Jurasz, A. Beluco, and F. A. Canales, "The impact of complementarity on power supply reliability of small scale hybrid energy systems," *Energy*, vol. 161, pp. 737 –743, 2018, ISSN: 0360-5442. DOI: https://doi.org/10.1016/j.energy.2018.07.182.

[108] C. E. Hoicka and I. H. Rowlands, "Solar and wind resource complementarity: Advancing options for renewable electricity integration in Ontario, Canada," *Renewable Energy*, vol. 36, no. 1, pp. 97 –107, 2011.

[109] F. Monforti, T. Huld, K. Bódis, L. Vitali, M. D'Isidoro, and R. Lacal-Arántegui, "Assessing complementarity of wind and solar resources for energy production in Italy. a Monte Carlo approach," *Renewable Energy*, vol. 63, pp. 576 –586, 2014, ISSN: 0960-1481. DOI: https://doi.org/10.1016/j.renene.2013.10.028.

[110] W. Katzenstein, E. Fertig, and J. Apt, "The variability of interconnected wind plants," *Energy Policy*, vol. 38, no. 8, pp. 4400–4410, 2010.

[111] J. Apt, "The spectrum of power from wind turbines," *Journal of Power Sources*, vol. 169, no. 2, pp. 369 –374, 2007, ISSN: 0378-7753. DOI: https://doi.org/10.1016/j.jpowsour.2007.02.077.

[112] W. Li, S. Stadler, and R. Ramakumar, "Modeling and assessment of wind and insolation resources with a focus on their complementary nature: A case study of Oklahoma," *Annals of the Association of American Geographers*, vol. 101, no. 4, pp. 717–729, 2011. DOI: 10.1080/00045608.2011.567926.

[113] H. Zhang, Y. Cao, Y. Zhang, and V. Terzija, "Quantitative synergy assessment of regional wind-solar energy resources based on MERRA reanalysis data," *Applied Energy*, vol. 216, pp. 172 –182, 2018. DOI: 10.1016/j.apenergy.2018.02.094.

[114] A. A. Prasad, R. A. Taylor, and M. Kay, "Assessment of solar and wind resource synergy in australia," *Applied Energy*, vol. 190, pp. 354 –367, 2017, ISSN: 0306-2619. DOI: https://doi.org/10.1016/j.apenergy.2016.12.135.

[115] G. Ren, J. Wan, J. Liu, and D. Yu, "Characterization of wind resource in china from a new perspective," *Energy*, vol. 167, pp. 994 –1010, 2019, ISSN: 0360-5442. DOI: https://doi.org/10.1016/j.energy.2018.11.032.

[116] A. Beluco, P. K. de Souza, and A. Krenzinger, "A dimensionless index evaluating the time complementarity between solar and hydraulic energies," *Renewable Energy*, vol. 33, no. 10, pp. 2157 –2165, 2008, ISSN: 0960-1481. DOI: https://doi.org/10.1016/j.renene.2008.01.019.

[117] S. Rose and J. Apt, "What can reanalysis data tell us about wind power?" *Renewable Energy*, vol. 83, pp. 963–969, 2015. DOI: 10.1016/j.renene.2015.05.027.

[118] X. Fettweis, J. E. Box, C. Agosta, *et al.*, "Reconstructions of the 1900–2015 Greenland ice sheet surface mass balance using the regional climate MAR model," *The Cryosphere*, vol. 11, no. 2, p. 1015, 2017. DOI: 10.5194/tc-11-1015-2017.

[119] D. Radu, M. Berger, R. Fonteneau, *et al.*, "Complementarity assessment of South Greenland katabatic flows and West Europe wind regimes," *Energy*, vol. 175, pp. 393–401, 2019, ISSN: 0360-5442. DOI: https://doi.org/10.1016/j.energy.2019.03.048. [Online]. Available: https://www.sciencedirect.com/science/article/pii/S0360544219304529.

[120] A. Obermann, S. Bastin, S. Belamari, *et al.*, "Mistral and Tramontane wind speed and wind direction patterns in regional climate simulations," *Climate Dynamics*, vol. 51, pp. 1059–1076, 2016. DOI: 10.1007/s00382-016-3053-3.

[121] International Energy Agency (IEA), *Renewables 2020 Data Explorer*, 2020. [Online]. Available: https://www.iea.org/articles/renewables-2020-data-explorer.

[122] M. Segreto, L. Principe, A. Desormeaux, *et al.*, "Trends in Social Acceptance of Renewable Energy Across Europe—A Literature Review," *International Journal of Environmental Research and Public Health*, vol. 17, no. 24, 2020. DOI: 10.3390/ijerph17249161.

[123] "Renewable Power Generation Costs in 2019," International Renewable Energy Agency, Tech. Rep., 2020. [Online]. Available: https://www.irena.org/publications/2020/Jun/Renewable-Power-Costs-in-2019.

[124] J. Badger, I. Bauwens, P. Casso, *et al.*, *Global Wind Atlas 3.0*, 2021. [Online]. Available: https://globalwindatlas.info/.

[125] F. Geth, T. Brijs, J. Kathan, J. Driesen, and R. Belmans, "An Overview of Large-Scale Stationary Electricity Storage Plants in Europe: Current Status and New Developments," *Renewable and Sustainable Energy Reviews*, vol. 52, pp. 1212–1227, Dec. 2015. DOI: https://doi.org/10.1016/j.rser.2015.07.145.

[126] M. R. Milligan and R Artig, "Choosing Wind Power Plant Locations and Sizes Based on Electric Reliability Measures Using Multiple-Year Wind Speed Measurements," NREL, Tech. Rep. CP-500-26724, 1999. [Online]. Available: https://www.osti.gov/biblio/750939.

[127] M. Berger, D.Radu, R. Fonteneau, *et al.*, "Critical time windows for renewable resource complementarity assessment," *Energy*, vol. 198, 2020. DOI: 10.1016/j.energy.2020.117308. [Online]. Available: https://www.sciencedirect.com/science/article/abs/pii/S0360544220304151.

[128] S. Jerez, F. Thais, I. Tobin, *et al.*, "The CLIMIX model: A tool to create and evaluate spatially-resolved scenarios of photovoltaic and wind power development," *Renewable and Sustainable Energy Reviews*, vol. 42, pp. 1–15, 2015. DOI: doi:10.1016/j.rser.2014.09.041.

[129] R. Becker and D. Thrän, "Optimal siting of wind farms in wind energy dominated power systems," *Energies*, vol. 11, no. 4, p. 978, 2018, ISSN: 1996-1073. DOI: 10.3390/en11040978. [Online]. Available: http://dx.doi.org/10.3390/en11040978.

[130] A. Musselman, V. M. Thomas, N. Boland, and D. Nazzal, "Optimizing wind farm siting to reduce power system impacts of wind variability," *Wind Energy*, vol. 22, no. 7, pp. 894–907, 2019. DOI: https://doi.org/10.1002/we.2328.

[131] J. Hu, R. Harmsen, W. Crijns-Graus, and E. Worrell, "Geographical optimization of variable renewable energy capacity in China using modern portfolio theory," *Applied Energy*, vol. 253, p. 113 614, 2019, ISSN: 0306-2619. DOI: https://doi.org/10.1016/j.apenergy.2019.113614.

[132] M. Berger, D. Radu, A. Dubois, *et al.*, "Siting renewable power generation assets with combinatorial optimisation," *Optimization Letters*, 2020. [Online]. Available: https://orbi.uliege.be/handle/2268/251037.

[133] L. Baringo and A. J. Conejo, "Strategic wind power investment," *IEEE Transactions on Power Systems*, vol. 29, no. 3, pp. 1250–1260, 2014. DOI: 10.1109/TPWRS.2013.2292859.

[134] F. D. Munoz, B. F. Hobbs, J. L. Ho, and S. Kasina, "An engineering-economic approach to transmission planning under market and regulatory uncertainties: WECC case study," *IEEE Transactions on Power Systems*, vol. 29, no. 1, pp. 307–317, 2014. DOI: 10.1109/TPWRS.2013.2279654.

[135] W. Zappa, M. Junginger, and M. van den Broek, "Is a 100% renewable European power system feasible by 2050?" *Applied Energy*, vol. 233-234, pp. 1027–1050, 2019. DOI: doi:10.1016/j.apenergy.2018.08.109.

[136] L. Kotzur, P. Markewitz, M. Robinius, and D. Stolten, "Impact of different time series aggregation methods on optimal energy system design," *Renewable Energy*, vol. 117, pp. 474 –487, 2018, ISSN: 0960-1481. DOI: https://doi.org/10.1016/j.renene.2017.10.017.

[137] G. Wu, R. Deshmukh, K. Ndhlukulac, *et al.*, "Strategic siting and regional grid interconnections key to low-carbon futures in African countries," *Proceedings of the National Academy of Sciences*, vol. 114, 14 2017. DOI: doi:10.1073/pnas.1611845114.

[138] W. Zappa and M. van den Broek, "Analysing the potential of integrating wind and solar power in Europe using spatial optimisation under various scenarios," *Renewable and Sustainable Energy Reviews*, vol. 94, pp. 1192 –1216, 2018. DOI: doi:10.1016/j.rser.2018.05.071.

[139] D. Bertsimas and J. Tsitsiklis, "Simulated annealing," *Statist. Sci.*, vol. 8, no. 1, pp. 10–15, Feb. 1993. DOI: 10.1214/ss/1177011077.

[140] T. Mertens, K. Bruninx, J. Duerinck, and E. Delarue, "The impact of planning reserve margins and demand uncertainty in generation expansion models," *IAEE Proceedings*, 2018. [Online]. Available: https://www.mech.kuleuven.be/en/tme/research/energy_environment/Pdf/wp-en2018-16.

[141] C. Ensslin, M. Milligan, H. Holttinen, M. O'Malley, and A. Keane, "Current methods to calculate capacity credit of wind power, IEA collaboration," Aug. 2008, pp. 1 –3, ISBN: 978-1-4244-1905-0. DOI: 10.1109/PES.2008.4596006.

[142] I. Staffell and S. Pfenninger, "Using bias-corrected reanalysis to simulate current and future wind power output," *Energy*, vol. 114, pp. 1224 –1239, 2016, ISSN: 0360-5442. DOI: https://doi.org/10.1016/j.energy.2016.08.068. [Online]. Available: http://www.sciencedirect.com/science/article/pii/S0360544216311811.

[143] S. Pfenninger and I. Staffell, "Long-term patterns of European PV output using 30 years of validated hourly reanalysis and satellite data," *Energy*, vol. 114, pp. 1251 –1265, 2016, ISSN: 0360-5442. DOI: https://doi.org/10.1016/j.energy.2016.08.060. [Online]. Available: http://www.sciencedirect.com/science/article/pii/S0360544216311744.

[144] International Electrotechnical Commission, *IEC 61400-1:2019: Wind energy generation systems - Part 1: Design requirements*, 2019. [Online]. Available: https://webstore.iec.ch/publication/26423.

[145] European Commission - Joint Research Centre, *ENSPRESO - an open, EU-28 wide, transparent and coherent database of wind, solar and biomass energy potentials*, 2019. [Online]. Available: https://data.jrc.ec.europa.eu/collection/id-00138.

[146] Deutsche WindGuard GmbH, "Capacity densities of European offshore wind farms," VASAB, Tech. Rep., 2018. [Online]. Available: https://vasab.org/10564-2/.

[147] "Clean energy transition - technologies and innovations, accompanying the report on progress of clean energy competitiveness," European Commission, Tech. Rep., 2020. [Online]. Available: https://ec.europa.eu/energy/topics/technology-and-innovation/clean-energy-competitiveness_en.

[148] Danish Energy Agency, *Technology Data for Generation of Electricity and District Heating*, 2020. [Online]. Available: https://ens.dk/en/our-services/projections-and-models/technology-data/technology-data-generation-electricity-and.

[149] ENTSO-E, *Power Statistics*, 2021. [Online]. Available: https://www.entsoe.eu/data/power-stats/.

[150] European Commission - Joint Research Centre, *The Joint Research Centre Power Plant Database (JRC-PPDB)*, 2019. [Online]. Available: https://ec.europa.eu/jrc/en/publication/joint-research-centre-power-plant-database-jrc-ppdb.

[151] ——, *JRC Hydro-power plants database*, 2020. [Online]. Available: https://github.com/energy-modelling-toolkit/hydro-power-database.

[152] A. Beauvais, M. Herrero Cangas, N. Chevillard, M. Heisz, M. Labordena, and R. Rossi, "EU Market Outlook for Solar Power 2019-2023," Solar Power Europe, Tech. Rep., 2019. [Online]. Available: https://www.solarpowereurope.org/eu-market-outlook-for-solar-power-2019-2023/.

[153] D. Radu, A. Dubois, and M. Berger, *Assessing the impact of offshore wind siting strategies on the design of the European power system - dataset*, 2021. [Online]. Available: https://dox.uliege.be/index.php/s/u6kPFWKRGOGlDqg.

[154] D. Radu and M. Berger, *Resite - a framework for RES siting leveraging resource complementarity*, 2021. [Online]. Available: https://github.com/dcradu/resite_ip/releases/tag/v0.0.1.

[155] A. Dubois, D. Radu, and M. Berger, *Replan - a framework for bulk energy systems planning and analysis*, 2020. [Online]. Available: https://github.com/montefesp/replan/releases/tag/v0.0.4.

[156] C. M. Grams, R. Beerli, S. Pfenninger, I. Staffell, and H. Wernli, "Balancing europe's wind-power output through spatial deployment informed by weather

regimes," *Nature Climate Change*, vol. 7, 557–562, Jul. 2017. DOI: 10.1038/nclimate3338.

[157] N. Cortesi, V. Torralba, N. González-Reviriego, A. Soret, and F. J. Doblas-Reyes, "Characterization of european wind speed variability using weather regimes," *Climate Dynamics*, vol. 53, 4961–4976, Jun. 2019. DOI: 10.1007/s00382-019-04839-5.

[158] R. Wiser, J. Rand, J. Seel, *et al.*, "Expert elicitation survey predicts 37% to 49% declines in wind energy costs by 2050," *Nature Energy*, vol. 53, 4961–4976, Apr. 2021. DOI: 10.1038/s41560-021-00810-z.

[159] S. Collins, P. Deane, B. Ó Gallachóir, S. Pfenninger, and I. Staffell, "Impacts of inter-annual wind and solar variations on the european power system," *Joule*, vol. 2, no. 10, pp. 2076–2090, 2018, ISSN: 2542-4351. DOI: https://doi.org/10.1016/j.joule.2018.06.020. [Online]. Available: https://www.sciencedirect.com/science/article/pii/S254243511830285X.

[160] F. Neumann and T. Brown, "The near-optimal feasible space of a renewable power system model," *Electric Power Systems Research*, vol. 190, p. 106 690, 2021, ISSN: 0378-7796. DOI: https://doi.org/10.1016/j.epsr.2020.106690.

[161] F. Neumann, V. Hagenmeyer, and T. Brown, *Approximating power flow and transmission losses in coordinated capacity expansion problems*, 2020. arXiv: 2008.11510 [physics.soc-ph].

[162] N. Helistö, J. Kiviluoma, H. Holttinen, J. D. Lara, and B.-M. Hodge, "Including operational aspects in the planning of power systems with large amounts of variable generation: A review of modeling approaches," *WIREs Energy and Environment*, vol. 8, no. 5, e341, 2019. DOI: https://doi.org/10.1002/wene.341. eprint: https://wires.onlinelibrary.wiley.com/doi/pdf/10.1002/wene.341. [Online]. Available: https://wires.onlinelibrary.wiley.com/doi/abs/10.1002/wene.341.

[163] B. A. Frew, S. Becker, M. J. Dvorak, G. B. Andresen, and M. Z. Jacobson, "Flexibility mechanisms and pathways to a highly renewable us electricity future," *Energy*, vol. 101, pp. 65–78, 2016, ISSN: 0360-5442. DOI: https://doi.org/10.1016/j.energy.2016.01.079. [Online]. Available: https://www.sciencedirect.com/science/article/pii/S0360544216300032.

[164] M. Brown, W. Cole, K. Eurek, *et al.*, *Regional Energy Deployment System (ReEDS) Model Documentation: Version 2019*, NREL/TP-6A20-74111, 2019. [Online]. Available: https://www.nrel.gov/docs/fy20osti/74111.pdf.

[165] D. Lew, G. Brinkman, E. Ibanez, *et al.*, "Western Wind and Solar Integration Study Phase 2," Sep. 2013. DOI: https://dx.doi.org/10.2172/1095399. [Online]. Available: https://www.osti.gov/biblio/1095399.

[166] J. Deane, F. Gracceva, A. Chiodi, M. Gargiulo, and B. P. Gallachóir, "Assessing power system security. a framework and a multi model approach," *International Journal of Electrical Power & Energy Systems*, vol. 73, pp. 283–297, 2015, ISSN: 0142-0615. DOI: https://doi.org/10.1016/j.ijepes.2015.04.020.

[Online]. Available: https://www.sciencedirect.com/science/article/pii/S0142061515002021.

[167] K. Poncelet, E. Delarue, D. Six, J. Duerinck, and W. D'haeseleer, "Impact of the level of temporal and operational detail in energy-system planning models," *Applied Energy*, vol. 162, pp. 631–643, 2016, ISSN: 0306-2619. DOI: https://doi.org/10.1016/j.apenergy.2015.10.100. [Online]. Available: https://www.sciencedirect.com/science/article/pii/S0306261915013276.

[168] J. Kiviluoma, E. Rinne, and N. Helistö, "Comparison of flexibility options to improve the value of variable power generation," *International Journal of Sustainable Energy*, vol. 37, no. 8, pp. 761–781, 2018. DOI: 10.1080/14786451.2017.1357554.

[169] A. D. Mills and R. H. Wiser, "Changes in the economic value of photovoltaic generation at high penetration levels: A pilot case study of california," in *2012 IEEE 38th Photovoltaic Specialists Conference (PVSC) PART 2*, 2012, pp. 1–9. DOI: 10.1109/PVSC-Vol2.2012.6656763.

[170] A. Pina, C. A. Silva, and P. Ferrão, "High-resolution modeling framework for planning electricity systems with high penetration of renewables," *Applied Energy*, vol. 112, pp. 215–223, 2013, ISSN: 0306-2619. DOI: https://doi.org/10.1016/j.apenergy.2013.05.074. [Online]. Available: https://www.sciencedirect.com/science/article/pii/S030626191300487X.

[171] D. Pudjianto, M. Aunedi, P. Djapic, and G. Strbac, "Whole-systems assessment of the value of energy storage in low-carbon electricity systems," *IEEE Transactions on Smart Grid*, vol. 5, no. 2, pp. 1098–1109, 2014. DOI: 10.1109/TSG.2013.2282039.

[172] N. E. Koltsaklis and M. C. Georgiadis, "A multi-period, multi-regional generation expansion planning model incorporating unit commitment constraints," *Applied Energy*, vol. 158, pp. 310–331, 2015, ISSN: 0306-2619. DOI: https://doi.org/10.1016/j.apenergy.2015.08.054. [Online]. Available: https://www.sciencedirect.com/science/article/pii/S0306261915009873.

[173] B. S. Palmintier and M. D. Webster, "Impact of operational flexibility on electricity generation planning with renewable and carbon targets," *IEEE Transactions on Sustainable Energy*, vol. 7, no. 2, pp. 672–684, 2016. DOI: 10.1109/TSTE.2015.2498640.

[174] A. Flores-Quiroz, R. Palma-Behnke, G. Zakeri, and R. Moreno, "A column generation approach for solving generation expansion planning problems with high renewable energy penetration," *Electric Power Systems Research*, vol. 136, pp. 232–241, 2016, ISSN: 0378-7796. DOI: https://doi.org/10.1016/j.epsr.2016.02.011. [Online]. Available: https://www.sciencedirect.com/science/article/pii/S0378779616300177.

[175] F. Neumann and T. Brown, "Transmission expansion planning using cycle flows," in *Proceedings of the Eleventh ACM International Conference on Future Energy Systems*, ser. e-Energy '20, Virtual Event, Australia: Association for

Computing Machinery, 2020, 253–263. DOI: 10.1145/3396851.3397688. [Online]. Available: https://doi.org/10.1145/3396851.3397688.

[176] S. Haas, B. Schachler, and U. Krien, *Windpowerlib - a python library to model wind power plants*, 2020. [Online]. Available: 10.5281/zenodo.3403360.

[177] WindEurope, *Wind energy and on-site energy storage - exploring market opportunities*, 2017. [Online]. Available: https://windeurope.org/wp-content/uploads/files/about-wind/reports/Wind-energy-in-Europe-Scenarios-for-2030.pdf.

[178] B. Wiegmans, *Gridkit extract of entso-e interactive map [data set]. zenodo.* 2016. [Online]. Available: https://doi.org/10.5281/zenodo.55853.

[179] E. Commission, *Nomenclature of territorial units for statistics*, 2016. [Online]. Available: https://ec.europa.eu/eurostat/web/nuts/background.

[180] Eurostat, *Population density by NUTS 2 region*, 2021. [Online]. Available: https://ec.europa.eu/eurostat/web/products-datasets/-/tgs00024.

[181] ——, *Regional gross domestic product (million PPS) by NUTS 2 regions*, 2021. [Online]. Available: https://ec.europa.eu/eurostat/web/products-datasets/-/tgs00004.

[182] S. Gonzato, K. Bruninx, and E. Delarue, "Long term storage in generation expansion planning models with a reduced temporal scope," *Applied Energy*, vol. 298, p. 117 168, 2021, ISSN: 0306-2619. DOI: https://doi.org/10.1016/j.apenergy.2021.117168. [Online]. Available: https://www.sciencedirect.com/science/article/pii/S0306261921006000.

[183] J. H. W. Jr., "Hierarchical grouping to optimize an objective function," *Journal of the American Statistical Association*, vol. 58, no. 301, pp. 236–244, 1963. DOI: 10.1080/01621459.1963.10500845.

[184] S. Hagspiel, C. Jägemann, D. Lindenberger, T. Brown, S. Cherevatskiy, and E. Tröster, "Cost-optimal power system extension under flow-based market coupling," *Energy*, vol. 66, pp. 654–666, 2014, ISSN: 0360-5442. DOI: https://doi.org/10.1016/j.energy.2014.01.025. [Online]. Available: https://www.sciencedirect.com/science/article/pii/S0360544214000322.

[185] F. Neumann and T. Brown, "Heuristics for transmission expansion planning in low-carbon energy system models," in *2019 16th International Conference on the European Energy Market (EEM)*, 2019, pp. 1–8. DOI: 10.1109/EEM.2019.8916411.

[186] N. Kumar, *Update of Reliablity and Cost Impacts of Flexible Generation on Fossil-fueled Generators for Western Electricity Coordination Council*, 2020. [Online]. Available: https://www.wecc.org/Reliability/1r10726%20WECC%20Update%20of%20Reliability%20and%20Cost%20Impacts%20of%20Flexible%20Generation%20on%20Fossil.pdf.

[187] NREL, "Regional Energy Deployment System (ReEDS) model documentation: version 2018," National Renewable Energy Laboratory, Tech. Rep., 2019, https://www.nrel.gov/docs/fy19osti/72023.pdf.

[188] D. S. Ryberg, M. Robinius, and D. Stolten, "Methodological framework for determining the land eligibility of renewable energy sources," *arXiv preprint arXiv:1712.07840*, 2017.

[189] T. Tröndle, S. Pfenninger, and J. Lilliestam, "Home-made or imported: On the possibility for renewable electricity autarky on all scales in Europe," *Energy Strategy Reviews*, vol. 26, p. 100 388, 2019, ISSN: 2211-467X. DOI: https://doi.org/10.1016/j.esr.2019.100388. [Online]. Available: http://www.sciencedirect.com/science/article/pii/S2211467X19300811.

[190] Open Power System Data, *Data Package Time series*, https://data.open-power-system-data.org/time_series/2019-06-05, 2019. DOI: 10.25832/time_series/2019-06-05.

[191] A. Dubois, D. Radu, and M. Berger, *Model reduction in capacity expansion planning problems via renewable generation site selection - dataset*, https://dox.uliege.be/index.php/s/errFWRnFbfroi17, 2020.

[192] A. Malvaldi, S. Weiss, D. Infield, J. Browell, P. Leahy, and A. M. Foley, "A spatial and temporal correlation analysis of aggregate wind power in an ideally interconnected Europe," *Wind Energy*, vol. 20, no. 8, pp. 1315–1329, 2017.

[193] F. deLlano Paz, A. Calvo-Silvosa, S. I. Antelo, and I. Soares, "Energy planning and modern portfolio theory: A review," *Renewable and Sustainable Energy Reviews*, vol. 77, pp. 636–651, 2017, ISSN: 1364-0321. DOI: https://doi.org/10.1016/j.rser.2017.04.045. [Online]. Available: https://www.sciencedirect.com/science/article/pii/S136403211730552X.

[194] X. Yue, S. Pye, J. DeCarolis, F. G. Li, F. Rogan, and B. Gallachóir, "A review of approaches to uncertainty assessment in energy system optimization models," *Energy Strategy Reviews*, vol. 21, pp. 204–217, 2018, ISSN: 2211-467X. DOI: https://doi.org/10.1016/j.esr.2018.06.003. [Online]. Available: https://www.sciencedirect.com/science/article/pii/S2211467X18300543.

[195] J. F. DeCarolis, "Using modeling to generate alternatives (mga) to expand our thinking on energy futures," *Energy Economics*, vol. 33, no. 2, pp. 145–152, 2011, ISSN: 0140-9883. DOI: https://doi.org/10.1016/j.eneco.2010.05.002. [Online]. Available: https://www.sciencedirect.com/science/article/pii/S0140988310000721.

[196] M. Pichault, C. Vincent, G. Skidmore, and J. Monty, "Characterisation of intra-hourly wind power ramps at the wind farm scale and associated processes," *Wind Energy Science*, vol. 6, no. 1, pp. 131–147, 2021. DOI: 10.5194/wes-6-131-2021. [Online]. Available: https://wes.copernicus.org/articles/6/131/2021/.

[197] A. van Stiphout, K. De Vos, and G. Deconinck, "The impact of operating reserves on investment planning of renewable power systems," *IEEE Transactions on Power Systems*, vol. 32, no. 1, pp. 378–388, 2017. DOI: 10.1109/TPWRS.2016.2565058.

[198] L. Kotzur, P. Markewitz, M. Robinius, and D. Stolten, "Time series aggregation for energy system design: Modeling seasonal storage," *Applied Energy*, vol. 213, pp. 123–135, 2018, ISSN: 0306-2619. DOI: https://doi.org/10.1016/j.apenergy.2018.01.023. [Online]. Available: https://www.sciencedirect.com/science/article/pii/S0306261918300242.

[199] National Renewable Energy Laboratory, *Annual technology baseline*, https://atb.nrel.gov, 2020.

[200] MBB Group Pty Ltd, *AEMO Transmission Cost Database Report*, 2020. [Online]. Available: https://aemo.com.au/energy-systems/major-publications/integrated-system-plan-isp/2022-integrated-system-plan-isp/current-inputs-assumptions-and-scenarios.

[201] International Energy Agency, "Projected costs of generating electricity," 2020. [Online]. Available: https://www.iea.org/reports/projected-costs-of-generating-electricity-2020.

[202] Danish Energy Agency, *Technology data for energy storage*, 2020. [Online]. Available: https://ens.dk/en/our-services/projections-and-models/technology-data/technology-data-energy-storage.

[203] K. Mongird, V. Viswanathan, P. Balducci, *et al.*, "Energy Storage Technology and Cost Characterization Report," U.S. Department of Energy, Tech. Rep., 2019. [Online]. Available: https://www.energy.gov/sites/prod/files/2019/07/f65/Storage\%20Cost\%20and\%20Performance\%20Characterization\%20Report_Final.pdf.

[204] A. L'Abbate and G. Migliavacca, "Review of costs of transmission infrastructures, including cross border connections," 2011. [Online]. Available: https://realisegrid.rse-web.it/Publications-and-results.asp.

[205] A. Akhil, G. Huff, A. Currier, *et al.*, "DOE/EPRI Electricity Storage Handbook in Collaboration with NRECA," Sandia National Laboratories, Tech. Rep., 2013. [Online]. Available: https://prod-ng.sandia.gov/techlib-noauth/access-control.cgi/2015/151002.pdf.

[206] G. Simbolotti and G. Tosato, "Technology Brief E12 - Electricity Transmission and Distribution," IEA, Tech. Rep., 2014. [Online]. Available: https://iea-etsap.org/E-TechDS/PDF/E12_el-t&d_KV_Apr2014_GSOK.pdf.

[207] D. McGowan, T. Rzepczyk, C. Sonmez, *et al.*, "TYNDP 2020 Scenario Report," ENTSO-E; ENTSO-G, Tech. Rep., 2019. [Online]. Available: https://www.entsos-tyndp2020-scenarios.eu/wp-content/uploads/2019/10/TYNDP_2020_Scenario_Report_entsog-entso-e.pdf.

[208] D. Gómez, J. Watterson, A. Branca, *et al.*, "IPCC Emissions Factor Database," IPCC, Tech. Rep., 2006. [Online]. Available: https://ghgprotocol.org/Third-Party-Databases/IPCC-Emissions-Factor-Database.

[209] European Environment Agency, *CO2 Intensity of Electricity Generation*, 2020. [Online]. Available: https://www.eea.europa.eu/data-and-maps/data/co2-intensity-of-electricity-generation.

[210] International Energy Agency, *Data and statistic - CO2 emissions by sector*, 2020. [Online]. Available: https://www.iea.org/data-and-statistics?country=WORLD&fuel=CO2\%20emissions&indicator=CO2\%20emissions\%20by\%20sector.

[211] K. Van den Bergh and E. Delarue, "Cycling of conventional power plants: Technical limits and actual costs," *Energy Conversion and Management*, vol. 97, pp. 70–77, 2015, ISSN: 0196-8904. DOI: https://doi.org/10.1016/j.enconman.2015.03.026. [Online]. Available: https://www.sciencedirect.com/science/article/pii/S0196890415002368.

[212] Gurobi Optimization, *Gurobi 9.1 - Parameters*, 2021. [Online]. Available: https://www.gurobi.com/documentation/9.1/refman/parameters.html.

[213] M. Wittenstein and G. Rothwell, "Projected Costs of Generating Electricity," IEA, Tech. Rep., 2015. [Online]. Available: https://www.oecd-nea.org/ndd/pubs/2015/7057-proj-costs-electricity-2015.pdf.

[214] Danish Energy Agency and Energinet, "Technology Data for Energy Storage," Danish Energy Agency, Tech. Rep., 2020. [Online]. Available: https://ens.dk/en/our-services/projections-and-models/technology-data/technology-data-energy-storage.

[215] S. Samsatli, I. Staffell, and N. J. Samsatli, "Optimal design and operation of integrated wind-hydrogen-electricity networks for decarbonising the domestic transport sector in great britain," *International Journal of Hydrogen Energy*, vol. 41, no. 1, pp. 447 –475, 2016, ISSN: 0360-3199. DOI: https://doi.org/10.1016/j.ijhydene.2015.10.032. [Online]. Available: http://www.sciencedirect.com/science/article/pii/S0360319915300574.

[216] P. Härtel and M. Korpås, "Aggregation methods for modelling hydropower and its implications for a highly decarbonised energy system in europe," *Energies*, vol. 10, no. 11, p. 1841, 2017, ISSN: 1996-1073. DOI: 10.3390/en10111841.

[217] ENTSOE, *Water Reservoirs and Hydro Storage Plants*, 2020. [Online]. Available: https://transparency.entsoe.eu/dashboard/show.

[218] B. Lehner, C. R. Liermann, C. Revenga, *et al.*, "High-resolution mapping of the world's reservoirs and dams for sustainable river-flow management," *Frontiers in Ecology and the Environment*, vol. 9 (9), pp. 494–502, 2011. [Online]. Available: http://globaldamwatch.org/grand/.

[219] ECMWF, *ERA5 hourly data on single levels from 1979 to present*, 2020. [Online]. Available: https://cds.climate.copernicus.eu/cdsapp#!/dataset/reanalysis-era5-single-levels?tab=overview.

[220] Eurostat, *Gross and net production of electricity and derived heat by type of plant and operator*, 2020. [Online]. Available: https://ec.europa.eu/eurostat/web/products-datasets/-/nrg_ind_peh.